Differential binding specificity of the bacterial effector protein AvrPto to plant receptor-like kinase virulence targets

Dissertation

der Mathematisch-Naturwissenschaftlichen Fakultät

der Eberhard-Karls Universität Tübingen

zur Erlangung des Grades eines

Doktors der Naturwissenschaften

(Dr. rer. nat.)

vorgelegt von

Dipl. Biol. André Reinhard

aus Hadamar

Tübingen

2016

Gedruckt mit Genehmigung der Mathematisch-Naturwissenschaftlichen Fakultät der Eberhard Karls Universität Tübingen.

Tag der mündlichen Qualifikation:	02.06.2016
Dekan:	Prof. Dr. Wolfgang Rosenstiel
1. Berichterstatter:	Prof. Dr. Thorsten Nürnberger
2. Berichterstatter:	Prof. Dr. Georg Felix

TABLE OF CONTENTS

LIST OF FIGURES

LIST OF TABLES

NOMENCLATURE

Acronyms

T_m	Melting temperature (of nucleic acids)
AA	Acrylamide
AC	Affinity chromatography
ACD6	Accelerated cell death 6
ADP	Adenosine diphosphate
AP	Affinity purification
APS	Ammonium persulfate
ATP	Adenosine triphosphate
BAA	Bisacrylamide
BAK1	BRI1-associated kinase 1
BiFC	Bi-molecular fluorescence complementation
BIK1	Botrytis-induced kinase 1
BIR	BAK1-interacting receptor-like kinase
BKK1	BAK1-like kinase 1
BR	Brassinosteroid
BRI1	Brassinosteroid-insensitive 1
BSA	Bovine serum albumin
BSK3	BR-signalling kinase 3
CBB	Coomassie brilliant blue
CC	Coiled coil
CD	Cytoplasmic domain
CDG1	Constitutive differential growth 1
cDNA	Complementary DNA
CFA	Coronafacic acid
CLR	C-type lectin receptors
CMA	Coronamic acid
CNL	Coiled coil-domain NLR
Co-IP	Co-immunoprecipitation
COI1	COR-insensitive 1
COR	Coronatine

CRISPR	Clustered regularly-interspaced short palindromic repeats
CrRLK1L	*Catharanthus roseus* receptor-like kinase
CV	Column volumes
CyA	Calmodulin-dependent adenylate cyclase
DAMP	Damage-associated molecular pattern
DNA	Desoxyribonucleic acid
DORN1	Does not respond to nucleotides 1
dsRNA	Double-stranded RNA
EC_{50}	Half-maximal effective concentration
EDTA	Ethylenediaminetetraacetic acid
EF-Tu	Elongation factor Tu
EFR	EF-Tu receptor
EGFR	Epidermal growth factor receptor
EPF	Epidermal patterning factor
ER (organelle)	Endoplasmic reticulum
ER (receptor)	Estrogen receptor
ETI	Effector-triggered immunity
ETS	Effector-triggered susceptibility
FC	Flow cell (SPR)
Fen	Fenthion sensitivity kinase
flg22	Flagellin (epitope)
FLS2	Flagellin-sensing 2
GlcNAc	*N*-acetylglucoasmine
GPI	Glycophosphatidylinositol
HAMP	Herbivory-associated molecular pattern
HOP	Hrp outer protein
HR	Hypersensitive response
hrp	Hypersensitive response and pathogenicity
IMAC	Immobilized metal affinity chromatography
IPTG	Isopropyl β-D-1-thiogalactopyranoside
IR	Infrared
IRAK	Interleukin-1 receptor associated kinase
ITC	Isothermal titration calorimetry
JA	Jasmonic acid
KAPP	Kinase-associated protein phosphatase
LB	Lysogeny broth

Lec	Lectin
LED	Light-emitting diode
LORE	Lipooligosaccharide-specific reduced elicitation
LPS	Lipopolysaccharide
LRR	Leucine-rich repeat
LysM	Lysine motif
MAMP	Microbe-associated molecular pattern
MAPK	Mitogen-activated protein kinase
MCS	Multiple cloning site
MES	2-(N-morpholino)ethanesulfonic acid
MLST	Multi-locus sequencing typing
MMDB	Molecular modeling database
MS	Mass spectroscopy
MST	Microscale thermophoresis
NADPH	Nicotinamide adenine dinucleotide phosphate
NB	Nucleotide-binding
NLP	Necrosis and ethylene-inducing peptide 1-like protein
NLR	NOD-like receptor
NLR	Nucleotide-binding leucine-rich repeat
NOD	Nucleotide-binding oligomerization domain
OD	Optical density
PAMP	Pathogen-associated molecular pattern
ParAMP	Parasitism-associated molecular pattern
PBL	PBS1-like
PCR	Polymerase chain reaction
PDB	Protein data bank
PEG	Polyethylene glycol
PEPR1	Pep1 receptor 1
pFRK1	Promoter of flg22-induced receptor-like kinase
pI	Isoelectric point
PKA	Protein kinase A
PKI	Protein kinase A inhibitor
PM	Plasma membrane
PP2A	Protein Ser/Thr phosphatase type 2A
Prf	*Pseudomonas* resistance / fenthion sensitivity
PRR	Pattern recognition receptor

PSSM	Position specific scoring matrix
PTI	PAMP-triggered immunity
PUB	Plant u-box E3 ubiquitin
R	Resistance
RBOHD	Respiratory burst oxidase D
RFP	Red fluorescent protein
RGB	Red/green/blue
RIN4	RPM1-interacting protein 4
RLCK	Receptor-like cytoplasmatic kinase
RLK	Receptor-like kinase
RLP	Receptor-like protein
RLR	RIG1-like receptor
RM	Restriction-modification
RMSD	Root-mean-square deviation
ROS	Reactive oxygen species
RPM1	Resistance to *Pseudomonas maculicola* 1
RPS2	Resistance to *Pseudomonas syringae* 2
SA	Salicylic acid
SDM	Site-directed mutagenesis
SDS	Sodium dodecyl sulfate
SDS-PAGE	Sodium dodecyl sulfate polyacrylamide gel electrophoresis
SEC	Size exclusion chromatography
SERK	Somatic embryogenesis receptor-like kinase
SipA	*Salmonella* invasion protein A
siRNA	Small interfering RNA
SOB	Super optimal broth
SOBIR1	Suppressor of BIR1-1
SOC	Super optimal broth with catabolite repression
SPR	Surface plasmon resonance
T3E	Type three effector
TAE	Tris / acetic acid / EDTA buffer
TALE	Transcription-activator-like effector
TB-HD	Terrific broth, high density
TEMED	Tetramethylethylenediamine
TIR	Toll-IL1 receptor
TLR	Toll-like receptor

TNL	TIR-domain NLR
TTSS / T3SS	Type three secretion system
UV	Ultraviolet
VAST+	Vector alignment search tool 'plus' (algorithm)
WAK1	Wall-associated kinase 1
Y2H	Yeast two-hybrid

Abbreviations

Avr	Avirulence
c	Concentration
e.g.	For example
fw	Forward
His	Histidine
i.e.	That is
log	Logarithm
Luc	Luciferase
pH	Power of hydrogen
pv.	Pathovar
rv	Reverse
S	Selectivity
Tris	Tris(hydroxymethyl)aminomethane
U value	Uniqueness value (SPR)
v/v	Volume per volume
vs.	*versus*
w/v	weight per volume

Mathematical Symbols and Constants

χ^2	Chi squared (statistics)
k_a	Association rate constant
K_D	Equilibrium dissociation constant
k_d	Dissociation rate constant

SI prefixes

c	Centi, 10^{-2}
f	Femto, 10^{-15}
G	Giga, 10^{9}

k	Kilo, 10^3
M	Mega, 10^6
m	Milli, 10^{-3}
n	Nano, 10^{-9}
p	Pico, 10^{-12}
µ	Micro, 10^{-6}

Taxa

At	*Arabidopsis thaliana* (thale cress)
Cr	*Catharanthus roseus*
Nb	*Nicotiana benthamiana*
Os	*Oryza sativa* (asian rice)
Pfu	*Pyrococcus furiosus*
Ps	*Pseudomonas syringae*
Pto	*Pseudomonas syringae* pv. *tomato*
Sl	*Solanum lycopersicon* (tomato)
Xcc	*Xanthomonas campestris* pv. *campestris*
Col-0	Columbia (*At* ecotype)
L*er*	Landsberg *erecta* (*At* ecotype)

Units

$\times g$	Multiple of standard gravity ($\sim 9.5\ \mathrm{m\,s^{-2}}$)
Å	Ångstrom
AU	Arbitrary units
g	Gram
h	Hour
L	Liter
M	Molar
m	Meter
min	Minute
RLU	Relative light units
rpm	Revolutions per minute
RU	Response units (SPR)
s	Second
U	Units (enzymatic activity)
°C	Degrees Celsius

CHAPTER 1

INTRODUCTION

1.1 Fundamentals of innate immunity

1.1.1 Life is immunity

Primal battlegrounds Life thrives on death – this biological paradigm succinctly describes why even the earliest and simplest of life forms on earth have evolved mechanisms to hold off would-be predators. Primal ecosystems such as marine water are dominated by parasitic agents; bacteriophage titres reach 5×10^7 mL^{-1} (**Danovaro et al., 2008**). To deal with this challenge, prokaryotes use the CRISPR/Cas system to degrade invading bacteriophage DNA (**Garneau et al., 2010**) - a very early form of an immune system that is present in ∼90 % of archaea and ∼40 % of bacteria (**Horvath and Barrangou, 2010**). Conceptually similar mechanisms include the prokaryotic use of restriction-modification (RM) systems, which encode specific methyl transferases to epigenetically mark domestic DNA as *self* and restriction endonucleases to cleave invading DNA that has not been properly modified and is thus classified as *non-self* (**Kobayashi, 2001**). This dichotomy of self against non-self, of host against pathogen, thus forms the very basis of the biological concept of immunity, which is retained from the simplest nucleic acids interacting with each other to complex multicellular eukaryotes.

Evolution of immunity Advancing along the tree of life presents an ever-increasing variety of strategies to cope with the assault of harmful organisms, and higher organisms often combine them to increase the efficiency of the immune response. Immunity mechanisms can be broadly categorized as being either *innate* or *adaptive*, based on whether they function as genetically preformed (and thus, inherited) systems or include responsive elements that allow fine-tuning to the specific nature of challenging pathogens, respectively. Conceptually, these strategies tie together by providing a layering effect: preformed systems do not require prior contact with the pathogen to be effective, while adaptive systems can be more specific (**Cooper and Alder, 2006**). This enhanced specificity allows adaptive immune responses to be both more finely tailored to the exact nature

of the pathogen and to incur higher metabolic costs, as their induction can be more tightly regulated (**Iwasaki and Medzhitov, 2010**). Arguably the most striking example of this concept is the vertebrate adaptive immune system, which uses somatic hypermutations and recombinations to achieve a far higher variety of very specific defence mechanisms than what could reasonably be encoded genetically (**Tonegawa, 1983**, **McBlane et al., 1995**). Additionally, the vertebrate adaptive immune system can create a specific immunity 'memory' which enhances the efficiency of subsequent responses to the same pathogen (**Ahmed and Gray, 1996**). In vertebrates, the innate and adaptive immune systems are efficiently integrated; beside providing defensive actions by itself, the innate immune system provides signals to the adaptive immune system which help to efficiently regulate immune responses (**Fearon and Locksley, 1996**). Recently, the critical importance of the innate immune system for animal health has gained increasing recognition (**Kawai and Akira, 2010**), and it has been shown that polymorphism in a single gene encoding for an innate immunity receptor is a significant factor in the development of human disease (**Hawn et al., 2003**). It should be noted that while the vertebrate adaptive immune system is the classical and most well-studied example of adaptive immunity, even evolutionarily ancient systems like the previously mentioned CRISPR/Cas system can provide some adaptive flexibility outside of the more rigid genetic framework generally classified as innate immunity (**Westra et al., 2014**).

Constitutive adaptations Organisms have evolved unspecific, constitutive biological adaptations as a first line of defence against potential pathogens. These include anatomical or physiological barriers to pathogen entry and survival, but due to their generalized nature, their effectiveness against any single type of pathogen is naturally limited, and successful pathogens evolved strategies to circumvent these defences (e.g. bacteriophages which can circumvent microbial cell envelopes or animal gut pathogens which survive passage through the stomach). Additionally, due to their constitutive presence, there is a strong need to balance the extent of these adaptations against the physiological needs of a healthy organism – resistant hosts are ecologically less competitive than non-resistant hosts in the absence of pathogens (**Schmid-Hempel and Ebert, 2003**), as immunity always has physiological tradeoffs (**Eichmann and Schäfer, 2015**).

Regulated immunity Stepping up in efficiency from purely unspecific, constitutive defences introduces the need for regulation. The basis of all regulated biological immunity functions – recognizing a present need to functionally activate dormant defence mechanisms – is mediated by receptors. The innate immune system genetically encodes receptor proteins for various molecular signals that alert the organism to a pathogen's

presence. The detection of these 'danger signals' can be either direct (e.g. recognizing molecular features that are only present in the pathogen) or indirect (e.g. recognizing the pathogen's actions). Once a signal is detected, the receptor provides input into a complex signalling network which can ultimately lead to an immune response (**Tena et al., 2011**). The multitude of negative feedback elements in immunity signalling emphasizes the critical importance of a well-regulated immune system (**Akira et al., 2006**), and some of the most intuitively drastic effects of immunity misregulation are apparent in the impact of human autoimmune diseases (**Sakaguchi et al., 2008**).

1.1.2 Danger signals as the basis of innate immunity

Pattern recognition A recurring theme of danger perception that occurs in innate immunity of higher organisms is that of molecular patterns (**Medzhitov and Janeway, 1997**). These perception systems are an evolutionary ancient part of innate immunity and are, in different forms, present in both plants and animals (**Nürnberger et al., 2004**, **Ronald and Beutler, 2010**). Although the general concept of pattern recognition is conserved in higher organisms, the specific perception systems seem to rather be a case of convergent evolution (**Ausubel, 2005**, **Zipfel and Felix, 2005**). Classically, such patterns have been defined as widely conserved, often simple molecular features (e.g. short peptide epitopes, carbohydrates, and small molecule ligands) that are recognized by corresponding pattern recognition receptors (PRRs).

MAMPs vs. DAMPs Patterns that are inherently specific to microbial life are excellent templates by which higher organisms can unequivocally detect the presence of microbes; these have been termed microbe-associated molecular patterns (MAMPs; also called PAMPs for pathogen-associated molecular patterns). Perception of MAMPs originating from microbial pathogens thus constitutes direct danger signals, as defined previously. Conversely, patterns which are endogenous in nature but only arise as a consequence of pathogen action ('modified self') have been classified as damage-associated molecular patterns (DAMPs), and thus constitute indirect danger signals. Pattern recognition in context of plant innate immunity is discussed in detail in section **1.4.1**.

Effectors Besides these simple molecular patterns, other signals of danger include the perception of specific pathogen proteins which act as virulence factors and have been termed effectors. Effector perception systems have been the basis of the classical gene-for-gene hypothesis in plant immunity (**Flor, 1971**; for details, also see section **1.4.2.1**), and have been described as a distinct branch of innate immunity (effector-triggered immunity, ETI) that can be contrasted with the previously described PRR-mediated immunity

(PAMP-triggered immunity, PTI; **Jones and Dangl, 2006**). Although the bulk of research on effector perception systems has been conducted on plants, emerging evidence shows that similar effector perception systems exist in animals (**Stuart et al., 2013**). Effectors in context of plant innate immunity are discussed in detail in section **1.4.2**.

Classification of danger signals Although the terms introduced in this section are widely used for classification purposes, there is ongoing debate whether such rigid classifications are appropriate, as a growing number of molecular examples are being discovered which defy these conventions (**Boller and Felix, 2009**, **Thomma et al., 2011**, **Cook et al., 2014**). Examples of specific danger signals and detailed discussion of their perception systems are provided in later sections describing the relevant concepts in the context of plant innate immunity (section **1.4**).

1.2 Microbial plant pathogens and plant diseases

The dawn of phytopathology In 1861, the population of Ireland was still feeling the impact of the calamity which would enter history books as the "Great Famine" of 1845 (**Klinkowski, 1970**) – a widespread outbreak of potato late blight, caused by *Phytophotora infestans* infection. This demonstration of the direct and drastic effect that plant disease can have on human culture contrasts the stark lack of knowledge about the origins of plant diseases at the time. It was only in 1861 that Anton de Bary, impressed by the recent events, demonstrated the causal link between microbial pathogens and the devastating potato disease (**Bary, 1861**). In stating that the oomycete caused the disease (he was describing it as a fungus at the time), he was rebuffing earlier reports which only mention fungal infection as a consequence of a prior existing disease (**Corda, 1847**).

Environmental factors to pathogenicity Plants are in the distinctly precarious position of not being able to evade harmful organisms through motility. In addition to this rather direct effect, the sessile lifestyle has other disadvantages: being forced to endure adverse abiotic environmental conditions (which might be favourable to pathogenesis) without possibility of avoidance puts additional strain on a plant's immune system. The causal interplay between environment, host and pathogen in the development of disease is therefore an early and central paradigm of plant pathology; host susceptibility to disease is a combination of multiple factors, with the actual presence of the pathogen being only one among others ('disease triangle', **Scholthof, 2007**).

Plant microbiomes Plants influence their own biotic environment by providing microbial habitats. The phyllosphere and rhizosphere are ecological niches rich in microbial

life (**Vorholt, 2012**, **Philippot et al., 2013**). Although environmentally quite different, there is significant overlap in microbial taxonomic distribution between these compartments (**Bai et al., 2015**). There is vivid two-way interaction between plants and their associated microbial communities, with distinct impacts on plant health (**Hardoim et al., 2008**, **Berendsen et al., 2012**, **De Coninck et al., 2014**); plants actively influence the composition of their microbiomes, e.g. through the secretion of metabolic compounds into the rhizosphere (**Badri et al., 2013**, **Bulgarelli et al., 2013**). The extent to which diverse factors such as soil type and plant identity influence the composition of root microbiomes is an emerging topic in plant science (**Lundberg et al., 2012**, **Bulgarelli et al., 2012**).

Friend or foe? As MAMPs are a significant danger signal to plants (section **1.1.2**), the question arises if and how the plant immune system can discriminate between beneficial and harmful microbes. In at least some cases, there is clear mechanistic similarity between the establishment of microbial symbiosis and pathogenicity (exemplified e.g. by legume-rhizobia interactions, **Oldroyd et al., 2011**). An increasing amount of data indicates that active suppression of the plant immune system by the putative symbiont is an important factor in establishment of symbiotic relationships (**Liang et al., 2013**), indicating that functional co-evolution of plants and symbiotic microorganisms has closer mechanistic ties to pathogenicity and the suppression plant innate immunity than thought previously (**Zamioudis and Pieterse, 2012**, **Gourion et al., 2015**, **Cook et al., 2014**).

Entry sites, attack vectors and pathogen synergy Animal action can facilitate microbial entry into plant tissues. Below the ground, nematodes infect roots and through this process transmit microbial plant pathogens (**Powell, 2012**), while above the ground, artificial lesions such as those occurring during herbivory or punctation by aphids have similar effects (**Stout et al., 2006**); these synergies between different classes of pathogens put additional strain on plant immunity. However, natural openings often suffice. A prime entry point for foliar bacterial pathogens is through stomata (**Underwood et al., 2007**). Far from being just passive gates of entry, active regulation and manipulation of stomatal opening is turning out to be a intense battleground between plants and their bacterial pathogens (**Montillet and Hirt, 2013**); while plants actively close their stomata in response to MAMP perception, pathogens have evolved virulence mechanisms to open them (**Melotto et al., 2006**), notably the use of specialized phytotoxins which manipulate plant hormonal signalling such as coronatine in *Pseudomonas syringae* and fusicoccin in various fungi (**Melotto et al., 2008**). Similarly, filamentous pathogens such as *Sclerotinia sclerotiorum* use stomata to aid hyphae extension through plant tissue and use oxalate as

a virulence factor to induce stomatal opening (**Stotz and Guimaraes, 2004**). Secondary effects of pathogen invasion may also include general impairment of stomatal function due to plant defence responses and/or epidermal cell death (**Mur et al., 2013**), as has been observed for the interaction between powdery mildew and barley ('stomatal lock open', **Prats et al., 2006**).

Crop disease Securing future food supply in a situation of a globally growing human population hinges heavily on effective agriculture which aims to minimize crop yield loss. Although total reduction in crop yield is affected roughly similarly by weeds, animal pests, and fungal/bacterial pathogens (9.4 %, 10.1 %, and 9.9 %, respectively), crop protection measures taken in current agricultural practise are less effective for the control of fungal/bacterial pathogens than for the other two groups (33.8 % efficacy compared to 42.4 % efficacy for animal pests and 70.6 % efficacy for weeds, respectively; **Oerke and Dehne, 2004**). Efforts to battle microbial plant pathogens in agricultural settings are aggravated by the fact that they evolve quickly and that current agriculture heavily relies on a narrow range of globally distributed crop plants of limited genetic diversity, often planted in monoculture settings (**Strange and Scott, 2005**). In recent years, there has been a remarkable increase in strongly virulent fungal disease outbreaks both in plant and animal hosts, which has already led to an unprecedented amount of host extinction events; this emerging fungal threat is probably aided by ubiquitous pathogen dispersal through an ever more globalized economy (**Fisher et al., 2012**). As mentioned before, environmental factors also strongly influence the outbreak of plant disease; global climate change might therefore pose further risks to food security as pathogens stand ready to exploit environmental changes to their benefit (**Gregory et al., 2009**).

1.3 *Pseudomonas syringae*, a model bacterial plant pathogen

1.3.1 Emergence as a model

The 'prime' bacterial plant pathogen In 2012, the journal *Molecular Plant Pathology* carried out a survey among its contributors, collecting 458 votes to determine which bacterial plant pathogen they consider 'the most scientifically and economically important', with first place going to *Pseudomonas syringae* pathovars (**Mansfield et al., 2012**). While certainly subjective, this anecdote serves to illustrate the perceived importance of *P. syringae* as a plant pathogen.

Historical discoveries for origins of pathogenicity The mentioned voting among scientists was surely influenced by the fact that many ground-breaking discoveries about

interactions of the plant immune system with bacterial pathogens were using *P. syringae* as a model organism. The *hrp* gene cluster, which forms the type III (three) secretion system (TTSS or T3SS), an important mechanism for effector delivery (and thus, pathogenicity) in many bacterial pathogens that infect eukaryotic organisms (**Galán and Wolf-Watz, 2006**), was elucidated in *P. syringae* pathovars (**Lindgren et al., 1986**, **He et al., 1993**). Subsequently, *P. syringae* has become a prime model organism for large-scale studies of secreted effector repertoires (**Guttman et al., 2002**, **Jamir et al., 2004**, **Chang et al., 2005**) and their workings in plant innate immunity (**Tao et al., 2003**), e.g. through repression of MAMP signalling (**Li et al., 2005**, **Block et al., 2008**, **Guo et al., 2009**) or being recognized as danger signals themselves (ETI, see section **1.4.2** for a more detailed look).

***P. syringae* genomes** In 2003, the genome of *P. syringae* pv. *tomato* (Pto) DC3000 was sequenced (**Buell et al., 2003**), which greatly aided the exploration of its effector secretome (**Collmer et al., 2002**). Since then, many other pathovars have been added to this list (**Joardar et al., 2005**, **Feil et al., 2005**), culminating in the possibility of a large-scale effort in comparative genomics among the different pathovars to elucidate their respective effector and phytotoxin secretomes and thus, the origins of differences in pathogenicity (**Baltrus et al., 2011**).

1.3.2 *P. syringae* lifestyle and pathogenicity

Ice, rain, and clouds An early and curious discovery about *P. syringae* was the fact that liquid cultures of some strains of the bacterium freeze at surprisingly high temperatures (-1.8 to -3.8 °C), due to induction of ice nucleation by intact *P. syringae* cells (**Maki et al., 1974**). Unlikely as it seems, the identification of the outer membrane proteins responsible for this phenomenon (**Wolber et al., 1986**) has revolutionized the artificial snow-making industry and prompted discussions about the ecology of ski pistes (**Rixen et al., 2003**). Since then, *P. syringae* strains have been found to be abundant in distinctly non-agricultural habitats such as pristine snow and even tropospheric clouds (**Amato et al., 2007**), which is remarkable for a species known primarily as a plant pathogen (**Morris et al., 2007**). The life-cycle of *P. syringae* has since been shown to be inherently linked to earth's water cycle, and environmentally isolated strains show striking similarity to agriculturally relevant pathogen strains (**Morris et al., 2008**). These circumstances contribute to the bacterium's success as a plant pathogen by providing ecological reservoirs independent of plant life and aiding in its wide distribution (**Monteil et al., 2013**). Water status of an infected plant also seems critical for virulence of *P. syringae* (**Beattie,**

2011), which can use mechanisms such as the production of extracellular polysaccharides to enhance its chances of survival in the apoplast (**Fett and Dunn, 1989**,**Yu et al., 1999**). Interestingly, resistant plants can correspondingly use ETI mechanisms to induce physiological adaptations which actively dehydrate the leaf environment around the invading pathogen (**Freeman and Beattie, 2009**). The importance of the aquatic aspect of *P. syringae* lifestyle and ecology is increasingly gaining recognition (**Morris et al., 2013**).

A successful plant pathogen The taxon *P. syringae* as a whole has an excessively large host distribution compared to other bacterial plant pathogens; *P. syringae* pv. *syringae* alone was determined to infect more than 80 host species (**Hirano and Upper, 2000**). *P. syringae* occurs mainly as a epiphytic leaf pathogen (**Hirano and Upper, 1990**). Not all strains are pathogenic; some have adapted to the life as a leaf commensal by losing key virulence factors such as the T3SS and effector genes (**Mohr et al., 2008**), and strains lacking the canonical T3SS have recently been described to be abundant in non-agricultural habitats (**Diallo et al., 2012**). In pathogenic *P. syringae*, host specificity and range varies widely among the different pathovars, and there is ongoing discussion on the rearragement of different pathovars into various *P. syringae* subspecies (**O'Brien et al., 2011**); also, pathovar designation often does not follow phylogeny (**Sawada et al., 1999**). As a crop pathogen, *P. syringae* has a global economic impact by infecting important crop species; a non-exhaustive listing in typical horticultural literature includes apples, beets, beans, cabbage, cucumbers, flowers, oats, olives, peas, tobacco, tomato, and rice (**Horst, 2013**). The topicality of *P. syringae* as a virulent plant pathogen is highlighted by recent developments like the epidemic spreading of a new and aggressive disease phenotype, 'bleeding canker disease' of European horse chestnut trees, which is caused by *P. syringae* pv. *aesculi* (**Green et al., 2010**). Historically, one of the best-studied disease phenotypes caused by *P. syringae* is the 'bacterial speck disease' of tomato, caused by Pto DC3000 (**Louws et al., 2001**). Interestingly, this strain can also infect the model plant *Arabidopsis thaliana* (**Preston, 2000**). By deleting a single effector gene from Pto DC3000, virulence on the tobacco model *Nicotiana benthamiana* can be established (**Wei et al., 2007**). The molecular determinants which lead to either resistance or susceptibility to this disease phenotype in various tomato cultivars and in *Arabidopsis* have since become a prime pathway for mechanistic studies on ETI and plant hormone signalling in context of immunity (**Xin and He, 2013**).

Determinants of *P. syringae* host specificity Host specificity of *P. syringae* can be interpreted on two different levels (**Heath, 2000**). On the first level, some plant species are susceptible to a certain pathovar of *P. syringae* while others are not ('nonhost resistance').

On the second level, different cultivars of a single, generally susceptible host species are (atypically) resistant to some strains of a generally pathogenic pathovar ('host resistance'). The presence or absence of specific effectors (or combinations thereof) has been identified as a key determinant for the divergent host specificity of the various *P. syringae* pathovars, and resistance (R) protein polymorphisms (which are, in *Arabidopsis*, highly abundant; **Clark et al., 2007**) in different plant species or cultivars can explain differential recognition of certain effectors, and thus, presence or absence of effective resistance (**Lindeberg et al., 2009**). Dissecting *P. syringae* genomes by multi-locus sequencing typing (MLST) suggests four main clades, with designated pathovars scattered among them (**Sarkar and Guttman, 2003**), and effector screens have been performed for members of each clade (**Cunnac et al., 2009**). Examples from closely related strains of bean pathovars *gylcinea* and *phaseolicola* show that differential effector arsenals can explain some, but not all, of the quantitative differences in cross-pathogenicity on the corresponding hosts (**Baltrus et al., 2012**). Evolutionary host shifts in pathovar lineages appear to correspond to conserved type three effector (T3E) repertoires; for example, the Pla106 strain (pathovar *lachrymans*, the causative agent of cucumber angular leaf spot disease) shares much of its T3E suite with two tomato pathogens, hinting to similar virulence strategies and making shifts between cucumber and tomato host systems more likely (**Baltrus et al., 2011**). Artificially engineering effectors originating from various pathovars into naturally non-pathogenic strains might lead to new insight into host specificity (**Mohr et al., 2008**). Evolutionary and functional aspects of effector repertoires are discussed in further detail in section **1.5.1**.

***P. syringae* phytotoxins** In addition to proteinacious virulence factors such as effectors, *P. syringae* pathovars are remarkable for exhibiting a variety of phytotoxins to increase their pathogenicity (**Hwang et al., 2005**). A particularly interesting example is coronatine (COR), a hybrid molecule consisting of the polyketide coronafacic acid (CFA) and the isoleucine-derived coronamic acid (CMA). The CFA moiety is structurally similar to jasmonates (JAs; **Weiler et al., 1994**), and coronatine was shown to target COR-insensitive 1 (COI1; **Feys et al., 1994**, **Xie et al., 1998**), a key component in JA perception (**Sheard et al., 2010**), in order to activate JA-dependent signalling and consequently suppress salicylic acid (SA)-dependent defence responses due to interference with physiological JA/SA hormonal crosstalk (**Brooks et al., 2005**). In addition to its detrimental effects on phytohormone-regulated immunity signalling, coronatine directly interferes with the regulation of stomatal closure, re-opening stomata that have been closed in response to MAMP signalling to facilitate bacterial entry into plant tissues (**Melotto et al., 2006**). Two other notable phytotoxins specific to *P. syringae*, syringomycin and syringopeptin

(**Gross and DeVay, 1977**, **Ballio et al., 1991**)), are lipopeptides that function similarly to detergents to form pores in plant plasma membranes (**Lavermicocca et al., 1992**), which facilitates the release of nutrients to the bacterium (**Hutchison and Gross, 1997**). Taking a wide view on the origins of pathogenicity leads to the conclusion that *P. syringae*'s unique arsenal of phytotoxins contributes significantly to its success as a broad-spectrum plant pathogen (**Bender et al., 1999**, **Geng et al., 2014**).

1.4 Danger perception systems in plants

An evolutionary view on danger perception As stated previously (section **1.1.2**), danger perception is a universal feature of innate immunity and a prerequisite for adequate and efficient defence responses. Observing the cladistic distributions of danger signals in pathogens and their corresponding perception systems in plants highlights some evolutionary aspects of plant innate immunity (**Boller and Felix, 2009**). While the microbial molecular features responsible for pattern recognition (MAMPs) are usually broadly conserved among pathogens and phylogenetically ancient, both widely and narrowly conserved MAMP perception systems exist in plants (figure **1.1**), indicating that there is continuing evolution of new perception systems for these ancient danger signals. Conversely, both microbial effectors and their corresponding perception systems in plants are usually more narrowly conserved. Genetic innovations which lead to new virulence factors in pathogens and new perception systems in plants have therefore been described as an 'evolutionary arms race', with important implications to pathogen host range and adaptation (**Schulze-Lefert and Panstruga, 2011**). It should be noted again that the historical distinction between MAMPs and effectors, while conceptually convenient, is subject to dissolution as more and more examples are being discovered which cannot be constrained by this rigid dichotomy (**Thomma et al., 2011**, also note the 'mixed shape' in figure **1.1**, **B**). The following sections keep the classical MAMP/effector nomenclature for mechanistic descriptions, while section **1.4.3** describes some of the current challenges to this classification in more detail.

1.4.1 Pattern-triggered immunity

1.4.1.1 Structural variety of PRR families

Animal PRRs Although the general concept of pattern recognition is similar in plant and animal innate immunity, some of the molecular features and functionality of PRRs are different in both systems. The most intensely studied mammalian PRRs belong to the

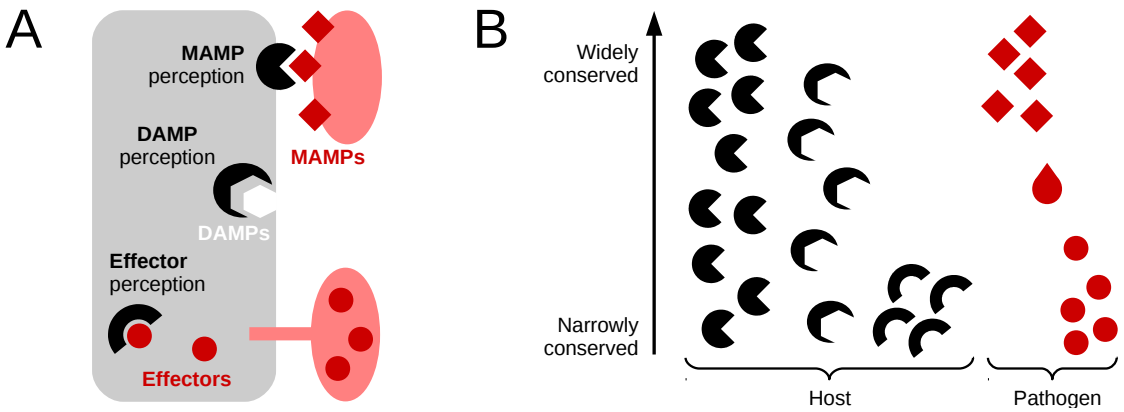

Fig. 1.1 Evolutionary aspects of danger perception in plants. **A**, Highly simplified, schematic representation of danger perception systems in a plant cell. Greyscale, host-derived components; red, pathogen-derived components (labels are given in figure). **B**, Relative conservation of danger signals and their corresponding perception systems. Meaning of symbols is the same as for (**A**), and number of symbols was chosen arbitrarily for illustrative purposes. The fluency of the MAMP/effector designation is symbolized by the mixed-form 'drop' shape. Pane (**B**) is modified from **Boller and Felix, 2009**.

class of toll-like receptors (TLRs) which act as prototypical MAMP receptors (**Song and Lee, 2012**) through extracellular leucine-rich repeat (LRR) domains, containing 19-25 LRRs each, and transduce danger signals into the cytoplasm using intracellular Toll-IL-1 Receptor (TIR) domains (**Akira and Takeda, 2004**). Interestingly, TLRs are in a way atypical LRR-domain receptors as most TLRs (with the exception of TLR5, which is involved in flagellin recognition; **Hayashi et al., 2001**) do not recognize proteinaceous ligands and do not bind their ligands on the concave surface of the ectodomain (as common in LRR-domain receptors; **Kang and Lee, 2011**, **Yoon et al., 2012**). Not all TLRs are functionally located at the cell surface; several perceive signals such as foreign nucleic acids within endosomes (**Werling et al., 2009**). A common theme in TLR-mediated pattern recognition is dimerization of TLRs (**Brodsky and Medzhitov, 2007**), which leads to signalling activation intracellularly and can increase the possible variety of perceived MAMP signals extracellularly through heterodimerization of ectodomains (**O'Neill and Bowie, 2007**). Recent advances demonstrate a role of other types of PRRs in animal immunity as well, among them C-type lectin receptors (CLRs), nucleotide-binding oligomerization domain (NOD)-like receptors (NLRs) and RIG-I-like receptors (RLRs), and there is active crosstalk between TLRs, these other PRRs, and various other 'adaptor'-type proteins to orchestrate immune responses (**Kawai and Akira, 2011**).

LRR-RLKs Similarly to the situation in the animal system, the classical plant PRRs were described as leucine-rich-repeat containing receptor-like kinases (LRR-RLKs), making comparisons to animal TLRs immediately tempting. However, the similarity

is mostly limited to using the same basic biochemical modules (LRRs) for pattern recognition, as both the structures of the LRR domains and the specific MAMP epitopes being recognized are significantly different in animal and plant systems, hinting to a case of convergent evolution (**Nürnberger et al., 2004**). The adaptability of the extracellular LRR domain to a wide variety of signals makes LRR-RLKs prototypical plasma membrane receptors, and consequently, they fulfil signalling functions not only in the context of innate immunity but also in developmental processes such as brassinosteroid (BR) signalling, stomatal patterning, and floral abscission (**Diévart and Clark, 2004**, **Wu et al., 2015**).

LRR-RLKs Plant LRR-RLKs also differ significantly from animal TLRs in their intracellular domains. While animal TLRs use TIR domains (both as cytoplasmic domain of the PRR and in various cytoplasmic adaptor proteins) to initiate signalling, LRR-RLK cytoplasmic domains are classical kinases, and form a monophyletic group together with several cytoplasmic animal receptor kinases, dubbed the RLK/Pelle family, or interleukin-1 receptor associated kinase (IRAK)/Pelle in animals (**Shiu and Bleecker, 2001**). While animals have few members of this family, it expanded vastly during plant evolution, with the *Arabidopsis* genome encoding for 600 proteins that contain this type of kinase domain (**Shiu and Bleecker, 2003**). Interestingly, while only a small subset of RLK/Pelle family members have been characterized as 'non-RD' kinases (due to the lack of a conserved arginine immediately preceding the catalytic aspartate in the activation loop; **Johnson et al., 1996**, **Nolen et al., 2004**), this subgroup is relatively common in characterized immunity-related PRRs. PRR subfamilies do not form a distinct clade, hinting that the biological PRR function has likely evolved multiple times in different groups of kinases, and thus, similar functional requirements might explain similar subsequent changes to the otherwise highly conserved RD motif (**Dardick et al., 2012**).

LRR-RLPs Like LRR-RLKs, LRR-receptor like proteins (LRR-RLPs) contain extracellular LRR domains for ligand binding and a single-pass transmembrane domain (**Fritz-Laylin et al., 2005**), and fulfil roles as receptors in immunity and developmental pathways (**Wang et al., 2008**). However, instead of a kinase domain, the intracellular portion of RLPs consists of a much shorter cytoplasmic domain. This poses obvious implications for signalling, and indeed RLP function has been fundamentally linked to that of adaptor proteins which can provide kinase function (**Gust and Felix, 2014**), a prime example of which is SOBIR1 (SUPPRESSOR OF BIR1-1/ EVERSHED), which has been shown to interact with a variety of LRR-RLPs in tomato (**Liebrand et al., 2013**). Importantly, this interaction is ligand-independent, indicating a fundamental necessity

of the interaction that makes the label 'bimolecular receptor kinase' for an RLP/adaptor complex appropriate (**Gust and Felix, 2014**).

LysM domain PRRs While the LRR domains of LRR-RLKs and LRR-RLPs show remarkable adaptability to peptide ligands, there are various types of PRRs with other types of ectodomains, enabling perception of danger signals corresponding to other molecular classes. Particularly well-studied are lysine motif (LysM) domain PRRs. The LysM domain is evolutionary ancient and occurs in bacteriophages, prokaryotes, and eukaryotes; the conserved function of LysM is binding of microbial structural carbohydrates such as bacterial peptidoglycan and fungal chitin via their *N*-acetylglucoasmine (GlcNAc) moieties (**Buist et al., 2008**, **Mesnage et al., 2014**). In plants, PRRs containing extracellular LysM domains fulfil functions in immunity- and symbiosis-related signalling (**Gust et al., 2012**). Apart from their extracellular domain, LysM domain PRRs exhibit a variety of protein topologies. LysM-RLKs are similar to LRR-RLKs and have cytoplasmic kinase domains for signalling, while LsyM-RLPs do not. In contrast to LRR-RLPs, LysM-RLPs also lack transmembrane and cytoplasmic domains altogether, being instead connected to the plant plasma membrane via glycophosphatidylinositol (GPI) anchors (**Gust et al., 2012**). Dimerization of LysM domain PRRs has emerged as a central theme to signalling in response to microbial cell envelope MAMPs (**Liu et al., 2012**, **Hayafune et al., 2014**), and differences in perception among plant species are currently being elucidated (**Shinya et al., 2012**).

1.4.1.2 A model system for MAMP perception: flg22 and FLS2

The 'classical' MAMP Arguably, the prime example of a MAMP (by virtue of being the most clearly characterized and intensively studied) is flg22, an active epitope of bacterial flagellin (**Felix et al., 1999**). As a structural protein and main component of the bacterial flagellum (**Samatey et al., 2001**), flagellin (FliC) is relatively conserved among mobile microbes and an important factor contributing to their ecological fitness, and —in case of pathogens— virulence, both in plant and in animal systems (**Tans-Kersten et al., 2001**, **Taguchi et al., 2010**, **Josenhans and Suerbaum, 2002**). Therefore, bacteria cannot easily avoid detection by losing flagellin altogether without incurring major fitness penalties, a theme that recurs in other MAMPs as well and makes them ideal templates for danger recognition. Interestingly, both *Agrobacterium* and commensalistic *Rhizobium* have evolved a variant of flagellin that retains functionality yet manages to avoid an immune response (**Felix et al., 1999**), and studies using *Xanthomonas campestris* pv. *campestris* (*Xcc*) show that single amino-acid polymorphisms of the epitope can

lead to quantitatively altered magnitudes of flg22 perception (**Sun et al., 2006**). Similar results have been obtained in the animal system, as it has been demonstrated that certain strains of human pathogenic bacteria exhibit mutations that render their flagellin versions undetectable, along with complementary mutations that restore motility function (**Andersen-Nissen et al., 2005**).

FLS2 Flagellin perception is widespread among plant phyla, and presence of in both angiosperms and gymnosperms indicates an evolutionary ancient perception system (**Albert et al., 2010b**). Genetic analysis led to the identification of Flagellin-sensing 2 (FLS2) as necessary for flg22 perception (**Gómez-Gómez and Boller, 2000**) and induction of plant defences in response to flg22 stimulation (**Zipfel et al., 2004**); subsequently, after previous indications that the FLS2 ectodomain is crucial for flg22 perception (**Gómez-Gómez et al., 2001**), a physical interaction between flg22 and FLS2 was demonstrated, establishing a direct ligand-receptor relationship (**Chinchilla et al., 2006**). Elucidation of the crystal structure of the flg22-FLS2 ectodomain complex gave further insights into the structural requirements of flg22 perception, and demonstrated the vital necessity of a co-receptor, Brassinosteroid-insensitive 1 (BRI1)-associated kinase 1 (BAK1), for flg22 binding (**Sun et al., 2013a**; the role of BAK1 as a co-receptor is described in detail in section **1.4.1.5**). FLS2 binds flg22 with high sensitivity, leading to experimental difficulties in the discovery of other MAMPs due to contamination issues (**Mueller et al., 2012**); as a consequence, there has been intense controversy on whether FLS2 may be involved in the recognition of several fundamentally unrelated peptide epitopes (**Lee et al., 2011**, **Danna et al., 2011**, **Segonzac et al., 2012**, **Lee et al., 2012**).

Other flagellin epitopes and receptors Although flagellin is conserved as a MAMP in plant and animal immunity, different flagellin epitopes have emerged as template for danger signaling in these two kingdoms of life (**Zipfel and Felix, 2005**). Animal TLR5 senses a region composed of 13 amino acids within the conserved D1 domain of the flagellin monomer, and certain mutations in this region abrogated both recognition by TLR5 and bacterial motility function; single point mutations have a greater effect on motility than on recognition, indicating bacteria's challenges to evade detection by mutating the epitope (**Smith et al., 2003**), although, as mentioned before, some pathogens have adapted successfully (**Andersen-Nissen et al., 2005**). In contrast, the flg22 motif responsible for plant recognition through FLS2 is located in an N-terminal fragment (**Felix et al., 1999**) which has been deemed dispensable for animal recognition through TLR5, and purified flg22 did not cause an immune response in human cell culture (**Donnelly and Steiner, 2002**). Interestingly, flagellin harbors at least one more immunogenic

epitope: flg28 was identified as being distinct from flg22 and is recognized by a yet-unidentified PRR other than FLS2 that seems to be limited to Solanaceae species (a putative 'FLS3'); furthermore, allelic variety in flagellin epitopes and their corresponding receptors seems to significantly shape flagellin responses (**Clarke et al., 2013**). The tomato (*Solanum lycopersicum*) orthologue of *At*FLS2, *Sl*FLS22, also recognizes flg22, but exhibits some important differences in the characteristics of binding, as it additionally recognized a shorter version of the epitope, flg15, which is unresponsive in *Arabidopsis* (**Robatzek et al., 2007**). Rice (*Oryza sativa*) also has a functional FLS2 orthologue, as expression of *Os*FLS2 in *Arabidopsis fls2* mutants restored flg22 recognition; however, in rice itself flg22 stimulation leads to much weaker responses (**Takai et al., 2008**). In summary, emerging evidence points to a large variety of nuances in both MAMP and receptor specificities for the model flg22/FLS2 pair that challenges the classical concept of strongly conserved and monolithic MAMP/receptor systems.

1.4.1.3 Variety of MAMP perception

Proteinaceous MAMPs Since the initial description of immunogenic short peptide motifs derived from specific pathogen proteins, the search for other proteinaceous MAMPs has been ongoing. Corresponding to the general evolutionary theory of MAMP recognition systems, large-scale genomic screens have been directed towards pathogen proteins under strong negative selection due to their critical function for the ecological fitness of the pathogen (**McCann et al., 2012**). However, many candidate MAMPs are still waiting for identification of their cognate perception systems, while on the other hand, many previously described PRRs detect unknown MAMPs ('orphan' MAMPs/receptors, **Boller and Felix, 2009**). Historically, the second proteinaceous MAMP to be characterized in greater detail as part of an unequivocal ligand-receptor pair was elf18 (**Kunze et al., 2004**), the N-terminally located active epitope of bacterial elongation factor Tu (EF-Tu), with its cognate plant PRR EF-Tu receptor (EFR), an LRR-RLK (**Zipfel et al., 2006**). EF-Tu is a highly conserved (**Lathe and Bork, 2001**), abundant (the most abundant protein in *E. coli*, **Pedersen et al., 1978**), and functionally essential bacterial protein, and thus perfectly fulfilling the classical definition of a MAMP template. EFR evolved in Brassicacae, making it a relatively narrowly distributed PRR perceiving a widely distributed MAMP; however, functional transfer of *Arabidopsis* EFR to tobacco and tomato show that downstream components seem to be conserved (**Lacombe et al., 2010**). Interestingly, recent studies showed that EF-Tu harbours another active epitope, EFa50, which can trigger defence-responses in rice, hinting to another yet-uncharacterised EF-Tu-perceiving PRR active in non-Brassicaceae (**Furukawa et al., 2014**). EFR shares

significant structural and functional similarity with FLS2, and switching of FLS2/EFR subdomains generally results in functional chimeric PRRs (**Albert et al., 2010a**). Beside LRR-RLKs, other receptor families have been implicated in the perception of proteinaceous MAMPs. The LRR-RLP RLP23 (**Albert et al., 2015**) detects a conserved 20 amino acid epitope present in Necrosis and ethylene-inducing peptide 1-like proteins (NLPs), which is exceedingly widely distributed; the NLP20 motif has been found in NLPs from bacteria, fungi, and oomycetes (**Böhm et al., 2014a**). This example provides another illustration of the duality inherent in many danger signals: cytotoxic NLPs are both important virulence factors for necrotrophic pathogens (**Qutob et al., 2006**, **Ottmann et al., 2009**) and direct MAMP signals. Interestingly, in some cases, the amino acid sequence of the recognized peptide epitope is not sufficient for detection, as plants have evolved PRRs to specifically detect modified epitopes; Required for activation of Xa21 (RaxX) is a peptide MAMP from *Xanthomonas* species whose perception in rice by the LRR-RLK XA21 depends on sulfation of a single tyrosine residue (**Pruitt et al., 2015**). In summary, peptide ligands originating from pathogen proteins form the basis of a broad variety of pattern recognition strategies in plant innate immunity.

Carbohydrate MAMPs Beside pathogen proteins, a second extensive class of molecules functioning as MAMPs is that of pathogen carbohydrates, which often fulfil important structural functions in microbial pathogens (**T. J. Silhavy, D. Kahne and Walker, 2010**, **Bowman and Free, 2006**). As noted before (section **1.4.1.1**), PRRs containing LysM domains are the prime example, recognizing bacterial peptidoglycan (**Willmann and Lajunen, 2011**, **Gust, 2015**) and fungal chitin (**Cao et al., 2014**, **Liu et al., 2012**, **Hayafune et al., 2014**). However, perception of carbohydrate patterns is not limited to LysM domain PRRs. Receptor-like kinases with other types of extracellular lectin domains (LecRLKs; **Vaid et al., 2012**) have been implicated in carbohydrate binding as well (**Singh and Zimmerli, 2013**, **De Schutter and Van Damme, 2015**); comparisons to the animal system (Dectin-1, a C-type lectin; **Gantner et al., 2003**) make them potential candidates for β-glucan perception, but the molecular identity of the corresponding receptor in plants remains elusive (**Fesel and Zuccaro, 2015**).

Other MAMPs Bacterial lipopolysaccharide (LPS), a critical immunogenic compound in the Gram-negative cell envelope (**Erbs and Newman, 2012**), is sensed by the B-type lectin LecRLK lipooligosaccharide-specific reduced elicitation (LORE) in Brassicaceae; the recognition is based on the lipid A moiety (**Ranf et al., 2015**). Other microbial cell envelope components also fulfil the definition of a MAMP; fungal ergosterol has

immunogenic properties in plants (**Tugizimana et al., 2012**), but its receptor remains elusive (**Klemptner et al., 2014**).

1.4.1.4 DAMPs ... and *AMPs

Endogenous peptides DAMPs pose a second major class of danger signals that are perceived via PRRs, and can be generally defined as host-derived molecules released during host-pathogen interaction (**Lotze et al., 2007**). Early research into this molecular class focused on plant-derived peptides. An 23 amino-acid peptide, Pep1, was described as a potent elicitor of plant immunity and is generated from a precursor (proPep1) that is induced by wounding, methyl jasmonate and ethylene signaling (**Huffaker et al., 2006**). Concurrently, the receptor for this peptide was identified as the LRR-RLK Pep1 receptor 1 (PEPR1) (**Yamaguchi et al., 2006**). Pep1 is a member of a family of related DAMP peptides, designated Pep1-Pep7. Interestingly, a second PRR, PEPR2, was found to perceive Pep family ligands, and the differential receptor-ligand specificities have been elucidated, with PEPR1 being the receptor for Pep1-6, and PEPR2 being a receptor for Pep1 and Pep2 (**Yamaguchi et al., 2010**). The function of endogenous peptide DAMPs seems to be that of an internal amplifier of defence responses, with functional integration into MAMP perception and hormone signalling (**Ma et al., 2012b**, **Tintor et al., 2013**), as well as a general mediator of herbivory defence widely conserved in range of plant clades (**Huffaker et al., 2013**). These recent studies highlight that there is a certain degree of fluency in classifying these endogenous peptides, as their release seems to be more specifically regulated and functionally varied than thought initially (**Bartels and Boller, 2015**), and may thus be functionally closer to cytokines than to true DAMPs.

Small-molecules for danger assessment Pathogen action can lead to the release of small molecule ligands that would not circulate within the plant normally, making them excellent DAMPs. Examples of this concept include the wall-associated kinase 1 (WAK1), which perceives liberated cell wall components (**Decreux and Messiaen, 2005**, **Brutus et al., 2010**), and Does not Respond to Nucleotides 1 (DORN1), a novel lectin-domain receptor for extracellular ATP (**Tanaka et al., 2010**) unrelated to previously identified animal ATP receptors (**Choi et al., 2014**).

Non-microbial pathogen signatures Pattern recognition is not limited to perception of microbial or endogenous damage-associated signatures, although these have been studied in most detail; it seems that for every interaction of a plant with another organism, there are corresponding foreign patterns being recognized, as in the case of insect herbivory (herbivory-associated molecular patterns - HAMPs, **Mithöfer and Boland, 2008**,

Acevedo et al., 2015), or plant-plant parasitism (parasite-associated molecular patterns - ParAMPs, **Kaiser et al., 2015**; Markus Albert, personal communication).

1.4.1.5 BAK1, a central co-receptor in plant immunity

Brassinosteroid signalling The receptor-like kinase BRI1-associated kinase 1 (BAK1) was first described for its role in brassinosteroid signalling as a modulator of Brassinosteroid-Insensitive 1 (BRI1) activity (**Li et al., 2002**, **Vert et al., 2005**). Brassinosteroid signalling by the BRI1/BAK1 complex has been shown to be mediated by sequential transphosphorylation events between the respective kinase domains (**Wang et al., 2008**). Subsequently, elucidation of the BRI1 ectodomain crystal structure provided further hints towards BAK1 as a true co-receptor (**Hothorn et al., 2011**), a notion which was reinforced by the finding that the BAK1 ectodomain is essential for complex formation (**Jaillais et al., 2011**) and unequivocally confirmed through a dedicated BRI1/brassinolide/BAK1 co-crystal (**Sun et al., 2013b**).

Immunity signalling BAK1 was first established as a component in plant immunity due to its involvement in the containment of the cell-death response in a BR-independent manner (**Kemmerling et al., 2007**). Concurrently, other studies highlighted its direct role in PRR signalling by its ligand-dependent association with FLS2 and the fact that *bak1* plants are impaired in FLS2-mediated immunity, both in *Arabidopsis* and tobacco (**Chinchilla et al., 2007**, **Heese et al., 2007**). Initial experiments included in these studies hinted that the involvement of BAK1 might not be limited to FLS2, and indeed other PRRs such as EFR and PEPR1 were found to interact rapidly with BAK1 and undergo transphosphorylation in a ligand-dependent manner; (**Schulze et al., 2010**), demonstrating a general role of BAK1 in MAMP recognition (**Chinchilla et al., 2009**). An FLS2/BAK1 ectodomain co-crystal structure demonstrated BAK1 has an active role in binding the ligand, with the flg22 peptide acting as 'molecular glue' between the BAK1/FLS2 LRR domains (**Sun et al., 2013a**). Cogent to its central role in immunity signalling, BAK1 was found to be targeted by microbial effectors (**Shan et al., 2008**); this aspect is discussed in more detail in section **1.5.2**. Focusing on BAK1 phosphorylation has provided several mechanistic insights; the structural impact of activation-loop phosphorylation was demonstrated (**Yan et al., 2012**) and the differential roles of BAK1 could be separated in a phosphorylation-dependent manner by a novel mutant allele, *bak1-5*, which is impaired in its PRR-mediated signalling functions but not in in BR signalling or cell death control (**Schwessinger et al., 2011**).

SERKs BAK1 is also known as SERK3, and part of a protein family named Somatic Embryogenesis Receptor-like Kinases (SERKs) for their initially discovered role in embryogenesis (**Schmidt et al., 1997**). The SERK family consists of five members and is highly conserved among plant clades (**Schwessinger and Rathjen, 2015**). Although the general protein architecture (4.5-5 LRR extracellular domain, single-pass transmembrane domain, kinase domain) is conserved among SERKs, modular domain functions have diverged during evolution, explaining the wide variety of co-receptor functions that SERKs are involved in (**Li, 2010**, **Aan den Toorn et al., 2015**). There is partial functional redundancy among SERK proteins; for example, four out of the five members of the SERK family – SERK1, SERK2, SERK3/BAK1, and SERK4/BKK1 (BAK1-like kinase 1) – can function as co-receptors for BRI1 (**He et al., 2007**, **Albrecht et al., 2008**, **Gou et al., 2012**). Recently, mathematical modelling of the BRI1/SERK interactome helped to put these data into context by describing SERK action as differential modulators of physiological output (**Esse et al., 2013**). Similarly, both SERK3/BAK1 and SERK4/BKK1 interact with FLS2, EFR, and PEPR1/2 to provide co-receptor redundancy to PRR-mediated immunity signalling (**Roux et al., 2011**), and the same proteins confer similar redundancy to the cell-death control pathway (**He et al., 2007**). Although SERK5, an extremely close homologue of SERK4, is not functional in the model *Arabidopsis* ecotype Col-0 due to a natural mutation in the RD motif, recent studies using SERK5 in the Landsberg *erecta* (L*er*) ecotype demonstrate its interaction with BRI1 and subsequently, its function in BR signalling (**Wu et al., 2015**).

1.4.1.6 PRR regulation networks

Positive regulation As the variety of identified PRRs is constantly increasing, subsequent mechanistic studies continue to unveil their extended interactoms and regulatory networks (**Böhm et al., 2014b**). The botrytis-induced kinase 1 (BIK1) was initially described as a plasma-membrane located regulatory kinase that modulates early responses to pathogen infection (**Veronese and Nakagami, 2006**). Subsequently, BIK1 was shown to associate with both FLS2 and BAK1 and to be involved in transphosphorylation events following flg22 perception (**Lu et al., 2010a**); similar data has since been obtained for other PRRs (**Zhang et al., 2010**, **Liu et al., 2013a**). Mechanistically, BIK1 works as a positive regulator of PRR immunity and directly phosphorylates the Nicotinamide adenine dinucleotide phosphate (NADPH) oxidase Respiratory burst oxidase D (RBOHD) to induce reactive oxygen species (ROS) production (**Kadota et al., 2014**). BIK1 is part of a family of Receptor-like cytoplasmatic kinases (RLCKs) called PBS1-like (PBL)

kinases; its homologues PBL1, PBL2, and PBS1 seem to be functionally additive (**Zhang et al., 2010**, **Liu et al., 2013b**).

Negative regulation The use of FLS2 as a model PRR has revealed mechanisms for signal attenuation after ligand perception, showing that FLS2 gets internalized after flg22 binding (**Robatzek et al., 2006**) and is a direct substrate for ubiquitination by two plant u-box E3 ubiquitin (PUB) ligases, PUB12 and PUB13, which are activated by BAK1 transphosphorylation in the active receptor complex (**Lu et al., 2011**); another negative regulator is the kinase-associated protein phosphatase (KAPP) which interacts with FLS2's kinase domain (**Gómez-Gómez et al., 2001**). As a common co-receptor for multiple PRRs, BAK1 is also a prime target for regulation. The BAK1-interacting receptor-like kinase 1 (BIR1) was identified as a BAK1-dependent negative regulator in immunity and cell death processes (**Gao et al., 2009**). Subsequently, a co-immunoprecipitation approach using BAK1 yielded two novel interactors belonging to the same protein family, named BIR2 and BIR3, which differentially regulate PRR complexes in a ligand-dependent manner through BAK1 (**Halter et al., 2014b**, **Halter et al., 2014a**, **Imkampe, 2015**). BAK1 is also the direct target of a phosphatase, protein Ser/Thr phosphatase type 2A (PP2A), which constitutively associates with BAK1 (but not with FLS2 or BIK1) and modulates its phosphorylation status (**Segonzac et al., 2014**); negative regulation of the common co-receptor BAK1 is thus emerging as a prime element of PRR regulation and underlines the importance of BAK1 as a central hub in MAMP signalling.

1.4.2 Effector-triggered immunity

1.4.2.1 Early models putting ETI into context of plant immunity

Going vertical The 'gene-for-gene' hypothesis of plant defence (**Flor, 1971**) was one of the earliest attempts to describe the genetic background of plant immunity, proposing complementary genetic systems in host and pathogen leading to 'vertical' resistance; i.e., resistance mediated by a single gene in host and pathogen each, following Mendelian inheritance patterns, and thus leading to qualitative resistance effects (**Plank, 1968**). This was contrasted with 'horizontal' resistance, which was defined as being polygenic and non-race specific (**Parlevliet and Zadoks, 1977**). According to this model, host genes leading to immunity were termed resistance genes (R-genes) and the corresponding pathogen genes being recognized by these R-genes were termed avirulence genes (Avr genes). However, this model left an open question regarding pathogen evolution: How does the pathogen benefit from the presence of an Avr gene? This problem was resolved by the discovery that an Avr gene product of *Xanthomonas campestris*, AvrBs2, is necessary

for full virulence (**Kearney and Staskawicz, 1990**); subsequently, an increasing number of Avr genes was associated with virulence functions, and it became clear that virulence and avirulence are indeed often two sides of the same coin, based on a single pathogen protein (**Swords et al., 1996**, **Vivian and Gibbon, 1997**). Since then, the term 'effector' has been used increasingly instead of 'Avr protein' in order to reconcile virulence and avirulence characteristics of the same protein under a more neutral term (**Kjemtrup et al., 2000**).

Going 'Zig-Zag' In an effort to unify the apparently two-sided nature of plant immunity (MAMP/PAMP triggered immunity based on pattern recognition (PTI), broadly corresponding to the historic 'horizontal' resistance, and effector triggered immunity (ETI) based on effector recognition, broadly corresponding to the historic 'vertical' resistance), the 'zig-zag' model was introduced (**Jones and Dangl, 2006**). This model explains the interplay of PTI and ETI as a staggered process in which PTI can be overcome by effector virulence action to result in effector-triggered susceptibility (ETS), which can then in turn be overcome through the evolution of novel R-genes against specific effectors, resulting in ETI; the process would be repeated over and over in an 'evolutionary arms race' (**Jones and Dangl, 2006**, **Boller and He, 2009**). Importantly, this model defined quantitative differences in magnitude of the defence response as a hallmark division between PTI and ETI, with only ETI reaching the highest possible magnitude, exemplified by the hypersensitive response (HR), a form of localized cell death (**Heath, 2000**).

1.4.2.2 ETI systems

Structural aspects Recognition events in early ETI studies using tobacco and tomato pathosystems (**Whitham et al., 1994**, **Salmeron et al., 1996**) were soon found to be linked to a distinct class of immune receptors, termed NB-LRR or NLR proteins for their domain structure, which includes a nucleotide binding (NB) domain and a number of LRRs (**Bent, 1996**, **Meyers et al., 1999**). NLR-like immune receptors exist in animals and plants, but despite structural and functional similarity, they are likely a product of convergent evolution (**Bonardi and Dangl, 2012**). In contrast to animal NLRs, plant NLRs are numerous and highly polymorphic (**Bakker et al., 2006**, **Guo et al., 2011**); the expanded role in plant immunity is likely caused by the increased need for specificity due to lack of an adaptive immune system (**Yue et al., 2012**). Two major classes of NLRs in plants have been defined by the presence of either a TIR domain or a coiled coil (CC) domain at the N terminus adjacent to the NB domain, resulting in a tripartite domain architecture of TIR/CC-NB-LRR domains; these classes are termed TNL and CNL,

respectively (**Takken and Goverse, 2012**, **Ma et al., 2012a**). The crystal structures of TIR and CC domains have been elucidated and, in an intriguing similarity to animal TLR function, revealed self-association and homodimerization as a crucial element in receptor activation; importantly, CNLs self-associate before, TNLs after effector-triggered activation (**Bernoux et al., 2011**, **Maekawa et al., 2011**). Mechanistically, structural data indicates that NLRs bind ADP in an autoinhibited, resting state and conformationally change into the signalling-competent R proteins upon effector perception, exchange ADP to ATP, and undergo further conformational changes initiating downstream signalling which ultimately leads to defence gene activation in the nucleus and a HR response (**Takken and Goverse, 2012**, **Qi and Innes, 2013**). Interestingly, downstream pathways triggered by NLRs seem to be strongly conserved in the plant kingdom despite the high degree of NLR polymorphism (**Maekawa et al., 2012**), and NLR proteins have been implicated in immunity-related functions other than the recognition of pathogen effectors (**Bonardi et al., 2011**).

Guards and decoys As many microbial effector proteins are secreted into the plant cell, intracellular perception was defined as an important difference of ETI compared to the generally membrane-bound PTI mechanisms (**Jones and Dangl, 2006**). Early work with R-gene systems has therefore focused on dissecting intracellular recognition mechanisms (**Hammond-Kosack and Jones, 1996**). The most immediately intuitive way of effector recognition is direct, physical interaction with a plant receptor, and indeed this mode of recognition has been observed in diverse host/pathogen systems such as rice blast (**Jia et al., 2000**), bacterial wilt caused by *Ralstonia solanacearum* (**Deslandes et al., 2003**), and flax rust (**Dodds et al., 2006**, **Catanzariti et al., 2010**). However, a large number of effector / R-protein recognition pairs does not operate via direct physical interaction. To explain this phenomenon, the 'guard' hypothesis was introduced, which states that the effector's action on a virulence target is perceived indirectly by the R-protein, with the R-protein thus acting as 'guard' to a effector-targeted 'guardee' (**Van Der Biezen and Jones, 1998**, **Dangl and Jones, 2001**). As an example, the *Arabidopsis* protein Resistance to *Pseudomonas maculicola* 1 (RPM1)-interacting protein 4 (RIN4), a multi-faceted component in immunity regulation (**Day et al., 2006**, **Liu et al., 2009**), is targeted by multiple *P. syringae* effectors via distinct molecular mechanisms (**Kim et al., 2005b**, **Kim et al., 2005a**, **Wilton et al., 2010**, **Sun et al., 2014**). However, effector modification of RIN4 is sensed by two classical R-proteins, RPM1 and Resistance to *Pseudomonas syringae* protein 2 (RPS2), to induce ETI responses (**Axtell and Staskawicz, 2003**, **Mackey et al., 2003**). In addition to dispensing with the need for direct interaction, the guard model resolved another perceived internal contradiction of the original gene-for-

gene hypothesis; namely, the fact that a single R-protein can detect multiple effectors (**Dangl and Jones, 2001**). Intriguingly, recent studies demonstrated that a single NLR R-protein can indeed directly interact with and recognize multiple effectors (**Cesari et al., 2013**). However, the guard model posed some other conceptual problems: to avoid virulence action by effectors, a guarded target should be under evolutionary pressure to evade effector binding, which would in turn limit the use of guard proteins in effector recognition. Thus, the 'decoy model' was proposed as a refinement to the guard model; in essence, it postulates that a guarded protein might have evolved to serve no other intrinsic molecular function than to be bound by the effector and thus, serve as a danger signal to the corresponding guarding R-protein (**Hoorn and Kamoun, 2008**, **Khan et al., 2016**). This model implies that decoy proteins are effectively a molecular mimicry of the effector's original virulence target, and may have evolved either independently or from these virulence targets by gene duplication. Interestingly, recent studies show that molecular decoys could exist not only as dedicated proteins but rather as single functional domains within R-proteins, such as NLRs carrying C-terminal WRKY domains which mimic effector-targeted WRKY transcription factors (**Le Roux et al., 2015**, **Sarris et al., 2015**). However, as the designation of a plant protein as decoy is by necessity based on negative data (apparent lack of a molecular function of the guarded protein), there is ongoing discussion whether the decoy designation is appropriately reflecting biological reality (**Block and Alfano, 2011**).

1.4.2.3 The Pto-Prf system

Indirect recognition The classical *P. syringae* / tomato gene-for-gene resistance pair *avrPto* / *Pto* (**Ronald et al., 1992**, **Martin et al., 1993**, **Rommens et al., 1995**), the critical determinant for the resistance to bacterial speck disease in tomato (**Scofield et al., 1996**), was described to be functionally dependent on another tomato gene, Pseudomonas resistance / fenthion sensitivity (*Prf*), a member of the NB-LRR family with an atypically long N-terminal extension (**Salmeron et al., 1996**). Initiation of ETI signalling in response to AvrPto perception was linked to direct physical interaction between AvrPto and Pto, a serine-threonine kinase (**Tang et al., 1996**). Mutational analysis of Pto showed that its kinase activity is not necessary for the interaction with AvrPto, but for the Prf-dependent induction of HR; additionally, constitutively kinase-active Pto led to Prf-dependent HR in the absence of AvrPto (**Rathjen et al., 1999**, **Sessa et al., 2000**). These data strengthened the notion that Pto works in conjunction with Prf to form a signalling-competent complex (**Mucyn et al., 2006**, **Balmuth and Rathjen, 2007**), a model generally consistent with the previously described guard hypothesis (**Xiao et al.,**

2003). In addition to AvrPto, a second sequence-unrelated *P. syringae* effector, AvrPtoB, is also recognized through interaction with Pto (**Kim et al., 2002**, **Dong et al., 2009**).

Phosphorylation switches The structure of the AvrPto-Pto complex was resolved in 2007, demonstrating the mechanistic basis for effector perception through manipulation of discreet phosphorylation residues on Pto (**Xing et al., 2007**). AvrPto acts as a kinase inhibitor, and its interaction with the Pto P+1 loop occurs structurally similar to that of the cAMP-dependent protein kinase A (PKA) with its pseudosubstrate peptide inhibitor PKI (**Bossemeyer et al., 1993**), directly manipulating the activation segment of Pto; beside the structural data, quantitative AvrPto-dependent inhibition of *in vitro* Pto autophosphorylation could be demonstrated (**Xing et al., 2007**), in clear contrast to previous postulations that activation of Pto kinase activity by AvrPto recognition initiated ETI signalling (**Tang et al., 1999**). However, mutational analysis showed that AvrPto-mediated inhibition of kinase activity is not the signal trigger *per se*, as discreet point-mutated variants of Pto, which were insensitive to kinase-inhibition by AvrPto, constitutively triggered HR (**Xing et al., 2007**). This suggested a negative-regulatory function of Pto acting on Prf, which could be abolished through disrupting the Pto P+1 loop by AvrPto binding; a notion which gained further traction in subsequent studies linking negative regulation of Prf by Pto-like kinases to Fen, a kinase structurally similar to Pto and required for fenthion sensitivity in tomato (**Mucyn et al., 2009**).

Dimerization model of Pto-Prf function These findings could be substantiated in later studies, which proposed refinements to the molecular function of the Pto/Prf complex. The complex was found to be oligomeric, with at least two Prf molecules associating with Pto; both Prf dimerization and Pto association were found to be mediated by the previously mentioned atypical, extended N-terminal domain of Prf (**Gutierrez et al., 2010**, **Saur et al., 2015**). Detailed investigation of differentially phosphorylated forms of Pto led to a dimerization-based model for complex activation (**Ntoukakis et al., 2013**). In its resting state, autophosphorylated Pto associated with Prf acts as a sensor domain in a multimeric receptor complex, with different Pto moieties brought into close proximity to each other through Prf dimerization. Upon AvrPto binding to Pto, disruption of the Pto P+1 loop through the kinase-inhibiting function of AvrPto activates the second Pto molecule (either directly or through Prf), which acts as 'helper' moiety and subsequently transphosphorylates the first Pto moiety to result in a fully activated complex, thus acting as a 'helper kinase'. Taken together, this model postulates the evolution of an intricate 'bait-switch' type of receptor complex acting as a 'molecular trap' of effector molecules (**Ntoukakis et al., 2014**).

1.4.3 Limits of classification

Obvious limitations Recent reviews pointed out limitations to the classical 'zig-zag' model postulating two distinct branches of plant innate immunity (PTI and ETI), as it fails to describe cases such as necrotrophic pathogens benefiting from host cell death, neglects DAMPs, postulates a staggered sequence of events that occur on vastly different spatial and time scales, and marks a quantitative nature to defense response outputs that cannot in reality be constrained to monolithic perception categories (**Pritchard and Birch, 2014**).

Danger signal continuum Additionally, as briefly mentioned previously, the classification of a danger signal as either 'MAMP' and 'effector' is problematic by itself (**Boller and Felix, 2009**, **Thomma et al., 2011**): Whenever a pathogen molecule harboring a MAMP motif contributes to the virulence of the pathogen, it might be labeled an effector, as in the case of cytolytic NLPs (**Böhm et al., 2014a**). Detection of molecules classically labeled as effectors is not limited to the intracellular space, as in the case of bacterial harpins, which are targeted and perceived extracellularly; additionally they are widely conserved in different bacterial clades (as in the the classical definition of a MAMP) and lead to immune responses similar to classical ETI responses (**Tampakaki and Panopoulos, 2000**, **Chang and Nick, 2012**, **Choi et al., 2013**).

Signalling networks It is hard to separate downstream responses as belonging solely to PTI or ETI; for example, significant overlap exists between the responses induced by flg22 or an apoplastic oomycete effector, Avr9 (**Navarro et al., 2004**); it has been proposed that the observed differences in PTI and ETI responses arise from differential input into the same downstream network (**Tsuda and Katagiri, 2010**, **Gassmann and Bhattacharjee, 2012**), and quantitative differences might result from the ETI branch removing negative regulation of the PTI branch (**Cui et al., 2015**). Additionally, upstream PTI and ETI components are partially confounded, as proteins generally linked to either branch of immunity exist as physically associated complexes at the plasma membrane, suggesting mechanistic integration (**Qi et al., 2011**).

Removing barriers Recently, in an effort to reduce category barriers in plant innate immunity signalling, an inclusive 'invasion model' has been proposed which aims to strictly classify molecules according to their physiological role in the originator organism, and summarize any perception in another organism as 'invasion pattern perception' agnostic of the exact result of this perception, which might include different types of defence response or symbiosis (**Cook et al., 2014**). In summary, while straightforward descriptive models of the interplay between host and microbes are conceptually helpful,

the underlying mechanisms governing such interactions are apparently too complex to be accurately described by such models; and as the expanding body of research moves away from a few intensely-studied model systems, the growing number of 'exceptions to the rule' only heightens the awareness of these conceptual limitations and illustrates the need for more integrative models.

1.5 Microbial effectors: molecular agents of virulence

1.5.1 Effector evolution, networks, and interplay

Evolution shaping the 'effectome' A pathogen's effector repertoire is a critical determinant of its virulence and thus, its success of host adaptation, as reflected through host range and specificity (also see section **1.3.2**). Effector genes have been found flanked by mobile elements (**Kim et al., 1998**); horizontal gene transfer is an important mechanism for the evolution of effector repertoires (**Nogueira et al., 2009**), and pathogen strains contain both recently acquired and evolutionary ancient effectors (**Rohmer et al., 2004**). The fact that many pathogen effectors lack homology to other bacterial proteins posed questions towards their origin, and indeed the similarity of several effectors to bacteriophage proteins has led to the hypothesis that phages serve as important vectors for the introduction of novel effectors into bacterial genomes (**Stavrinides et al., 2008**). Beside horizontal transfer of novel effectors, pathoadaptation (clonal descent with modifications in classical Darwinian form) is a major drive to effector diversification, and can mediate the 'arms race' to avoid detection while conserving the virulence function (**Ma et al., 2006**, **McCann and Guttman, 2008**). Conservation of a large part of effectors in different *P. syringae* pathovars suggests the maintenance of a core set of effectors to maintain general virulence (**Sarkar et al., 2006**). With the increasing availability of sequenced genomes, this concept has been extended to other pathogens such as *Xanthomonas campestris* (**Guy et al., 2013**) and *Ralstonia solanacearum* (**Ailloud et al., 2015**).

Virulence targets As the discovery of novel effector proteins has continued at a steady pace, a variety of different virulence strategies has become apparent (**Abramovitch and Martin, 2004**, **Block et al., 2008**, **Deslandes and Rivas, 2012**), occuring at all stages of infection (**Asai and Shirasu, 2015**). Even limiting analysis to intracellular effectors and the *P. syringae* model pathogen, the array of virulence functions is dazzling: various effectors interfere with host protein turnover (**Nomura et al., 2006**), subcellular localization (**Jelenska et al., 2014**), transcription processes (**Nicaise et al., 2013**), hor-

mone homoeostasis (**Hann et al., 2014**), and phosphorylation-dependent downstream signalling (**Zhang et al., 2007**). Beside host proteins, some effectors target nucleic acids; transcription-activator-like effectors (TALEs) mimic transcription factors and bind to host promoter regions (**Boch et al., 2009**) to modulate gene expression to the pathogen's benefit (**Kay et al., 2007**, **Römer et al., 2007**). A large-scale genomic analysis has provided insight into the effector-effector target interactome, indicating that a wide variety of effectors from multiple pathogen clades evolved to bind relatively few, highly connected host targets (**Mukhtar et al., 2011**); an example would be the previously mentioned RIN4 (**Sun et al., 2014**). From the pathogen's viewpoint, this is highly advantageous as targeting these 'hubs' maximizes the amount of disruption to the host's immune system and results in difficulty for the plant to evolutionarily eliminate targeted proteins due to their functional involvement in multiple pathways. Conversely, these findings conceptually support the guard hypothesis, as effector-targeted hubs are also good candidates for guarding by R-proteins.

1.5.2 BAK1 as an effector target

One stone, many birds Due to its central role as a co-receptor in PRR signalling (section **1.4.1.5**), BAK1 would be a prime 'hub' type target for pathogen effectors. Indeed, prompted by the curious discovery that *Arabiopsis* plants constitutively expressing the *P. syringae* effector AvrPto phenotypically mimic weak *bri1* mutants, suggesting an effect on a component involved in BR signalling, an interaction between AvrPto and BAK1 (but not BRI1) could be observed *in vivo* in immunoprecipitation assays (**Shan et al., 2008**). Additionally, the same interaction could be observed for AvrPtoB. This provided an elegant explanation for previous observations that AvrPto and AvrPtoB interfere with multiple PRR pathways (**He et al., 2006**), although AvrPto was hypothesized to additionally target BAK1-independent PRRs (**Lu et al., 2010a**).

More stones In additon to AvrPto and AvrPtoB, another *P. syringae* effector, Hrp outer protein F2 (HopF2), an ADP ribosyltransferase previously shown to inhibit mitogen-activated protein kinase (MAPK) cascades (**Wang et al., 2010**), was found to target BAK1 (**Zhou et al., 2013**). Taken together, these studies demonstrate a striking redundancy in *P. syringae*'s effector arsenal indicative of a truly high-value target. Targeting BAK1 is not limited to the *P. syringae* model pathogen – a recent study shows that Xoo2875, an effector of the rice pathogen *Xanthomonas oryzae* with various conserved homologs in *Xanthomonas* species, targets *Os*BAK1 (**Yamaguchi et al., 2013**).

Targeting kinases – a common theme? Elucidation of the co-crystal structure of AvrPtoB bound to BAK1 demonstrated similarities of the molecular determinants for both AvrPtoB's virulence, mediated through BAK1, and recognition, mediated through Pto (**Cheng et al., 2011**). Importantly, this together with the previously mentioned studies pointed to a common theme – the structural similarity of intracellular kinase domains of RLKs might prompt the same effector to bind multiple targets, as demonstrated by previous studies showing AvrPtoB-mediated degradation of FLS2 (**Göhre et al., 2008**) and AvrPto binding to both FLS2 and EFR (**Xiang et al., 2008**). Recently, the effector HopAO1, a tyrosine phosphatase (**Underwood et al., 2007**), was demonstrated to directly reduce EFR tyrosine phosphorylation, an important regulatory switch in PRR signalling; subsequent experiments also demonstrated interaction with FLS2, but notably, not with BAK1 or CERK1 (**Macho et al., 2014**). The precise molecular mechanisms which determine binding specificity of kinase-targeting effectors thus remain to be elucidated.

1.6 Aims of this thesis

Previous studies resulted in conflicting datasets regarding the virulence target of the *Pseudomonas syringae* effector AvrPto in the model organism *Arabidopsis thaliana*, either demonstrating interaction with FLS2 (**Xiang et al., 2008**, **Xiang et al., 2011**), but not BAK1 (**Xiang et al., 2011**), or demonstrating interaction with BAK1, and qualitatively weaker interaction with FLS2 (**Shan et al., 2008**, **Zhou et al., 2013**). A common aspect of these studies was the reliance on experimental *in vivo* approaches for determining protein-protein interactions, thereby precluding quantitative analysis, which is a hallmark of *in vitro* techniques (**Lalonde et al., 2008**). The initial working hypothesis of this thesis was that the conflicting datasets of the previous studies could at least partially be explained if AvrPto binds to all previously reported plant RLK virulence targets (due to its mechanistic background as a kinase inhibitor), but with differential affinity obscured by the qualitative nature of the experiments. To address this issue, the aim of this thesis was the use of *in vitro* approaches to describe the molecular interactions between AvrPto and its putative virulence targets quantitatively, thereby permitting conclusions regarding the effector's evolutionary background and its primary mode of action in the establishment of virulence.

CHAPTER 2

MATERIALS

2.1 Consumables

The following tables list suppliers of chemicals (table **2.1**), commercial biologicals (table **2.2**), and miscellaneous consumables (table **2.3**) which have been used in this work.

Table 2.1 Chemicals

Type	**Supplier (location)**
Basic Chemicals	Sigma Aldrich (Taufkirchen), Carl Roth (Karlsruhe), Fisher Chemical (Schwerte), Merck (Darmstadt), VWR (Darmstadt), Serva (Heidelberg), Avantor (Griesheim), BD Biosciences (Heidelberg), Nanotemper (München),
Antibiotics	Carl Roth (Karlsruhe)
Pharmaceuticals	Roche (Grenzach-Wyhlen)

Table 2.2 Commercial biologicals

Type	**Supplier (location)**
Oligonucleotides	Eurofins MWG Operon (Ebersberg)
Peptides	GenScript (Piscataway)
Enzymes	Thermo Fisher (Braunschweig), Duchefa (Haarlem), Yakult (Tokyo)
Antibodies	Sigma Aldrich (Taufkirchen), Thermo Fisher (Braunschweig), Chromotek (München)

Table 2.3 Miscellaneous consumables

Type	Supplier (location)
Consumables for Nucleic Acid and Protein Methods	Thermo Fisher (Braunschweig), Carl Roth (Karlsruhe), Sartorius (Göttingen), GE Healthcare (München), Nanotemper (München)
Laboratory Plastics	MultiMed (Kirchheim/Teck), Eppendorf (Hamburg)

2.2 Microbiological media

All media (table **2.4**) were prepared with the listed components dissolved in ultra-pure water (Milli-Q® system, Merck Millipore). Unless stated otherwise, all given percentages are weight per volume (w/v). Solid media were prepared by adding agar-agar to liquid media at a concentration of 15 $g\,L^{-1}$. All media were autoclaved (121 °C, 20 min) before use. For resistance-based selection of microbes, antibiotics (table **2.5**) were added at the indicated concentrations after autoclaving.

Table 2.4 Microbiological media

Type	Formulation	
	Component	**Concentration** ($g\,L^{-1}$)
Lysogeny Broth (**LB**)	Tryptone	10
	Yeast Extract	5
	NaCl	10
Terrific Broth, High Density (**TB-HD**), pH 7.5	Tryptone	10
	Yeast Extract	24
	Glycerol	3.16
	KH_2PO_4*	0.23
	K_2HPO_4*	1.25
Super Optimal Broth (**SOB**)	Tryptone	20
	Yeast Extract	5
	NaCl	0.5
	KCl	0.19
Super Optimal Broth with catabolite repression (**SOC**)	*same as SOB, but including:*	
	D-Glucose*	3.6

Components marked with an asterisk (*) were sterilized seperately and added after autoclaving

Table 2.5 Antibiotics

Type	Concentration ($\mu g\,mL^{-1}$)
Carbenicillin	100
Chloramphenicol	34
Tetracyclin	15
Kanamycin	20

2.3 Plasmid constructs

Table **2.6** lists the plasmid constructs used in this work.

Table 2.6 Plasmids and synthetic constructs

Name	Usage	Reference
pet22-BAK1K	bac. expression, *At*BAK1 kinase domain	N. Wagener
pet22-S286A	bac. expression, *At*BAK1 S286A mutant	this work
pet22-K317E	bac. expression, *At*BAK1 K317E mutant	this work
pet22-Y403F	bac. expression, *At*BAK1 Y403F mutant	this work
pet22-T324G	bac. expression, *At*BAK1 T324G mutant	this work
pet22-T324D	bac. expression, *At*BAK1 T324D mutant	this work
pet22-BRI1K	bac. expression, *At*BRI1 kinase domain	N. Wagener
pet22-FLS2K	bac. expression, *At*FLS2 kinase domain	N. Wagener
pJC40-BAK1K	bac. expression, *At*BAK1 kinase domain	this work
pJC40-mOAvrPto	bac. expression, *Ps*AvrPto-mOrange	this work
pJC40-Pto	bac. expression, *Sl*Pto	this work
pUri	bac. expression, *At*Uricase	R. Willmann
pGWB17-BAK1	Protoplast expression, *At*BAK1	this work
pFRK1-Luc	Protoplast expression, *At*FRK1	**(Zheng et al., 2014)**
pAvrPto	Protoplast expression, *Ps*AvrPto	**(Zheng et al., 2014)**

2.4 Bacteria

Table **2.7** lists the bacterial strains used in this work. All listed strains belong to the bacterial species *Escherichia coli*.

Table 2.7 Bacterial strains

Name (Supplier)	Genotype	Usage
XL1-BLUE (Stratagene)	endA1 gyrA96(nalR) thi-1 recA1 relA1 lac glnV44 F'[::Tn10 proAB+ lacIq Δ(lacZ)M15] hsdR17(rK- mK+)	Molecular Cloning, Plasmid Propagation
ROSETTA(DE3)PLYSS (Novagen)	F- ompT hsdSB(RB- mB-) gal dcm λ(DE3 [lacI lacUV5-T7 gene 1 ind1 sam7 nin5]) pLysSRARE (CamR)	Bacterial Expression
BL21(AI) (Thermo Fisher)	F- ompT galdcm lon hsdSB(rB- mB-) araB::T7RNAP-tetA	Bacterial Expression

2.5 Plants

Table **2.8** lists the genotypes of *Arabidopsis thaliana* used in this work. All mutant genotypes are in the Columbia (Col-0) background. Plants were used for the isolation of protoplasts as described in section **3.2.2**.

Table 2.8 Plant genotypes

Name	Stock Name	Reference
Col-0	N/A	N/A
bak1-4	SALK_116202	**Kemmerling et al., 2007**
bak1-5 × *bkk1-1*	N/A	**Schwessinger et al., 2011**

CHAPTER 3

METHODS

3.1 Microbiological methods

3.1.1 General handling of bacteria

3.1.1.1 Transformation of *E. coli*

Chemically competent *E. coli* of strains listed in Table 2.7 were created using a high-efficiency protocol **(Inoue et al., 1990)**.

To transform chemically competent bacteria, frozen aliquots (-80 °C) were thawed on ice for 10 min. Plasmid DNA ($c = 100 - 500\ \mathrm{ng\,\mu L^{-1}}$) was added to thawed cells followed by an incubation period of 15 min on ice. After resuspension by careful swirling, cells were subjected to a heat shock of 42 °C for 45 sec., then briefly cooled on ice. 250 µL of sterile room-temperature SOC medium (see table **2.4**) without antibiotic was added to the cells. The cells were then incubated at 37 °C for 1 h to allow expression of plasmid-borne resistance markers. After this growth period, cells were collected by centrifugation (5000 $\times g$, 5 min) and resuspended in 50 µL of SOC medium. The cells were then plated on LB-Agar plates containing the appropriate selection marker (see tables **2.4** and **2.5**) and incubated overnight at 37 °C.

3.1.1.2 Propagation and storage of *E. coli*

To propagate *E. coli*, freshly transformed single colonies were picked from a LB-Agar plate and used to inoculate 20 mL of LB medium containing the appropriate antibiotic for selection. The liquid culture was incubated in a shaker (37 °C, 200 rpm) until an OD_{600} of 0.6 to obtain a vital culture in the mid-log growth phase. This liquid culture was then used as a starter culture for further use in DNA or protein preparations (see sections **3.1.1.3** and **3.1.2.1**).

For long-term storage of *E. coli*, an aliquot of 300 µL of a mid-log phase culture was

mixed with sterile glycerol to a final glycerol concentration of 40 % and flash-frozen in liquid N_2. The frozen stock was then kept at −80 °C until further use.

3.1.1.3 Cultivation of *E. coli* for DNA extraction

To cultivate *E. coli* for DNA extraction, a mid-log phase starter culture was used to inoculate either 5 mL (small-scale) or 500 mL (large-scale) of LB medium containing the appropriate selection marker. The cultures were incubated for 16 h in a shaker (37 °C, 200 rpm). After incubation, cultures were spun down in a centrifuge (Sorvall RC-6+) and either used directly or stored at −25 °C until further use. Subsequently, DNA extraction was performed as described in sections **3.3.1.1** (small-scale) and **3.3.1.2** (large-scale).

3.1.2 Heterologous protein expression in bacteria

3.1.2.1 Cultivation of *E. coli* for protein extraction

For heterologous expression of proteins, synthetic constructs containing complementary DNA (cDNA) coding for proteins of interest were cloned into plasmids suitable for bacterial expression (see table **2.6** for an overview of all constructs). Plasmids were transformed into *E. coli* strains ROSETTA or BL21AI (see table **2.7**).

A single colony was picked from the transformation plate and used to inoculate a starter culture of 20 mL of LB medium containing the appropriate selection marker. The starter culture was then cultivated in a shaker (overnight; 22 °C, 240 rpm) until an OD_{600} of 0.6. At this point, the culture was used to inoculate 500 mL of pre-warmed selective medium (LB for expression in ROSETTA, TB-HD medium for expression in BL21AI; see table **2.4**) and transferred to a larger cultivation vessel (Erlenmeyer flask, total capacity 2 L). Bacteria were incubated further until an OD_{600} of 0.6. At this point, the expression culture was scaled up to its final volume by distributing the starter culture into 5 flasks with a final volume of 400 mL of pre-warmed selective growth medium each. Cultivation was then continued until an OD_{600} of 0.6 to allow induction of protein expression at optimal cell vitality.

3.1.2.2 Induction of protein expression

To induce protein expression, inducer was added to mid-log growth phase cultures (OD_{600} of 0.6).

For expression in ROSETTA, Isopropyl β-D-1-thiogalactopyranoside (IPTG) was added to a final concentration of 1 mM. After addition of IPTG, cells were transferred to 28 °C and

incubation was continued at 250 rpm. After 4 h, cells were harvested by centrifugation (8000 rpm, 15 min), shock-frozen in liquid N_2 and stored at -80 °C until further use.

For expression in BL21AI, L-Arabinose was added to a final concentration of 0.05 %. After addition of L-Arabinose, cells were transferred to 18 °C and incubation was continued at 250 rpm. After 16 h, cells were harvested and stored as described above.

3.1.2.3 Optimization of expression parameters

In order to optimize expression of proteins of interest, parameters such as inducer concentration, expression temperature, expression time, and presence of detergent during protein extraction were analysed.

Inducer concentration To test optimal inducer concentrations, three identical small-scale cultures (20 mL in Erlenmeyer flasks of 100 mL total volume) in mid-log growth phase were induced in parallel with hundred-fold titrations of inducer. For IPTG, concentrations of 10 µM, 100 µM, and 1 mM were tested. For L-Arabinose, concentrations of 0.005 %, 0.05 %, and 0.5 % were tested. Expression was performed (as described in section **3.1.2**), total soluble protein was extracted (as described in section **3.1.2.4**) and the amount of the protein of interest in raw extracts was visualized via Sodium dodecyl sulfate polyacrylamide gel electrophoresis (SDS-PAGE) followed by Coomassie brilliant blue (CBB) staining (as described in section **3.4.4**).

Expression time and temperature To test optimal expression time and temperature, time-course experiments were performed. Two identical small-scale cultures were prepared as described above. Just before induction, a sample of 1 mL was collected, spun down in a microcentrifuge (10000 $\times g$, 1 min), and flash-frozen in liquid N_2. After induction, the flasks were incubated further at 28 °C and 18 °C, respectively. For the culture grown at 28 °C, samples were collected as described above at time points 0.5 h, 1 h, 2 h, 3 h, 5 h, and 16 h. For the culture grown at 18 °C, samples were collected at time points 3 h, 5 h, and 16 h. At each time point, the OD_{600} of the culture was measured to normalize for cell number. After collection of all samples, total protein was extracted as described in section **3.1.2.4**. The amount of extraction buffer used for each protein extraction was kept proportional to the amount of cells as measured by OD_{600}. Total amount of protein was visualized by SDS-PAGE followed by CBB staining as referenced above.

Protein solubility To test the solubility of the protein of interest dependent on expression conditions, expression parameters were analysed as described above and soluble

total protein extraction (as described in section **3.1.2.4**) was performed. After soluble protein extraction, the cell pellet was resuspended again in extraction buffer supplemented with 1 % (w/v) Sodium lauroyl sarcosinate (sarkoysl). Protein extraction, SDS-PAGE and CBB staining was then performed as referenced above.

3.1.2.4 Extracting total soluble protein from *E. coli*

To extract total soluble protein from *E. coli*, frozen cell aliquots were thawed on ice. Then, pre-chilled extraction buffer (50 mM Tris pH 7.6, 150 mM NaCl) was added to cell aliquots. The amount of extraction buffer used depended on the amount of liquid culture at the end of expression time as listed in table **3.1**. Cells were resuspended and kept on a water-ice slurry for the remainder of the procedure. The resuspended cells were then sonicated in burst mode (Bandelin Sonoplus, probe MS-72; sonication 1 s, pause 3 s) using the culture-dependent parameters listed in table **3.1**.

Table 3.1 Conditions for extracting total protein from *E. coli*

$\mathbf{V}_{culture}$ (mL)	$\mathbf{V}_{buffer}$ (µL)	**Amplitude** (%)	Σ **Energy** (kJ)
1	100	20	0.05
500	20	65	1.5
$\geq$ 2000	50*	65	3

*sonicated as two consecutive aliquots of 25 mL

After sonication, cell suspensions were spun down in a pre-cooled centrifuge (12000 $\times g$, 15 min, 4 °C). The supernatant was separated from the pelleted cell debris and kept on ice until further use.

3.2 Plant methods

3.2.1 Growth conditions for *A. thaliana*

General cultivation A number of seeds were sown in pots on commercial soil supplemented with an Imidacloprid-containing insecticide (Confidor WG70, Bayer). To synchronize germination times, the seeds were stratified by storing them in a cold room (4 °C) for 24 h. The vernalized seeds were then transferred to a climate-controlled growth chamber (Saia-Burgess, Murten) with the following conditions: photoperiod of 8 h, light intensity of 110 mE $m^{-2} s^{-1}$, relative humidity of 60 %. Approximately 14 days after germination, seedlings were transplanted to single pots (⌀ 6 cm) for further cultivation.

Seed production Conditions were analogous to those listed above but with a photoperiod of 16 h to induce flowering. Upon inflorescence formation, flowering stems were sealed into paper bags to collect seeds. Plants were allowed to dry, and seeds were harvested ∼4 weeks after flower formation.

3.2.2 Protoplast methods

3.2.2.1 Isolation of *A. thaliana* leaf mesophyll protoplasts

For isolation of *Arabidopsis thaliana* leaf mesophyll protoplasts, a protocol slightly modified from **Yoo et al., 2007** was used. Plants were grown under short-day conditions for 5 weeks as described in section **3.2.1**. Plants were then transferred to a temperature-controlled room (20 °C) for further processing. All further steps in the protoplast isolation and transfection protocols were performed at 20 °C, unless specified otherwise.

Leaf harvesting Plants were pre-selected according to size (rosette diameter ∼5 cm for Col-0 plants, ∼3.5 cm for *bak1* mutant plants) and generally healthy phenotype. As a second selection step, up to three of the most well-formed (regularly shaped, sufficient size) leaves from each plant were cut near the base using a razor blade. Subsequently, the leaves were cut into thin (∼0.5 mm) strips, excluding ∼2 mm from the leaf tip and base each and taking care not to crush any tissue at the cutting site. The leaf strips were then transferred to a Petri dish containing 10 mL of enzyme solution (see table **3.2**) and carefully submerged using a forceps. About 50 leaves per plant genotype were cut in total, resulting in ∼150 leaf strips per 10 mL of enzyme solution.

Protoplast extraction In order to allow the enzyme solution to penetrate the leaf tissue, the Petri dish containing the leaves submerged in enzyme solution was placed in a darkened desiccator and vacuum-infiltrated for 30 min. The Petri dish was then removed from the desiccator and incubated further in the dark for 3 h. After incubation, the enzyme solution containing the leaf strips was gently transferred to a larger Petri dish and washed by addition of 10 mL of W5 washing buffer (see table **3.2**). Protoplasts were then released from the leaf strips by gentle swirling. The suspension was filtered through nylon mesh to separate the leaf strips from the protoplast suspension. Protoplasts were harvested by centrifugation in round-bottom tubes (4 °C, 100 $\times g$, 2 min). The supernatant was discarded and protoplasts were resuspended in 4 mL W5 washing buffer. An aliquot of 15 µL was taken for protoplast quantification, and protoplasts were incubated in the dark on ice for 2 h.

Protoplast quantification To quantify protoplast yield, 15 µL of protoplast solution (see above) were transferred to a hemocytometer (type Fuchs-Rosenthal, Paul Marienfeld). The number of vital protoplasts (i.e. intact, spheroid, even distribution of chloroplasts) was counted in 4 grid squares and the average used for volumetric calculations.

Table 3.2 Buffers and solutions for protoplast isolation

Type	**Component**	**Concentration**	
		mM	% (w/v)
Enzyme solution	Mannitol	400	
	KCl	20	
	$CaCl_2$	10	
	MES pH 5.7	20	
	Cellulase R10		1.5
	Macerozyme R10		0.4
	BSA		0.1
W5 washing buffer	NaCl	154	
	$CaCl_2$	125	
	KCl	5	
	MES pH 5.7	2	

3.2.2.2 Transfection of *A. thaliana* leaf mesophyll protoplasts

Transfection of protoplasts was performed using a protocol slightly modified from **Yoo et al., 2007**.

Preparation After the last incubation step in the protoplast preparation protocol (see section **3.2.2.1**), the supernatant was removed from the settled protoplasts. The protoplasts were gently resuspended in a volume of MMG solution (see table **3.3**) calculated to yield a protoplast concentration of 2×10^5 mL^{-1}.

Transfection Aliquots of 600 µL of protoplast suspension (resuspended in MMG as described above) per transfection were added to round-bottom tubes containing plasmid DNA for the desired transfections (prepared as described in section **3.3.1.2**). The protoplast suspension was mixed with the plasmid DNA by gentle swirling, then 660 µL of PEG solution (see table **3.3**) was added. The transfection was stopped after 5 min by addition of 2.64 mL of W5 washing buffer. Protoplasts were harvested by centrifugation (4 °C, 100 $\times g$, 2 min) and resuspended in 600 µL of W5 washing buffer. Protoplasts were then ready to be used for a pFRK1-Luciferase assay as described in section **3.8.1**.

Table 3.3 Solutions for protoplast transfection

Type	Component	Concentration	
		mM	% (w/v)
MMG solution	Mannitol	400	
	$MgCl_2$	15	
	MES pH 5.7	4	
PEG solution	Mannitol	200	
	$CaCl_2$	100	
	PEG 4000		40

3.3 Nucleic acid methods

3.3.1 Plasmid preparation from bacteria

3.3.1.1 Small-scale preparation of plasmids

Small-scale preparation of plasmids was carried out using the GeneJET® kit (Thermo Fisher) according to the manufacturer's instructions, using a culture size of 5 mL.

3.3.1.2 Large-scale preparation of plasmids

Large-scale preparation of plasmids was carried out using the NucleoBond® Xtra Midi kit (Macherey-Nagel) according to the manufacturer's instructions, using a culture size of 500 mL.

3.3.2 DNA quantification

The amount of DNA in liquid preparations was determined using the built-in nucleic acid quantification protocol of a NanoDrop 2000 spectrophotometer (Thermo Fisher).

3.3.3 DNA sequencing

For DNA sequencing, the LIGHTRUN™ service by GATC Biotech (Konstanz) was used according to the service provider's instructions. Sequencing data was analysed using the CLC Main Workbench suite (CLCbio / Qiagen).

3.3.4 Agarose gel electrophoresis and DNA visualization

Dissolved DNA samples were separated into their constituent molecular species by agarose gel electrophoresis.

Gel preparation Agarose was suspended in 1× TAE buffer (40 mM Tris pH 8.5, 1 mM EDTA), the agarose concentration being dependent on the required resolving range as summarized in table **3.4**.

Table 3.4 Agarose concentrations for resolving DNA species of differential size

$\%_{\text{Agarose}}$(w/v)	**Resolving Range** (kbp)		
0.5	1	–	30
0.7	0.8	–	12
1.0	0.5	–	10
1.2	0.4	–	7
1.5	0.2	–	3

Gel casting Suspended agarose was heated until boiling to facilitate dissolving, then allowed to cool to 50 °C. Ethidium bromide was then added to the agarose solution at a final concentration of 0.5 $\mu g\,mL^{-1}$ before casting the gels. After solidifying, agarose gels were transfered to a horizontal electrophoresis chamber (BioRad) containing 1× TAE buffer.

Sample loading To prepare DNA samples for gel electrophoresis, the samples were mixed with 5×DNA loading buffer (10 mM Tris pH 7.5, 60 mM EDTA, 60 % (v/v) glycerol, 0.25 % bromphenol blue) to a final 1× concentration. Subsequently, samples were loaded into the agarose gel and electrophoresis was performed at 100 V until the dye front reached the lower edge of the gel.

DNA visualization After electrophoresis, stained DNA bands were visualized by UV illumination in an E-BOX gel documentation system (Peqlab).

3.3.5 DNA extraction from agarose gels

For preparative DNA extraction from agarose gels, the GeneJET gel extraction kit (Thermo Fisher) was used according to the manufacturer's instructions.

3.3.6 Polymerase Chain Reaction (PCR) methods

3.3.6.1 Primer design for molecular cloning

To design primer pairs for the amplification of cDNA inserts for molecular cloning, regions of template suitable for hybridisation were chosen manually to yield annealing temperatures between 50 °C and 60 °C, with a maximum internal divergence of 4 °C per pair. Melting temperatures were calculated using the salt-adjusted algorithm of the online

tool OligoCalc (Northwestern University, Evanston), which uses the following equation **(Nakano et al., 1999)**:

$$T_m = (wA + xT) \cdot 2 + (yG + zC) \cdot 4 - 16.6 \cdot \log(0.050) + 16.6 \cdot \log([Na^+]) \qquad (3.1)$$

where w,x,y,z are the number of the bases A,T,G,C in the sequence, respectively.

Other molecular features such as stop codons, tags, spacers, linkers, and recognition sites for type-III restriction enzymes were added in-frame to the target template hybridizing region. Finally, the primers were tested *in silico* using the predefined PCR tools of the CLC Main Workbench Suite (CLCbio / Qiagen).

3.3.6.2 Generation of cDNA inserts for molecular cloning

For the generation of cDNA inserts for molecular cloning, PCR reactions were set up as summarized in the following table **3.5**.

Table 3.5 Standard PCR reaction mix, Σ 50 µL

Component	**Volume** (µL)
H_2O (MILLIQ)	36
10× Polymerase buffer	5
10× dNTP mix (2 mM each)	5
Primer (fw) (50 µM)	1
Primer (rv) (50 µM)	1
Template DNA (∼1 ng µL^{-1})	1
DNA Polymerase (5 U µL^{-1})	1

To achieve maximum fidelity, *Pyrococcus furiosus* (*Pfu*) DNA polymerase (Thermo Fisher) and its corresponding buffer stock was used for the generation of cDNA inserts. Amplification was carried out in a thermocycler (Peqlab Primus 96$^{\text{advanced}}$) using a protocol summarized in table **3.6**.

Table 3.6 Standard PCR amplification parameters

	Step №	**Temperature** (°C)	**Duration** (min)	**Cycle Purpose**
	1	95	5	Initial Melting
×25	2	95	0.5	Melting
×25	3	$(T_m - 4)$	0.5	Primer Annealing
×25	4	72	x	Elongation
	5	72	5	Final Elongation

where $x = Length_{(template\ sequence\ in\ kb)} \times 2$ min.

After amplification, PCR reactions were stored at −20 °C until further use.

3.3.6.3 Colony PCR for analytical purposes

To analyse successful ligation of an insert into a vector backbone, colony PCR was used. Ligated plasmids were transformed into chemically competent XL1BLUE as described in section **3.1.1.1**. Single colonies were picked from the resulting transformation plate and streaked on fresh selective agar plates. To provide plasmid template for the colony PCR, the pipette tips which have been used for streaking the colonies were briefly dipped into the reaction mixture. The remainder of the PCR mix and protocol are analogous to the ones given in tables **3.5** and **3.6**, respectively, with the following differences: *Thermus aquaticus* (Taq) DNA polymerase (recombinant, home-made) and its corresponding buffer (67 mM Tris pH 8.8, 16 mM $(NH_4)_2SO_4$, 2.5 mM $MgCl_2$, 0.01 % Tween-20) were used, and elongation cycle duration was $Length_{(template\ sequence\ in\ kb)} \times$ min.

To detect whether the insert has been cloned in the correct topology, the forward primer was chosen to be vector-specific and the reverse primer to be insert-specific. After amplification, PCR products were separated by agarose gel electrophoresis, followed by visualization via UV illumination as described in section **3.3.4**. Appearance of clear bands at the expected size indicated successful ligation. Single colonies from the agar plates which have been used as template were then used for inoculation of small-scale liquid cultures as described in **3.1.1.3** and the subsequent isolation of plasmids as described in **3.3.1.1**.

3.3.6.4 Site-Directed Mutagenesis (SDM) PCR

In order to generate point mutations in DNA to result in specific amino-acid exchanges in coding sequences, a protocol modified from the commercial Quikchange 2 XL kit (Agilent technologies) was used. This approach is a linear PCR technique based on full-circle amplification of plasmids carrying the desired mutation.

Primer design The online tool provided by Agilent for use in the Quikchange 2 XL kit was used to generate primer sequence pairs with T_m between 78 °C and 81 °C and a minimal amino-acid exchange mutation in the center of the primer.

SDM protocol The PCR mix used for SDM PCR was identical to the standard PCR mix which is listed in table **3.5**. *Pfu* DNA polymerase was used. Table **3.7** lists the amplification parameters for SDM PCR.

Table 3.7 SDM PCR amplification parameters

	Step Nº	**Temperature** (°C)	**Duration** (min)	**Cycle Purpose**
	1	95	1	Initial Melting
×18 {	2	95	0.833	Melting
	3	60	0.5	Primer Annealing
	4	68	x	Elongation
	5	68	5	Final Elongation

where $x = Length_{(plasmid\ sequence\ in\ kb)} \times 2$ min.

After amplification, the PCR mix was supplemented with 0.5 µL of DpnI restriction enzyme (10 U μL^{-1}) and incubated for 1 h at 37 °C to specifically cleave methylated DNA (template plasmid). After DpnI digestion, 10 µL of the reaction was transformed into 100 µL of chemically competent XL1BLUE cells as described in section **3.1.1.1**.

Analysis of SDM Mutagenesis was evaluated by sequencing 3 clones per reaction as described in section **3.3.3** with suitable primers upstream of the mutated site and aligning the DNA sequences with the wild-type template sequence.

3.3.7 Molecular cloning

Depending on the vector backbone used, cDNAs were cloned via either restriction-ligation (section **3.3.7.1**) or the commercial GATEWAY system (section **3.3.7.2**).

3.3.7.1 Restriction-ligation cloning

Insert preparation For restriction-ligation type cloning, inserts were generated by PCR as described in section **3.3.6** with primers containing the appropriate type-III restriction enzyme recognition sites. Recognition sites were chosen in a way that excluded them both from the insert coding sequence and from the vector backbone outside of the multiple cloning site. To generate 3' overhangs for cloning, PCR products were gel-purified as described in sections **3.3.4** and **3.3.5**, followed by restriction with the appropriate enzymes (double digest). A sample restriction digest mix is summarized in table **3.8**.

Table 3.8 Standard restriction reaction mix, Σ 100 µL

Component	**Volume** (µL)
H_2O (MILLIQ)	25
10× Restriction enzyme buffer	10
Restriction enzyme № 1 (10 U μL^{-1})	5
Restriction enzyme № 2 (10 U μL^{-1})	5
Gel-purified PCR product	50

Notes: Restriction enzyme buffer was chosen to provide the best possible performance for both restriction enzymes and to avoid star activity. Relative amounts of both restriction enzymes were varied according to their activity in the chosen buffer, e.g. double amount of a restriction enzyme was chosen if it was expected to exhibit a 50 % reduction of activity in the buffer used.

Following restriction digest, restriction enzymes were heat-inactivated according to the supplier's instructions and the restriction fragments were separated by agarose gel electrophoresis as described in section **3.3.4**. The target band corresponding to the digested insert fragment was then excised as referenced in section **3.3.5**.

Vector preparation Plasmid DNA was extracted from *E. coli* cultures as described in section **3.3.1.1**. The plasmids were then digested (with the same restriction enzymes used to prepare the insert) to linearize the plasmids via double strand breaks, excise the fragment of multiple-cloning-site between the restriction enzyme recognition sites, and create 3' overhangs suitable for ligation, analogous to the process described above. The plasmid DNA was then separated and gel-purified as referenced above.

Ligation To ligate the previously prepared insert and vector DNA, a ligation mix was prepared as summarized in table **3.9**. The ligation reaction was incubated for 12-16 h at 16 °C, followed by heat-inactivation of ligase (80 °C, 15 min).

Table 3.9 Standard ligation reaction mix, Σ 20 µL

Component	**Volume** (µL)
H_2O (MILLIQ)	13
10× T4 DNA ligase buffer	2
T4 DNA ligase (5 Weiss U μL^{-1})	1
Vector DNA	2
Insert DNA	2

Note: The ratio of vector DNA to insert DNA was varied according to their relative length (in bp) to provide a 1:1 molar ratio of cohesive ends.

Following ligation, the reaction mixture was digested with a restriction enzyme chosen to only cut any original ('empty') vector DNA still present to optimize transformation of the ligation mix. This was achieved by selecting a recognition site present in the piece of multiple-cloning site that was expected to be eliminated during vector preparation. Restriction was performed by adding 1 µL of the corresponding restriction enzyme (10 U μL^{-1}) directly to the heat-inactivated ligation mix and incubating at 37 °C for 30 min. Following restriction, the restriction enzyme was heat-inactivated according to the supplier's instructions. An aliquot of 1 µL of the ligation mix was then used to transform chemically competent XL1BLUE as described in section **3.1.1.1**.

3.3.7.2 GATEWAY® cloning

Cloning using the GATEWAY® system (Thermo Fisher) was performed according to the manufacturer's instructions.

3.4 General biochemical methods

3.4.1 Storage and handling of purified protein samples

Unless specified otherwise, purified protein samples were kept on ice at all times during use. For short-term storage (up to 16 h), samples were stored at 4 °C. For long-term storage, samples were divided into single-use aliquots, flash-frozen by immersion in liquid N_2 and then stored at −80 °C. For use, stored samples were thawed quickly by addition of room-temperature buffer solution and vortexing (thawing by hand if no further dilution of sample was desired). As soon as the sample was thawed completely, it was transferred to ice for further use.

3.4.2 Dialysis

Buffer exchange was achieved by dialysis. Dialysis tubing of suitable molecular weight cut-off and internal diameter was chosen and rinsed with H_2O (MILLIQ) for 10 min, followed by equilibration in target buffer for another 10 min. The dialysis tubing was then closed on one end by clamping, filled with sample, and closed on the other end as well. The tubing was transferred to a suitably large vessel (volume at least 1000× sample

volume) filled with pre-chilled (4 °C) buffer solution. Dialysis was performed for 16 h (4 °C, stirring-rod agitation).

3.4.3 Protein quantification

Crude extracts and partially purified proteins Estimative quantification was performed by separation on SDS-PAGE as described in section **3.4.4**, followed by CBB staining. For reference, a titration of bovine serum albumin (BSA) standard (1 $\mu g\,mL^{-1}$, 10 $\mu g\,mL^{-1}$, 100 $\mu g\,mL^{-1}$, 1 $mg\,mL^{-1}$) was included on the same gel. Sample protein amount was estimated by comparing band intensity with the BSA standard.

Purified proteins ($\geq$90 %, $\geq$100 $\mu g\,mL^{-1}$) Purified protein stock solutions of sufficiently high concentrations were quantified using the built-in methods of a Nanodrop 2000 spectrophotometer, taking into account the calculated molecular weight and molecular extinction coefficient at a wavelength of 280 nm **(Gill, SC; von Hippel, 1989)**. These parameters were calculated based on protein sequence using the ProtParam online tool of the ExPASy bioinformatics resource portal (Swiss Institute of Bioinformatics), which uses the following equation for calculation of the extinction coefficient:

$$\varepsilon_{Protein} = N_{(Tyr)} \times \varepsilon_{(Tyr)} + N_{(Trp)} \times \varepsilon_{(Trp)} + N_{(Cystine)} \times \varepsilon_{(Cystine)} \tag{3.2}$$

$$\text{where } \varepsilon_{(Tyr)} = 1490,\ \varepsilon_{(Trp)} = 5500,\ \varepsilon_{(Cystine)} = 125.$$

Purified proteins ($\geq$90 %, $\leq$100 $\mu g\,mL^{-1}$) Estimative quantification of dilute purified protein samples was performed using the commercial Roti® -Nanoquant system (Carl Roth) according to the manufacturer's instructions.

3.4.4 SDS-PAGE

Sodium dodecyl sulfate polyacrylamide gel electrophoresis (SDS-PAGE, **Laemmli, 1970**) was used to separate proteinaceous samples under denaturing conditions. 12 % polyacrylamide (PAA) gels were prepared to the specifications summarized in table **3.10**.

Gel casting Separating gels were cast between glass plates in a vertical casting rack (BioRad) and the top surface was covered with thin layer of isopropanol. After polymerization of the separating gel, the isopropanol was discarded and the stacking gel was cast on top of the separating gel. A comb for creating pockets for sample loading was inserted.

Table 3.10 Gel composition for SDS-PAGE. SDS, Sodium dodecyl sulfate; AA, Acrylamide; BAA, Bisacrylamide; APS, Ammonium persulfate; TEMED, Tetramethylethylenediamine

Type	Component	Concentration	Volume (mL)
Resolving gel	H_2O (MILLIQ)		3.2
	Acrylamide mix	30 % (AA) 0.8 % (BAA)	4
	Tris pH 8.8	1.5 M	2.6
	SDS	10 %	0.1
	APS	10 %	0.1
	TEMED		0.004
Stacking gel	H_2O (MILLIQ)		2.975
	Acrylamide mix	30 % (AA) 0.8 % (BAA)	0.67
	Tris pH 6.8	0.5 M	1.25
	SDS	10 %	0.1
	APS	10 %	0.05
	TEMED		0.002

After polymerization of the stacking gel, the casting rack was disassembled and the gels were either used directly or stored at 4 °C for up to 7 days.

Sample preparation Samples were mixed with 5 × loading buffer (250 mM Tris pH 6.8, 10 % (w/v) SDS, 50 % (w/v) gylcerine, 5 % (w/v) β-mercaptoethanol, 0.002 % (w/v) bromphenol blue) and incubated at 95 °C for 5 min. Samples were then loaded into the sample pockets of the stacking gel.

Electrophoresis Gels were placed in a vertical electrophoresis chamber (BioRad), and the chamber was filled with SDS running buffer (190 mM Glycine, 25 mM Tris pH 8.3, 1 % (w/v) SDS). Electrophoresis was then performed with a limiting current of 25 mA per gel.

Staining of PAA gels After electrophoresis, gels were stained by immersion in Coomassie-Brilliant-Blue (CBB) staining solution (1 $g\,L^{-1}$ CBB, 50 % isopropanol, 10 % acetic acid) for $0.5-2$ h. To increase band contrast, gels were de-stained after staining by immersion in de-staining solution (50 % isopropanol, 10 % acetic acid) for $0.5-4$ h.

3.5 Protein purification

General considerations For protein purification, ÄKTA systems (ÄKTA Explorer, ÄKTA Pure; GE Healthcare) were used. Temperature for all purification steps was 4 °C. Before starting a purification procedure, the systems were prepared and washed according

to the manufacturer's instructions. Standard flow rates for all purification steps were 1 $\mathrm{mL\,min^{-1}}$. All buffers used for purification were filtered, degassed and pre-chilled before use.

3.5.1 Affinity Chromatography (AC)

Affinity chromatography was performed as a first step to purify tagged proteins. For purification via hexahistidine tag (His-tag, **Hochuli et al., 1988**), Immobilized Metal ion Affinity Chromatography (IMAC) columns containing Ni^{2+} ions bound to a sepharose matrix (HisTrap FF 1 mL, GE Healthcare) were used.

Sample loading Total soluble protein was extracted from *E. coli* as described in section **3.1.2.4**, using extraction buffer containing a low amount of imidazole to decrease unspecific absorption to the column during loading (50 mM Tris pH 7.6, 150 mM NaCl, 20 mM imidazole). The same buffer was used as a running buffer during purification (buffer inlet A). Raw extracts were then loaded using the system's sample pump at a flow rate of 1 $\mathrm{mL\,min^{-1}}$. To maximize the loaded sample amount, the sample tubing was flushed with an aliquot of buffer directly after sample application (while still being connected to the column) until UV absorption at 280 nm returned to baseline levels.

Sample elution After sample loading, an imidazole gradient was established by using the system's mixing unit to mix running buffer (see above) with elution buffer (50 mM Tris pH 7.6, 150 mM NaCl, 500 mM imidazole). A two-step gradient was then performed, consisting of a pre-wash step using a maximum imidazole concentration of 70 mM (90 % (v/v) running buffer, 10 % (v/v) elution buffer), followed by an elution step using a maximum imidazole concentration of 500 mM (100 % elution buffer). Figure **3.1** shows a schematic representation of a typical elution profile. During the elution gradient step, fractions ($V = 1$ mL) were collected continuously and stored at 4 °C. After elution was completed, the column was washed with running buffer, and the purification procedure was completed.

Fraction handling After collection, fractions were analysed for purity and yield by SDS-PAGE and CBB staining as described in section **3.4.4**. Depending on purity, fractions were then either used as input for further purification procedures (e.g. size exclusion chromatography (SEC), see section **3.5.2**) or dialysed into protein storage buffer (50 mM Tris ph 7.6, 150 mM NaCl) as described in section **3.4.2**.

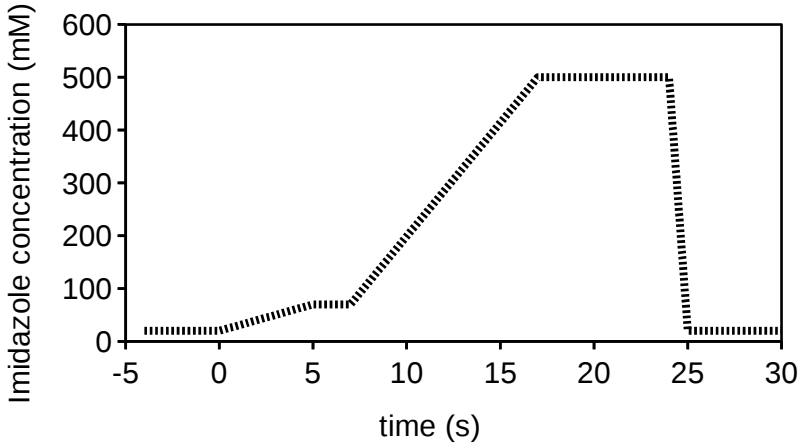

Fig. 3.1 Typical elution profile for IMAC. The pre-elution washing gradient step was performed between time points 0 min and 7 min, the elution gradient step between time points 7 min and 17 min. Elution is continued at 100 % buffer B to elute any strongly bound material prior to column storage.

3.5.2 Size Exclusion Chromatography (SEC)

Size exclusion chromatography was performed using a gel filtration column filled with a matrix of cross-linked agarose and dextran, with a total bed volume of 120 mL (HiLoad 16/600 Superdex 75 PG, GE Healthcare). The column was equilibrated with 240 mL (2 column volumes, CV) of running buffer (50 mM Tris pH 7.6, 150 mM NaCl) before use.

Sample loading Samples were loaded manually into an injection loop of suitable diameter (250 µL to 25 mL) using a syringe. The contents of the loaded injection loop were injected into the column after equilibration.

Sample elution Fractions ($V = 1$ mL) were collected continuously starting 120 mL (1 CV) after sample injection.

Fraction handling Fractions were analyzed for purity and yield, and then processed further, as described in section **3.5.1**.

3.6 Kinase activity assays

Kinase activity assays were performed using a protocol modified from **Horn and Walker, 1994**. Recominbinant proteins with hypothetical kinase activity were expressed and purified as described in sections **3.1.2** and **3.5**.

Labelling reaction A total amount of 1 µg per sample protein was incubated in kinase assay buffer (50 mM HEPES pH 7.6, 20 mM $MgCl_2$, 1 mM DTT, 10 µM ATP, 10 µCi

γ-AT^{32}P). The reaction was incubated at room temperature for 1 h, then stopped by addition of 5 $\times$ SDS sample buffer (see section **3.4.4**).

Gel processing Samples were incubated at 90 °C for 15 min, then separated by SDS-PAGE, stained and destained as described in section **3.4.4**. The gels were then dried by placing them on filter paper (Whatman, GE Healthcare) and incubating them in a vacuum/heat gel drying apparatus (VWR) at 80 °C for 3 h.

Autoradiography visualization After drying, gels were placed on top of a storage phosphor screen (BAS, GE Healthcare) and incubated inside an autoradiography cassette for 16 h. After incubation, the screen was removed from the cassette in the dark and transfered to a laser-based fluorescent image scanning unit (Hitachi FMBIO® III) and exposed according to the manufacturer's instructions.

3.7 *In vitro* interaction assays

Sample preparation *In vitro* interaction assays have been performed with aliquots of purified proteins. Recombinant proteins were expressed and purified as described in sections **3.1.2** and **3.5**. Prior to each experiment, protein stock solutions were quantified as described in section **3.4.3**. All subsequent dilutions were made in interaction assay buffer (50 mM Tris pH 7.6, 150 mM NaCl, 0.01% Tween-20), which is identical to protein storage buffer except for the addition of detergent to suppress unspecific interactions.

3.7.1 Microscale Thermophoresis

3.7.1.1 Background

Molecular principle Microscale thermophoresis (MST) assays are based on the motion of particles in a temperature gradient (*thermophoresis*; also called thermodiffusion or Ludwig-Soret effect, **Ludwig, 1856**). This effect applies to particles ranging in size from macroscopic colloids and aerosols to single ions in solution. Although thermophoresis has been known for a long time, the precise molecular mechanisms governing this motion remain largely elusive. For typical biomolecules in aqueous solutions, important factors include size of the molecule, charge, and extent of the hydration shell; the complex interplay of these and other factors make accurate prediction of thermophoretic behaviour of biomolecules difficult. Experimentally, biomolecules may exhibit positive (movement from hot to cold) or negative (movement from cold to hot) thermophoresis. Taking general molecular diffusion into account, a steady-state situation will be reached for any

given temperature gradient when the thermophoretic force acting on a particle equals the diametric force of back-diffusion (see figure **3.2** for an illustration).

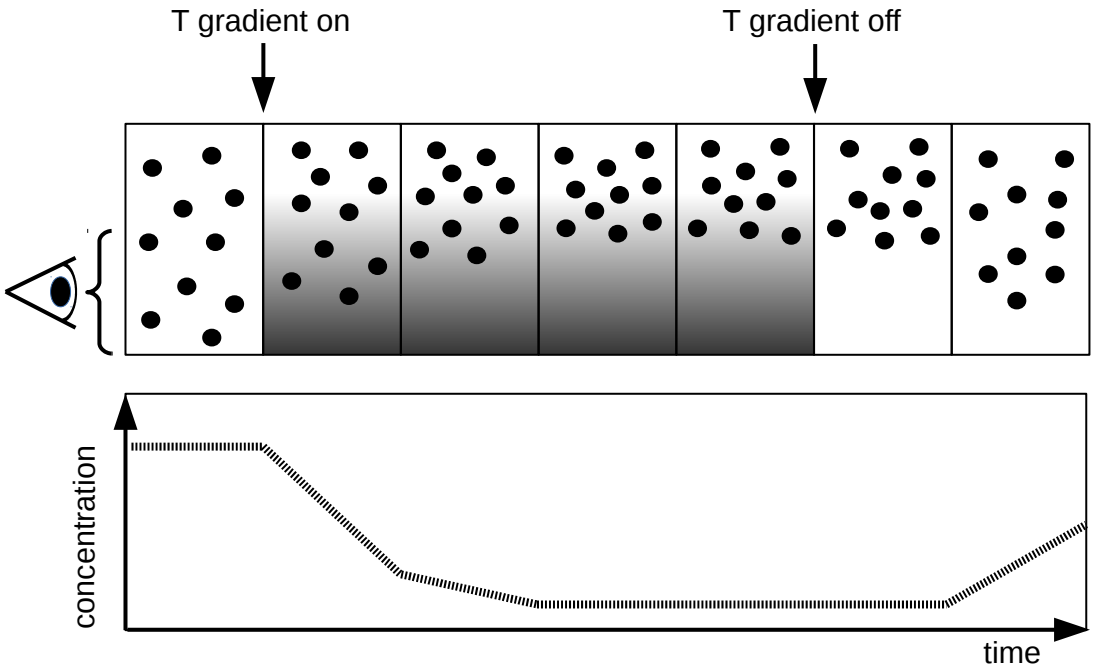

Fig. 3.2 Molecular principle for thermophoresis. **Top**: Compartment representation. Particles (black dots) are evenly and randomly distributed in a solution. Upon establishment of a temperature gradient (grey), particles move due to thermophoresis until a steady-state has been reached. Upon abolishment of the temperature gradient, particles redistribute in the solution by diffusion. The eye symbolizes an external observer. **Bottom**: Apparent particle concentration over time (dashed line) as seen by the observer .

Application to protein-protein interactions When biomolecular interactions take place, the complex that is being formed exhibits thermophoretic behaviour that is different to that of its isolated constituent molecules. MST assays take advantage of this by tracking the movement of a specific biomolecule through fluorescence and using the differential thermophoretic behavior of its possible states (i.e. isolated vs. complex-bound) to infer the amount of complex formation (figure **3.3 A**). In practise, quantitative determination of binding affinities is possible for pairs of biomolecules by using a titration approach. While the concentration of the observed molecule is held constant, the second molecule is titrated over a broad range of concentrations. By setting the amount of complex being formed into relation with the concentration of the second molecule, the affinity of the interaction can be determined (figure **3.3 B, C**).

Instrument technical background Instruments for MST assays as have been used in this study (NT.115 platform, Nanotemper) use coupled optical systems to induce tem-

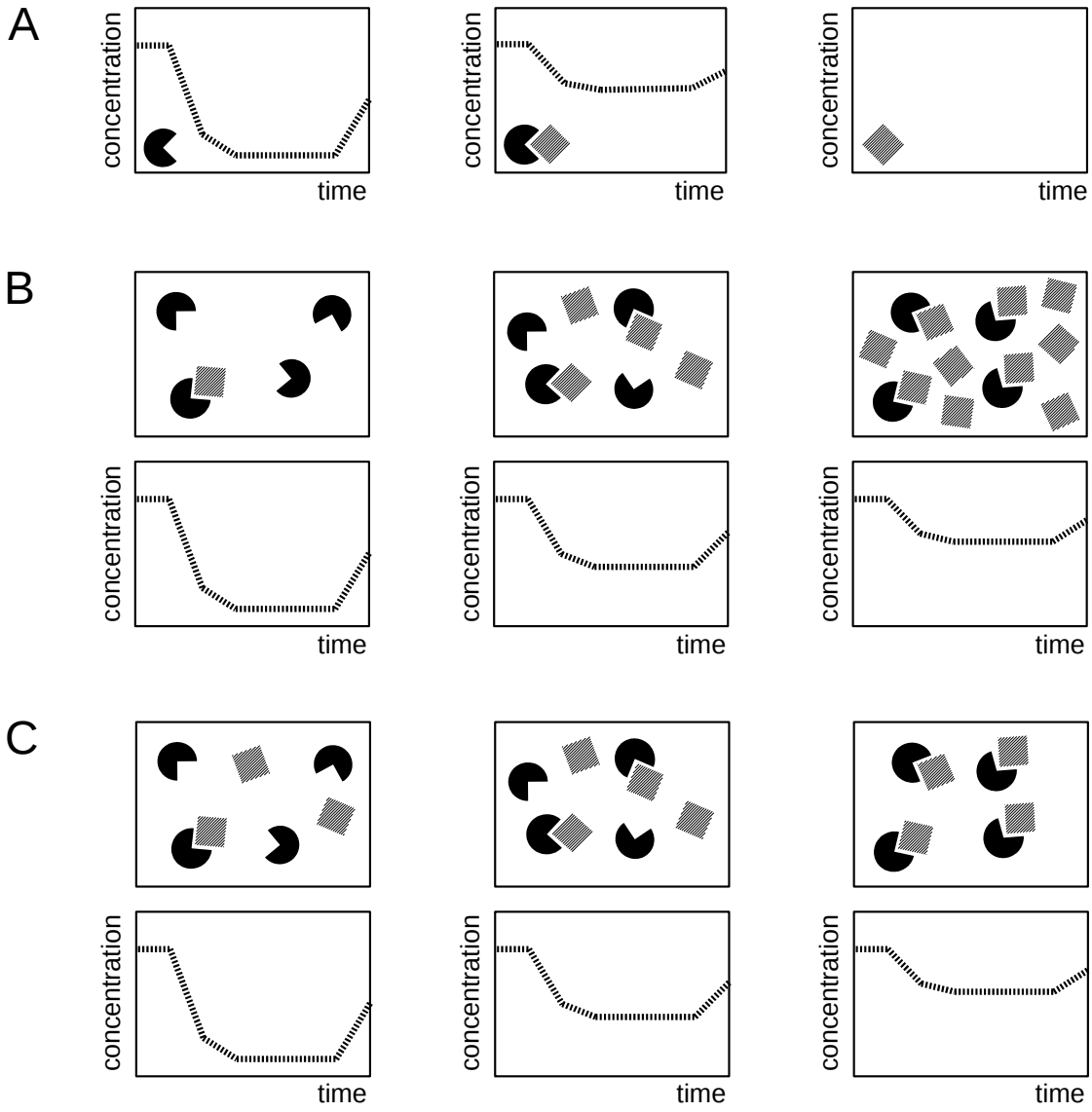

Fig. 3.3 Complex formation and thermophoresis. Thermophoresis-induced concentration shifts (dashed lines) are depicted analogous to figure 3.2. One of the biomolecules (black shape) can be observed through fluorescence, while the other (shaded diamond) can not. **A**, Complex formation is reflected by a shift in thermophoretic mobility. **B**, Titration of the nonobserved molecule leads to concentration-dependent shifts in apparent thermophoretic mobility for any given affinity of the interaction. **C**, At a single constant concentration of the non-observed molecule, differences in affinity are visible as differences in thermophoretic mobility.

perature gradients (infrared laser) and measure fluorescence (UV-vis detector, excitation by LED, emission filtering using RGB color channels) in glass capillaries of 10 µL total internal volume. The temperature gradients induced by the infrared laser are spheroid with a radius of ∼200 µm between the center point (highest temperature) and a 70 % temperature drop point (**Jerabek-Willemsen et al., 2011**). Temperature gradients are typically on the order of 2 to 6 °C (depending on the user-adjustable instrument infrared laser power). Typical time scales for a single capillary measurement are about 60 s with a laser-heated phase of 30 s and continuous fluorescence signal recording. The intensity of the fluorescence signal can be manipulated by the adjustment of excitation LED power and the choice of a specific emission filter set. Measurements over multiple capillaries (typically 8 to 16 capillaries per interaction) are used to calculate thermophoretically induced signal shifts dependent on concentration of the unlabeled molecule.

3.7.1.2 Assay development and experimental procedure

Instrument and consumables Thermophoresis measurements were performed using a NT.115 instrument (Nanotemper) with a red/green filterset. Capillaries with various coatings (uncoated, hydrophilic, hydrophobic) and capillary trays were obtained from the same manufacturer.

Optimization of fluorescence signal For binary interactions between the bacterial effector protein *Ps*AvrPto and *A. thaliana* RLK kinase domains, *Ps*AvrPto was used as the observed molecule. To this end, *Ps*AvrPto was expressed and purified with a fused C-terminal mOrange fluorescence tag (**Shaner et al., 2004**). The green filter of the instrument and hydrophilically coated capillaries were chosen for optimal signal of mOrange fluorescence. Using a concentration of labeled *Ps*AvrPto of 50 nM, a fluorescence signal of ∼ 500 counts was observed (LED power 80 %), which is within the linear range of the instrument and was chosen as the experimental concentration.

Titrations and sample preparation Serial titrations over a total of 16 capillaries were used. Titrations were performed in PCR tubes in a specific manner to minimize artefacts due to pipetting inaccuracies. To each tube except the first one, 10 µL of interaction buffer (see section **3.7**) were added. An aliquot of 20 µL of the unlabelled protein at two times the highest experimental concentration was added to the first tube. From the first tube, an aliquot of 10 µL of protein solution was then taken, mixed with the volume of buffer in the second tube using the same pipette tip, and transferred to the next tube, where the same procedure was repeated. The procedure was then repeated continuously until the last tube, after which the remaining 10 µL of sample dilution were discarded, yielding 16

tubes with 10 µL of serially diluted unlabelled protein each. To each of the tubes, labelled protein was then added at two times the final experimental concentration using a fresh pipette tip for each tube. Samples were mixed by flicking, spun down (1000 $\times g$, 30 s) and transferred to capillaries by directly immersing the capillaries into the tubes. The capillaries were then transferred to an aluminium rack (figure **3.4**) and inserted into the instrument.

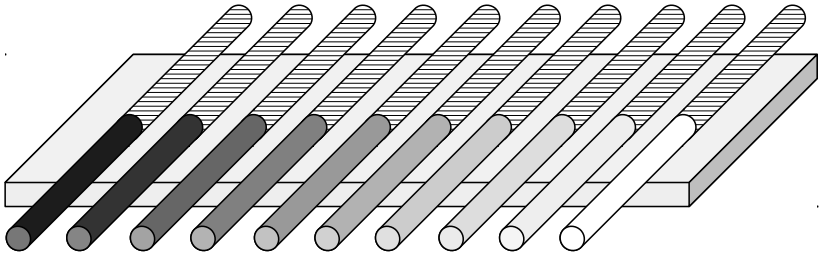

Fig. 3.4 Serial dilution capillary setup for MST. Equal volumes of two protein solutions are used. The labelled protein is used at the same concentration in each capillary (shaded part of capillary), while the unlabelled protein is diluted over the range of capillaries (grey-scale gradient, with darker colors corresponding to higher concentration). *Note*: the two different protein solutions are in reality homogeneously distributed in each capillary; an artificial division in the center of each capillary was used for illustrative purposes.

Measurement Capillaries were measured for total fluorescence using the automated capillary scan method of the NT.115 control software. Thermophoresis measurements were initiated if the variance in total fluorescence between all capillaries was below 10 % for at least 15 out of 16 capillaries (measurements with single outliers were performed discarding the outlier capillary). Measurements were performed twice for each sample set at 20 % and 40 % infrared laser power, respectively.

3.7.1.3 Data evaluation

Affinity determination Data evaluation was performed using the NT.115 analysis software provided by the manufacturer. For each measurement curve, normalized fluorescence values of a two-second window immediately before IR laser heating (cold fluorescence) were divided by normalized fluorescence values of a four-second window immediately before the end of IR laser heating (hot fluorescence). These values were then plotted against the concentration of the unlabelled molecule. Curve fitting was then performed using the built-in algorithms for a 1:1 binding model, which determines normalized fluorescence values for the corresponding bound and unbound molecular states and calculates the K_{D} using the inflection point of the sigmoidal dose-response curve.

Normalization To account for different signal amplitudes between individual experiments, fluorescence values were normalized by dividing maximum fluorescence (corresponding to the unbound state) by minimum fluorescence (corresponding to the bound state) and plotting these normalized values as fraction bound.

3.7.2 Surface Plasmon Resonance

3.7.2.1 Background

Molecular principle Surface Plasmon Resonance (SPR) is the most widely used method to quantitatively determine protein-protein interaction parameters **(Myszka, 1997)**. Using an optical biosensor approach, the total molecular mass accumulated on a sensor surface can be quantified in real time with a maximum molecular weight resolution of $\sim$200 Da. Molecular interactions can be studied by fixing one of the binding partners (termed 'ligand') on the sensor surface and injecting the other binding partner (termed 'analyte') in a time-controlled manner. Binding events between these molecules then lead to accumulation of mass on the sensor surface which can be detected directly. In SPR assays, data is obtained as curves of system response (plotted as arbitrary resonance units, RU) over time. The signal is proportional to mass, with 1 RU corresponding to $\sim$1 pg mm^{-2} of molecules **(Stenberg et al., 1991)**. For a detailed description of the physical background of the method, see **Mayo and Hallock, 1989**.

System overview SPR instruments consist of a microfluidics system with automated sample injection mechanisms and constant flow regulated through a peristaltic pump (flow rates 10 µL min^{-1} to 30 µL min^{-1}). The reaction chamber (flow cells, see figure **3.5 A**) is created by docking a sensor chip to the instrument, which closes the internal microfluidics system. The reaction chamber is enclosed in a temperature-controlled jacket (temperature accuracy $\pm$ 0.005 °C) in order to achieve a stable environment for kinetic measurements.

Sensor surface molecular environment One of the most commonly used types of sensor chip (type CM5, GE Healthcare) was used in this study. CM5 chips (figure **3.5**) consist of a thin gold surface on a glass substrate to which a carboxymethylated dextran hydrogel matrix has been covalently attached by the manufacturer to a thickness of $\sim$100 nm, which corresponds to 0.2 % of the flow cell height **(Myszka et al., 1998)**. For immobilization of proteinaceous ligands, an amine coupling chemistry can be used which covalently links the N-terminus and lysine ε-amino groups of the ligand to the matrix carboxyl groups. This type of coupling results in a random, flexible, and three-dimensional distribution of ligand molecules within the dextran matrix (figure **3.5 B**),

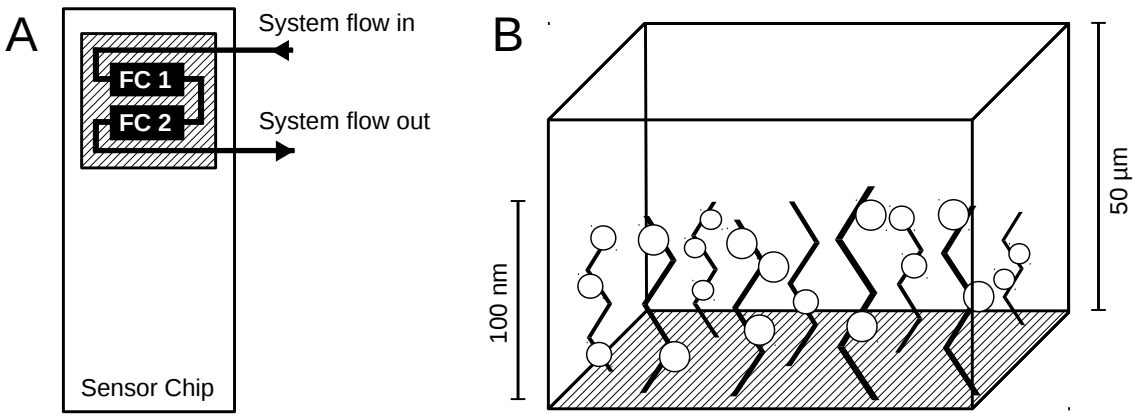

Fig. 3.5 Sensor chip for SPR measurements (not to scale). **A**, each sensor chip is made up of two flow cells (black boxes) which are gold-coated microscopic cavities etched into the glass substrate (shaded). Upon inserting the chip into the instrument, these cavities dock with corresponding cavities in the instrument to create the reaction volumes. System flow runs sequentially through both flow cells. By convention, flow cell 1 (FC1) is used as a reference flow cell, while flow cell 2 (FC2) is used as the sample flow cell. **B**, Simplified view of a single flow cell. The ligand (white spheres) is attached to flexible dextran chains (black sticks), which are in turn covalently fused to the gold surface (shaded area).

increasing the sensor's binding capacity compared to that of a purely planar surface and minimizing potential steric hindrance by decreasing the apparent ligand density in the flow system **(Johnsson et al., 1991)**. However, in context of analyte diffusion across this third dimension, the thickness of the dextran layer can usually be neglected for practical experimental considerations **(Karlsson and Fält, 1997, Wofsy and Goldstein, 2002)**.

Analyte injections and binding events Injecting analyte into the system's flow cell (see figure **3.6**) causes the total surface response signal to increase rapidly due to the presence of the analyte molecules in the laminar flow close to the surface. This does not necessarily indicate binding events. In the absence of binding the signal will return to the baseline value rapidly after the analyte sample flow has been switched off and the flow cell has been emptied of non-bound analyte (figure **3.6 A**). However, if a binding event takes place, the signal will initially remain at a high value after the analyte sample flow has been switched off and decrease more slowly. The following signal decrease is then due to dissociation of the complex, and the rate of this signal decrease is directly linked to the binding reaction's dissociation rate constant (figure **3.6 B**).

Kinetic analysis Under certain circumstances, quantitative determination of binding parameters is possible using sensorgram data generated by analyte injection. Taking the predefined concentration of the analyte into account, an idealized binding event

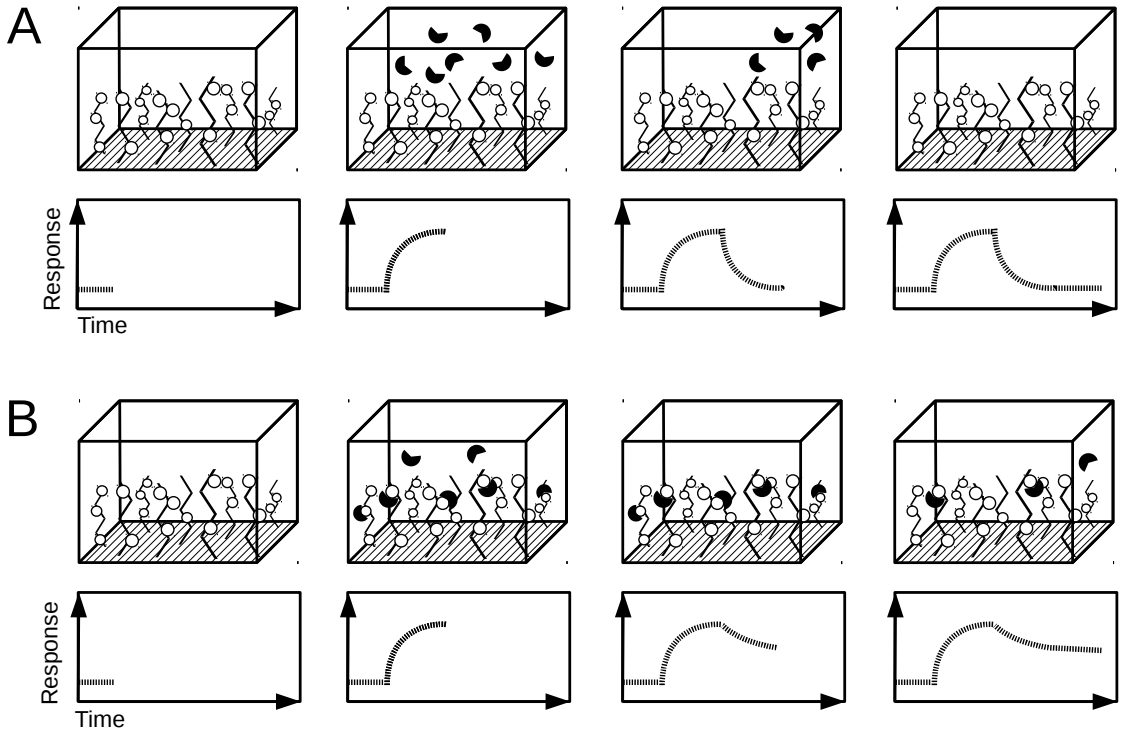

Fig. 3.6 Compartment representations (top) and sensorgrams (bottom) for analyte injections. **A**, if no interaction takes place between ligand (white spheres) and analyte (black shapes), the signal will rise temporarily during injection but fall back to baseline levels after injection has finished. **B**, if an interaction takes place between ligand and analyte, the signal decrease after injection is more gradual and depends on the rate of dissociation between ligand and analyte. *Note*: axis labels are shown on first sensorgram only.

corresponding to a theoretical model (e.g. a simple 1:1 Langmuir binding of the analyte (A) to a given ligand (B), see equation **3.3**) can be predicted.

$$A + B \underset{k_d}{\overset{k_a}{\rightleftharpoons}} AB \tag{3.3}$$

By varying flexible parameters in the model iteratively (e.g. association rate constant, k_a, and dissociation rate constant, k_d), the data can be fitted to the model until a minimum deviation is achieved (see figure **3.7 A)**. At this point, the quality of the fit can be evaluated using tools such as residual plots and uniqueness (U) values (see section **3.7.2.3** for details on the exact procedure).

Kinetic titration On recent SPR platforms (such as the Biacore X100 that has been used in this study), kinetic analysis via single-cycle titration is possible. In this work flow, the analyte is injected consecutively at increasing concentrations (see figure **3.7 B)**. In between injections, the analyte partially dissociates from the ligand. Although one injection of analyte at a known concentration would yield enough data to determine the

kinetic constants, using a titration series increases the robustness of the fit by cancelling out artefacts potentially arising at certain analyte concentrations. For best resolution, the titration should be performed around the expected K_D of the interaction, i.e. analyte should be injected at concentrations both below and above the expected K_D. Analysis is then performed on the entire sequence of injections (*global analysis*, see **Rich and Myszka, 2000**).

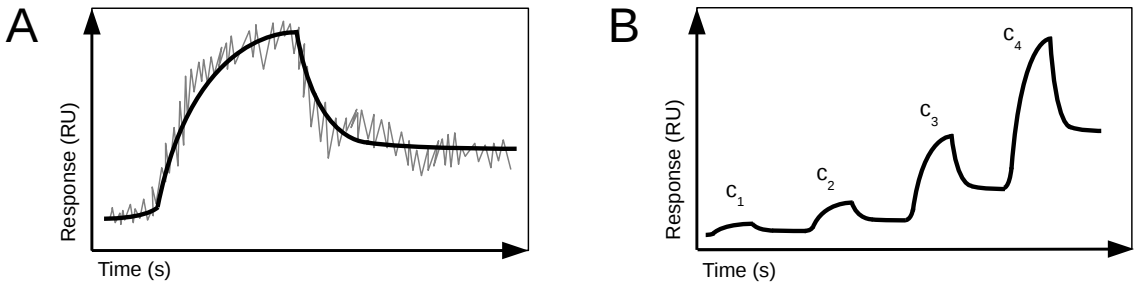

Fig. 3.7 Exemplary SPR interaction kinetics analysis. **A**, data for a single analyte injection (grey curve, noisy) is being fitted to a mathematical model describing the interaction (black curve, smooth). **B**, kinetic titration experiment. Multiple injections of increasing concentration (c_1, c_2, c_3, c_4) have been performed during the same experimental run. The kinetic fit has been performed over the timeframe of the whole experiment. *Note*: only the fit curve is shown for clarity.

3.7.2.2 Assay development and experimental procedure

Instrument and consumables For SPR measurements, a Biacore X100 system (GE Healthcare) was used. Sensor chips and all kits for sensor chip preparation were obtained from the same manufacturer.

Sensor chip preparation To prepare a sensor chip for ligand capture purposes, a fresh, unmodified sensor chip (carboxymethylated dextran covalently attached to gold surface, type CM5) was inserted into the instrument and equilibrated with 1 $\times$ PBS buffer (137 mM NaCl, 2.7 mM KCl, 10 mM Na_2HPO_4, 2 mM KH_2PO_4) for 1 h (flow rate 10 $\mu L\,min^{-1}$). The chip surface was then activated in both flow cells using an amine coupling kit (GE healthcare) according to the manufacturer's instructions with an activation time of 7 min. Following activation, an α-RFP nanobody (RFPtrap®, Chromotek) was injected to both chip flow cells at a concentration of 50 $\mu g\,mL^{-1}$ in 10 mM acetate, pH 5.5., for 7 min. After nanobody injection, the surface was deactivated for another 7 min. This protocol resulted in total nanobody amounts of $\sim$3000 response units (RU) per sensor surface flow cell. After deactivation, the buffer was switched

to interaction assay buffer (see section **3.7**), the system was primed and subsequently equilibrated for another 2 h before starting a ligand capture protocol.

Ligand capture Ligand was captured by injecting mOrange-tagged purified protein at a concentration of 100 nM to the second (sample) flow cell of a chip coupled with an α-RFP nanobody (as described above). Injection was performed using the instrument control software's built-in RU target method to a set amount of 250 RU. The system was then equilibrated (flow rate 30 µL min^{-1}) until signal decrease due to ligand dissociation reached the linear baseline phase with dissociation rates of less than 1 RU min^{-1} ($\sim$3 h), indicating negligible dissociation of ligand from the nanobody. Actual ligand binding levels at the end of equilibration varied between approx. 180 and 220 RU.

Kinetic titration experiment Kinetic titration experiments were performed using a single-cycle kinetics assay workflow. The sensor chip was loaded with ligand on the sample flow cell and equilibrated as described above. The flow rate was set to 30 µL min^{-1} to minimize the extent of the unstirred solvent layer effect above the dextran matrix and therefore potential mass-transfer limitations (**Goldstein et al., 1999**). Before analyte injection, a blank run was performed by injecting buffer for 4 to 5 times (120 s each). Then the analyte was injected as a series of 4 to 5 injections (120 s each) at increasing concentrations, with partial dissociation phases (120 s each) between each injection event. Analyte concentrations were chosen from a set of threefold serial dilutions (12.3 nM, 37 nM, 111 nM, 333 nM, 1 µM, 3 µM, 9 µM) according to the expected affinity of the interaction to provide a maximum concentration of at least ten-fold the expected K_D. After analyte injection, a replicate blank run was performed as before.

Alternative setup using α-his antibody As an alternative to using the mOrange moiety to capture ligand molecules, a α-his antibody was used to capture ligand via fused his tag. α-his antibody (GE Healthcare) was loaded onto both surfaces of a CM5 chip according to the manufacturer's instructions. As all the purified proteins used for interaction study carried his-tags, a blocking step was necessary between ligand loading and analyte injection (see figure **3.8**). The aim of the blocking step was to suppress secondary binding events occurring between the analyte his-tag and the α-his antibody on both flow cells. As a blocking protein, his-tagged *Arabidopsis thaliana* Uricase (**Willmann, 2011**) was used for its convenience in recombinant expression and purification. Uricase was expressed in *E. coli* (BL21AI) as described in section **3.1.2** and purified as described in section **3.5**. Purified Uricase was diluted to 1 mg mL^{-1} and injected manually into both flow cells (contact time 600 s) after ligand loading. Injections were repeated until no further

increase in signal could be observed, indicating a saturation of α-his binding sites in both flow cells. The remainder of the assay protocol was performed as described before.

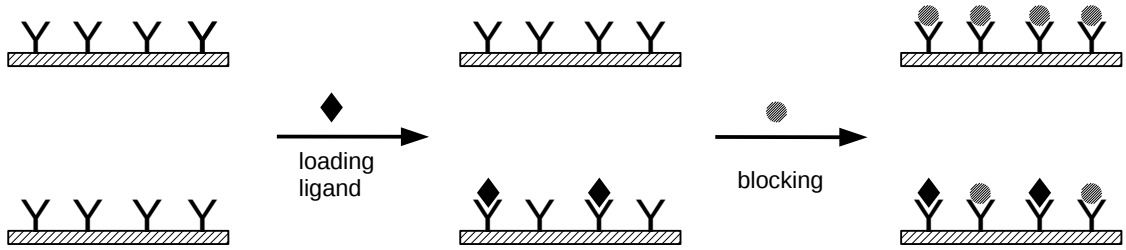

Fig. 3.8 Alternative SPR setup using an α-his antibody (black Y shapes). The sensor chip surface is symbolized by shaded rectangles. **Top**, reference surface; **bottom**, sample surface. After loading the ligand (black diamonds), excess antibody binding sites on the sample surface as well as all binding sites on the reference surface are blocked by injecting a non-interacting his-tagged protein (shaded circles).

3.7.2.3 Data evaluation

Curve fitting Using the system's evaluation software, single-cycle kinetics curves were processed by subtracting the signal from the reference flow cell from the signal of the sample flow cell. Systemic baseline drift and injection artifacts were taken into account by subtracting the averaged values of the two blank runs from the values of the analyte run **(Rich and Myszka, 2000)**. Sample data were then fitted to a 1:1 binding model using the built-in methods of the system's analysis software.

Quality control Residual plots including upper and lower thresholds for acceptable deviations were generated using the built-in methods and examined for relevant signal deviations. To examine the mathematical robustness of the fit, iteratively calculated uniqueness values (U values, **Önell and Andersson, 2005**) were determined for all possible combinations of parameter pairs using the built-in methods. Only curve fittings passing stringent quality control (non-artifact residual deviations within the lower calculated threshold, U-values < 15) were used for determination of kinetic constants and K_{D}.

3.8 *In vivo* interaction assays

In-vivo interaction assays have been performed to see whether the binding events which have been characterized quantitatively *in vitro* can also be observed in a more natural system. To this end, an *A. thaliana* leaf mesohpyll protoplast system which has originally

been established to characterize effector function via transient expression (**Yoo et al., 2007**, **Zheng et al., 2014)** has been adapted.

3.8.1 *A. thaliana* protoplast system to study effector interactions

Basic principle Using the adapted *A. thaliana* leaf mesohpyll protoplast system, interaction between effectors and their putative targets is observed indirectly by monitoring the effector's ability to suppress immunity signalling. Plants carrying a knock-out mutation for a certain effector target gene are complemented by transient expression of the knocked-out wild-type protein or a corresponding mutational construct. By co-transforming an effector, a repression of immunity signalling is expected if the effector is able to bind its natural target. If this is not the case (e.g. because mutations in the target protein decrease its affinity to the effector), effector expression is expected to have a far lower (or no) effect on repression of immunity signalling (see figure **3.9** for a schematic overview of the basic principle).

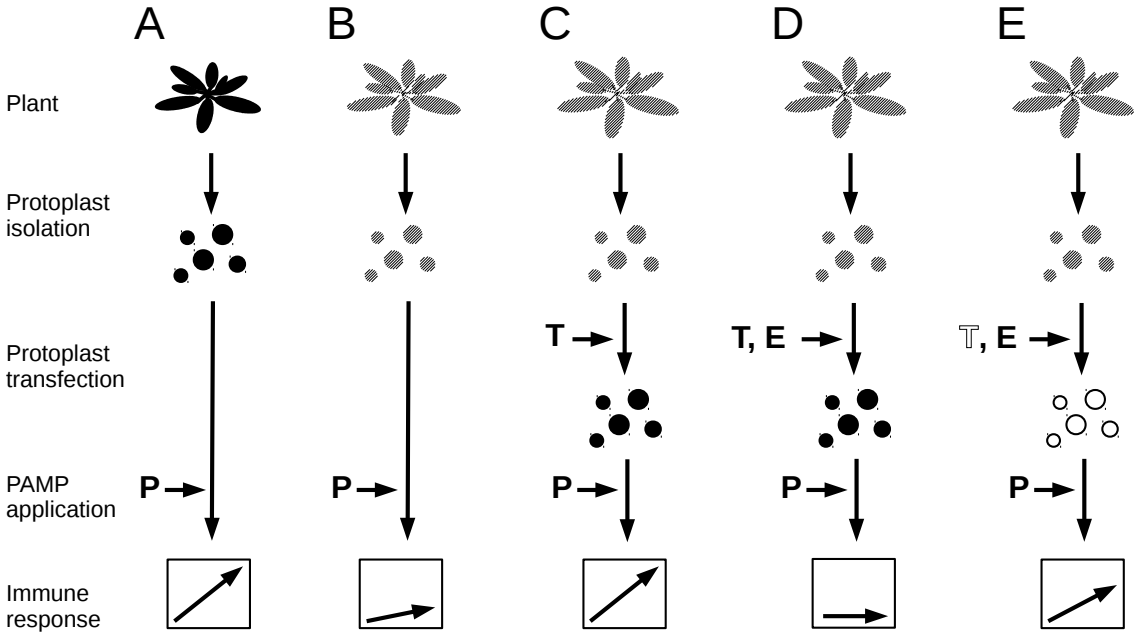

Fig. 3.9 Protoplast system adapted to study effector-target interactions. **A**, Wild-type plants respond normally to PAMP (P) treatment (raised arrow in box). **B**, Effector target mutant protoplasts (shaded circles) show decreased response to PAMP treatment. **C**, Effector target mutant protoplasts complemented with the wild-type effector target (T) show restored response to PAMP treatment. **D**, Effector target mutant protoplasts complemented with the wild-type effector target and cotransformed with the effector (E) show strongly decreased response to PAMP treatment. **E**, Effector target mutant protoplasts (outlined circles) complemented with a mutant effector target which shows less binding activity to the effector (outlined T) and cotransformed with the effector show higher response to PAMP treatment (compared to wild-type target with effector expression).

pFRK1-Luciferase assay *A. thaliana* protoplasts were isolated as described in section **3.2.2.1** and transfected as described in section **3.2.2.2** with one or more plasmid(s) encoding for the following (see table **2.6** for details):

- The firefly luciferase (*Luc*) reporter gene under control of the flg22-induced receptor-like kinase 1 (FRK1) promoter (*pFRK1*) to monitor immunity signalling
- The *Pseudomonas syringae* effector protein AvrPto (*Ps*AvrPto)
- The *A. thaliana* immunity-related co-receptor BAK1 (*At*BAK1), either in its wild-type or in a mutated form

After transfection, protoplast suspensions were supplemented with the luciferase substrate D-Luciferin to a final concentration of 200 nM and mixed carefully. For each sample, six aliquots of 100 µL protoplast suspension each were then transferred to individual wells of a 96-well microtiter plate and incubated overnight (∼15 h, 20 °C). After this incubation step, the microtiter plate containing the protoplast suspensions was transferred to a luminometer (Berthold) and luminescence was measured for each well (initial luminescence). After measuring initial luminescence, the plate was incubated in the dark for 30 min. After this incubation step, the six wells per sample were divided into two groups of three wells each. To the first group, 1 µL of flg22 solution (10 µM, 0.1 % (v/v) dimethylsulfoxide (DMSO)) was added, yielding a final flg22 concentration of 100 nM. To the second group, 1 µL of 0.1 % (v/v) DMSO was added as a control. Then luminescence was measured as before. After this measurement, the plate was shaken gently and incubated in the dark for 90 min before the next measurement. Measurements were then continued in 90 min intervals until 6 h after addition of flg22.

Data evaluation Measurements were plotted as relative light unites (RLU) vs. time after PAMP treatment. To calculate relative induction, averaged RLU values of DMSO-treated sample replicates (controls) were substracted from averaged RLU values of the corresponding PAMP-treated sample replicates for each time point. To calculate fold induction, averaged RLU values of PAMP-treated sample replicates were divided by averaged RLU values of control replicates.

3.9 Bioinformatics

3.9.1 Structural modeling of proteins

Structural homology modelling was performed using an enhanced version of the Vector Alignment Search Tool (VAST+; **Madej et al., 2014**), a tool which uses geometric

datasets based primarily on crystal structures annotated in the Molecular Modelling Database (MMDB; **Madej et al., 2012**). Partial structural alignments were generated in a sequence-agnostic way by searching for conserved so-called "biounits" using the VAST+ algorithm, which is based on position specific scoring matrices (PSSMs, **Kann et al., 2005**). Aligned biounits were visualized using the Cn3D tool (**Wang et al., 2000**). Non-aligned biounits were then added to the visualization by pulling the respective geometric datasets from the MMDB structural data.

3.10 Statistics

Unpaired Student's *t* test was performed using the GraphPad QuickCalc *t* test calculator (GraphPad Software, La Jolla, USA).

CHAPTER 4

RESULTS

4.1 Heterologous expression and purification of target proteins from *E. coli*

4.1.1 Synthetic constructs for heterologous expression

Synthetic constructs containing cytoplasmic domains (CDs) of *A. thaliana* BAK1, BRI1, and FLS2 with C-terminal His-tags for purification in the bacterial expression vector pet22 have been provided by N. Wagener (unpublished data, figure **4.1**). A synthetic construct linking full-length *S. lycopersicum* Pto with a N-terminal His-tag for purification (figure **4.2**) has been cloned into the bacterial expression vector pJC40 as described in section **3.3.7**. As MST experiments need a fluorescent label to monitor protein-protein interactions (see section **3.7.1.1**), a synthetic construct for expressing *P. syringae* (DC3000) AvrPto linked to an mOrange fluorescent tag (figure **4.3**) has been generated as described before. Table **4.1** summarizes the molecular properties of all synthetic constructs and introduces the short-hand construct nomenclature that will be used for the remainder of this chapter.

Table 4.1 Molecular properties for synthetic expression constructs

Construct	**Nº AAs**	**MW** (kDa)	**pI**	**Organism of origin**
BAK1-CD	353	39.8	5.81	*A. thaliana*
BRI1-CD	340	37.8	6.49	*A. thaliana*
FLS2-CD	330	36.9	5.65	*A. thaliana*
Pto	345	39.2	6.51	*S. lycopersicum*
mO-AvrPto	432	48.4	6.56	synthetic / *P. syringae*

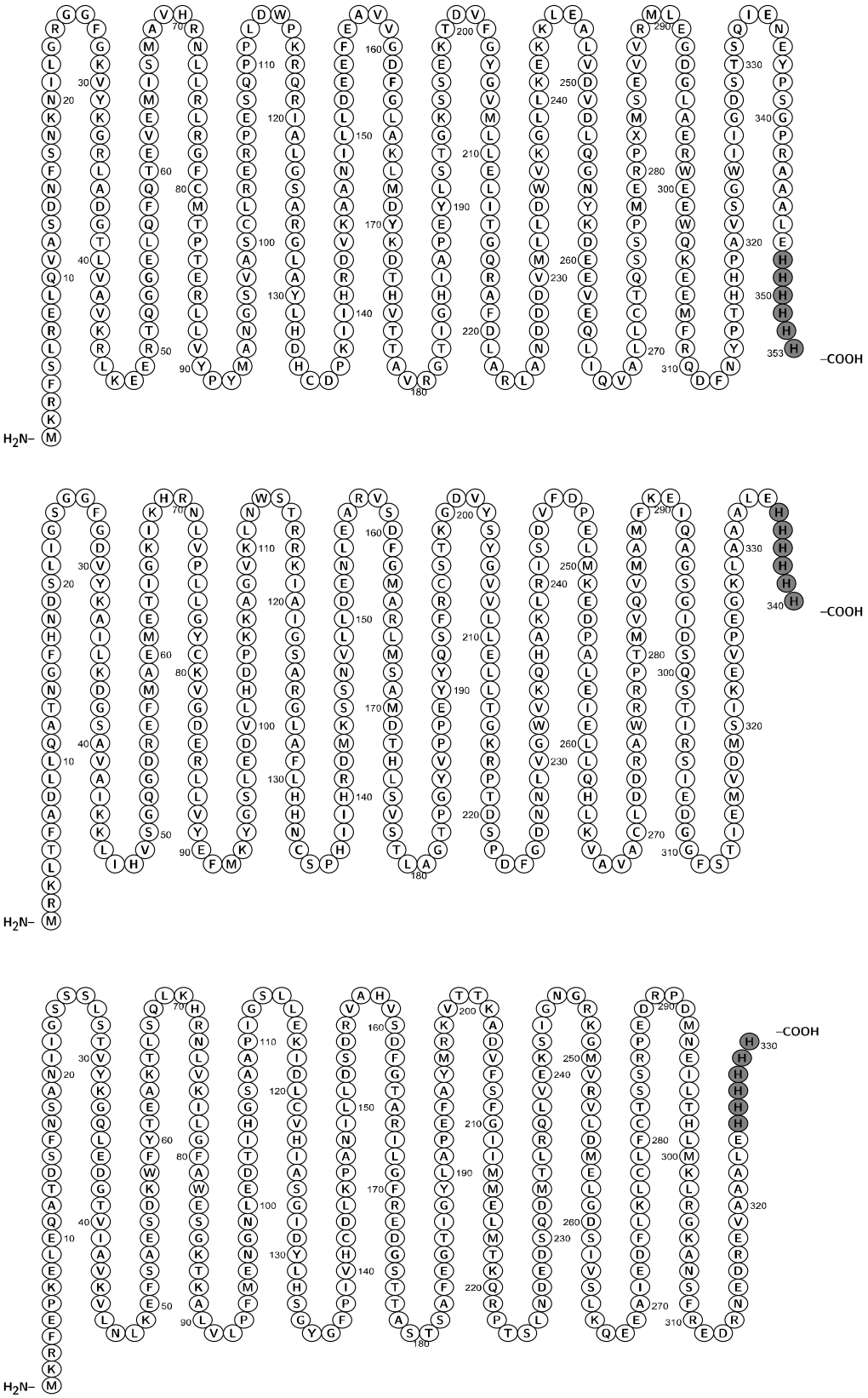

Fig. 4.1 *A. thaliana* RLK-CD his-tagged constructs (amino acid sequence). **A**, BAK1-CD, **B**, BRI1-CD, **C**, FLS2-CD. Functional domains are indicated by shading. Dark grey, His tag (purification tag); white, CD. Amino acids are given in single-letter code. *Note*: numbering is specific to the synthetic construct and does not correspond to any database annotated residue numbers.

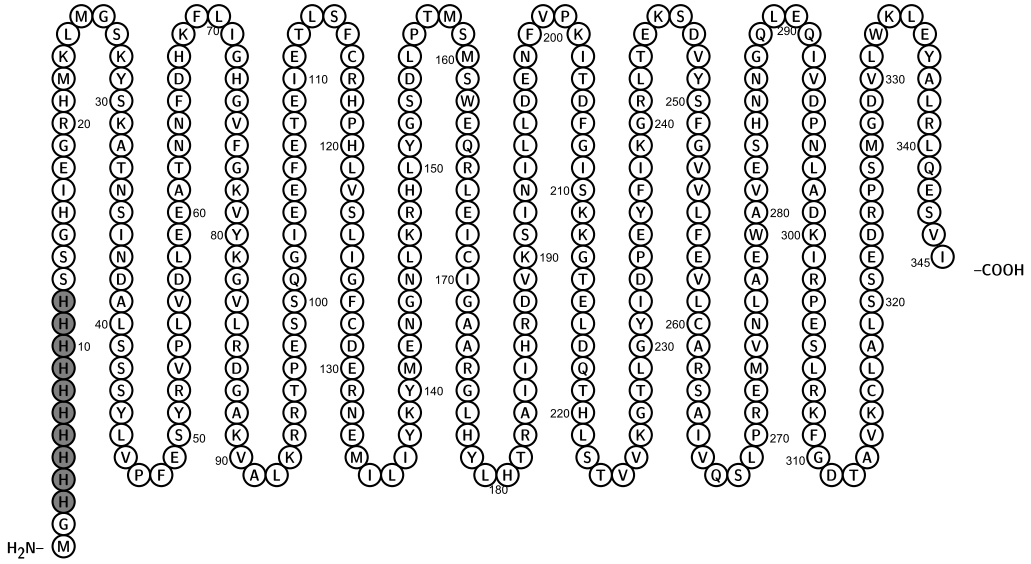

Fig. 4.2 Pto his-tagged construct (amino acid sequence). Functional domains are indicated by shading. Dark grey, His tag (purification tag); white, Pto. Amino acids are given in single-letter code. *Note*: numbering is specific to the synthetic construct and does not correspond to any database annotated residue numbers.

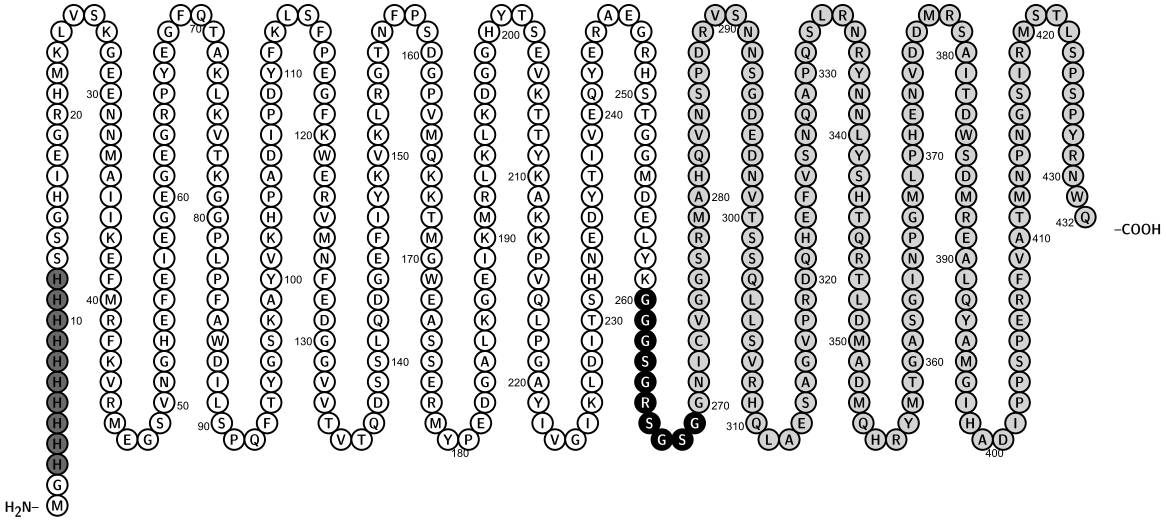

Fig. 4.3 mOrange-AvrPto fusion construct (amino acid sequence). Functional domains are indicated by shading. Dark grey, His tag (purification tag); white, mOrange (fluorescence tag); black, flexible linker (domain separator); light grey, AvrPto (effector). Amino acids are given in single-letter code. *Note*: numbering is specific to the synthetic construct and does not correspond to any database annotated residue numbers.

4.1.2 Expression analysis

Time course experiments Expression analysis of *A. thaliana* RLK-CD clones (figure **4.4**) was performed as described in section **3.1.2.3**. In the case of BAK1-CD, phosphorylation can be observed indirectly in a CBB-stained gel as an apparent shift in migration size (**Peck, 2006**; the shift is indicated by solid arrow in figure **4.4**). Prolonged expression time increased the ratio of phoshorylated to unphosphorylated BAK1-CD with a maximum at 2-3 h post induction. This phosphorylation-dependent shift in apparent migration size is not visible for BRI1-CD at the attained expression levels, although kinase activity assays demonstrated autophosphorylation activity (see section **4.1.4**). Consistent with previous reports that FLS2 is a weak kinase with undetectable autophosphorylation activity *in vitro* (**Schwessinger et al., 2011**), the expression product migrates as a single band. In contrast to BAK1-CD and BRI1-CD, maximum expression levels were obtained by expressing for 16 h at 18 °C (figure **4.4**, **C**). Very low soluble expression levels and a severe reduction in bacterial growth rates were obtained using expression strain ROSETTA, indicating toxicity of the expression product to *E. coli*; this problem could be partially abrogated by the use of strain BL21AI, which provides more stringent repression of expression in the non-induced state by controlling expression through the arabinose-inducible araBAD promoter (**Chao et al., 2002**). However, expression levels for FLS2-CD remained relatively low compared to those obtained for all other proteins used in this work.

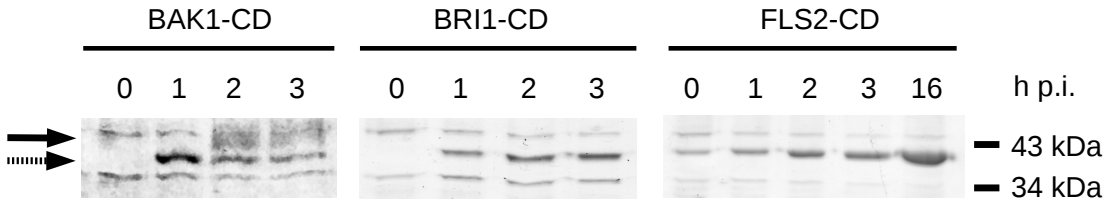

Fig. 4.4 *A. thaliana* RLK-CDs expression time course experiment (expression strain ROSETTA, total cell extracts loaded on gel). SDS-PAGE with CBB staining. Expression temperature was 28 °C for time points 0 - 3 h p.i. and 18 °C for time points 16 h p.i. Solid arrow, phosphorylated form of BAK1-CD, dashed arrow, unphosphorylated form. h p.i., hours post expression. *Note*: composite image, not quantitative; individual image brightness has been adjusted.

Expression product is only partly soluble To test the amount of soluble vs. insoluble protein that resulted from heterologous expression in *E. coli*, protein extraction was performed as described in section **3.1.2.4** but in the presence of varying amounts of sodium lauroyl sarcosinate (sarkosyl) to facilitate the solubilization of inclusion bodies (**Frankel et al., 1991**). Figure **4.5** shows a pilot experiment demonstrating that a large amount of BAK1-CD is retained in the insoluble fraction and can be solubilized using sarkosyl.

However, due to the fact that the solubilized protein was shown to lack autophoshorylation activity (see section **4.1.4**, figure **4.10 B**), the amount of BAK1-CD in the soluble fraction was increased by varying expression parameters; optimization experiments showed that while prolonged expression (>3 h) increased the total amount of expressed protein, the maximum amount of soluble protein was obtained using short expression times (1–3 h at 28 °C); this correlated with a high amount of autophosphorylation activity as observed in the appearance of a slower-migrating phosphorylated state (as described previously).

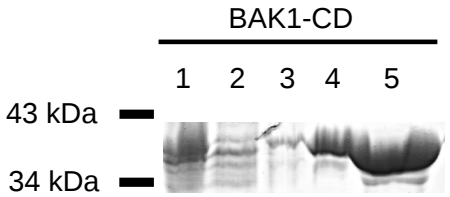

Fig. 4.5 Extraction of *A. thaliana* BAK1-CD from *E. coli* (expression 16 h at 18 °C) in the absence or presence of sarkosyl. SDS-PAGE with CBB staining. **1**, whole cell lysis; **2**, soluble extract (buffer without sarkosyl); **3**, 0.1 % (w/v) sarkosyl; **4**, 1 % (w/v) sarkosyl; **5**, 10 % (w/v) sarkosyl. Equal amounts (by volume) were loaded onto the gel for each lane.

Expression of mOrange-AvrPto Expression conditions for the synthetic mOrange-AvrPto fusion construct were optimized (section **3.1.2.3**), indicating little soluble expression at higher temperatures ($\geq$28 °C, data not shown) and using expression strain ROSETTA, but high amounts of soluble expression after 16 h at 18 °C using expression strain BL21AI, as shown in figure **4.6**. In induced cells, the appearance of a double band can be observed (Figure **4.6 C**) with the main target band corresponding to a size of 45 kDa. A secondary band at an apparent size of $\sim$30 kDa likely corresponds to a truncated version or a degradation product (for more detail, see section **4.1.3**).

Summary of optimized conditions Table **4.2** gives a brief overview of the optimized bacterial expression conditions for the synthetic constructs used in this work.

Table 4.2 Optimized bacterial expression conditions

Construct	**Strain**	$c_{inducer}$	**t** (h)	**T** (° C)
BAK1-CD	ROSETTA	1 mM	3	28
BRI1-CD	ROSETTA	1 mM	3	28
FLS2-CD	BL21AI	0.05 %	16	18
Pto	BL21AI	0.05 %	16	18
mO-AvrPto	BL21AI	0.05 %	16	18

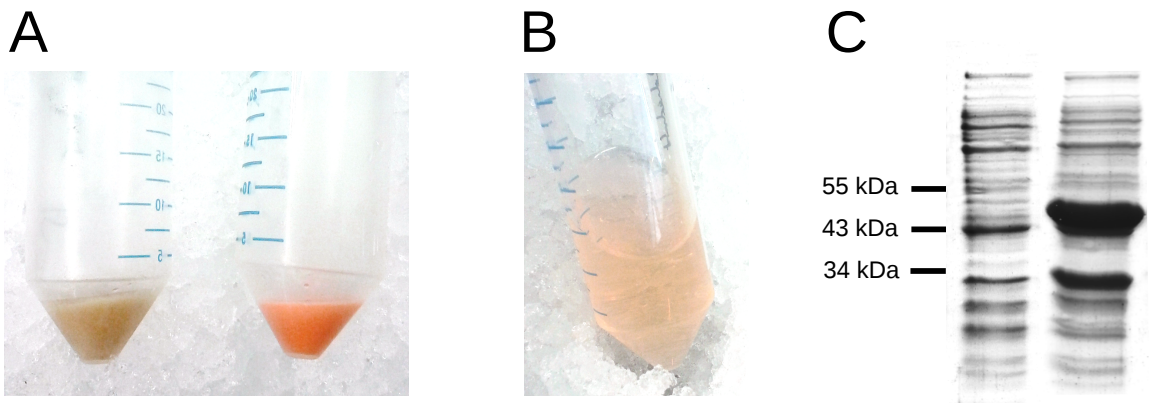

Fig. 4.6 Bacterial expression (BL21AI) of mOrange-AvrPto fusion construct. Cells were harvested after 16 h of expression at 18 °C. **A**, orange color originating from the mOrange moiety fluorescence can be observed in cell pellet after expression (right tube). **B**, the color is retained in the soluble crude extract. **C**, soluble crude extract of noninduced (left) and induced (right) cells in SDS-PAGE with CBB staining.

4.1.3 Purification

***A. thaliana* CDs and Pto** Optimization of purification procedures was performed using BAK1-CD as described in section **3.5**, using affinity chromatography (AC) and size exclusion chromatography (SEC) steps, followed by SDS-PAGE to examine yield and purity, and *in vitro* kinase activity assays (section **4.1.4**) to determine biochemical functionality of the purified protein. The resulting optimized work flow was limited to a single AC step, as subsequent further purification steps resulted in reduced yield and post-purification concentration of protein resulted in loss of observable kinase activity (see section **4.1.4**, figure **4.10**, **B**). A representative purification is shown in figure **4.7**. Purification procedures for mutagenized variants of BAK1-CD, BRI1-CD, FLS2-CD, and Pto was performed analogously to that of BAK1-CD.

mOrange-AvrPto Affinity chromatography purification of mOrange-AvrPto (figure **4.8**, **A**, **B**) consistently resulted in the presence of secondary bands migrating at a lower molecular weight than the predicted target protein size in addition to the dominant band (figure **4.8**, **C**). Further attempts of purification by size exclusion chromatography (SEC) failed to show an effect, as the different apparent molecular sizes could not be resolved. The chromatogram shows two prominent peaks (figure **4.9**, **A**), which both contain the same molecular species (figure **4.9**, **B**; the first elution peak likely corresponds to higher-order complexes of mOrange-AvrPto).

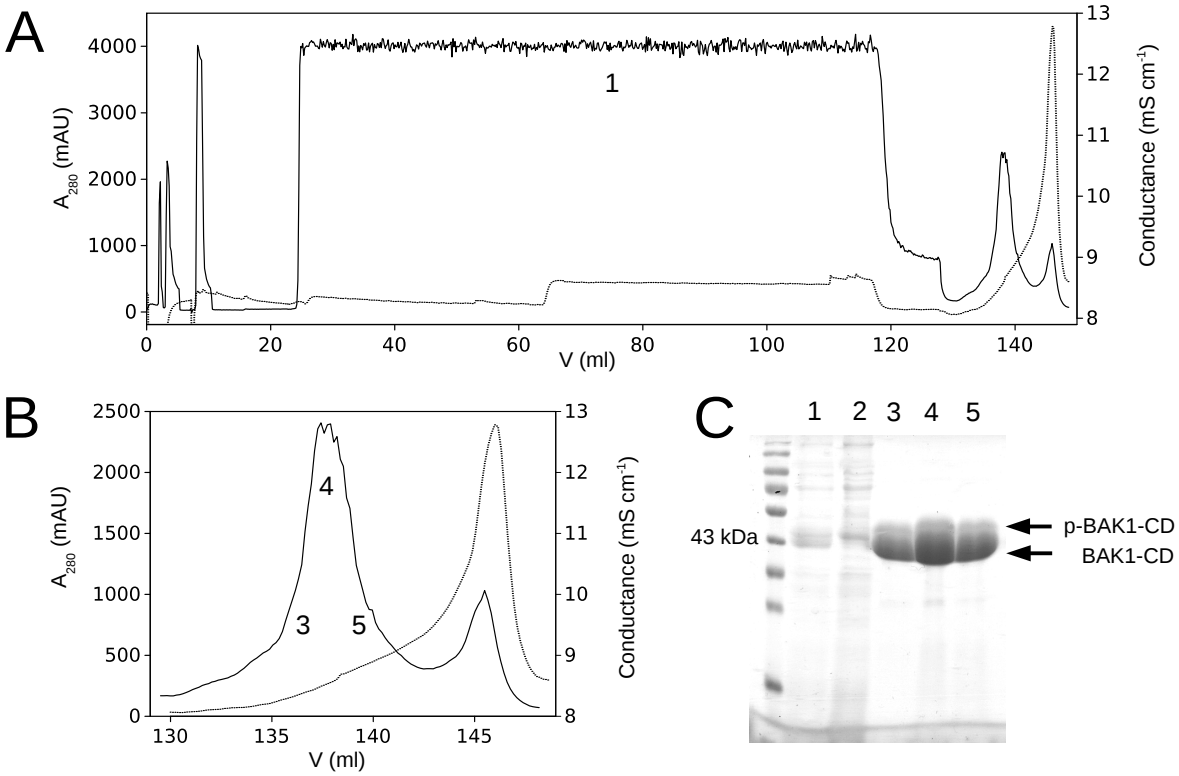

Fig. 4.7 Purification of BAK1-CD. **A**, affinity chromatography (AC; GE Healthcare HisTrap, 1 ml), complete run. Initial signal peaks are washing steps. Bacterial crude extract was applied to the column at cumulative volume of ∼25 mL, and sample loading was stopped at cumulative volume of ∼125 mL. Elution (imidazol gradient) was started at cumulative volume of ∼130 mL. A final wash is performed after the main elution peak at a cumulative volume of ∼143 mL Black curve is total absorption at 280 nm, indicating amount of protein. Dotted curve is conductance, indicating elution gradient (imidazol). The numbers indicate the corresponding lanes in (**C**). **B**, enlargement of elution step. Curves are as described above. The numbers indicate the corresponding lanes in (**C**). **C**, SDS-PAGE on different steps of purification procedure. 1, raw extract; 2, flow-through (non-bound material during column loading); 3, 4 and 5 correspond to different time points during elution, as seen in (**B**). Each lane was loaded with 20 µL of the indicated sample.

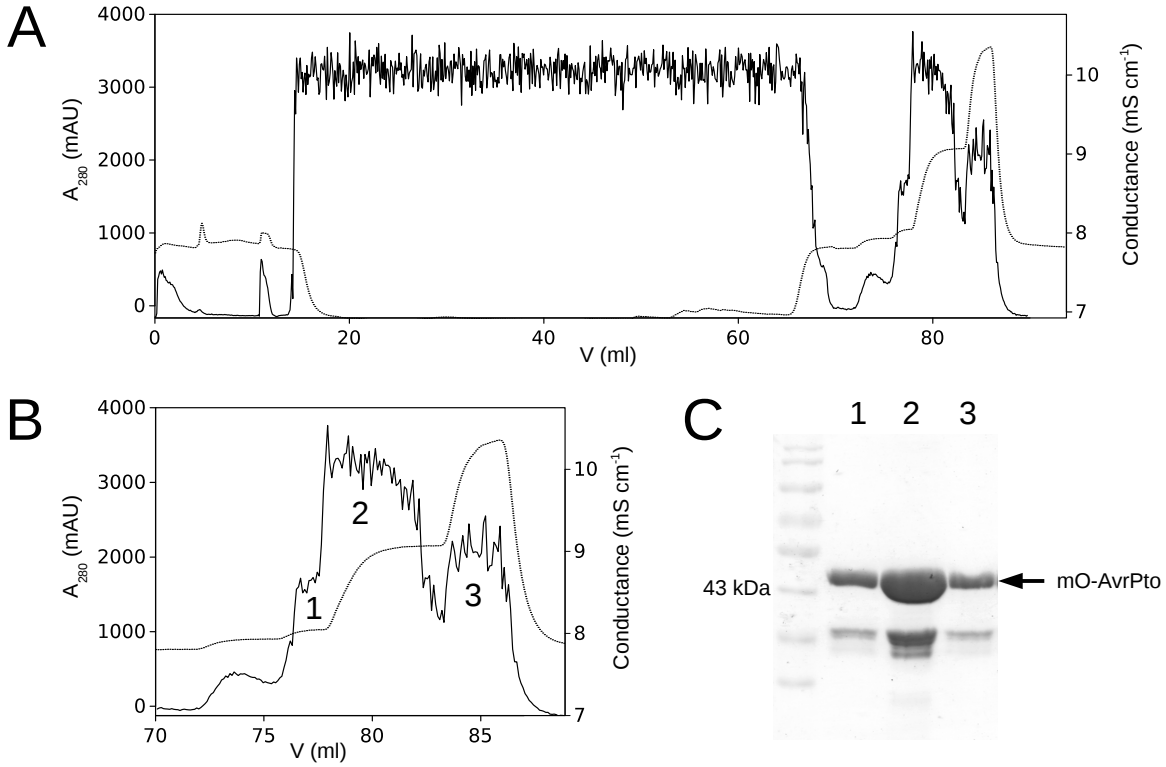

Fig. 4.8 Purification of mO-AvrPto. **A**, affinity chromatography (GE Healthcare HisTrap, 1 ml), complete run. Initial signal peaks are washing steps. Bacterial crude extract was applied to the column at cumulative volume of ∼15 mL, and sample loading was stopped at cumulative volume of ∼70 mL. Elution (imidazol step gradient: 50 mM, 250 mM, 500 mM) was started at cumulative volume of ∼72 mL. Black curve is total absorption at 280 nm, indicating amount of protein. Dotted curve is conductance, indicating elution gradient (imidazol). **B**, enlargement of elution step. Curves are as described above. The numbers indicate the corresponding lanes in (**C**). **C**, SDS-PAGE on AC elution fractions. 1, 2 and 3 correspond to different time points during elution (steps of gradient), as seen in (**B**). Each lane was loaded with 2 µL of the indicated sample.

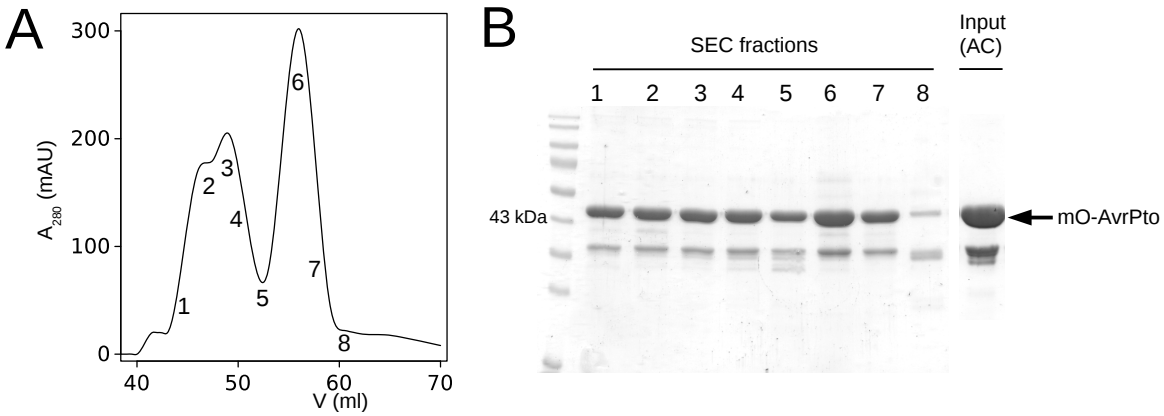

Fig. 4.9 Attempted further purification of mO-AvrPto. **A**, size exclusion chromatography (SEC; GE Healthcare HiLoad 16/600, Superdex 75). Peak fractions were harvested from 42 to 62 ml. Cumulative volume is relative to sample injection. Numbers indicate the harvested fraction as analysed in (**B**). **B**, SDS-PAGE on SEC elution fractions. SEC fraction lanes were loaded with 20 µL of sample each. The input (AC faction) is given for comparison purposes. *Note*: picture is a composite image consisting of lanes run on different gels (SEC fractions / input), and is only intended for visual comparison of band patterns.

4.1.4 *In vitro* kinase activity assays

Viability of *in vitro* kinase assays It has been demonstrated before that autophosphorylation of purified BAK1-CD can be observed *in vitro* (**Wang et al., 2008**). Similar findings have been obtained for BRI1-CD; in contrast, FLS2-CD kinase activity seems to be hardly detectable *in vitro* using the same assay format (**Schwessinger et al., 2011**). In this study, kinase activity assays have been performed mainly to validate the molecular function of purified proteins, in order to establish streamlined expression, purification, and handling procedures for subsequent use of protein samples in interaction assays.

Kinase activity assays for purified BAK1-CD To test the influence of different handling steps in protein purification on kinase activity, several aliquots were treated differently and tested in the same format. Figure **4.10** shows autoradiographs obtained from various aliquots of purified BAK1-CDs which were either stored under different conditions (figure **4.10 A**) or have undergone treatments to optimize soluble protein concentration (figure **4.10 B**). Storage of BAK1-CD for 7 d at 4 °C has a detrimental effect on autophosphorylation, while short-term storage for 1 d at 4 °C or a single freeze-thaw-cycle result in similarly high amounts of autophosphorylation. Precipitating purified BAK1-CD with ammonium sulfate and re-suspending the precipitate in a smaller volume of buffer to increase soluble concentration results in a complete loss of autophosphorylation activity. Similarly, purifying BAK1-CD from the insoluble fraction of bacterial expression using sarkosyl detergent also results in a complete loss of autophosphorylation activity. Due

to these results, the standard work flow adopted for all subsequent protein purification procedures consisted of a single affinity chromatography step, immediately followed by dialysis (16 h, 4 °C) to remove the imidazol used for elution, and subsequent flash-freezing (liquid N_2) of single-use aliquots; no post-purification attempts at increasing protein concentration were performed due to their negative effect on BAK1-CD kinase activity. All purified proteins used for downstream interaction assays were prepared in the same manner for reproducibility.

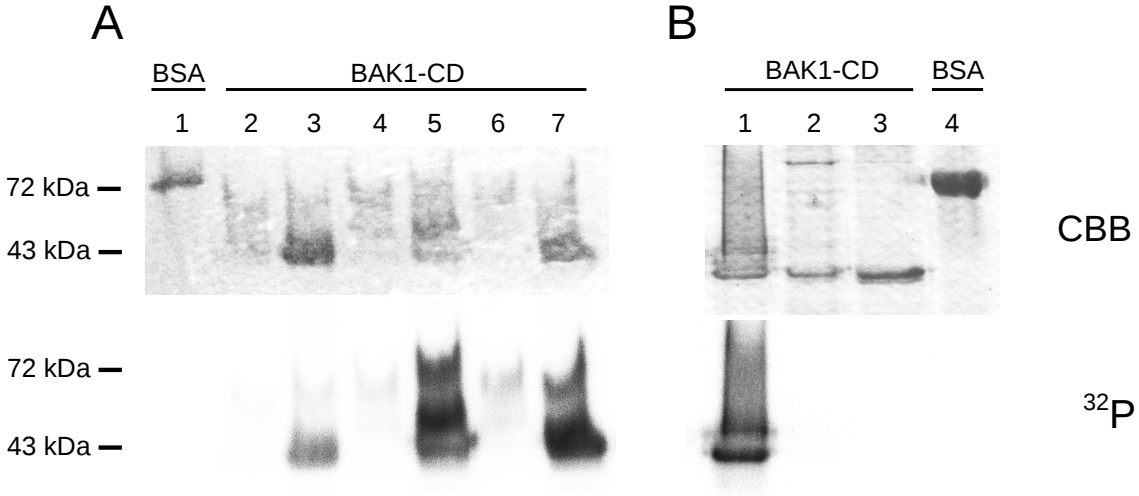

Fig. 4.10 Kinase activity assay of *A. thaliana* BAK1-CD using different treatments post-purification. **A**, influence of storage conditions. **1**, BSA (5 µg); **2**, BAK1-CD stored for 7 d at 4 °C (5 µg); **3**, BAK1-CD stored for 7 d at 4 °C (10 µg); **4**, BAK1-CD stored for 1 d at 4 °C (5 µg); **5**, BAK1-CD stored for 1 d at 4 °C (10 µg); **6**, BAK1-CD frozen and thawed once (5 µg); **7**, BAK1-CD frozen and thawed once (10 µg). **B**, influence of treatments for optimizing concentration. **1**, BAK1-CD without further treatment (10 µg); **2**, BAK1-CD concentrated threefold by ammonium sulfate precipitation (10 µg); **3**, BAK1-CD solubilized from inclusion bodies using sarkosyl (10 µg); **4**, bovine serum albumin (BSA, 10 µg).

Kinase activity assays for purified BRI1-CD *In vitro* autophosphorylation of recombinant BRI1-CD has been demonstrated before (**Wang et al., 2005**). To test whether the BRI1-CD purification procedure resulted in kinase-active protein, a kinase activity assay using BRI1-CD (and BAK1-CD for comparison purposes) has been performed (figure **4.11**). Purified BRI1-CD shows a strong autophosphorylation that is similar in magnitude to that of purified BAK1-CD, despite the apparent lack of a distinct second, slower-migrating band due to phosphorylation-induced mobility shift in SDS-PAGE (section **4.1.2**). These results indicate that purification of BRI1-CD results in similarly kinase-active protein as BAK1-CD, confirming the suitability of the expression and purification work flow for RLK cytoplasmic domains.

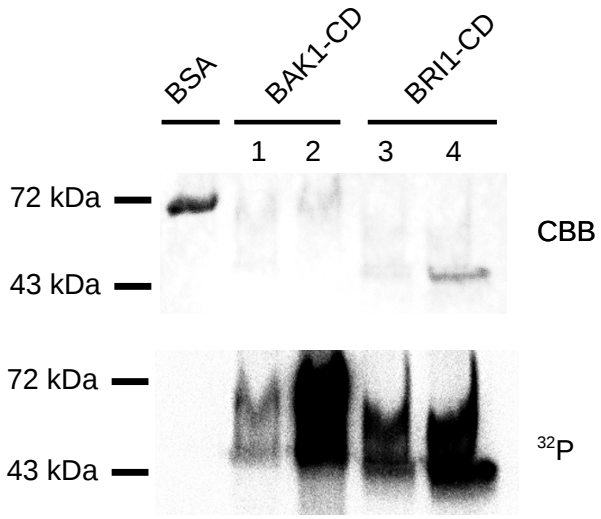

Fig. 4.11 Kinase activity assay of purified *A. thaliana* BAK1-CD and BRI1-CD. **1**, BAK1-CD aliquot 1 (5 µg; **2**, BAK1-CD aliquot 2 (5 µg); **3**, BRI1-CD aliquot 1 (3 µg); **4**, BRI1-CD aliquot 2 (5 µg). Bovine serum albumin (BSA, 5 µg) was used as a control.

Influence of AvrPto on BAK1-CD kinase activity AvrPto was described as an inhibitor of Pto kinase activity in previous studies (**Xing et al., 2007**) and was shown to lower FLS2-CD autophosphorylation *in vitro* (**Xiang et al., 2008**). On the other hand, AvrPto was previously reported to be phosphorylated *in planta* by a Pto- and Prf-independent kinase activity (**Anderson et al., 2006**). To test the influence of AvrPto on *in vitro* BAK1 phosphorylation, a titration experiment has been performed using equal amounts of BAK1-CD and varying amounts of AvrPto (figure **4.12**). The presence of purified mOrange-AvrPto is seen as the appearance of a double band with the upper band corresponding to the full-length construct with an apparent size of ∼45 kDa and a secondary lower band with an apparent size of ∼30 kDa. Total signal corresponding to labeled phosphates remains approximately constant in all lanes; upon increasing the concentration of mOrange-AvrPto, phosphorylation slightly decreases on BAK1-CD and increases on mOrange-AvrPto. No similar transphosphorylation is seen on the BSA control. A very similar effect has been observed before for the interaction of a different effector protein, AvrPtoB, with BAK1-CD (**Cheng et al., 2011**). While transphosphorylation of mO-AvrPto by BAK1-CD is readily apparent, it is more diffcult to determine if the effect on BAK1-CD autophosphorylation is truly indicative of mO-AvrPto-mediated inhibition of autophosphorylation activity. The total magnitude of BAK1-CD autophosphorylation signal intensity shift during the mO-AvrPto titration (figure **4.12**, lanes 2-5), considering the amount of mO-AvrPto used, is rather low (roughly, <50 %); together with the fact that the 'BAK1-CD + BSA' sample (lane 6) shows less autophosphorylation signal than BAK1-CD alone (lane 1), although the amount of BAK1-CD loaded onto the

gel was the same (CBB staining), these results preclude quantitative analysis. Although not strictly comparable due to different experimental formats, it should be noted previous studies based on protoplast Co-IP did not show a difference in (BL-stimulated) BAK1 and BRI1 phosphorylation in the presence or absence of AvrPto (**Shan et al., 2008**, supplemental).

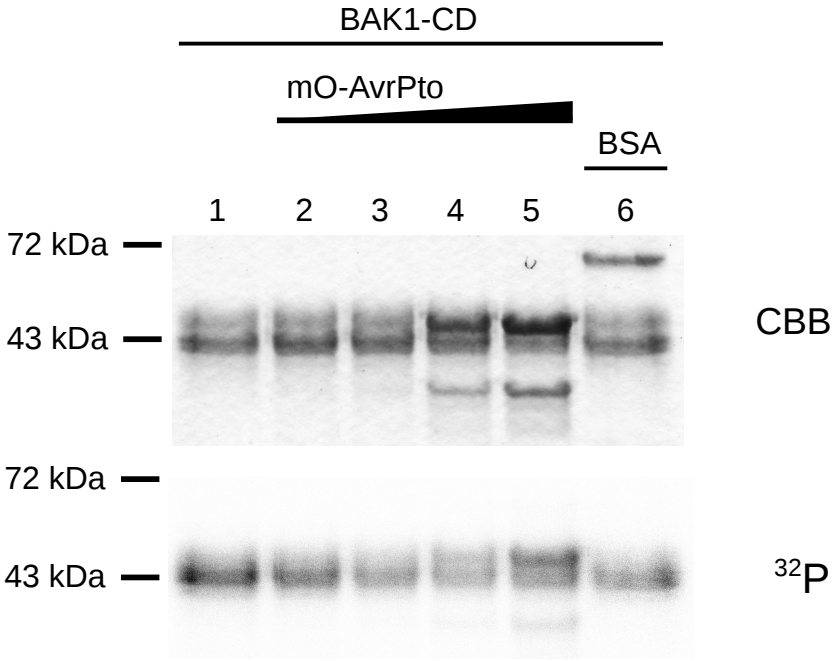

Fig. 4.12 Kinase activity assay of *A. thaliana* BAK1-CD with different concentrations of mOrange-AvrPto (mO-AvrPto). **1**, BAK1-CD (2 µg); **2**, BAK1-CD (2 µg) + mO-AvrPto (10 ng); **3**, BAK1-CD (2 µg) + mO-AvrPto (100 ng); **4**, BAK1-CD (2 µg) + mO-AvrPto (1 µg); **5**, BAK1-CD (2 µg) + mO-AvrPto (2 µg); **6**, BAK1-CD (2 µg) + BSA (2 µg).

4.2 Determination of steady-state binding affinities for AvrPto / RLK interactions

4.2.1 AvrPto interacts with BAK1 in MST experiments

Steady-state affinity for binary interactions between mO-AvrPto and BAK1-CD was determined by MST, using fluorescently labelled mO-AvrPto at fixed concentrations of 50 nM and titrations of BAK1-CD over four orders of magnitude (between approximately 0.5 nM and 5 µM). Averaged affinity for the interaction (at 40 % gradient intensity, $n = 3$ experiments) was 45 ($\pm$8) nM. Experimental data allowed fitting to an idealized steady-state binding model with good fidelity, with a clear inflection point and both baseline (no complex formation) and saturation (full complex formation) levels being

reached (figure **4.13**). Notably, the steady-state affinity of BAK1-CD to AvrPto is higher than any formerly reported affinity of AvrPto to other putative interactants as determined in previous studies (see section **4.2.3, figure 4.16** for quantitative comparisons and corresponding citations).

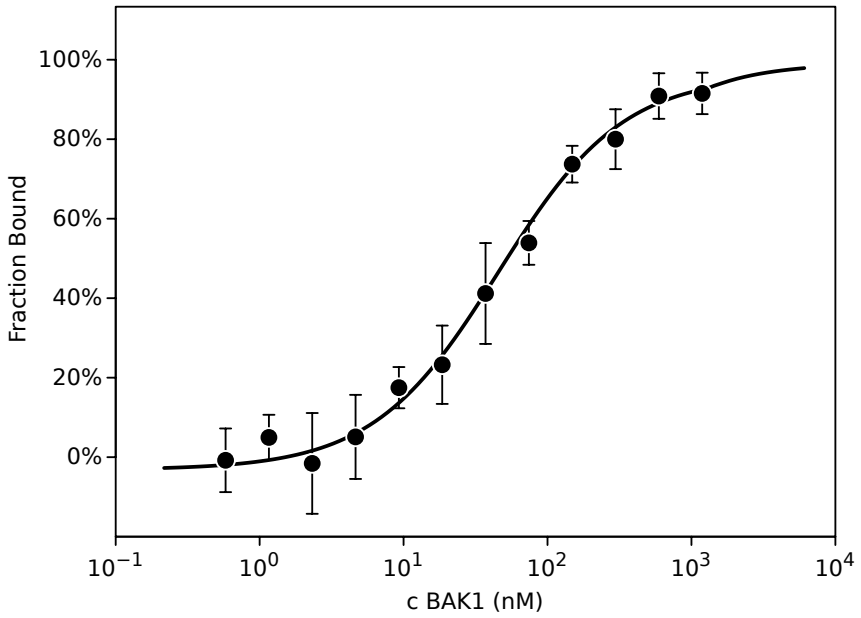

Fig. 4.13 Steady-state affinity determination for the interaction pair BAK1-CD and mOrange-AvrPto. The fraction bound was plotted in dependence of BAK1-CD concentration in each capillary. Each data point was averaged from 3 independent experiments. Error bars are SD.

4.2.2 Temperature gradient strength does not significantly influence binding

To test whether the affinity is influenced by the intensity of the experimentally induced temperature gradient, experiments were additionally performed at 20 % and 80 % gradient intensity, yielding affinities of 33 ($\pm$17) nM and 39 ($\pm$4) nM, respectively (figure **4.14**; $n = 3$ experiments), which are insignificant differences ($p = 0.50$ and 0.18, respectively) compared to the value obtained for experiments using a 40 % gradient intensity.

4.2.3 Pto and FLS2 show weaker interaction with AvrPto

Full-length Pto and FLS2-CD were tested for interaction with mOrange-AvrPto analogous to BAK1-CD. Affinities determined (at 40 % gradient intensity) were 239 ($\pm$82) nM for FLS2-CD (figure **4.15 A**, $n = 3$ experiments) and 133 ($\pm$46) nM (figure **4.15 B**, $n = 3$ experiments) for Pto. There is a noticable increase in systematic noise at low protein

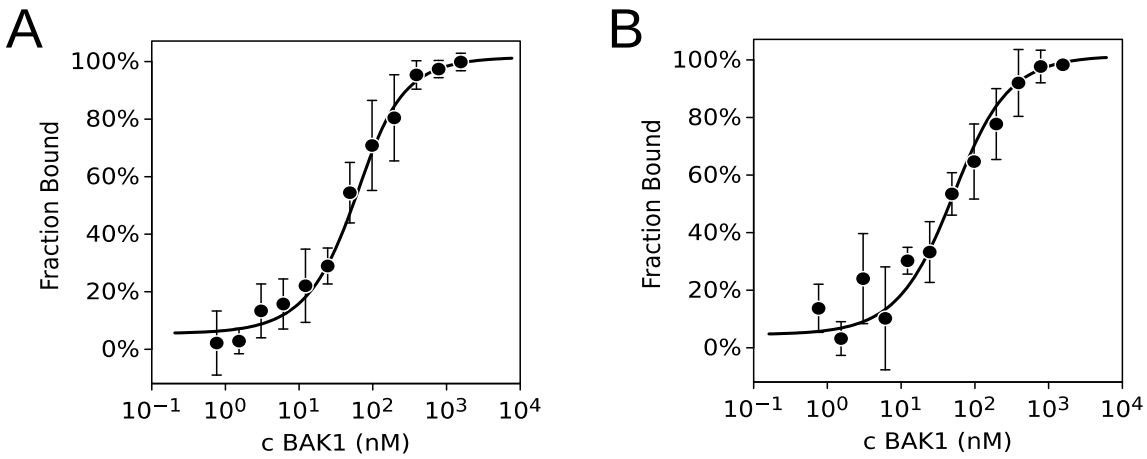

Fig. 4.14 Steady-state affinity determination for the interaction pair BAK1-CD and mOrange-AvrPto at different temperature gradient settings. **A**, 20 % gradient intensity; **B**, 80 % gradient intensity. The fraction bound was plotted in dependence of BAK1-CD concentration in each capillary. Data is averaged from 3 independent experiments. Error bars are SD.

concentrations compared to the experiments including BAK1-CD, which is due to an overall lower magnitude of fluorescence shift for these experiments. Due to solubility issues, higher concentrations of FLS2-CD could not be obtained, which decreases the fidelity of the determination of the lower bound of steady-state affinity, as it is difficult to determine whether the saturation phase of the reaction has truly been reached (note fitting curve at high FLS2 concentrations, figure **4.15**, **A**). Figure **4.16**, **A** shows a comparative overview of the different steady-state affinities as determined by MST. These results demonstrate that compared to the interaction with BAK1-CD, the interaction of mO-AvrPto with FLS2-CD is approximately 5 times weaker, and the interaction with Pto is approximately 3 times weaker. For comparison purposes, previous experimental data for AvrPto binding affinities obtained by other groups is given in figure **4.16**, **B**, indicating generally good agreement of these datasets to the results obtained in this study.

4.2.4 No interactions can be observed for AvrPto with BRI1 and negative controls

Using the same experimental setup as in the previously described MST experiments, no interaction could be observed for the interaction pair mO-AvrPto with BRI1-CD (Figure **4.17, A**). Two additional interaction pairs were studied as negative controls: mO-AvrPto was tested for interaction with bovine serum albumin (BSA, figure **4.17, B**) and BAK1-CD was tested for interaction with mOrange (lacking the AvrPto moiety; figure **4.17, C**). No interaction could be observed for the negative controls ($n = 2$ experiments each).

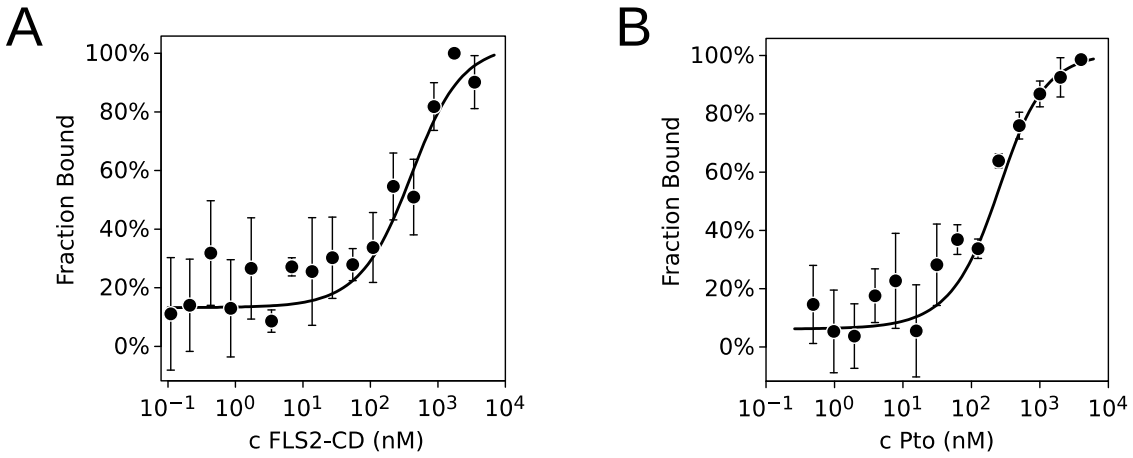

Fig. 4.15 Steady-state affinity determination for the interaction pairs FLS2-CD and mOrange-AvrPto (**A**), as well as Pto and mOrange-AvrPto (**B**). The fraction bound was plotted in dependence of unlabeled protein concentration in each capillary. Data is averaged from 3 independent experiments. Error bars are SD.

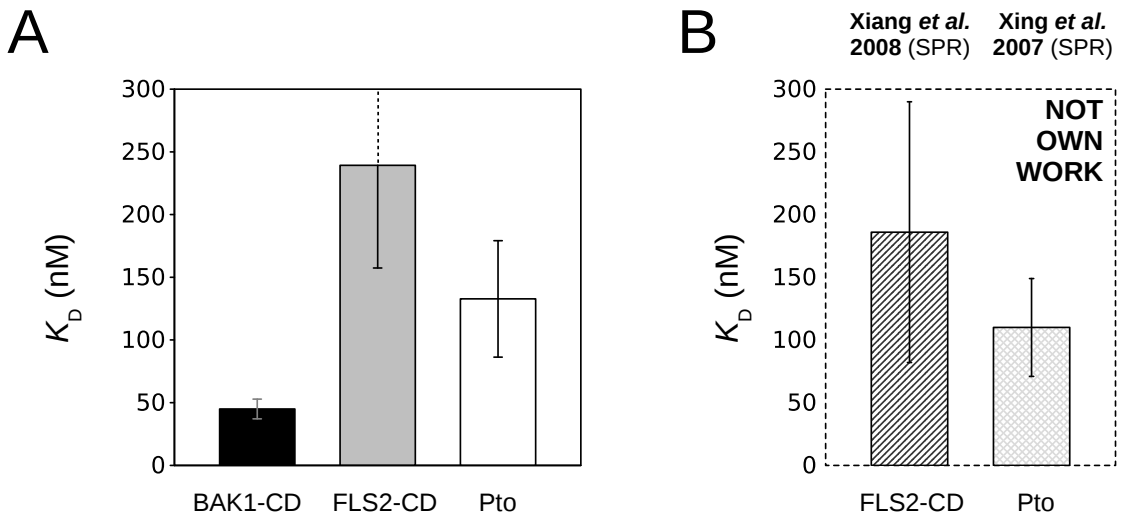

Fig. 4.16 **A**, Overview of steady-state affinities as determined by MST. Black bar, BAK1-CD; grey bar, FLS2-CD; white bar, Pto. Only the lower margin of error is shown for FLS2-CD, as determination of the upper bound was not possible with sufficient certainty using this assay setup. **B**, Previously determined affinities of AvrPto to FLS2-CD (**Xiang et al., 2008**), and AvrPto to Pto (**Xing et al., 2007**). These experiments were performed using SPR in a steady-state configuration.

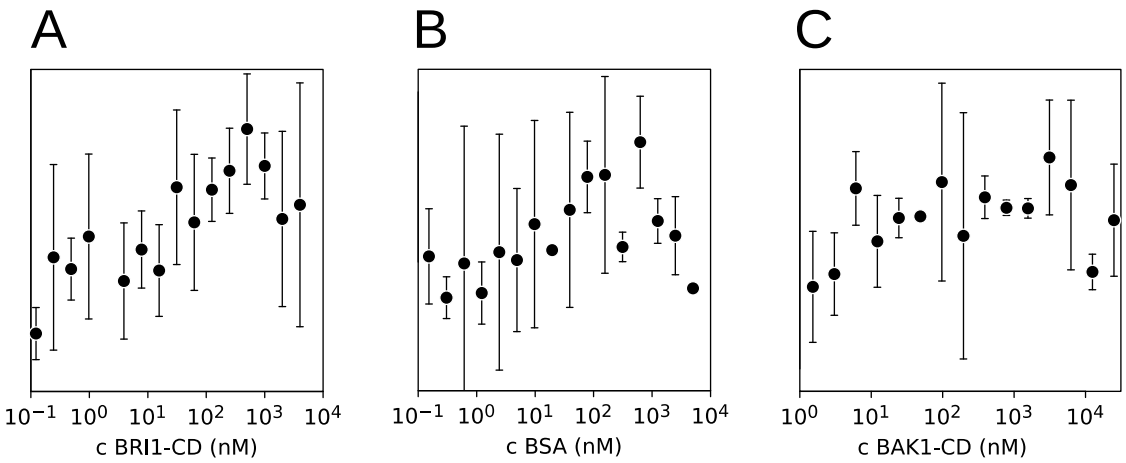

Fig. 4.17 Steady-state MST experiments for interaction pairs which showed no binding; **A**, BRI1-CD / mO-AvrPto, as well as control experiments **B**, BSA / mO-AvrPto; and **C**, BAK1-CD / mOrange. The normalized response values (calculated as in experiments with binding response) were plotted in dependence of unlabelled protein concentration in each capillary. Data is averaged from 2 independent experiments. Error bars are SD. *Note*: The ordinate axis has been omitted in these diagrams as plotting a fraction bound (as in the experiments including a fitting curve) would not be meaningful in this context.

4.3 Kinetic characterization of AvrPto / RLK interactions

As MST experiments give information only on steady-state affinities for any given interactions, surface plasmon resonance (SPR) experiments were performed to elucidate the kinetic background of all interactions described in this study. Additionally to the kinetic characterization, these experiments represent an fundamentally different methodology to arrive at quantitative affinity data.

4.3.1 BAK1 binds AvrPto with high affinity due to fast complex formation

Kinetic parameters To determine kinetic parameters of the mO-AvrPto–BAK1-CD interaction, a single-cycle kinetics titration approach was used. In this experimental set-up, mO-AvrPto was transiently captured on a α-RFP nanobody (RFP-Trap, Chromotek) with very high affinity (< 1 RU min^{-1} baseline signal slope); subsequently, BAK1-CD was serially injected in increasing three-fold concentration steps, with continuous signal recording. Blank- and FC1- referenced experimental cycles were then used for kinetic analysis (for details on referencing methodology, see section **3.7.2.2**). Data curves were fitted using a 1:1 Langmuir binding model via the instrument's evaluation software, resulting in generally good fitting according to quality control (section **3.7.2.3**); this indicates

that the interaction corresponds reasonably well to a simple 1:1 binding stoichiometry without rate-limiting conformational changes or excessive complexity, although minor complexity not accounted for by the model was generally visible as systematic deviations within the quality control thresholds. Kinetic parameters were determined from fitting curves; in turn, affinity was determined from kinetic parameters, yielding non-steady state affinity data. Figure **4.18** shows a representative kinetic experiment with model fitting ($K_D = 40$ nM, pane **A**) and the corresponding quality control using a residuals plot, wich shows deviations of experimental data from the model (pane **B**). Averaging values from three individual experiments, the association rate constant (k_a) for the mO-AvrPto with BAK1-CD interaction was determined as 4.5×10^4 ($\pm$ 2.0×10^4) $mol^{-1}\,s^{-1}$, while the dissociation rate constant (k_d) was determined as 1.45×10^{-3} ($\pm$ 2.7×10^{-4}) s^{-1}. The affinity (K_D) inferred from kinetic parameters was 36 $\pm$ 13 nM.

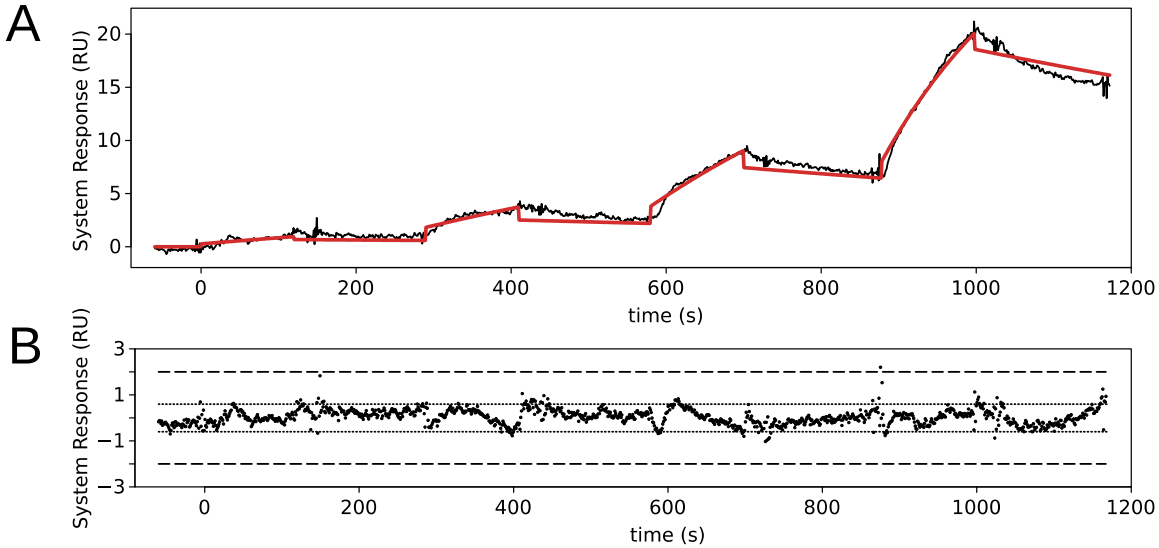

Fig. 4.18 Interaction kinetics of mO-AvrPto and BAK1. **A**, data (black curve) and global kinetic fit to a 1:1 binding model (red curve; $\chi^2 = 0.115$ RU^2, U-value = 1). Injected concentrations were 12.3 nM, 37.5 nM, 111 nM, and 333 nM. **B**, residuals plot showing deviations between data and model. Quality control levels are indicated by the dotted line (inner threshold) and dashed line (outer threshold). The experiment was repeated 3 times with similar results.

Alternative capturing system Due to the difficulties in using an α-RFP nanobody in the FLS2-CD experiments (see section **4.3.3**), and to test the dependence of the interaction on ligand/analyte status for the interactants, kinetic experiments were alternatively performed using an α-his antibody for ligand capture (see section **3.7.2.2**). The roles of ligand and analyte were switched compared to the α-RFP experiments by using BAK1-CD as ligand and mO-AvrPto as analyte. Using this alternative system yielded kinetic parameters similar to those obtained for α-RFP mediated capture (Figure **4.19**,

k_a = 5.9 $\times 10^4$ mol^{-1} s^{-1} , k_d = 1.5 $\times 10^{-3}$ s^{-1}, K_D = 25 nM), indicating that the interaction occurs similarly independent of setting each interactant as either ligand or analyte. This reinforces the notion that the parameters governing the interaction dynamics can be described with reasonable accuracy by a simple 1:1 binding model, as the surface topology and environment of the flow cell does not seem to be influencing binding parameters in a significant way. Note that although the kinetic fitting curve visually appears to better correspond to the data in figure **4.19 A** compared to figure **4.18 A**, this is a secondary effect of the higher total signal amplitude in the former experiment and has no relevance for the actual fitting quality, as observable in the corresponding residual plots (**B** panes), which show very similar acceptable deviations in both cases.

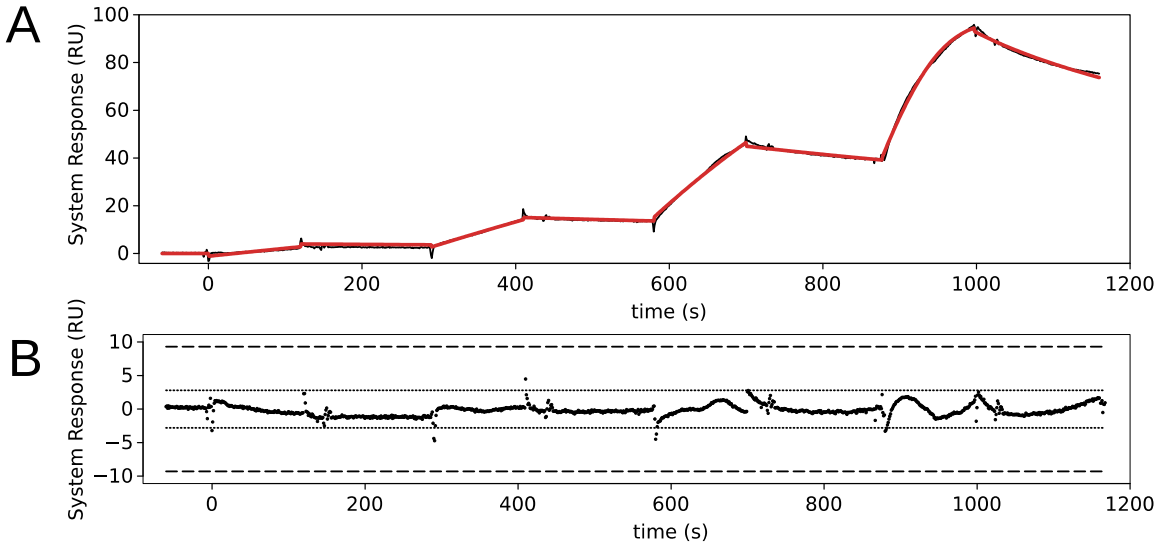

Fig. 4.19 Interaction kinetics of mO-AvrPto and BAK1 (alternative setup). **A**, data (black curve) and global kinetic fit to a 1:1 binding model (red curve; $\chi^2 = 0.744$ RU^2, U-value = 1). Injected concentrations were 12.3 nM, 37.5 nM, 111 nM, and 333 nM. **B**, residuals plot showing deviations between data and model. Quality control levels are indicated by the dotted line (inner threshold) and dashed line (outer threshold). The experiment was repeated 2 times with similar results.

4.3.2 Pto / AvrPto complex formation is slow but very stable

Kinetic paramters Kinetic parameters for mO-AvrPto / Pto interaction were determined using the same experimental setup as described before for the mO-AvrPto / BAK1-CD interaction pair. The association rate is an order of magnitude slower compared to BAK1-CD, with a k_a determined as 3.1 $\times 10^3$ ($\pm$ 1.9 $\times 10^3$) mol^{-1} s^{-1}. However, the dissociation rate is slower as well, with a k_d determined as 2.2 $\times 10^{-4}$ ($\pm$ 1.2 $\times 10^{-4}$) s^{-1}, indicating an exceptionally stable molecular complex. The affinity as determined

from the kinetic parameters was 119 ± 21 nM. Figure **4.20** shows a representative kinetic experiment (K_D = 90 nM).

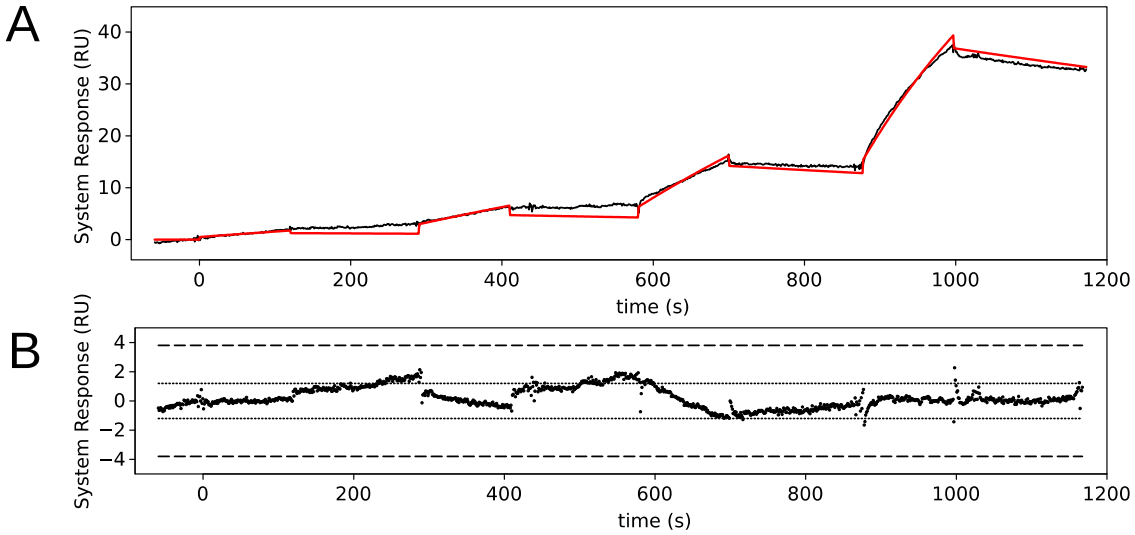

Fig. 4.20 Interaction kinetics of mO-AvrPto and Pto. **A**, data (black curve) and global kinetic fit to a 1:1 binding model (red curve; $\chi^2 = 0.55$ RU^2, U-value = 3). Injected concentrations were 12.3 nM, 37.5 nM, 111 nM, and 333 nM. **B**, residuals plot showing deviations between data and model. Quality control levels are indicated by the dotted line (inner threshold) and dashed line (outer threshold). The experiment was repeated 3 times with similar results.

4.3.3 FLS2 / AvrPto complex dissociates rapidly

FLS2-CD shows strong background binding to the α-RFP nanobody Using the same assay setup as described before for the mO-AvrPto / BAK1-CD and mO-AvrPto / Pto interaction assays resulted in FLS2-CD binding to both sample and reference flow cells, with slightly higher amount of binding in the reference flow cell (figure **4.21**). This indicates that FLS2-CD binds to the α-RFP nanobody which is used to capture mO-AvrPto in this assay setup. Corresponding to these circumstances, the observed binding in the sample flow cell is slightly lower due to partial covering of the nanobody surfaces with mO-AvrPto during ligand injection. Therefore, kinetic evaluation was not possible under these conditions.

FLS2-CD binding to AvrPto can be observed in alternate system To handle the issue of background binding in the α-RFP nanobody capture system, an alternative system using an α-his antibody for capture was used (see section **3.7.2.2**, figure **3.8**). Analogous to the alternative setup experiment with BAK1-CD (see section **4.3.1**), FLS2-CD was used as ligand, mO-AvrPto as analyte. Figure **4.22** shows the result of a representative experiment. Although there are clear binding events occurring, the data does not fit to a

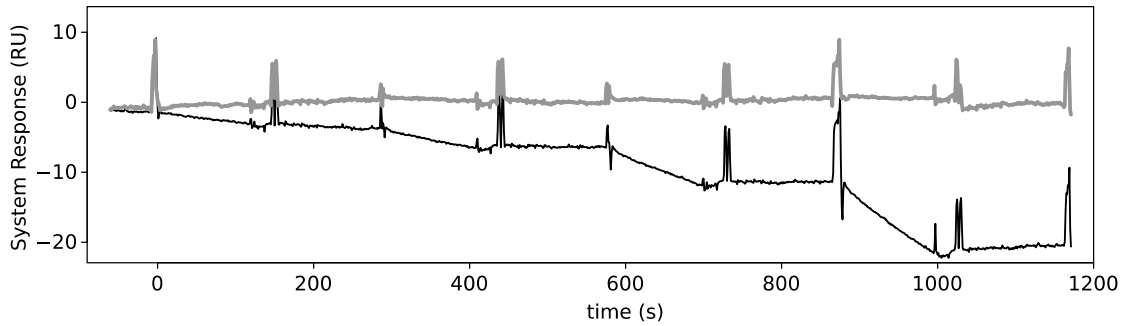

Fig. 4.21 SPR: FLS2-CD background binding. Black curve is reference-subtracted sample data. Injections were 111 nM, 333 nM, 1 µM, and 3 µM. Grey curve is buffer injection.

simple 1:1 binding model with sufficient quality over the whole range of injections (see residuals plot, figure **4.22 B**), making a quantitative kinetic evaluation by global kinetic fitting impossible. Attempts to facilitate kinetic evaluation by loading a smaller quantity of FLS2-CD (**Önell and Andersson, 2005**) did not result in improved data quality for global kinetic analysis (data not shown). It should be noted that this alternate system has inherent drawbacks, as binding of his-tagged analyte to the α-his antibody cannot be ruled out completely despite prior blocking and reference subtraction (also see section **3.7.2.2**).

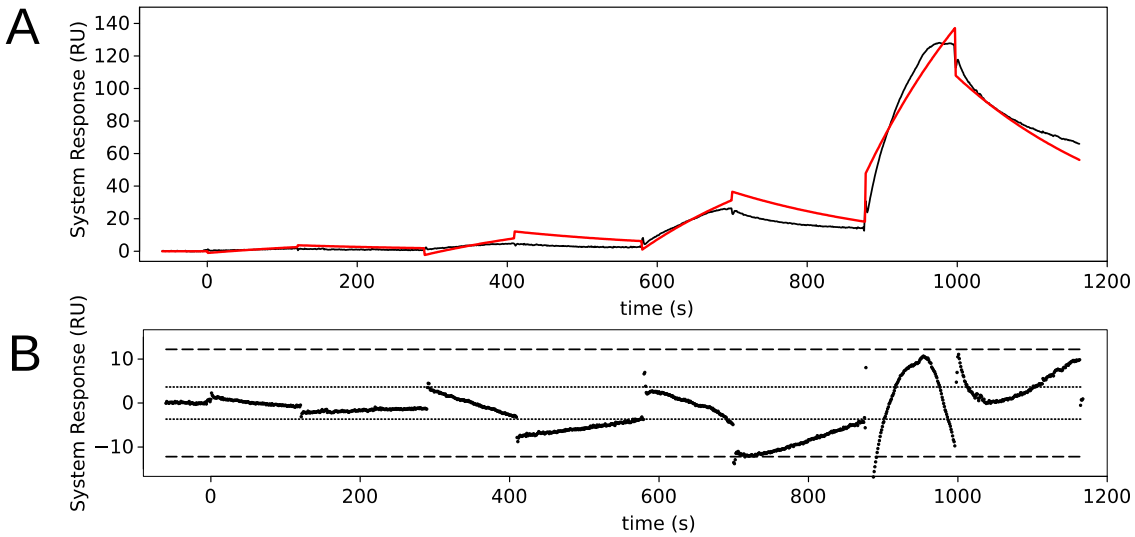

Fig. 4.22 Interaction kinetics of mO-AvrPto and FLS2-CD (alternative setup). **A**, data (black curve) and global kinetic fit to a 1:1 binding model (red curve; $\chi^2 = 31$ RU^2, U-value $= 15$). Injected concentrations were 12.3 nM, 37.5 nM, 111 nM, and 333 nM. **B**, residuals plot showing deviations between data and model. Quality control levels are indicated by the dotted line (inner threshold) and dashed line (outer threshold). *Note*: the kinetic fit is shown only for descriptive purposes, as the fit quality is not sufficient to infer meaningful kinetic data.

Analysis of dissociation phases Removing complexity from the experiment by restricting analysis to the dissociation phases results in acceptable fitting quality (see figure **4.23**), which allows isolated estimation of the dissociation rate constant. Kinetic fitting was performed for three individual concentrations of mO-AvrPto. It should be noted that the reliability of a single parameter determination is inherently less robust than global kinetic analysis, as reflected in the higher U-values in figure **4.23**. Dissociation rate constants estimated from this analysis were 0.04 s^{-1} (111 nM mO-AvrPto injection, figure **4.23 A**), 0.07 s^{-1} (333 nM mO-AvrPto injection, figure **4.23 b**), and 0.06 s^{-1} (1 µM mO-AvrPto injection, figure **4.23 C**), respectively. While not allowing determination of a kinetics-based affinity due to lack of reliable association-phase data, these data indicate that the complex of mO-AvrPto with FLS2 dissociates far more rapidly than those of mO-AvrPto with either BAK1-CD or Pto, which argues for a much weaker complex formation (thus, lower affinity), which is in line with the previously determined steady-state data.

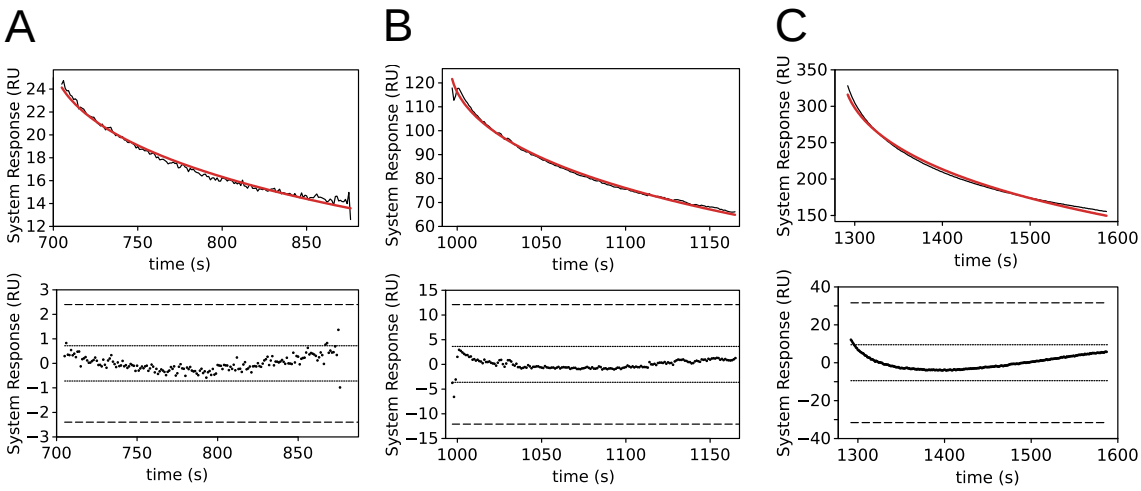

Fig. 4.23 Kinetic analysis (**top**) and residuals plot (**bottom**) of mO-AvrPto / FLS2-CD interaction, dissociation phases only. Black curves in top panels show data, red curves show kinetic fit to a 1:1 binding model. Shown are three different injected concentrations of mO-AvrPto: **A**, 111 nM (fit: $\chi^2 = 0.102$ RU^2, U-value = 12); **B**, 333 nM (fit: $\chi^2 = 0.604$ RU^2, U-value = 2); **C**, 1 µM (fit: $\chi^2 = 12.4$ RU^2, U-value = 9). Quality control levels are indicated by the dotted line (inner threshold) and dashed line (outer threshold) in the lower panels.

4.3.4 BRI1 and BSA do not bind AvrPto

Using the same assay setup as for the characterization of mO-AvrPto / BAK1-CD and mO-AvrPto / Pto interactions yielded no apparent binding for the BRI1-CD (figure **4.24**, **A**). The same was true for the BSA control (figure **4.24**, **B**). Loading the sensor surface with free mOrange (without an AvrPto moiety) and injecting BAK1-CD as has been done in mO-AvrPto / BAK1-CD experiments has a similar effect (figure **4.24**, **C**). These data

recapitulate the corresponding steady-state data as measured in MST experiments (section **4.17**).

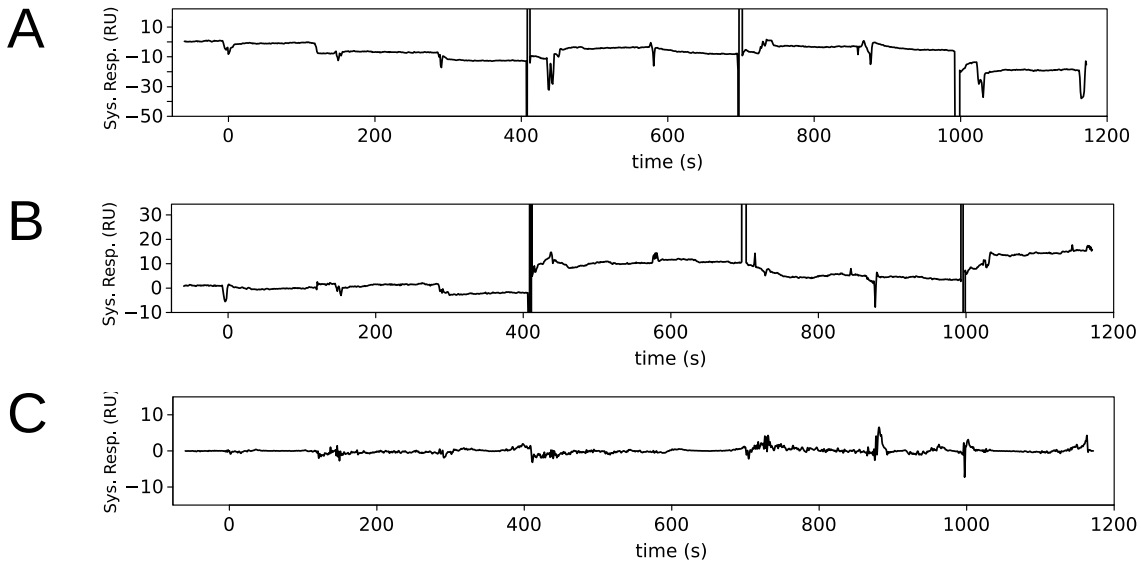

Fig. 4.24 SPR experiments for **A**, BRI1-CD; **B**, BSA; and **C**, BAK1-CD with mOrange alone. Injected concentrations were 37 nM, 111 nM, 333 nM and 1 µM for BRI1-CD, 111 nM, 333 nM, 1 µM and 3 µM for BSA, and 12.3 nM, 37 nM, 111 nM, and 333 nM for BAK1-CD, respectively. Curves are reference-substracted data. The experiments were repeated 2 times with similar results. *Note*: large signal spikes are injection artefacts.

4.3.5 Comparison of binding kinetics

Quantitative comparison Figure **4.25** shows an overview of kinetic constants as determined by SPR analysis. The affinities calculated from kinetic constants (figure **4.25 C**, solid bars) agree with steady-state affinities as have been measured in MST experiments (figure **4.25 C**, shaded bars; also see section **4.2**).

Qualitative comparison Figure **4.26** shows an overlay of the kinetic experiments using the alternate SPR setup (section **3.8**) for the mO-AvrPto / BAK1-CD and mO-AvrPto / FLS2-CD interaction pairs. Both experiments were conducted under identical conditions, allowing a qualitative comparison of the respective kinetic profiles (as has been noted before, the kinetic experiment for FLS2-CD does not allow quantitative global kinetic fitting). The higher dissociation rate constant for the mO-AvrPto / FLS2-CD interaction pair is readily apparent in the dissociation segments. The lower affinity of the interaction is also visible as a proportionally lower relative response at lower injected mO-AvrPto concentrations.

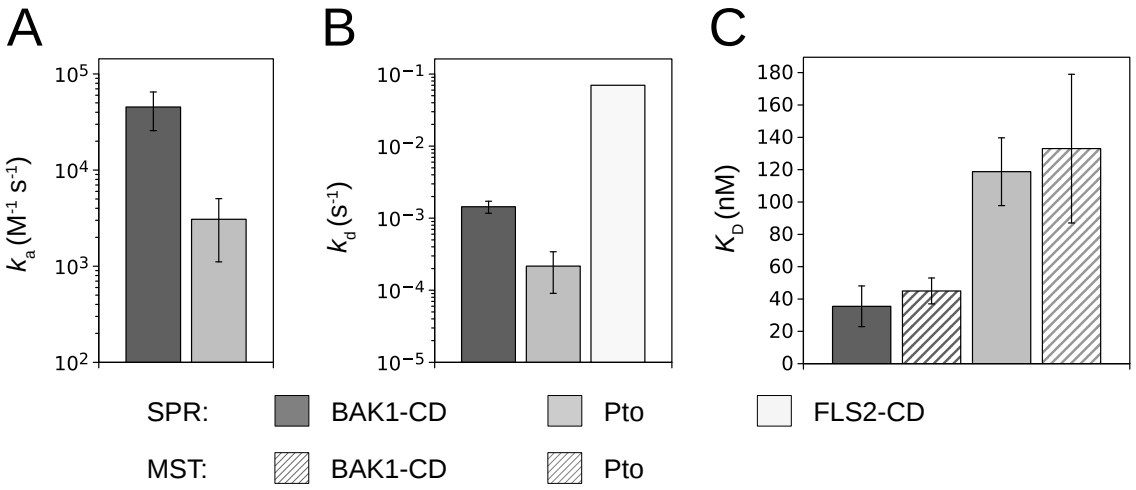

Fig. 4.25 Comparison of kinetic parameters obtained from SPR experiments. **A**, association rate constant (k_a); **B**, dissociation rate constant (k_d); **C**, affinity (K_D; steady-state affinities (shaded bars) are provided for reference). *Note*: logarithmic scales in (**A**) and (**B**). The dissociation rate constant given for FLS2-CD is taken from the fitting with the smallest U-value, as described in section **4.3.3**, and should be considered estimative. This value is based on a single experiment; all other values are based on three independent experiments.

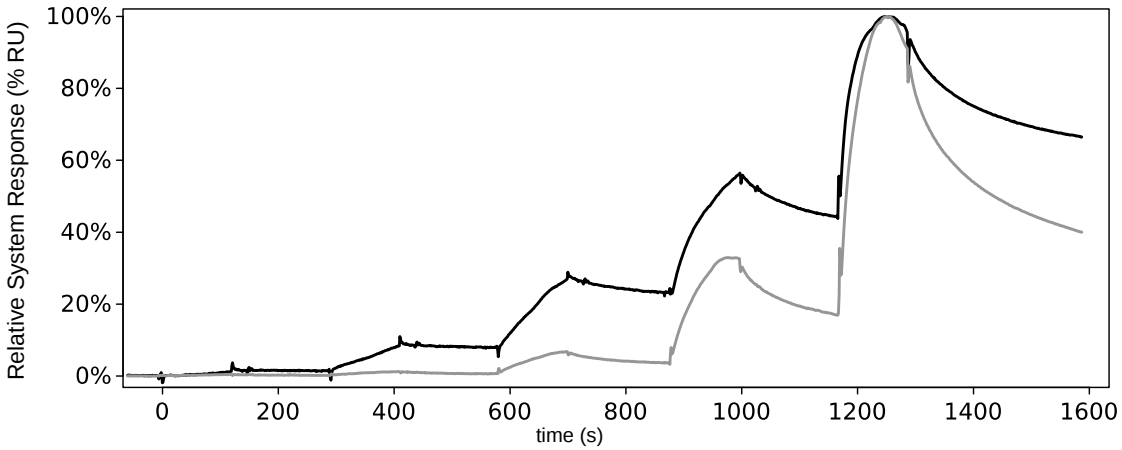

Fig. 4.26 SPR: Comparison of kinetic profiles for mO-AvrPto / BAK1-CD and mO-AvrPto / FLS2-CD interactions. Consecutive injections were mO-AvrPto at concentrations of 12.3 nM, 37 nM, 111 nM, 333 nM, and 1 µM, respectively. Only the data points are shown. Data was normalized as % of maximum response (at end of 1 µM mO-AvrPto injection).

4.4 Putative interaction-mediating residues of BAK1

Relevant crystal structure data Previous studies reported extensive high-quality crystal structure data on AvrPto (**Wulf et al., 2004**, **Xing et al., 2007**), Pto (**Xing et al., 2007**, **Dong et al., 2009**), BRI1 (LRR domain, **Hothorn et al., 2011**), BAK1 (cytoplasmic domain, **Cheng et al., 2011**), and FLS2 (LRR domain, **Sun et al., 2013a**). Of particular interest for the scope of this study is the availability of co-crystallization data for the interaction pairs AvrPto / Pto (protein data bank (PDB) identifier 2QKW, **Xing et al., 2007**), AvrPtoB / Pto (PDB identifier 3HGK, **Dong et al., 2009**), and AvrPtoB / BAK1 (PDB identifier 3TL8, **Cheng et al., 2011**).

Hypothesis of shared interaction interfaces Although the effectors AvrPto and AvrPtoB are sequence-unrelated, they share one of two proximate interaction interfaces on the Pto molecule (**Dong et al., 2009**). Also, BAK1 is very similar to Pto both in primary sequence as well as in solution structure, and was demonstrated to interact with AvrPtoB as well (**Cheng et al., 2011**). Therefore, it seemed plausible that there may be significant local overlap between the previously determined AvrPto-interacting region in Pto and a putative AvrPto-interacting region in BAK1.

4.4.1 BAK1 kinase domain can be homology modelled to Pto

Using the VAST+ tool (**Madej et al., 2014**, also see section **3.9.1**), BAK1-CD was homology-modelled to Pto based on geometric criteria inferred from the previously cited BAK1-CD / AvrPtoB and Pto / AvrPto co-crystal structural datasets, yielding 267 aligned residues with a root-mean-square deviation (RMSD) of 2.27 Å. (figure **4.27**). It should be noted that the RMSD is calculated over the complete superposition of all attempted alignments in the query structures (thus including AvrPto / AvrPtoB alignments), indicating that this number underestimates the quality of the BAK1-CD / Pto alignment. This alignment ranked second position out of a total number of 3745 geometric alignments in the database query (based on number of aligned residues), position one being the alignment with the second Pto crystal structure in the database (PDB identifier 3HGK, as cited before).

4.4.2 AvrPto / BAK1 geometrical analysis

Addition of the AvrPto structure to the aligned BAK1-CD / Pto superimposition (figure **4.28 A**) shows that the relevant local structures are geometrically well aligned, indicating three spatially adjacent putative interaction interfaces (figure **4.28 B**). Although these

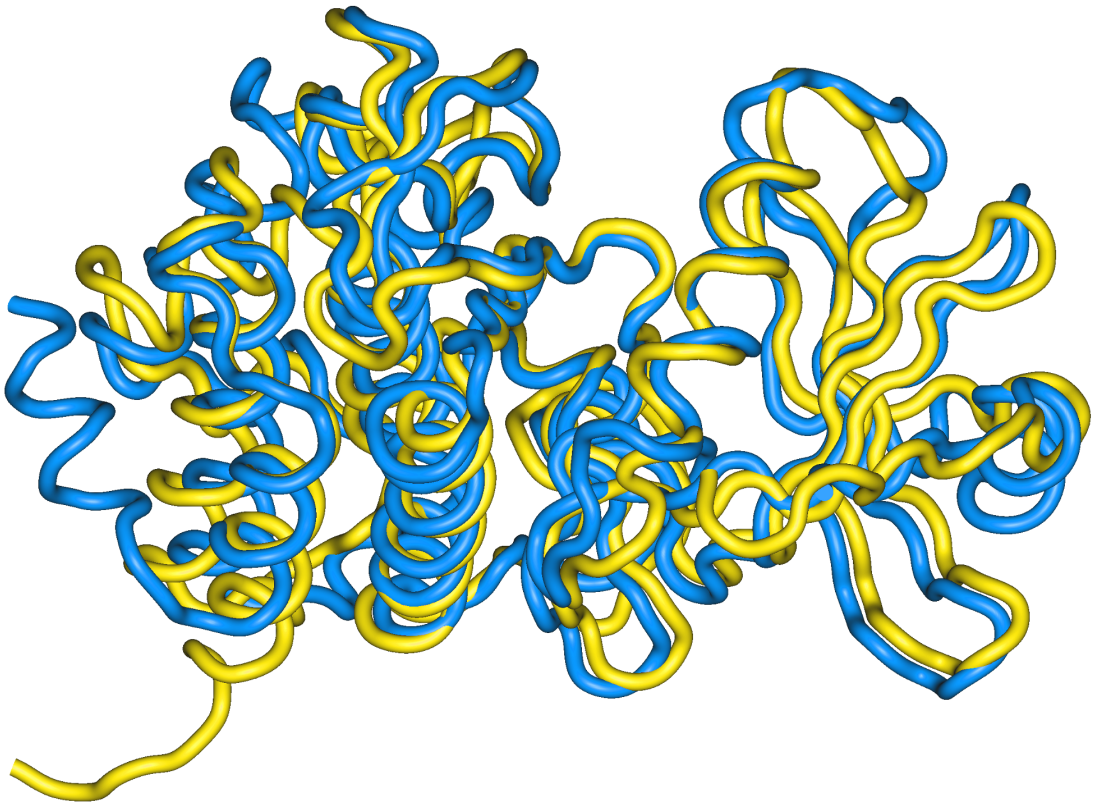

Fig. 4.27 Structural superimposition of BAK1-CD (blue) to Pto (yellow) without side chains, based on geometric alignment.

putative interaction interfaces are located close to each other in the three-dimensional structure, their sequence-based location reaches across approximately the first half of the intracellular kinase domain (figure **4.28 C**).

4.4.3 Selection of point mutations

In an effort to understand the structural basis for the strong interaction between BAK1-CD and AvrPto, a series of single point mutations was introduced into BAK1-CD. The selection of point mutations was based on three general approaches, which are briefly summarized below.

Global phosphorylation status For the first approach, mutations were introduced that lock BAK1-CD either in an unphosphorylated or in a phosphorylated form, with the aim to test whether global phosphorylation status of the BAK1-CD has any influence on its affinity to AvrPto. Previous reports indicated that Pto activation loop phosphorylation, which leads to the active conformation, is necessary for kinase activity and interaction with AvrPto (**Xing et al., 2007**), and similarly, a kinase-inactive mutation of FLS2 was

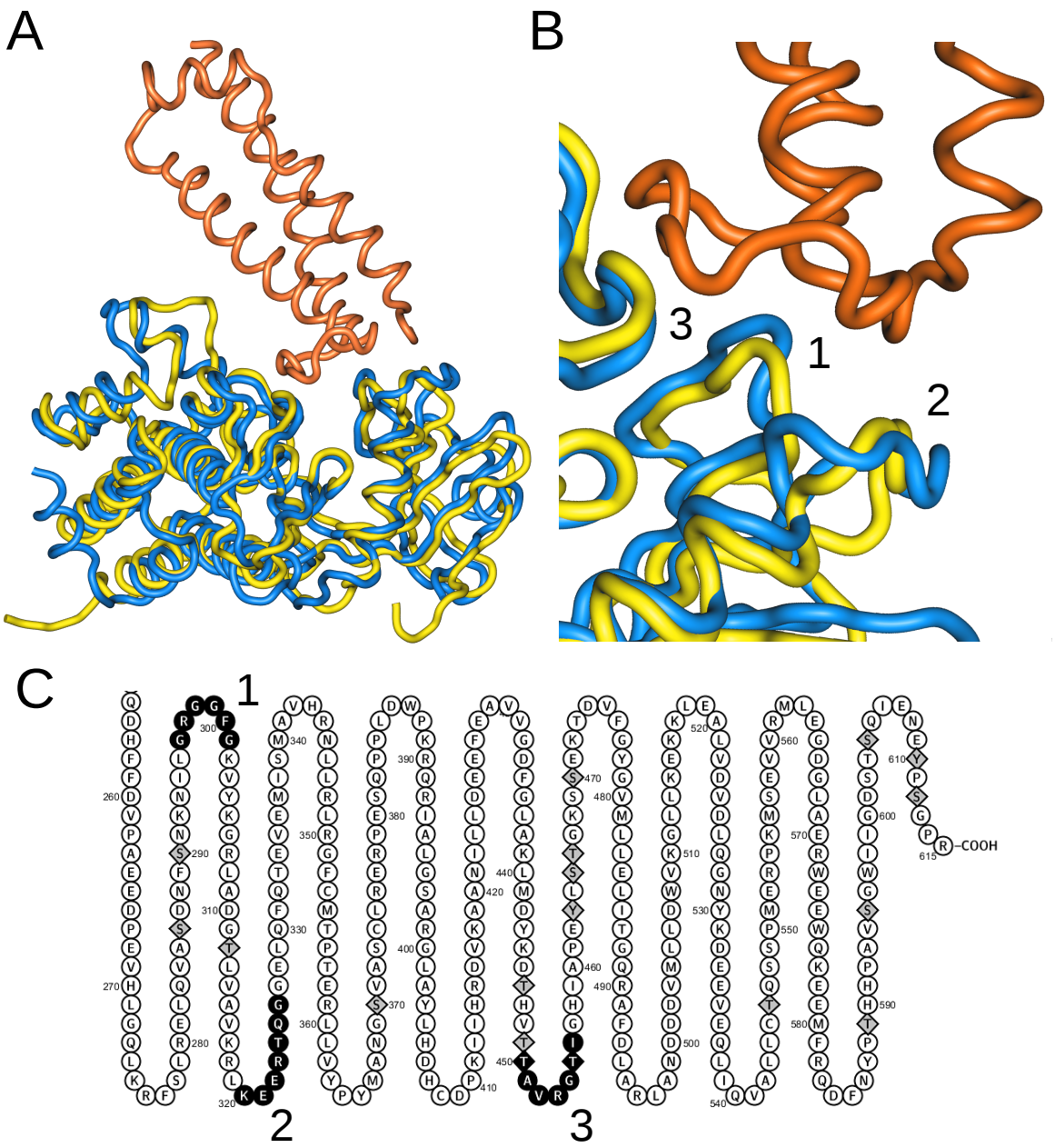

Fig. 4.28 Putative AvrPto / BAK1 interaction interfaces. **A**, Structural superimposition of BAK1-CD (blue) to Pto (yellow) with added AvrPto structure (orange). **B**, enlargement of contact area. Numbers indicate three putative interaction interfaces on the aligned BAK1 structure (direction of counting from N to C terminus). **C**, location of interaction interfaces (black residues) in the BAK1 amino acid sequence (N-terminally truncated). Big numbers correspond to interaction interface numbering in (**B**). Grey and black diamond-shaped residues indicate phosphorylation sites annotated in the UniProt database (**The UniProt Consortium, 2015**). Small numbers indicate annotated residue numbers as retrieved from the UniProt database. Amino acids are given in single-letter code.

found to abolish its interaction with AvrPto (**Xiang et al., 2008**). Additionally, structural studies investigating the interaction of BAK1-CD with AvrPtoB indicate that the active conformation of BAK1 is necessary for this interaction (**Cheng et al., 2011**). Taken together, these studies indicate that phosphorylation status may be a significant parameter governing the interaction between AvrPto and its putative virulence targets (**Zong et al., 2008**).

Local environment The second approach was based directly on geometrical analysis of the interaction interfaces; mutations were introduced in amino acids which were both physically close to the putative interaction interfaces and whose modification would have a large direct impact on their immediate vicinity; for this reason, residues were selected which had the potential to be phosphorylated, as presence or absence of phosphorylation marks a strong change in a protein's local environment. To simulate the effects of a phosphorylated state, phosphomimetic aspartate substitutions were used on threonine and tyrosine residues; to simulate the effects of an unphosphorylated state, glycine and phenylalanine substitutions were used on threonine and tyrosine residues, respectively.

Conservation in interactants The third approach was based on previous experiments in this study which indicated that AvrPto was able to bind BAK1-CD, FLS2-CD and Pto, but not BRI1-CD. Therefore, alignments were generated and residues were determined which were conserved in all the interactants, but not in BRI1-CD. Subsequently, the corresponding BRI1 residue was introduced into BAK1-CD. Again, as in the previous approaches, focus was placed primarily on amino acids which have the potential to be phosphorylated.

4.5 Influence of BAK1 and AvrPto point mutations on interaction characteristics

4.5.1 BAK1 global phosphorylation status and kinase activity

4.5.1.1 Constitutively phosphorylated BAK1 binds AvrPto with wild-type affinity

S286A mutant BAK1 residue S286 has an important regulatory function for global phosphorylation status, acting as a major negative regulatory switch (**Wang et al., 2008**), and phosphorylation at this residue likely occurs in response to BAK1-FLS2 interaction (**Wang et al., 2014a**). Therefore, an S286A mutation was introduced to create a constitutively phosphorylated version of BAK1-CD. As expected, the mutation results in a strong shift towards the BAK1-CD phosphorylated form during bacterial expression, as

can be seen in the migration pattern during SDS-PAGE (figure **4.29 A**). In SPR analysis the association constant (k_a) was determined as 5.4 $\times 10^4$ ($\pm$ 5.3 $\times 10^3$) mol^{-1} s^{-1}, while the dissociation rate constant (k_d) was determined as 1.2 $\times 10^{-3}$ ($\pm$ 1.3 $\times 10^{-4}$) s^{-1}. The affinity (K_D) inferred from kinetic parameters was 24 $\pm$ 6 nM. Figure **4.29** shows a representative kinetic experiment (K_D = 28 nM). These results indicate that the S286A mutant interacts with AvrPto similarly to WT BAK1-CD, and suggests that the constitutively phosphorylated state of residues which result from forced BAK1 autophosphorylation pose no obstacle to interaction with AvrPto.

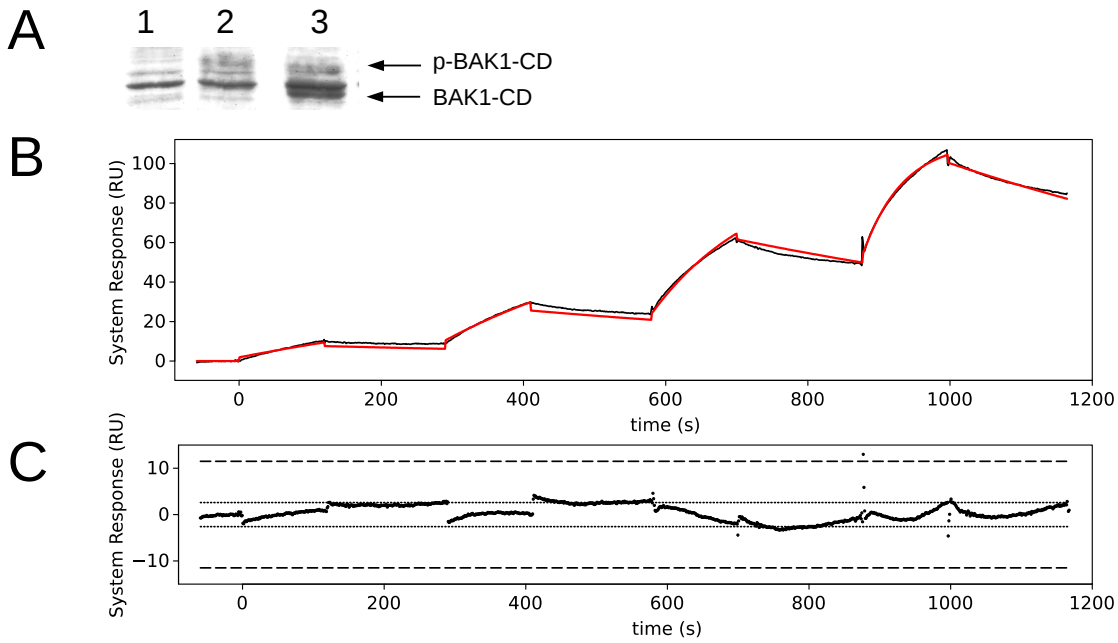

Fig. 4.29 Interaction kinetics of mO-AvrPto and the S286A mutant. **A**, SDS-PAGE of soluble extracts from *E. coli* (ROSETTA) expressing (**1**) no protein, (**2**) BAK1-CD S286A mutant, or (**3**) BAK1-CD WT form. Arrows indicate phosphorylated and unphosphorylated form of BAK1-CD as indicated. *Note*: picture is a composite image consisting of non-adjacent lanes of the same gel, and is only intended for visual comparison of band patterns. **B**, data (black curve) and global kinetic fit to a 1:1 binding model (red curve; χ^2 = 3.19 RU^2, U-value = 2). Injected concentrations were 12.3 nM, 37.5 nM, 111 nM, and 333 nM. **C**, residuals plot showing deviations between data and model. Quality control levels are indicated by the dotted line (inner threshold) and dashed line (outer threshold). The experiment was repeated 2 times with similar results.

4.5.1.2 Kinase-inactive BAK1 does not bind AvrPto

K317E mutant BAK1 K317E is a well-characterized point mutation resulting in complete loss of kinase activity (**Li et al., 2002**, **Bajwa et al., 2013**). Injection of the BAK1 K317E mutant using the same SPR assay setup as has been used for analysis of wild-type BAK1-CD and other SDM mutants resulted in a pure baseline signal (data not shown).

Subsequently, maximum concentration of K317E in the assay was raised to 3 µM in an attempt to increase the observation window for binding events. Figure **4.30** shows the result of a representative experiment; there is no binding visible that would allow kinetic evaluation; the very slight binding event occurring at the highest concentration is due to unspecific background absorption to the reference flow cell, as indicated by the negative magnitude of the response. These findings support previous data by other groups (as cited before) that the active conformation of kinase interactants is crucial for their interactions with AvrPto.

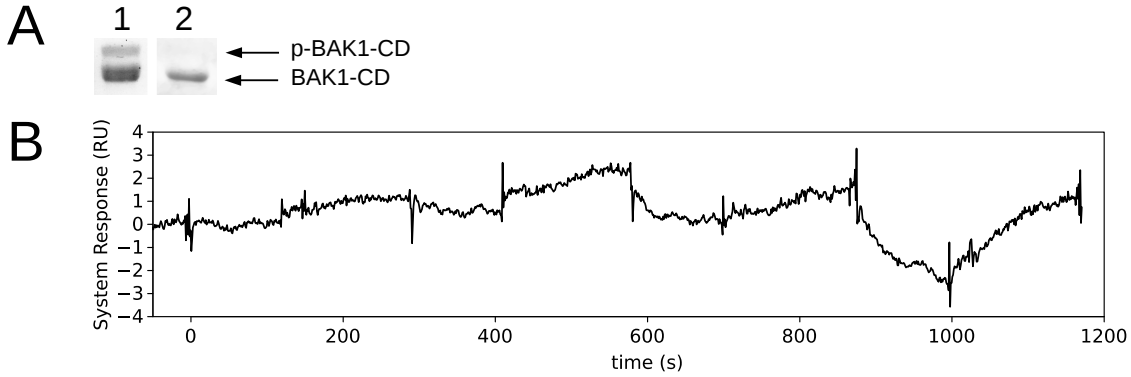

Fig. 4.30 Interaction kinetics of mO-AvrPto and the kinase-inactive K317E mutant. **A**, SDS-PAGE of purified protein; (**1**) BAK1-CD WT, (**2**) BAK1-CD K317E mutant. Arrows indicate phosphorylated and unphosphorylated form of BAK1-CD as indicated. *Note*: picture is a composite image consisting of lanes run on different gels, and is only intended for visual comparison of band patterns. **B**, data curve for K317E injections. Injected concentrations were 111 nM, 333 nM, 1 µM, and 3 µM. The experiment was repeated 2 times with similar results.

4.5.2 The BAK1 Y403F mutation has no influence on its affinity to AvrPto

Y403 identification The BAK1 residue Y403 was identified by looking for potential functionally relevant single amino acid divergences in conservation among the interactants (also see section **4.4.3**). Y403 is conserved as a tyrosine in BAK1, FLS2, and Pto, but not in BRI1 (figure **4.31**, **B**).

Y403 as putative effector target? Interestingly, the homologous position in *A thaliana* EFR, Y836, was recently described to be required for EFR activation and downstream immunity signalling, as well as to be targeted by another *P. syringae* effector protein, HOPAO1. This effector acts as a tyrosine phosphatase and suppresses immunity signalling by dephosphorylating EFR Y836 (**Macho et al., 2014**).

Y403F analysis Y403 is located distal to the putative AvrPto / BAK1-CD interaction interfaces (**4.31**, **A**). SPR analysis shows that the Y403F mutation has no significant effect on its binding to AvrPto (figure **4.31** shows a representative experiment), as both kinetics and affinity for the interaction are similar to WT BAK1-CD ($k_a = 2.1 \times 10^4$ ($\pm 9.3 \times 10^3$) $mol^{-1}\,s^{-1}$, $k_d = 7.3 \times 10^{-4}(\pm\ 5.7 \times 10^{-5})\ s^{-1}$, $K_D = 35$ (± 14) nM), indicating that the single amino acid divergence at the Y403-equivalent position in BRI1-CD is not the determinant for AvrPto interaction specificity.

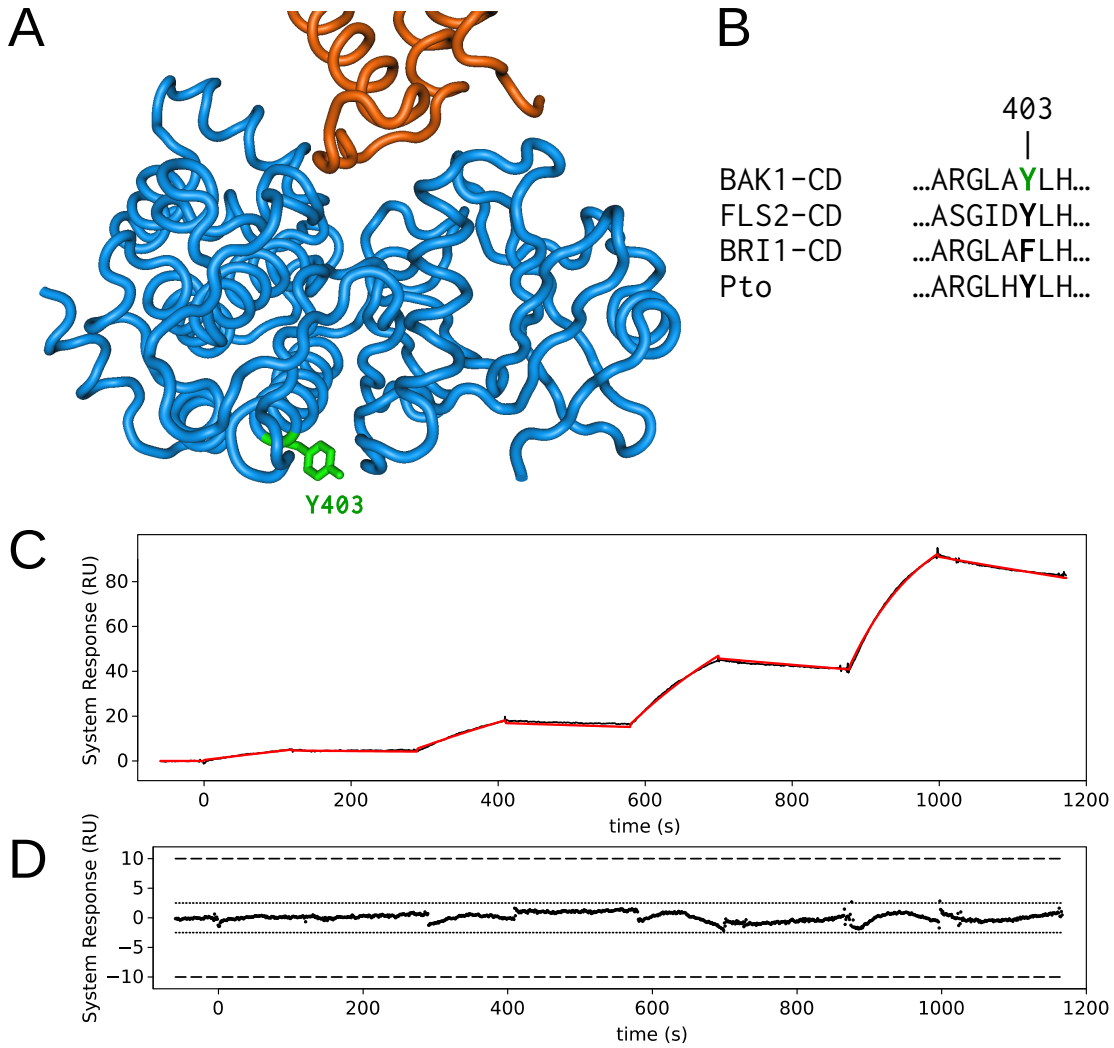

Fig. 4.31 Y403F analysis. **A**, The Y403 residue (green) is located distal to the putative BAK1-CD (blue) / AvrPto (orange) interaction interfaces (aligned Pto is not shown for clarity). **B**, alignment showing conservation of Y403 (numbering corresponds to BAK1 only). **C**, SPR analysis, data (black curve) and global kinetic fit to a 1:1 binding model (red curve; $\chi^2 = 0.50\ RU^2$, U-value = 1). Injected concentrations were 12.3 nM, 37.5 nM, 111 nM, and 333 nM. **D**, SPR analysis, residuals plot showing deviations between data and model. Quality control levels are indicated by the dotted line (inner threshold) and dashed line (outer threshold). The experiment was repeated 2 times with similar results.

4.5.3 BAK1 T324 mutations significantly alter its affinity to AvrPto due to altered interaction kinetics

T324 identification The second putative interaction interface (see figure **4.28**, **B**, **C**) contains a single phosphorylatable residue, T324. T324 locates centrally in this interface, with the residue and its corresponding phosphate group (the crystal structure used to build the model exhibited phosphorylation at this residue) extended into the direction of the putative location of the AvrPto structure (figure **4.32**, **A**). Besides location, this residue was also chosen because of its conservation status. FLS2 and Pto contain a serine, another phosphorylatable residue, at the homologous position of BAK1 T324. However, in the BRI1 sequence, the homologous residue is a glycine instead (figure **4.32**, **B**).

T324G associates rapidly Surprisingly, mutating BAK1-CD T324 to a glycine to mimic the situation in BRI1-CD resulted in increased affinity to mO-AvrPto in SPR experiments, with a K_D of 6.3 ± 1.2 nM (figure **4.32**, **C** shows a representative experiment, $K_D = 7$ nM), an approximately six-fold increase compared to WT BAK1-CD. Kinetic analysis reveals that the increased affinity of the T324G mutant to mO-AvrPto is due to an increased association rate of the complex ($k_a = 1.2 \times 10^5$ $(\pm 3.0 \times 10^4)$ $\mathrm{mol}^{-1}\,\mathrm{s}^{-1}$), which is about 3 times faster than that of WT BAK1-CD. In contrast, the dissociation rate is about as fast as that observed for WT BAK1-CD ($k_d = 7.7 \times 10^{-4}$ $(\pm 1.2 \times 10^{-5})$ s^{-1}).

T324D dissociates quickly To further analyse the observed effect of the T324G mutant, the functionally opposed phosphomimetic mutation was introduced to BAK1-CD (T324D). Correspondingly, the affinity of T324D to mO-AvrPto was significantly lower than that of WT BAK1-CD or the T324G mutant ($K_D = 170.0 \pm 40.0$ nM). In regards to kinetics, this mutation has the opposite effect to T324G as well: while the association rate for complex formation with mO-AvrPto is about the same as that of WT BAK1-CD ($k_a = 2.8 \times 10^4$ $(\pm 1.2 \times 10^4)$ $\mathrm{mol}^{-1}\,\mathrm{s}^{-1}$, the dissociation rate for the complex is about 5 times faster ($k_d = 4.9 \times 10^{-3}$ $(\pm 1.8 \times 10^{-3})$ s^{-1}).

T324 as 'interface marker' T324 has not been reported as a BAK1 *in vivo* phosphorylation site previously in *A. thaliana* ('Arabidopsis2010' database, **Clouse et al., 2008**). However, it can be subject to autophosphorylation during heterologous expression in the *E. coli* system, as has been demonstrated in a phosphoproteomics study (**Wu et al., 2012**), and the homologous residue in tomato BAK1 (*Sl*BAK1) was also shown to autophosphorylate *in vitro* (**Bajwa et al., 2013**). As the T324G mutations results in increased affinity to AvrPto, the initial hypothesis that the non-phosphorylatable single amino acid divergence of the T324-homologous position in BRI1 may be a contributor to

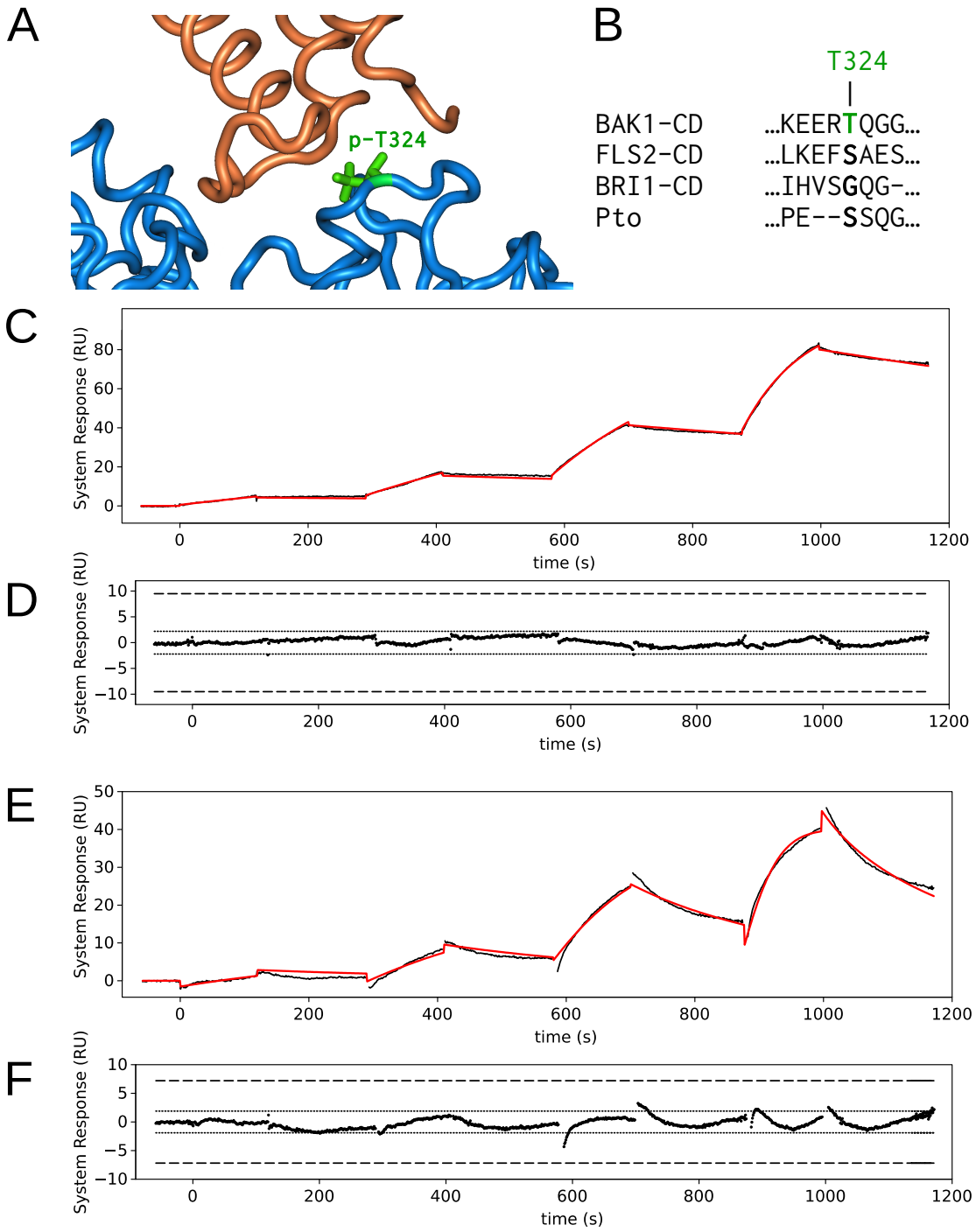

Fig. 4.32 T324 analysis. **A**, The T324 residue (green) is located in the middle of the second putative BAK1-CD (blue) / AvrPto (orange) interaction interface (aligned Pto is not shown for clarity). **B**, alignment showing conservation of T324 (numbering corresponds to BAK1 only). **C**, T324G SPR analysis, data (black curve) and global kinetic fit to a 1:1 binding model (red curve; $\chi^2 = 0.53$ RU^2, U-value = 1). Injected concentrations were 12.3 nM, 37 nM, 111 nM, and 333 nM. **D**, T324G SPR analysis, residuals plot showing deviations between data and model. Quality control levels are indicated by the dotted line (inner threshold) and dashed line (outer threshold). The experiment was repeated 3 times with similar results. **E**, T324D SPR analysis, data (black curve) and global kinetic fit to a 1:1 binding model (red curve; $\chi^2 = 0.95$ RU^2, U-value = 3). Injected concentrations were 37 nM, 111 nM, 333 nM, and 1 µM. *Note*: Injection artefacts were removed at the beginning and end of injections. **F**, T324D SPR analysis, residuals plot (as described above). The experiment was repeated 3 times with similar results.

the differential RLK-CD interaction specificity of AvrPto can be ruled out. However, it seems plausible that the differential effects on AvrPto/BAK1 binding affinity and kinetic behaviour resulting from the T324G and T324D mutations may be due to steric hindrance of a phosphate group at this position; this would in turn reinforce the notion that the BAK1 loop containing this residue indeed forms part of the interaction interface and thus substantiate the initial hypothesis that the interactions between AvrPto and either BAK1 or Pto occur similarly on a structural level (section **4.4.2**).

4.5.4 AvrPto mutation Y89D strongly diminishes interaction with BAK1

Y89D in literature AvrPto Y89D has previously been described as a mutant which abolishes binding of AvrPto to Pto and loses wild-type AvrPto's negative effect on Pto autophoshorylation (**Xing et al., 2007**). Very similar findings have been reported regarding the Y89D mutant's effects on putative virulence targets FLS2 and EFR; interaction with these proteins was strongly diminished and no effect on FLS2 or EFR autophosphorylation could be observed, in contrast to wild-type AvrPto (**Xiang et al., 2008**).

Y89 analysis AvrPto Y89 extends towards the putative AvrPto / BAK1-CD interfaces (figure **4.33**, **A**). The effect of AvrPto Y89 on interaction with Pto has previously been described as mediating hydrophobic contact with Pto V51; however, in BAK1, the homologous residue is a glycine (G299; figure **4.33**, **B**, **C**). These residues are located in the corresponding BAK1 and Pto loops forming the first putative interaction interface (also see figure **4.28**). Interestingly, residue T324 (which is located in the BAK1 loop forming the second putative interaction interface) extends towards AvrPto Y89 (figure **4.33**, **D**). Mutating Y89 to a phosphomimetic aspartate has a strong effect on interaction with BAK1, reducing binding to a very low residual level (figure **4.33**, **E**). It seems likely that the strong reduction in binding occurs mechanistically analogously to the situation in the Pto/AvrPto interaction (**Xing et al., 2007**), and that a phosphomimetic aspartate in the Y89 position leads to strong steric hindrance. These findings can be set into relation with the previously described T324 mutations, as in both cases aspartate mutations have qualitatively (though not quantitatively) similar results, further substantiating the putative alignment of the interaction interfaces.

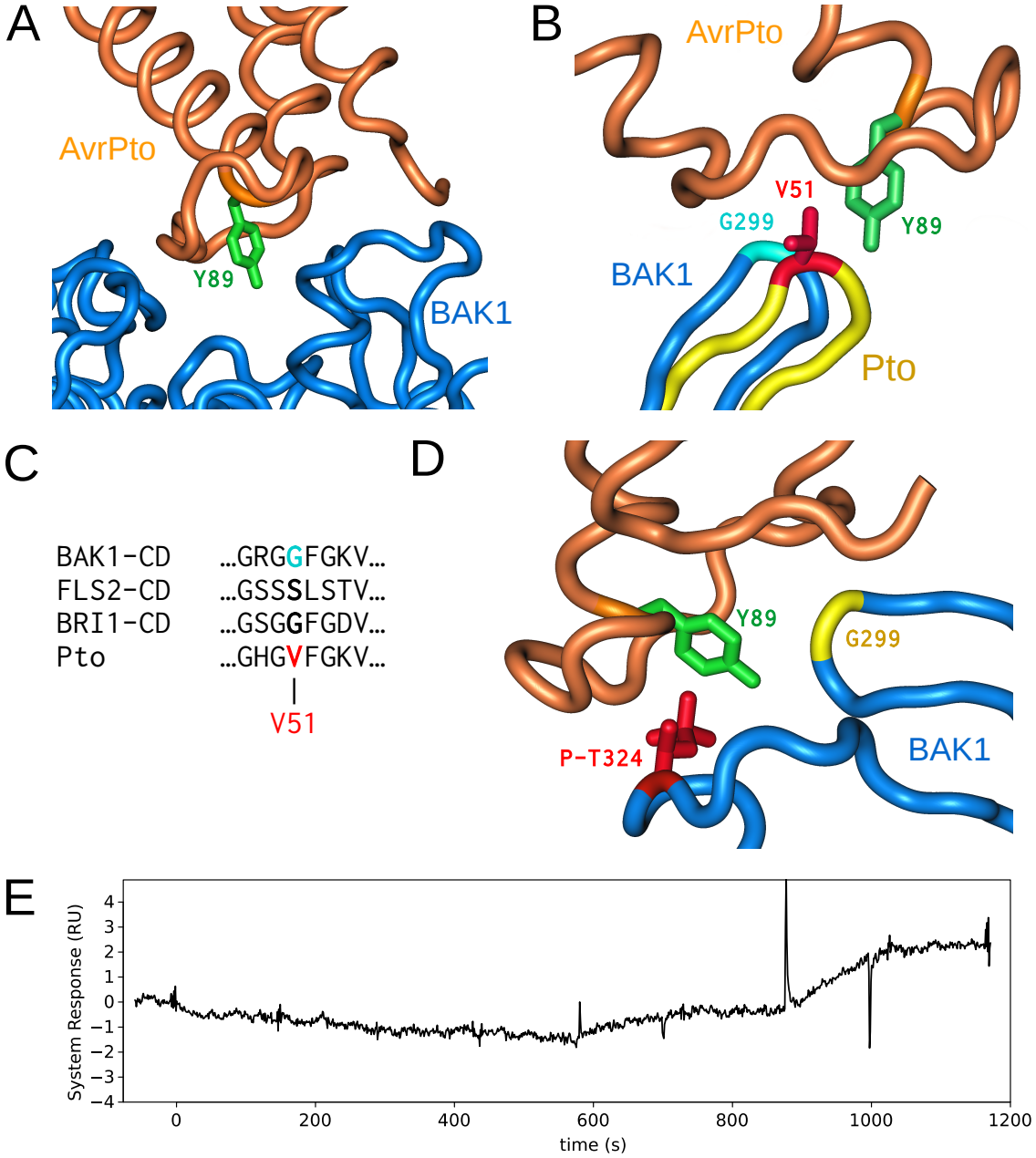

Fig. 4.33 Y89D analysis. **A**, AvrPto Y89 (green) extends towards the putative BAK1 (blue) interaction interfaces. **B**, AvrPto Y89 faces residues V51 in Pto (red residue on yellow structure) and G299 in BAK1 (cyan residue on blue structure), respectively. Only the relevant loops on the Pto and BAK1 structures are shown for clarity. **C**, alignment showing conservation of Pto V51 (numbering corresponds to Pto only; colors correspond to pane **B**). **D**, AvrPto Y89 locates close to both BAK1 G299 (yellow) and BAK1 T324 (red). **E**, AvrPto Y89D shows drastically reduced interaction with BAK1-CD in SPR experiments. Injected BAK1-CD concentrations were 37 nM, 111 nM, 333 nM, and 1 µM, respectively. This signal was not sufficient for meaningful kinetic evaluation. The experiment was repeated 2 times with similar results.

4.5.5 Mutational analysis kinetics comparison

Quantitative comparison Figure **4.35** shows a quantitative overview of kinetic constants for BAK1-CD mutant interactions with mO-AvrPto as determined by SPR experiments and presents statistical analysis which compares the kinetic behaviour of the mutants to wild-type BAK1-CD. There are no significant differences in kinetic behaviour between wild-type BAK1 and the mutants S286A and Y403F. However, significant differences could be observed for both T324 mutants. The divergence in affinity of T324G and T324D compared to wild-type BAK1 (which is higher, and lower, respectively (figure **4.35**, **C**)); is reflected through markedly different interaction kinetics. While the T324G mutant exhibits an approximately three-fold faster complex formation compared to wild-type BAK1 and all other mutants (figure **4.35**, **A**), the dissociation of the complex is slightly slower compared to wild-type BAK1 (figure **4.35**, **B**). The opposite is true for T324D: formation of the complex occurs similarly as in wild-type BAK1 (figure **4.35**, **A**), while it exhibits an approximately five-fold faster complex dissociation (figure **4.35**, **B**).

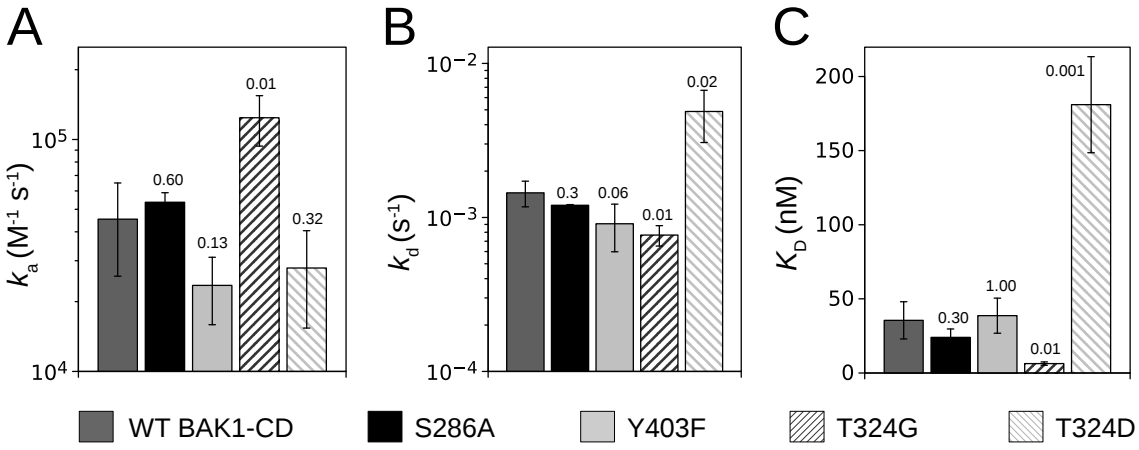

Fig. 4.34 Comparison of kinetic parameters obtained from SPR experiments for BAK1 mutants. **A**, association rate constant (k_a); **B**, dissociation rate constant (k_d); **C**, affinity (K_D). *Note*: logarithmic scales in (**A**) and (**B**). Values are given as means ± SD. The values are based on three independet experiments, with the exception of the S286A and Y403F mutants, which are based on two independent experiments. P values (unpaired Student's *t*-test) are indicated above the error bars.

Qualitative comparison Normalizing the data obtained from kinetic experiments with WT BAK1-CD and its corresponding T324 mutants as fraction of maximum response and plotting an overlay of the respective kinetic curves visualizes the different kinetic behaviours (figure **4.35**).

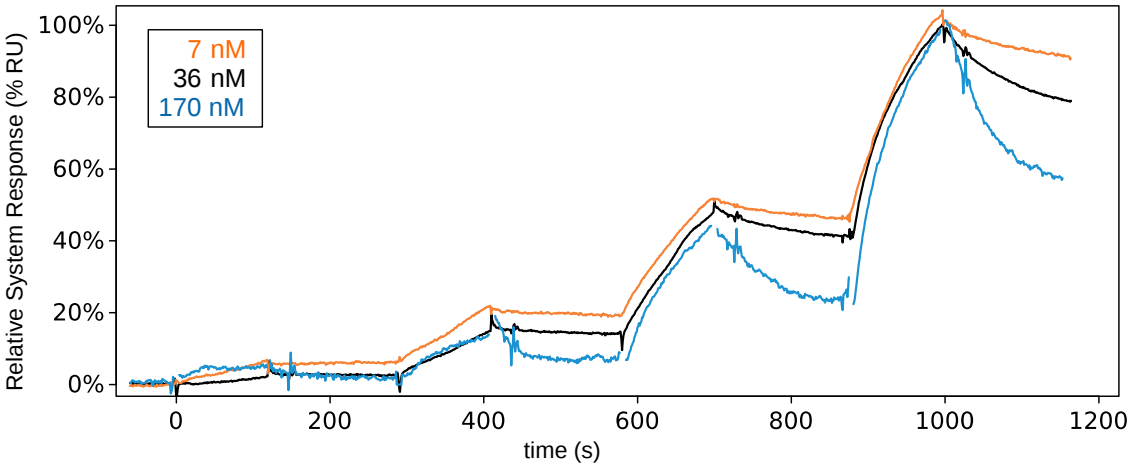

Fig. 4.35 Qualitative comparison of BAK1 mutant kinetics. Black, wild-type BAK1-CD; orange, T324G mutant; blue, T324D mutant. Only data curves are shown for clarity. Injections were 12.3 nM, 37 nM, 111 nM, and 333 nM. Curves have been normalized as % of maximum response (at the end of 333 nM injection) to facilitate comparison. Injection artefacts have been removed from the T324D curve (note missing data points). Affinities (K_D) are given in the inset box for reference.

4.6 AvrPto interactions *in planta* using a protoplast system

Declaration of collaboration All *in vivo* experiments as described in the following sections were performed in collaboration with T. Schmidt and have been included in the corresponding M.Sc. thesis (**Schmidt, 2015**). The contribution of T. Schmidt was as follows: Discussions concerning the planning of experiments, preparation of stock solutions and isolation of plasmids for use in the experiments, sowing and care of plants for use in protoplast isolation, manual assistance during protoplast isolation and the performance of the experiments.

4.6.1 BAK1 SDM variants can functionally complement the *bak1* mutant phenotype in flg22-triggered immunity signalling

To test whether the BAK1 point mutations generated for the *in vitro* study can still provide the natural BAK1 function *in vivo*, wild-type BAK1 or its point mutated variants were expressed in *A. thaliana* protoplasts as described in section **3.2.2**. BAK1 function was studied using a *pFRK1*-luciferase assay as described in sections **3.8.1** (also see figure **3.9**, **A** to **C** for a schematic overview of the system and its use to study functional complementation). Comparing protoplasts isolated from Col-0 plants with protoplasts isolated from *bak1-5 bkk1-1* mutant plants shows a significant ($p \leq 0.05$) reduction in luciferase activity 3 h post induction (figure **4.36, A**, $p = 0.034$). This phenotype can

be rescued by transforming plasmids containing full-length BAK1 under control of the 35S promoter into the *bak1-5 bkk1-1* protoplasts (figure **4.36, B**). Except for the kinase-inactive mutant K317E, which does not show a significant *pFRK1* induction compared to noncomplemented protoplasts ($p = 0.19$), all tested BAK1 point mutations could rescue the phenotype, indicating that these point mutations do not impair natural BAK1 function in context of immunity signalling (represented by flg22-triggered *pFRK1* induction). However, the resolution of the asssay does not allow conclusions in regard to quantitative differences in the point mutants' ability to rescue the *bak1-5 bkk1-1* phenotype when compared to complementation with wild-type BAK1.

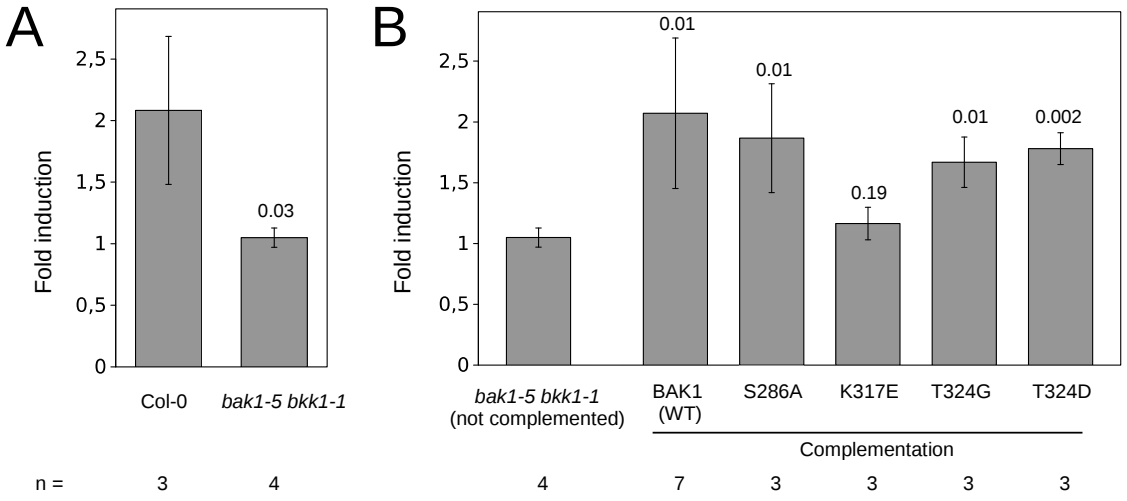

Fig. 4.36 Complementation of *bak1-5 bkk1-1* mutant phenotype in flg22-triggered FRK1 induction by transiently expressing BAK1 or point-mutated variants in protoplasts . **A**, *bak1-5 bkk1-1* mutant protoplasts are impaired in flg22-triggered immunity signalling (represented by *pFRK1* induction). **B**, wild-type BAK1 or BAK1 point mutations can complement BAK1 function when expressed transiently in *bak1-5 bkk1-1* mutant protoplasts. Point mutations are described by single-letter amino-acid abbreviations and PDB annotated BAK1 sequence numbering. Fold change is given as the quotient in luminescence of flg22-stimulated vs. unstimulated protoplasts 3 h after flg22 treatment. Values are given as mean ± SD; the number of independent experiments on which the values are based are given below the data labels. *P* values (unpaired Student's *t*-test) are indicated above the error bars.

4.6.2 Differences in affinity as observed *in vitro* are not visible in the functional assay

To test whether the differences in binding affinity between AvrPto and the different point-mutated BAK1 variants that have been determined *in vitro* (see section **4.5**) can also be observed *in vivo*, the *A. thaliana* protoplast system was used to investigate AvrPto function in *bak1-5 bkk1-1* protoplasts which have been complemented with either wild-type BAK1

or one of the point-mutated variants as described in section **4.6.1** (also see figure **3.9**, **C** to **E** for a schematic overview of the system and its use to study effector function). Addition of plasmid enabling expression of AvrPto to *bak1-5 bkk1-1* protoplasts complemented with either wild-type BAK1 or one of its point-mutated variants results in reduction of luciferase activity (figure **4.38**). However, in the case of K317E and T324G mutants, the observed difference between *pFRK1* induction in samples without or with AvrPto expression is not large enough for the difference to be significant ($p = 0.51$ and 0.08, respectively). In this assay, the *in vitro* affinity differences between AvrPto and wild-type BAK1, T324G, or T324D, respectively, are not reflected in a differential ability of AvrPto to repress immunity signalling, likely due to the overexpression situation for both the different BAK1 variants and AvrPto. Thus, while not achieving the necessary resolution to reflect the differential binding specificity between AvrPto and BAK1 variants as observed *in vitro*, this assay qualitatively demonstrates the physiological action of AvrPto *in vivo*.

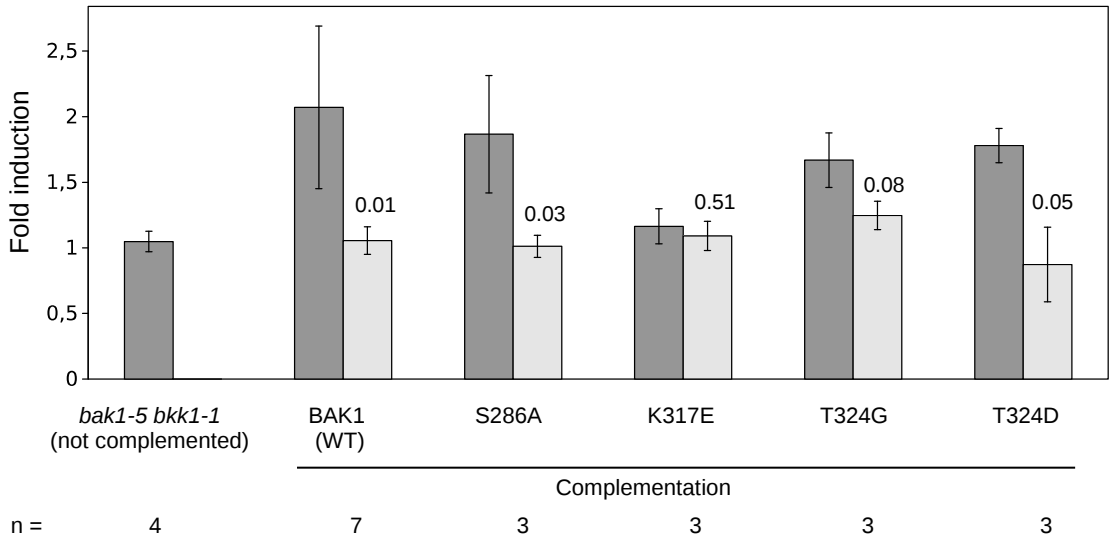

Fig. 4.37 AvrPto function in *bak1-5 bkk1-1* mutant protoplasts complemented by transiently expressing BAK1 or SDM variants. Dark bars, without AvrPto; light bars, with AvrPto. Point mutations are described by single-letter amino-acid abbreviations and PDB annotated BAK1 sequence numbering. Fold change is given as the quotient in luminescence of flg22-stimulated vs. unstimulated protoplasts 3 h after flg22 treatment. Values are given as mean ± SD; the number of independent experiments on which the values are based are given below the data labels. *P* values (unpaired Student's *t*-test) are indicated above the error bars.

4.6.3 AvrPto additionally acts on BKK1 in the functional assay

In addition to the *bak1-5 bkk1-1* double knockout mutant protoplasts, experiments have been performed in *bak1-4* mutant protoplasts to study the contribution of BKK1, which has previously been found to interact with AvrPto through Co-IP experiments (**Shan et al.,**

2008) and indirectly through phenotypical readouts such as stomatal patterning (**Meng et al., 2015**). While expression of AvrPto in *bak1-5 bkk1-1* protoplasts complemented with the kinase-inactive K317E BAK1 mutant has no effect 3 h after flg22 treatment (as there is no visible pFRK1 induction to begin with), there is visible *pFRK1* induction in *bak1-4* protoplasts complemented with the K317E BAK1 mutant 3 h after flg22 treatment and a corresponding reduction upon expression of AvrPto, likely mediated through BKK1. However, this result is based on a single experiment only, and should be confirmed through additional experiments.

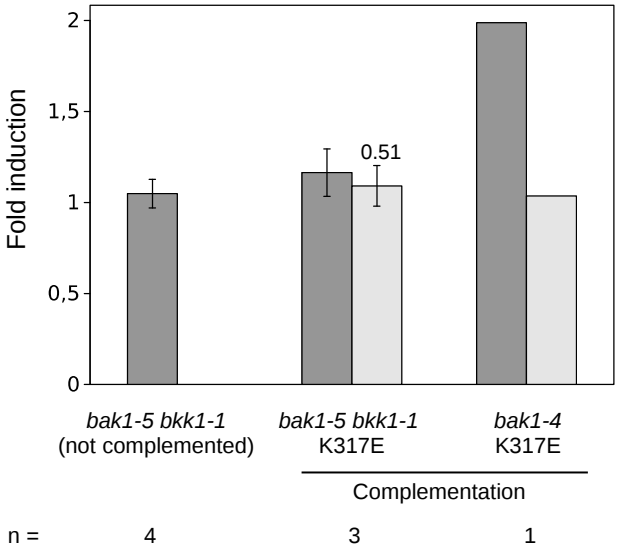

Fig. 4.38 AvrPto functional difference in *bak1-5 bkk1-1* and *bak1-4* mutant protoplasts complemented by transiently expressing BAK1 K317E. Dark bars, without AvrPto; light bars, with AvrPto. Fold change is given as the quotient in luminescence of flg22-stimulated vs. unstimulated protoplasts 3 h after flg22 treatment. Values are given as mean ± SD; the number of independent experiments on which the values are based are given below the data labels. *P* values (unpaired Student's *t*-test) are indicated above the error bars. The *bak1-4* data is based on a single experiment.

CHAPTER 5

DISCUSSION

This study provides novel insights into the virulence strategy of *Pseudomonas syringae* mediated through the effector protein AvrPto, which has served as an important model for the study of effector function in the plant immunity field. AvrPto was previously shown to be involved in the suppression of multiple MAMP-induced defence pathways (**He et al., 2006**), but a conflict in the literature has evolved over the molecular background of these findings. A number of previous studies identified several putative virulence targets but critically, failed to reach consensus on the identity, providing two conceptually different explanations for the observed virulence phenomena – describing AvrPto as either targeting various single PRRs or a common co-receptor (section **5.1**). In contrast to the previous experimental approaches, this work provides a novel way to address this conflict by using comparative quantitative methodology to highlight critical differences in specificity and binding kinetics for the interaction of AvrPto with its multiple virulence targets, as well as with the well-studied avirulence target Pto (section **5.2**). The insights gained from quantitative elucidation of effector virulence mechanisms open up new directions for future research extending quantitative analysis to other facets of the plant immunity field (section **5.3**).

5.1 AvrPto's virulence targets: nuances of a spectrum?

5.1.1 Moving targets are harder to hit

AvrPto targets kinases The plasma membrane localization (**Shan et al., 2000**) and virulence action at an early stage of immune signalling (**He et al., 2006**) gave important clues towards the localization and mechanistic nature of AvrPto's elusive virulence target. As component of the classical gene-for-gene resistance pair *avrPto* / *Pto* (**Ronald et al., 1992**, **Martin et al., 1993**, **Rommens et al., 1995**), it became clear that immunity mediated through AvrPto recognition relies on the direct interaction between AvrPto and an intracellular Ser/Thr kinase (**Scofield et al., 1996**, **Tang et al., 1996**). Taking these separate findings together with the guard model (see section **1.4.2.2**), it was reasonable

to conclude that the virulence target of AvrPto should be a plasma membrane-localized, intracellular kinase acting early in immunity signalling.

PRRs as virulence targets Thus it came at no surprise that the first study pointing towards specific virulence targets identified the intracellular domains of two PRRs, FLS2 and EFR, as virulence targets using evidence of complex formation with the effector by co-immunoprecipitation (Co-IP) experiments (**Xiang et al., 2008**). Importantly, the study highlighted AvrPto's virulence action on multiple PTI pathways and speculated towards a larger array of yet-unidentified PRR-kinase virulence targets. From an evolutionary and physiological point of view, this study reached a conclusion both important and intuitively logical: AvrPto, a kinase inhibitor, binds to several, closely related PRR kinase domains (likely due to their structural similarity) and thus inhibits more than one PTI pathway – AvrPto thus acts as a multifunctional and effective tool evolved by *P. syringae* specifically to shut down early PTI responses, a major factor determining the virulence of bacterial pathogens (**Macho and Zipfel, 2015**), as most clearly underlined by the fact that ectopic expression of AvrPto in *Arabidopsis* fully restores virulence of *P. syringae hrp* mutants completely lacking the T3SS (**Hauck et al., 2003**).

Targeting PRR complexes The discovery of BAK1 as a central co-receptor in various PTI pathways (section **1.4.1.5**), however, changed the big picture of MAMP perception in several important ways, one of them concerning the virulence strategy of effectors. The virulence effects of AvrPto which have been observed in previous studies could now be logically and parsimoniously explained by a mechanism other than that of targeting various different PRRs – targeting the common co-receptor. This new concept was taken up immediately in the second 2008 publication concerning itself with AvrPto's virulence targets (**Shan et al., 2008**); using a similar Co-IP approach to **Xiang et al., 2008**, AvrPto was found to interact with BAK1. Curiously, association of AvrPto with FLS2 was detected in some, but not all of the Co-IP experiments performed in the study; when co-expressing BAK1 and FLS2 in protoplasts together with moderate amounts of AvrPto, Co-IPs resulted in only BAK1 being pulled down with AvrPto. The authors thus concluded that the binding event between AvrPto and FLS2, while observable in specific circumstances, may be an artefact of overexpression. Mechanistically, binding of AvrPto to BAK1 was shown to interfere with flg22-triggered BAK1/FLS2 association, and it was postulated that this physical inhibition of complex formation between a MAMP receptor and its co-receptor, rather than any influence on the target's kinase activity, was the basis of virulence. This finding was consistent with the previous observation in other studies that AvrPto is a relatively weak kinase inhibitor (10^5 times less potent

than PKI, **Grove et al., 1987**, **Xing et al., 2007**), and might not reach necessary levels for its kinase-inhibiting activity to become physiologically relevant during infection in the *in vivo* situation. Beside the direct evidence of BAK1/AvrPto interaction, Shan and co-workers also found indirect evidence pointing towards involvement of BAK1 (rather than different PRRs) in AvrPto virulence action, as AvrPto-overexpressing plants phenotypically resemble plants impaired in BR responses such as *bri1* mutants (**Shan et al., 2008**), a phenotype which could be explained due to the direct involvement of BAK1 as a co-receptor for BL (**Sun et al., 2013b**).

Second thoughts The conflicting datasets obtained from the previously cited studies prompted both groups involved to conduct follow-up experiments; however, these failed to resolve the issue, instead broadening the divide between the previous observations. Further Co-IP experiments using both protoplasts and seedlings, reinforced by bimolecular fluorescence complementation (BiFC) assays in protoplasts, demonstrated interaction between AvrPto and FLS2; critically, no interaction of AvrPto with BAK1 could be observed under the same circumstances (**Xiang et al., 2011**). To address the issue of overexpression, a Co-IP was performed from plants expressing tagged AvrPto, but no tagged targets; detection with antibodies raised against native FLS2 or BAK1 yielded endogenous FLS2, but no BAK1, in the immunoprecipitate. The discrepancy of the results was not limited to the identity of the putative virulence target; mechanistically, the study showed that the flg22-triggered FLS2/BAK1 association occurred independently of the presence or absence of AvrPto; instead, a direct inhibition of FLS2 kinase activity was postulated and reasoned to be visible as a reduction in phosphorylation of BIK1, a downstream substrate of FLS2 kinase activity, in FLS2 but not *fls2* mutant protoplasts (**Zhang et al., 2010**). However, this observation arguably does not rule out the direct involvement of BAK1, as the same group previously showed that BAK1 is essential for flg22-triggered BIK1 phosphorylation, consistent with its role as a co-receptor (**Zhang et al., 2010**). Additional evidence against this line of reasoning stems from the fact that BIK1 was previously shown by the Shan group to be directly phosphorylated by BAK1 *in vitro* (**Lu et al., 2010b**), although *in vivo* this event occurs on flg22 treatment and depends on the presence of both kinase-active FLS2 and BAK1 simultaneously, indicating that transphosphorylation events between FLS2 and BAK1 are essential for subsequent BIK1 phosphorylation. In further response to the findings of **Shan et al., 2008**, Xiang and co-workers provided an alternative explanation for the AvrPto overexpressor *bri1*-like phenotype: AvrPto was shown to interact with two receptor-like cytoplasmatic kinases implicated in BR signalling, the BR-signaling kinase 3 (BSK3), and constitutive differential growth 1 (CDG1), which are downstream substrates of BRI1 (**Tang et al., 2008**, **Kim**

et al., 2011). As the follow-up study by Xiang and coworkers included a broader array of interaction assays to characterize the AvrPto-FLS2 interaction, a similarly targeted follow-up study by the other group analogously expanded the experimental procedures for the AvrPto-BAK1 interaction, and additionally characterized the interaction of another *P. syringae* effector, HopF2, with BAK1 (**Zhou et al., 2013**). BiFC experiments were added, showing interaction of AvrPto with BAK1; additionally Co-IPs were performed using protoplasts in the *fls2* mutant background, again showing interaction with BAK1 and further indicating that this interaction occurs independently from FLS2. The previous findings regarding developmental phenotype were reinforced; constitutive AvrPto overexpressor constructs (35S::AvrPto-HA) did not result in plants producing viable seeds in the Col-0 or *fls2* background; however, using a *bak1-4* mutant background led to reduced severity of the developmental phenotype and to plants producing viable seeds, indicating BAK1 as the physiological virulence target of AvrPto.

AvrPto and stomatal patterning Additional phenotypical evidence leading to BAK1 (and other SERKs) as AvrPto's virulence target was presented in a recent study by the Shan group investigating the function of SERKs in stomatal patterning. Upon perception of epidermal patterning factor (EPF) ligands (**Lee et al., 2012**), SERKs heterodimerize with ERECTA family RLKs to regulate stomatal patterning independent of BR signalling (**Meng et al., 2015**). Ectopic expression of AvrPto causes a stomatal clustering phenotype which disrupts regular stomatal patterning (similar effects were observed for AvrPtoB). This is likely due to AvrPto acting on all functional SERKs, as there is a remarkable redundancy in SERK function in the context of stomatal patterning: single and any double mutants do not show a phenotype, while only one triple mutant combination, *serk1-1*/*serk2-1*/*bak1-4* shows clustered stomata, indicating strong contribution of these three SERKs and somewhat weaker contribution of SERK4. Consistent with these data, AvrPto overexpressor plants show a stronger stomatal clustering phenotype than the mentioned triple mutant (a quadruple null mutant is embryo lethal), indicating suppression of residual functionality by AvrPto targeting SERK4.

Overview: new data in context How do the main findings described in this thesis fit into the context of the previous literature? AvrPto was found to interact with BAK1, Pto, and FLS2, with differential specificity ranked from strongest to weakest interaction in the listed order. In brief, this supports the qualitative data obtained in both **Shan et al., 2008** and **Xiang et al., 2008**, as well as one of the direct follow-up studies, **Zhou et al., 2013**, but not the data in **Xiang et al., 2011**, which ruled out interaction between AvrPto and BAK1. Importantly, the quantitative data for all studied AvrPto interactions are fully

compatible with previous quantitative characterizations as described in **Xing et al., 2007** and **Xiang et al., 2008** (section **4.2.3**, figure **4.16**, **B**). More detailed discussion about quantitative implications of these findings adding new insights to previous studies is given in section **5.2**.

5.1.2 Target subpools and availability at the plasma membrane

The inner plasma membrane: AvrPto's habitat AvrPto contains a myristoylation motif on its second glycine (G2), targeting it to the interior surface of the plant plasma membrane (PM) during secretion via the T3SS; this localization is critical for both its recognition by Pto (**Shan et al., 2000**) and its virulence activity (**He et al., 2006**). As AvrPto interacts with several proteins, which themselves might occur in differential states at the plasma membrane, elucidation of AvrPto's virulence strategy benefits from knowledge about the dynamics of its putative virulence targets in order to determine their spatio-temporal accessibility to the effector.

FLS2 at the PM As a classical model PRR, FLS2 has been the topic of several studies dissecting trafficking and compartmentalization of MAMP receptors, laying the foundation of our current understanding of PRR dynamics at the plasma membrane. FLS2 is in dynamic balance, undergoing ligand-induced endocytosis (**Robatzek et al., 2006**, **Beck et al., 2012**) and secretory trafficking controlled by the endoplasmic reticulum (ER) (**Tintor and Saijo, 2014**, **Inada and Ueda, 2014**) to maintain a signalling-competent receptor pool at the cell surface (**Robatzek and Kuhn, 2015**). MAMP perception leads to dynamic reorganization of protein composition at the plasma membrane, including many PRRs (**Keinath et al., 2010**). Interaction of FLS2 with BAK1 upon ligand perception results in a marked reduction in its membrane mobility; unelicited FLS2 however is highly mobile (**Ali et al., 2007**, **Schulze et al., 2010**). However, localized redistributions of PRRs in direct response to pathogens at the infection site may play a role, and has been demonstrated for FLS2, although paradoxically in response to a fungal pathogen (**Nielsen and Thordal-Christensen, 2013**); the functional relevance of these findings remains to be seen. It is therefore hard to determine the distribution of PRR targets such as FLS2 encountered at the plasma membrane by AvrPto upon secretion into the plant cell; the hypothetical physiological implications of receptor quantity for immunity suppression by AvrPto are discussed in further detail in section **5.3.1**.

Dynamic insights for BAK1 Molecular dynamics of BAK1 populations have been elucidated mainly in the context of brassinosteroid signalling. However, due to the striking structural and mechanistic similarity of BAK1's role in either BR or flg22-induced

signalling, insights obtained from these studies may be relevant for transfer to BAK1-related immunity signalling. Similar to FLS2, BAK1 is constantly recycled to maintain a signalling-competent population at the PM; however, endocytosis of BAK1/BRI complexes seems to be ligand-independent (**Russinova et al., 2004**). This is likely a result of the different dynamic needs of stimulus perception – constant, slower response to endogenous developmental signals vs. fast, flexible response to a MAMP (**Geldner et al., 2007**). A recent study visualizing localizations of fluorescently tagged BAK1 and BRI1 in real time shows that the two proteins constitutively associate in absence of ligand ('pre-formed complexes'), but only about 10 % of the total population of BRI1 at the PM exists as a heterooligomer with BAK1 upon application of exogenous ligand (**Bücherl et al., 2013**), which is in line with earlier semi-quantitative Co-IPs showing that less than 5 % of total BAK1 is recruited by BRI1 upon ligand perception (**Albrecht et al., 2012**). However, ligand perception leads to an increase of $\sim$50 % of receptor heterooligomers, implicating a role for ligand-mediated receptor recruitment (**Bücherl et al., 2013**). Comparing the studies investigating BAK1 dynamics with FLS2 and BRI1 strengthened the notion that BAK1 exists in distinct sub-pools which are not freely interchangeable between developmental and immunity signalling; consequently, the growth-inhibition effect of MAMP signalling does not occur due to any rate limiting caused by BAK1 availability to either pathway, and uncoupling is likely mediated through differential phosphorylation (**Schwessinger et al., 2011**, **Belkhadir et al., 2014**, **Wang et al., 2014a**). However, AvrPto is likely able to bind BAK1 present in both pathways (or at least a hypothetical 'precursor' state of BAK1 feeding into both pathways) as indicated by the growth phenotypes described before and the findings in the present work that AvrPto binds to constitutively fully-phosphorylated BAK1-CD with the same affinity as to the wild-type protein *in vitro* (see section **4.5.1.1**). Although the exact molecular determinants of the differential BAK1 states in developmental and immunity signalling are not yet entirely clear, site-specific differential phosphorylation mediated through BAK1-interacting RLKs was recently demonstrated (**Wang et al., 2014b**). In addition to the direct evidence concerning specific phosphorylation states, a recent study investigating the negative regulatory pseudokinase BIR2 demonstrated a crucial role for BIR2 in segregating BAK1 into distinct pools which can be specifically adressed by the corresponding ligand (**Halter et al., 2014a**).

Redundancy in BAK1 function Homology among members of the SERK family leads to a large degree of functional redundancy in various pathways, including immunity signalling (section **1.4.1.5**). The degree in which the different SERKs can functionally stand in for each other probably depends on the specific PRR involved; while EFR strongly

interacts with all SERKs except SERK5, FLS2 seems to preferentially interact with BAK1 and to a lesser degree, SERK2, while the interaction with SERK1 and BKK1/SERK4 was limited (**Roux et al., 2011**). Consistent with observations that even in *bak1* mutant plants AvrPto was able to suppress MAMP signalling, AvrPto was found to associate with BKK1/SERK4 and SERK5, and may thus be targeting the closest BAK1 homologues to maximize its virulence effects (**Shan et al., 2008**); a later study expanded these findings to SERK1 and SERK2 (**Meng et al., 2015**). These results could be confirmed in this work in the functional assay, as AvrPto was able to suppress the residual flg22-triggered FRK1 induction in *bak1-4* mutant plant protoplasts, likely indicating its action on other SERKs still functionally present in the protoplasts (section **4.6.2**).

5.1.3 Biological significance of target spectrum

Intention or artefact? The notion that AvrPto is an exceptional example of a promiscuous effector, targeting a variety of proteins, is now well established in the literature and has been confirmed through this work. The quantitative data obtained in this work add crucial information to this picture and show that AvrPto is a not only a promiscuous, but also relatively selective effector (**Mandell and Kortemme, 2009**), as there are significant differences in binding affinity to its various targets. However, the question remains whether this broad target range is of direct biological relevance or rather a secondary effect of a relative lack of differentiation in regard to the structural determinants of interactions between AvrPto and its targets. These issues are speculative, as it is difficult to design meaningful experiments directly addressing this question and yielding data that would conclusively rule out either one of these options. As crystallographic structural analysis of the AvrPto-BAK1 and AvrPto-FLS2 interactions was outside the scope of this work, the structural aspect is discussed briefly in section **5.1.4**, while putative implications of the novel quantitative data on AvrPto-target interactions obtained in this work are discussed in detail in sections **5.2** and **5.3.1**.

5.1.4 Molecular aspects of kinase binding

Structural insights The structural data available for AvrPto-Pto and AvrPtoB-BAK1 co-crystals enabled the homology-based modeling of a putative AvrPto-BAK1 complex structure in this work (section **4.4**). The viability of this approach was validated through the determination of a single previously uncharacterised residue on BAK1, T324, which can either increase or decrease the affinity of BAK1 to AvrPto when mutated to a glycine or a phosphomimetic aspartate, respectively. In SPR experiments, these affinity

differences were demonstrated to be caused by altered interaction kinetics (section **4.5.5**, figure **4.32**). The T324 residue is central to a BAK1 loop extending towards the putative location of the AvrPto structure, into close vicinity to AvrPto Y89 (figure **4.33**, **D**). The corresponding aspartate mutant of AvrPto, Y89D, has been previously described to strongly suppress interaction with Pto (**Xing et al., 2007**) and FLS2 (**Xiang et al., 2008**), a finding that could be independently verified through this work (section **4.5.4**, figure **4.33**, **E**). Based on these data, it is most likely that steric hindrance of negatively charged groups (either phosphorylated threonine or the phosphomimetic aspartate residue) mediates the lowered affinity of AvrPto Y89D and BAK1 T324D mutants through electrostatic repulsion. This demonstrates that the AvrPto-BAK1 and AvrPto-Pto interactions occur similarly on a structural level, involving analogous interaction interfaces. The biological significance of BAK1 phosphorylation on T324 is not clear yet, but this phosphorylation was demonstrated *in vitro* for the BAK1-AvrPtoB co-crystal (**Cheng et al., 2011**), and the BAK1 T324D mutant can still functionally complement flg22-triggered immunity signalling in *Arabidopsis* protoplasts (section **4.6.2**, figure **4.36**, **B**).

Interaction determinants Consistent with previous findings that reached similar conclusions for FLS2 (**Xiang et al., 2008**) and Pto (**Xing et al., 2007**), this work demonstrated that an active conformation of BAK1's catalytic loop (which can be disrupted through the K317E kinase-inactive mutation) is crucial for AvrPto interaction (section **4.5.1.2**). In contrast to T324 and K317, no other single-point-mutated BAK1 variants tested in this work showed a significant difference in AvrPto interaction compared to wild-type BAK1 (section **4.5.5**, figure **4.5.5**), indicating that further mutational analysis, possibly including higher order combinations of amino acid substitutions, may be necessary to unravel the exact primary sequence determinants which allow BAK1 (in contrast to, for example, BRI1) to interact with AvrPto. A putative future co-crystal structure of AvrPto in complex with BAK1, once available, will significantly facilitate this task and allow independent verification of the homology-based *in silico* model described in this work.

Kinase inhibition? Elucidation of the AvrPto-Pto co-crystal structure (**Xing et al., 2007**) demonstrated a significant structural similarity to the well-studied complex of the cAMP-dependent protein kinase (also known as protein kinase A, PKA) and its corresponding small inhibitory peptide, protein kinase A inhibitor (PKI, **Bossemeyer et al., 1993**). These findings explain the autophosphorylation-inhibitory effect observed *in vitro* by **Xiang et al., 2008** for FLS2 and, in this work, for BAK1 (section **4.1.4**, figure **4.12**). The effect is likely based on competitive inhibition through a pseudosubstrate

mechanism, as both PKI and the corresponding loop of AvrPto localize close to the ATP binding pocket of PKA and Pto, respectively (**Dalton and Dewey, 2006**, **Xing et al., 2007**), thus limiting access of ATP substrate. A similar reduction of BAK1 autophosphorylation has been shown for the interaction between AvrPtoB and BAK1 (**Cheng et al., 2011**). However, it has been shown that AvrPto is drastically less effective in inhibiting Pto autophosphorylation when compared to the PKI/PKA pair (K_is of 11 µM and 1 nM, respectively, a difference of 4 orders of magnitude; **Xing et al., 2007**, **Shan et al., 2008**). Interestingly, while the interaction of AvrPtoB with BAK1 is significantly weaker than that of AvrPto (steady-state affinity of 3.5 µM, or approximately 100-fold lower than that of AvrPto to BAK1), its inhibitory effect on BAK1 autophosphorylation is significantly stronger in relative terms (**Cheng et al., 2011**). It thus appears likely that the inhibition of BAK1 kinase activity through AvrPto, while demonstrable, may be a secondary effect of its complex localization, not its primary molecular virulence function.

5.2 A novel quantitative look at effector-target interactions

5.2.1 Methodology of this work compared with previous studies

Black, white, or grey? The collection of previous studies providing specific data towards the identification of AvrPto's putative virulence target (**5.1.1**) had one important methodological aspect in common: the reliance on qualitative approaches such as Co-IP and BiFC for describing bimolecular interactions. Compared to high-throughput screening methods such as yeast two-hybrid (Y2H) or affinity purification followed by mass spectrometry (AP-MS), these methods provide lower rates of false negatives or positives, thereby increasing the fidelity of the interaction data at the cost of throughput (**Berggård et al., 2007**, **Lalonde et al., 2008**). Co-IP, when performed with specific antibodies, can faithfully report the presence of a complex including two or more proteins of interest. However, quantitative conclusions are very limited. While it may be possible to qualitatively rank affinities between multiple interaction pairs by carefully choosing expression levels (as has been performed in **Shan et al., 2008**, demonstrating that compared to FLS2, a larger amount of BAK1 can be co-immunoprecipitated with AvrPto), true quantitative information such as dissociation constants (K_Ds) cannot be obtained. Moreover, it is difficult to conclude that an interaction characterized by Co-IP is really indicative of a binary, direct contact between two proteins, as a third (possibly undetected) protein might mediate the physical association between the two proteins of interest. Very similar limitations apply to BiFC analysis, as association of proteins at a distance of $\sim$7 nm can reconstitute the fluorophore and thus lead to a positive signal (**Hu et al., 2005**, **Fan et al.,**

2008); this distance scale is well within the range of higher-order protein complexes (**Erickson, 2009**).

In vivo* vs. *in vitro The most significant conceptual advantage of these methods compared to the main methods used in the present work is their higher similarity to native biological conditions, as they can be performed inside living cells or complete organisms mimicking the situation as it would occur in nature. However, it is impossible to achieve truly native conditions in controlled laboratory experimental environments, and each method necessarily includes deviations from the natural system (such as changes in protein expression levels or down-stream analytical manipulations); therefore, conceptually, there are arguably no practically attainable 'native' conditions, but rather varying degrees of 'artificial'. Advancing along the scale towards more artificial conditions allows the control of an increasing number of experimental parameters. Under purely *in vitro* conditions, protein-protein interactions can be studied quantitatively because the use of purified proteins in aqueous buffer environments rules out a large number of (potentially, unknown) complicating factors, and allows quantification of individual protein concentrations. Thus, the critical advantage of *in vitro* methodology is the possibility of quantitative analyis. It is important to carefully consider the advantages and disadvantages of each method; ultimately, *in vivo* and *in vitro* methods ideally complement each other to yield different types of information which then allow to characterize a protein-protein interaction in greatest depth (**Piehler, 2005**).

5.2.2 Seeing both sides of a coin: steady-state affinity and kinetics for quantitative characterization of an interaction

Steady-state affinity A common way to quantify the intensity of biomolecular interactions is the determination of binding affinity – ultimately a thermodynamic description of the sum of attractive and repulsive intermolecular forces that govern the interaction. Fundamentally, biomolecular interactions can often be reasonably described by simple binding models which are governed by the law of mass action; formation of a biological complex can thus be described succinctly as the reversible formation of a product made up of two reactants A and B: $A + B \longrightarrow AB$. Steady-state affinity determination assays take advantage of the fact that such reactions eventually reach chemical equilibrium; that is, the association and dissociation rates of the complex are equal and there is no net change in the amount of complex. If the concentration of the reactants can be predetermined and the amount of complex can be observed, experimental titration approaches allow quantification of the interaction's binding affinity. In this work, steady-state binding affini-

ties were measured through microscale thermophoresis (MST), an optical technology for quantitative interaction analysis (section **3.7.1.1** and figure **3.4** illustrate the titration concept applied to MST). The most common way to describe affinity in context of biologically relevant interactions is that of the dissociation constant, K_D, which is defined as the concentration of free A at which half of B is associated with A. It is important to note that while often quantitatively linked, dissociation constants of functionally relevant biomolecular interactions do not always reflect the actual functional output of the system (e.g. as described by the EC_{50} of dose-response curves).

Kinetics Kinetic affinity determination reaches the same type of information via a different pathway; instead of observing reactions that have reached chemical equilibrium, the rates of association and dissociation of the complex are measured directly. Formation of the complex AB is described by a forward reaction ($A + B \longrightarrow AB$), which is governed by the association rate constant, k_a. Conversely, dissociation of the complex AB is described by a backward reaction ($AB \longrightarrow A + B$), which is governed by the dissociation rate constant, k_d. The affinity of the interaction (K_D) can then be determined directly from the association and dissociation rate constants: $K_D = \frac{k_d}{k_a}$. Intuitively, a higher affinity thus corresponds to a faster association rate and a slower dissociation rate of the complex. Compared to steady-state analysis, kinetic analysis provides additional information to characterize an interaction, as two interactions with the same affinity can have different kinetic behaviours. In the present work, this is exemplified by the interactions between AvrPto and either BAK1 or Pto: although the binding affinity of these interactions differs by roughly a factor of 3, the interaction between AvrPto and BAK1 both associates and dissociates roughly 10 times faster (figure **4.25**). In this work, kinetic experiments have been performed using surface plasmon resonance spectroscopy (SPR; section **3.7.2**) in a single-cycle kinetic titration approach (figure **3.7**).

5.2.3 Quantitative differences in affinity: *quo vadis*?

Scales The highest affinity measured in the course of this work was that of AvrPto to BAK1-CD, with K_Ds determined as 45 $\pm$8 nM (steady-state, section **4.2.1**) and 36 $\pm$13 nM (kinetics, section **4.3.1**), respectively. How does this affinity compare to that of other well-known physiologically relevant biomolecular interactions? Botulinum neurotoxin of *Clostridium botulinum*, the most acutely lethal toxin currently known with an LD_{50} of 1.3–2.1 $ng\,kg^{-1}$ in rats (**Arnon et al., 2001**), binds its protein receptor with a K_D of $\sim$34 nM (**Jin et al., 2006**), an affinity very similar to the AvrPto-BAK1 interaction. The affinity ceiling in biological context is likely provided by two of the strongest currently

known non-covalent protein-ligand binding events, the interactions of avidin or streptavidin with biotin, which occur on a femtomolar affinity scale (**Weber et al., 1989**). However, such exceedingly strong interactions seem to be the exception rather than the rule, and most biologically relevant interactions, including protein-protein interactions, occur at affinities between roughly 1 nM and 1 mM, with some rare exceptions in the picomolar range (**Houk et al., 2003**, **Wang et al., 2004**, **Chen et al., 2013**). Specific protein-protein interactions, as exemplified by mammalian antibodies binding their cognate antigens, are typically in the nanomolar to low micromolar affinity range (**Griffiths et al., 1994**). However, more transient protein-protein interactions, as they typically occur in signalling, may be significantly weaker, often falling into the higher micromolar range (**Nooren and Thornton, 2003**). Importantly, the affinity of the effector AvrPtoB to BAK1 was previously determined as 3.5 μM in isothermal titration calorimetry (ITC) experiments (**Cheng et al., 2011**), an affinity 100-fold lower than that of AvrPto to BAK1 as determined in this work. In this context, the affinity of AvrPto to its virulence targets BAK1 and FLS2, as well as to the tomato avirulence target Pto, can generally be categorized as relatively specific, high-affinity protein-protein interactions, based on the relative affinity scale on which these interactions occur.

Factors The affinity difference between the interaction pairs AvrPto-BAK1 and AvrPto-FLS2, as determined in equilibrium binding analysis, is approximately 5-fold (figure **4.16 A**). What implications can a 5-fold difference in affinity have on biological context at the cellular scale? Or, stated more provocatively, is this enough of a quantitative separation to postulate meaningful physiological effects originating from such an affinity difference? Unfortunately, there is little quantitative data regarding effector-target interactions, or other similar interactions in the context of plant immunity; the greatest number of detailed quantitative analyses of biological interactions has been performed in context of medical and pharmaceutical science, especially cancer research. Studies investigating the functionality of animal **e**strogen **r**eceptors (ERs)) indicate that $\sim$4-fold ligand affinity differences between two receptor subtypes, ERα and ERβ, may be the molecular basis for tissue-specific differential action of estrogens (**Kuiper et al., 1997**), thus highlighting a relatively small difference in interaction affinity as a major factor encoding a physiological output (albeit on a receptor-ligand level). The human Dicer protein, which converts **d**ouble-**s**tranded RNA (dsRNA) substrates to **s**mall **i**nterfering RNA (siRNA) products, is dynamically regulated through differential binding affinities on a similar scale. Dicer is inhibited by processed siRNAs, which competitively bind the active site of the enzyme, but with an affinity 5-11 times weaker than the substrate dsRNAs (**Lima et al., 2009**). Obviously, the specificity factors necessary to achieve differential functional

output in complex interaction networks depends largely on the relative levels of all the interactants. To elucidate these quantitative relationships in complex interaction networks is a daunting task, and even the most well-studied interactions (such as those including the human **e**pidermal **g**rowth **f**actor **r**eceptors (EGFRs) are not fully understood yet on the quantitative scale (**Jones et al., 2006**).

Selectivity Looking at the physiological consequences of kinase inhibition, the medical literature provides some illustrative insights, as target selectivity of kinase inhibitors is a major issue in drug design. A large scale study comparing target binding specificity of a set of 38 pharmaceutical small-molecule kinase inhibitors to 287 human kinases ($\sim$ 55 % of the predicted kinome) show that selectivity varies significantly, with some inhibitors acting very selectively, some promiscously, and many strongly binding a primary target and additionally various 'off-targets' with differential specificity (**Karaman et al., 2008**). Qualitatively, the latter situation is remarkably similar to that of the putative AvrPto interactome. The authors quantified selectivity relative to primary targets $\left(S = \frac{K_{\mathrm{D}}(off-target)}{K_{\mathrm{D}}(primary\ target)}\right)$ and found that most small-molecule kinase inhibitors are quite selective to their primary targets, but some have significant affinity (defined as $S \leq 10$) to off-targets which are closely related to the primary target, and a few even to relatively unrelated off-targets. This differential specificity has been identified as a highly relevant factor in the design of anti-tumor and anti-angiogenic agents (**Morin, 2000**), and can lead to tissue-specific functional implications of these kinase inhibitors (**Sako et al., 1988**). Arguably, similar mechanisms could apply, in the context plant immunity, to differential specificity of effectors targeting multiple kinases (such as AvrPto and AvrPtoB). However, whether there is significant functional similarity between the well-characterized pharmaceutically relevant small-molecule kinase-inhibitors of animal kinases and macromolecular kinase inhibitors such as AvrPto is not known, and a lack of comparative quantitative data on the selectivity of other proteinaceous kinase inhibitors precludes direct comparisons. Thus, more quantitative studies on functionally similar protein-protein interactions are needed to clarify this issue and establish the functional importance of target selectivity in the context of effector virulence in plant immunity signalling.

Efficacy, a missing link? Studies quantitatively probing receptor-ligand relationships in depth, usually in the medical context of developing receptor antagonists in drug design, demonstrated that *efficacy* is a critical link between two independently quantitative elements, interaction affinity and physiological response (**Kenakin, 2002**). Efficacy can be summarized as differential functional output a given ligand causes at a given state of

receptor occupancy. Conceptually, the virulence effects of AvrPto could be described in this manner by quantitatively linking its target occupation to observed virulence results (effectively making AvrPto a 'ligand' to its virulence target 'receptors' in the nomenclature of classical efficacy studies). However, such analysis is complicated by the lack of a reliable physiological readout that is both close to native conditions and sensitive enough to detect quantitative differences in affinity between AvrPto and its virulence targets. In the present work, an adapted protoplast system using pFRK1 activation (and its repression through AvrPto) as physiological readout (sections **3.8.1** and **4.6.2**), while demonstrating the *in vivo* effects of AvrPto virulence, did not achieve sufficient resolution to significantly discriminate between ∼4-fold differences in affinity (section **4.6.2**), which was the highest difference obtained for the tested BAK1 single point mutations (figure **4.35**, **C**). Thus, the putative quantitative relationship between virulence target binding affinity and gradated physiological output (observed virulence effects) remains elusive at this point. Possibly, further mutational analysis using BAK1 variants concurrently mutated in multiple sites may achieve larger affinity shifts that may be reflected in the established pFRK1-Luc protoplast assay.

5.2.4 Implications from kinetics

Time is of the essence Kinetic analysis adds a critical temporal dimension to quantitative interaction analysis. While steady-state affinity is a very convenient measure to quantify the strength of an interaction, it conceptualizes a 'frozen' state of complex existence which realistically does not often occur in nature, as physiological interactions between biomolecules may never reach chemical equilibrium $\left(k_\mathrm{a} \times [A] \times [B] = k_\mathrm{d} \times [AB]\right)$ before the corresponding biological event has already concluded – as has been succinctly stated in a technical article on kinetic analysis, 'biological systems that have reached a state of equilibrium are typically necrotic' (**Önell and Andersson, 2005**). Many high-affinity interactions dissociate slowly enough that quantitative disruption of a complex, once formed, does not occur under physiological conditions. The most stable complex observed in the course of this work was that of AvrPto with Pto, with a dissociation rate constant 2.2×10^{-4} ($\pm 1.2 \times 10^{-4}$) s^{-1} (section **4.3.2**). How long would meaningful complex dissociation take under these circumstances? Calculating the half-life (first-order reaction kinetics) of the complex yields:

$$t_{1/2}\ \text{(AvrPto-Pto)} = \frac{\ln 2}{k_\mathrm{d}\text{(AvrPto-Pto)}} \approx \frac{0.693}{2.2 \times 10^{-4}\ \mathrm{s}^{-1}} = 3150\ \mathrm{s} = \boxed{52.5\ \mathrm{min}} \qquad (5.1)$$

It appears reasonably unlikely that a significant amount of AvrPto could be liberated once recognized by Pto, and depending on (currently unknown) relative effector/receptor levels in the physiological context of infection, this interaction may be irreversible for all practical purposes. The fact that tomato plants carrying the *Pto/Prf* R-gene system are highly resistant to Pto DC3000 infection argues for the effectiveness of this ETI defence pathway, and the idea that the robust induction of defence responses mediated through Prf/Pto can easily overcome the virulence effects of PTI suppression. In contrast to complex dissociation, the timing effects of complex association are harder to interpret, as according to the law of mass action, they are second-order reactions and critically depend on the actual concentrations of each individual interactant (termed 'A' and 'B' in the following differential equation) at the onset of complex formation:

$$\frac{\mathrm{d}[AB]}{\mathrm{d}t} = k_{\mathrm{a}} \times [A] \times [B] - k_{\mathrm{d}} \times [AB] \tag{5.2}$$

Thus, even relatively slow association rates may be practically overcome through interactor abundance, and it appears reasonable to assume that this would be the case for Pto. Possibly, future work investigating Pto and virulence target (*Sl*FLS2, *Sl*BAK1) protein levels in tomato plants under physiological conditions might reveal the currently missing concentration data components to predict the relative amounts of AvrPto-virulence target and AvrPto-Pto complexes forming during infection, and thus provide further insights into the Pto-mediated defence strategy evolved in tomato against AvrPto.

Evolutionary framework The interactions between AvrPto and its different binding partners occur on a relatively narrow affinity scale (one order of magnitude), but the kinetics are strikingly different – viewed qualitatively and relative to each other, AvrPto-BAK1 associates quickly and dissociates slowly, AvrPto-FLS2 associates slowly and dissociates quickly, and AvrPto-Pto associates slowly and dissociates slowly (section **4.3.5**). These data intuitively fit into a theoretical framework which aims to explain how the functionally different interactions of AvrPto with its multiple binding partners originated on an evolutionary level, possibly adressing the question of biological significance that was proposed earlier (section **5.1.3**). On the pathogen side, AvrPto likely evolved to quickly and quantitatively associate with BAK1 upon injection and targeting to the plant plasma membrane, thus effectively shutting down multiple early-timescale MAMP responses simultaneously. AvrPto would encounter various off-targets, namely the intracellular kinase domains of PRRs, due to their structural similarity with AvrPto's primary target BAK1. However, the specificity to BAK1 would be accomplished as binding to off-targets appears to occur on slower time scales, and additionally, as the dissociation of AvrPto

from PRR CDs is relatively fast, as exemplified by the FLS2 data. The AvrPto-FLS2 complex has a half-life of 9.9 s (calculated as shown before for the AvrPto-Pto complex, equation **5.1**); compared to the situation for the AvrPto-BAK1 complex, which has a half-life of 477 s (7.95 min), this almost 50-fold difference in complex stability indicates that binding events to off-targets would be relatively reversible and thus allow the effector to preferentially bind its primary target with high fidelity. Thus, the evolutionary pressure to abrogate binding to secondary targets might be rather low, and if any such evolutionary modifications would also lower the affinity to AvrPto's primary target (a likely possibility considering the structural similarities between the BAK1-CD and PRR-CDs), it might be opportune to sacrifice a certain amount of specificity to gain maximum affinity to the primary virulence target.

5.3 Transferring insights to more complex systems

The quantitative interaction analysis performed in this work delivers insights that help to evaluate the functional role of AvrPto in the origin of both virulence and avirulence responses in plants. The next steps to further our understanding of effector biology and virulence mechanisms now need to place these findings into physiological context. Pathways in plant immunity are being elucidated mechanistically in ever-greater detail, but critically, quantitative characterizations on an *in vivo* level remain rare. AvrPto acts early during infection to suppress PTI responses, and the evaluation of its physiological action, and thus, its virulence strategy, hinges heavily on information about the relative abundance of the effector, its various putative virulence targets, and (if present), avirulence targets.

5.3.1 Physiological consequences of protein levels

Dynamics of AvrPto delivery AvrPto gets secreted into the plant cell in a partially unfolded state in order to physically fit through the inner diameter of the T3SS apparatus (which is $\sim$2.5 nm, **Blocker et al., 2001**), and employs a pH-dependent folding switch to attain its active form within the plant cytoplasm (**Dawson et al., 2009**). Experiments quantifying effector delivery into host cells in real time using another bacterial model organism, enteropathogenic *E. coli*, demonstrate that the translocation kinetics of effectors can be strikingly different, resulting in a hierarchical delivery that may indicate timing as a strategy to coordinate effector function; 40 min after infection, delivery of 'quick' effectors may already have reached a steady-state while delivery of 'slow' effectors may be barely detectable, and effector concentration within the bacterial cell was found to

be a main determinant for translocation kinetics (**Mills et al., 2008**). In absolute terms, the kinetics for the effector translocation event can be very fast, as demonstrated by a study showing insertion of the *Salmonella* invasion protein (SipA) into the host cell ∼60 s after bacterial docking; the delivery then continued linearly until complete exhaustion of the intrabacterial effector pool (**Schlumberger et al., 2005**). The translocation kinetics for AvrPto are still unknown; studies using an AvrPto fusion protein with a calmodulin-dependent adenylate cyclase (Cya) reporter domain detected effective translocation at the first time point of the experiment, which was 3 h after inoculation of tomato plants with Pto DC3000 (**Schechter et al., 2004**), but the temporal resolution of this assay is too low to determine accurate translocation kinetics. It is therefore currently unknown which determinants govern the effective delivery of AvrPto into the plant cell, and the time scales involved; experimental approaches dynamically tracking AvrPto delivery (e.g. through observing fluorescently labeled AvrPto *in planta*) are needed to clarify this issue. However, it is reasonable to assume that in early stages of infection, the absolute amount of functional AvrPto able to interact with virulence targets *in situ* is rather low, as there are multiple potential rate-limiting steps involved: pathogen attachment, AvrPto delivery through the T3SS, pH-triggered AvrPto folding, and finally, diffusion towards the target protein.

Target abundance It is logical to assume that this effector scarcity early in the infection process implies that overly abundant virulence targets may not be effectively (i.e., quantitatively) bound by AvrPto. At this point, any significant differences in target levels would be crucial to determine the possible effectiveness of AvrPto; in extreme situations, this factor could theoretically even outweigh affinity differences. If, for example, the amount of immunity signalling-competent BAK1 present would outweigh the amount of FLS2 by a factor of 100 before flg22-triggered complex formation, AvrPto binding to FLS2 could have a greater effect despite its lower affinity, as a limiting amount of effector could block a larger relative fraction of FLS2 than BAK1 to inhibit FLS2/BAK1 complex formation. However, current knowledge about both FLS2 and BAK1 amounts *in planta* is relatively limited. A study highlighting functional variation of FLS2 across *A. thaliana* ecotypes and close relatives quantified total FLS2 abundance via Western Blot (using an antibody against sequence-identical epitopes), noting that FLS2 amounts vary widely, are apparently not correlated to transcript levels, and that functional differences in flg22 response observed in the various groups primarily depend on receptor levels, not differential affinity of MAMP to receptor (**Vetter et al., 2012**). These findings indicate that although the FLS2 perception system is generally well conserved, the actual amount of receptor present is highly variable; furthermore, it is currently unclear how the apparent

disconnection between transcript and protein levels observed by Vetter and colleagues can be explained mechanistically and physiologically, as regulation of FLS2 transcript levels has been observed in context of ethylene signalling (**Mersmann et al., 2010**). Another phytohormone, **s**alicylic **a**cid (SA), was recently shown to directly control the abundance of both FLS2 and BAK1 pools at the plasma membrane relative to non-plasma membrane fractions through the **A**ccelerated **C**ell **D**eath **6** (ACD6) protein, which directly associates with FLS2 and BAK1 and and likely acts on the secretory pathway to stimulate their maturation and export from the ER (**Zhang et al., 2014**, **Tateda et al., 2014**). Taking these findings together, it appears likely that hormonal modulation of plant immunity responses can have direct effects on AvrPto's effectiveness in PTI signalling suppression by increasing receptor amounts at the plasma membrane, although current approaches limit our understanding to relative, not absolute protein levels.

Sequestering by Pto? The binding event of AvrPto to Pto initiates ETI signalling in a classical R-protein-mediated response (section **1.4.2.3**). This effect is sufficient to explain the resistance of plants carrying the *Pto/Prf* system to Pto DC3000. However, the peculiar kinetics of the AvrPto/Pto interaction (figure **4.3.5**, section **5.2.4**) raise the question whether physical sequestering effects may also play a significant role. As formation of the AvrPto-Pto complex likely relies on significant amounts of available Pto (in order to overcome the relatively slow association), this fact combined with the exceptionally high complex stability may lead to a local depletion of AvrPto at the plasma membrane, providing a conceptually independent approach to mitigate AvrPto's virulence effects *in vivo*. Importantly, this hypothesis is consistent with an interesting effect observed by He and coworkers in an early study: ectopic expression of Pto in *Arabidopsis* protoplasts lowered AvrPto's ability to suppress flg22-triggered FRK1 activation (**He et al., 2006**); this would likely be mediated through the postulated sequestering effects, as these protoplasts lacked a signalling-competent Pto/Prf system. This putative double-edged defence strategy by R-protein complexes could provide an intriguing perspective for future research efforts, as there is currently no example for such a hypothetical 'bi-modal' guarded effector target.

5.3.2 Putative unknown targets

A wide interactome? The possibility of multiple virulence targets was recognized from the very beginning of investigations into AvrPto's interactome (section **5.1.1**). Although an increasing amount of evidence (including this work) points towards the central co-receptor BAK1 as the primary virulence target, AvrPto was previously shown

to additionally interact with the kinase domains of other SERKs (**Meng et al., 2015**), FLS2 (this work, **Shan et al., 2008**, **Xiang et al., 2008**), and EFR (**Xiang et al., 2008**). Besides these relatively well-characterized PRR targets, there is a number of proteins for which initial data also indicate association with AvrPto. Xiang and coworkers observed that AvrPto interacts with several RLCKs (**Xiang et al., 2011**); additionally, the same group previously found that AvrPto binds and inhibits the autophosphorylation of the kinase domain of At2g23200, a yet uncharacterized Ser/Thr kinase of the *Catharanthus roseus* receptor-like kinase (CrRLK1L) subfamily featuring malectin-like domains and putatively involved in plant immunity (**Xiang et al., 2008**, **Nissen et al., 2016**).

Delimiting the interactome's extent It thus appears highly likely that AvrPto is generally unselective enough to qualitatively (although probably not quantitatively) associate with a large group of kinases independent of their exact physiological function, and these probably represent 'off-targets' as discussed previously in the context of selectivity (section **5.2.3**). It is possible that we are just beginning to gather targets of this remarkably promiscuous effector, and have barely scratched the surface of its interactome. Although the affinity of AvrPto to BAK1 is high enough to confidently state this interaction to be highly specific and indicative of a primary target in evolutionary context, it cannot be ruled out completely that AvrPto interacts with other, yet unknown proteins with even greater specificity. At this point, the structural requirements that kinases need to meet in order to interact with AvrPto are not clear yet (section **5.1.4**), and it has been shown previously that it is hard to predict these interactions based on sequence similarity alone (**Shan et al., 2008**). As mentioned above, previous studies led to the discovery of several AvrPto-interacting proteins in a case-by-case manner, but the hypothetical interactome is large enough that other approaches may be necessary to fully understand its boundaries. If future work can determine specific residues which confer interaction with AvrPto to previously non-binding kinase targets (such as BRI1), it may finally be possible to comprehensively predict the extent of AvrPto's interactome based on sequence and structural data.

SUMMARY

Pseudomonas syringae is a widespread and highly adaptable bacterial plant pathogen that can infect both economically relevant crop plants and *Arabidopsis thaliana*, making it a highly relevant model pathogen for investigating the origin of pathogenicity in the plant immunity field. *P. syringae* uses a large and diverse arsenal of effector proteins secreted into the host cell to suppress plant immune responses during the infection process and thereby increase its virulence. One of these effectors, AvrPto, has historically been studied in-depth as a part of a classical gene-for-gene resistance pair in tomato. Though it has been the target of scientific inquiry for more than two decades, the virulence mechanism of AvrPto remained largely elusive. AvrPto binds the intracellular kinase domains of multiple plant plasma membrane pattern recognition receptors, and previous qualitative investigations into these interactions led to inconclusive and conflicting hypotheses regarding AvrPto's virulence target. This thesis provides insights into these unresolved questions by using quantitative methodology to investigate differences in binding specificity and interaction kinetics in AvrPto's multi-faceted interactome. AvrPto was shown to bind the intracellular domain of the PRR-interacting co-receptor *At*BAK1 with high affinity, while binding the equivalent domain of the PRR *At*FLS2 with demonstrable, but significantly lower affinity. Quantitative investigation into the interaction of AvrPto with *Sl*Pto, the guarded effector target forming the molecular basis for R-gene mediated immunity in response to AvrPto recognition in tomato, show that the affinity of this interaction ranks between those of AvrPto with either BAK1 or FLS2. These data indicate that AvrPto likely evolved to bind BAK1 homologues in various host plant species, and in turn, *Sl*Pto evolved in tomato to bind AvrPto and mediate its recognition. In contrast, binding to FLS2 likely occurs due to its structural similarity to the primary target BAK1. Importantly, additional kinetic analysis of these interactions provided a conceptually different methodological approach to corroborate the affinity data, and added temporal information consistent with the described evolutionary model. Although the exact molecular determinants of AvrPto's kinase binding specificity remain elusive, mutational analysis on BAK1's intracellular domain indicate that the interaction likely occurs structurally similarly to that of AvrPto with Pto, an interaction which has already been structurally elucidated.

ZUSAMMENFASSUNG

Pseudomonas syringae ist ein weitverbreitetes und hochgradig anpassungsfähiges pflanzenpathogenes Bakterium; da es sowohl wichtige Nutzpflanzen als auch den pflanzlichen Modellorganismus *Arabidopsis thaliana* befällt, wurde es zu einem wichtigen Modell für die Aufklärung von Virulenzmechanismen in der Pflanzenimmunitätsforschung. Von herausragender Bedeutung für die Pathogenität von *P. syringae* ist ein großes Repertoire verschiedener Effektorproteine, die in die Pflanzenzelle sekretiert werden und dort auf mannigfaltige Weise die Immunantwort des Wirtes unterbinden können. Eines dieser Effektorproteine, AvrPto, wurde in der Vergangenheit besonders intensiv untersucht, da es Bestandteil eines Resistenzpaares im Rahmen der klassischen Gen-für-Gen Hypothese der pflanzlichen vererbten Immunität ist. Trotz dieser Umstände verblieb die Identität des pflanzlichen Zielproteins, das von AvrPto zur Virulenzsteigerung angegriffen wird, lange ungeklärt. Dieser Arbeit vorangehende Studien konnten zwar zeigen, dass AvrPto in der Lage ist, die intrazellulären Domänen verschiedener pflanzlicher Rezeptorkinasen zu binden, allerdings verblieb die biologische Relevanz dieser Interaktionen ein bedeutsamer Streitpunkt. Durch quantitative Methodik, die sich von den bisherigen Ansätzen unterscheidet, konnten im Rahmen dieser Dissertation neue Erkenntnise zu diesem Thema gewonnen werden. Es konnte gezeigt werden, dass AvrPto die intrazelluläre Domäne des PRR-Korezeptors *At*BAK1 mit hoher Affinität bindet, während die äquivalente Domäne des PRRs *At*FLS2 deutlich schwächer gebunden wird. Im Vergleich dazu liegt die Affinität von AvrPto zu *Sl*Pto, dem Protein aus Tomate welches die spezifische Erkennung von AvrPto vermittelt, dazwischen. Evolutionsgeschichtlich gesehen lassen sich diese Umstände durch folgendes Modell erklären: AvrPto evolvierte wahrscheinlich, um das in vielen Pflanzenspezies konservierte Zielprotein BAK1 mit hoher Affinität zu binden, während in Tomate seinerseits das Protein Pto evolvierte, um AvrPto zu binden und seine Erkennung zu vermitteln; die Bindung von AvrPto zu FLS2 hingegen beruht vermutlich auf struktureller Ähnlichkeit zum Zielprotein BAK1. Kinetische Experimente ermöglichten eine methodisch unabhängige Verifizierung der Affinitätsdaten und stützen das beschriebene Evolutionsmodell durch dazu schlüssige zeitabhängige Aspekte der Bindungscharakteristik. Obwohl derzeitig noch nicht abschließend geklärt ist, welche molekularen Eigenschaften die Bindespezifität von AvrPto zu verschiedenen Kinasedomänen vermitteln, konnte durch Mutagenese von BAK1 gezeigt werden, dass die Bindung strukturell wahrscheinlich ähnlich zu der mit Pto stattfindet, für welche bereits Kristallstrukturdaten vorliegen.

REFERENCES

Aan den Toorn, M., Albrecht, C., and Vries, S. de (2015). "On the Origin of SERKs: Bioinformatics analysis of the Somatic Embryogenesis Receptor Kinases." In: *Mol. Plant* 8.5, pp. 762–782.

Abramovitch, R. B. and Martin, G. B. (2004). "Strategies used by bacterial pathogens to suppress plant defenses". In: *Curr. Opin. Plant Biol.* 7.4, pp. 356–364.

Acevedo, F. E. et al. (2015). "Cues from chewing insects - the intersection of DAMPs, HAMPs, MAMPs and effectors". In: *Curr. Opin. Plant Biol.* 26, pp. 80–86.

Ahmed, R. and Gray, D. (1996). "Immunological memory and protective immunity: understanding their relation." In: *Science* 272.5258, pp. 54–60.

Ailloud, F. et al. (2015). "Comparative genomic analysis of Ralstonia solanacearum reveals candidate genes for host specificity." In: *BMC Genomics* 16.270, pp. 1–11.

Akira, S. and Takeda, K. (2004). "Toll-like receptor signalling." In: *Nat. Rev. Immunol.* 4.7, pp. 499–511.

Akira, S., Uematsu, S., and Takeuchi, O. (2006). "Pathogen recognition and innate immunity." In: *Cell* 124.4, pp. 783–801.

Albert, I. et al. (2015). "An RLP23–SOBIR1–BAK1 complex mediates NLP-triggered immunity". In: *Nat. Plants* 1.10, pp. 1–9.

Albert, M. et al. (2010a). "*Arabidopsis thaliana* pattern recognition receptors for bacterial elongation factor tu and flagellin can be combined to form functional chimeric receptors". In: *J. Biol. Chem.* 285.25, pp. 19035–19042.

Albert, M. et al. (2010b). "Regulation of cell behaviour by plant receptor kinases: Pattern recognition receptors as prototypical models". In: *Eur. J. Cell Biol.* 89.2-3, pp. 200–207.

Albrecht, C. et al. (2008). "*Arabidopsis* SOMATIC EMBRYOGENESIS RECEPTOR KINASE proteins serve brassinosteroid-dependent and -independent signaling pathways". In: *Plant Physiol.* 148.1, pp. 611–619.

Albrecht, C. et al. (2012). "Brassinosteroids inhibit pathogen-associated molecular pattern-triggered immune signaling independent of the receptor kinase BAK1". In: *Proc. Natl. Acad. Sci. U. S. A.* 109.1, pp. 303–308. arXiv: arXiv:1408.1149.

Ali, G. S. et al. (2007). "Ligand-dependent reduction in the membrane mobility of Flagellin sensitive2, an *Arabidopsis* receptor-like kinase". In: *Plant Cell Physiol.* 48.11, pp. 1601–1611.

Amato, P. et al. (2007). "Microorganisms isolated from the water phase of tropospheric clouds at the Puy de Dôme: Major groups and growth abilities at low temperatures". In: *FEMS Microbiol. Ecol.* 59.2, pp. 242–254.

Andersen-Nissen, E. et al. (2005). "Evasion of Toll-like receptor 5 by flagellated bacteria". In: *Proc. Natl. Acad. Sci. U. S. A.* 102.26, pp. 9247–9252.

Anderson, J. C. et al. (2006). "Host-mediated phosphorylation of type III effector AvrPto promotes *Pseudomonas* virulence and avirulence in tomato." In: *Plant Cell* 18.2, pp. 502–514.

Arnon, S. S. et al. (2001). "Botulinum Toxin as a Biological Weapon". In: *JAMA* 285, pp. 1059–1070.

Asai, S. and Shirasu, K. (2015). "Plant cells under siege: Plant immune system versus pathogen effectors". In: *Curr. Opin. Plant Biol.* 28, pp. 1–8.

Ausubel, F. M. (2005). "Are innate immune signaling pathways in plants and animals conserved?" In: *Nat. Immunol.* 6.10, pp. 973–979.

Axtell, M. J. and Staskawicz, B. J. (2003). "Initiation of RPS2-specified disease resistance in *Arabidopsis* is coupled to the AvrRpt2-directed elimination of RIN4". In: *Cell* 112.3, pp. 369–377.

Badri, D. V. et al. (2013). "Application of natural blends of phytochemicals derived from the root exudates of *Arabidopsis* to the soil reveal that phenolic-related compounds predominantly modulate the soil microbiome". In: *J. Biol. Chem.* 288.7, pp. 4502–4512.

Bai, Y. et al. (2015). "Functional overlap of the *Arabidopsis* leaf and root microbiota". In: *Nature* 528.7582, pp. 364–369.

Bajwa, V. S. et al. (2013). "Identification and functional analysis of tomato BRI1 and BAK1 receptor kinase phosphorylation sites." In: *Plant Physiol.* 163.1, pp. 30–42.

Bakker, E. G. et al. (2006). "A genome-wide survey of R gene polymorphisms in *Arabidopsis*." In: *Plant Cell* 18.8, pp. 1803–1818.

Ballio, A. et al. (1991). "Syringopeptins, new phytotoxic lipodepsipeptides of *Pseudomonas syringae* pv. syringae." In: *FEBS Lett.* 291.1, pp. 109–112.

Balmuth, A. and Rathjen, J. P. (2007). "Genetic and molecular requirements for function of the Pto/Prf effector recognition complex in tomato and Nicotiana benthamiana." In: *Plant J.* 51.6, pp. 978–990.

Baltrus, D. A. et al. (2012). "The Molecular Basis of Host Specialization in Bean Pathovars of *Pseudomonas syringae*." In: *Mol. Plant-Microbe Interact.* 25.7, pp. 877–888.

Baltrus, D. a. et al. (2011). "Dynamic evolution of pathogenicity revealed by sequencing and comparative genomics of 19 *Pseudomonas syringae* isolates." In: *PLoS Pathog.* 7.7, e1002132.

Bartels, S. and Boller, T. (2015). "Quo vadis, Pep? Plant elicitor peptides at the crossroads of immunity, stress, and development." In: *J. Exp. Bot.* 66.17, pp. 5183–5193.

Bary, A. de (1861). *Die gegenwärtig herrschende Kartoffelkrankheit, ihre Ursache und ihre Verhütung.* Leipzig: A. Förstersche Buchhandlung.

Beattie, G. A. (2011). "Water relations in the interaction of foliar bacterial pathogens with plants." In: *Annu. Rev. Phytopathol.* 49.1, pp. 533–555.

Beck, M. et al. (2012). "Spatio-temporal cellular dynamics of the *Arabidopsis* flagellin receptor reveal activation status-dependent endosomal sorting." In: *Plant Cell* 24.October, pp. 1–16.

Belkhadir, Y. et al. (2014). "The growth-defense pivot: Crisis management in plants mediated by LRR-RK surface receptors." In: *Trends Biochem. Sci.* 39.10, pp. 447–456. arXiv: NIHMS150003.

Bender, C. L., Alarcón-Chaidez, F., and Gross, D. C. (1999). "*Pseudomonas syringae* phytotoxins: mode of action, regulation, and biosynthesis by peptide and polyketide synthetases." In: *Microbiol. Mol. Biol. Rev.* 63.2, pp. 266–292.

Bent, A. (1996). "Plant Disease Resistance Genes: Function Meets Structure." In: *Plant Cell* 8.10, pp. 1757–1771.

Berendsen, R. L., Pieterse, C. M., and Bakker, P. A. (2012). "The rhizosphere microbiome and plant health". In: *Trends Plant Sci.* 17.8, pp. 478–486.

Berggård, T., Linse, S., and James, P. (2007). "Methods for the detection and analysis of protein-protein interactions." In: *Proteomics* 7.16, pp. 2833–2842.

Bernoux, M. et al. (2011). "Structural and functional analysis of a plant resistance protein TIR domain reveals interfaces for self-association, signaling, and autoregulation." In: *Cell Host Microbe* 9.3, pp. 200–211.

Block, A. and Alfano, J. R. (2011). "Plant targets for *Pseudomonas syringae* type III effectors: Virulence targets or guarded decoys?" In: *Curr. Opin. Microbiol.* 14.1, pp. 39–46.

Block, A. et al. (2008). "Phytopathogen type III effector weaponry and their plant targets." In: *Curr. Opin. Plant Biol.* 11.4, pp. 396–403.

Blocker, A. et al. (2001). "Structure and composition of the Shigella flexneri 'needle complex', a part of its type III secreton." In: *Mol. Microbiol.* 39.3, pp. 652–663.

Boch, J. et al. (2009). "Breaking the code of DNA binding specificity of TAL-type III effectors." In: *Science.* 326.5959, pp. 1509–1512.

Böhm, H. et al. (2014a). "A conserved peptide pattern from a widespread microbial virulence factor triggers pattern-induced immunity in *Arabidopsis*." In: *PLoS Pathog.* 10.11, e1004491.

Böhm, H. et al. (2014b). "Immune receptor complexes at the plant cell surface." In: *Curr. Opin. Plant Biol.* 20, pp. 47–54.

Boller, T. and Felix, G. (2009). "A renaissance of elicitors: perception of microbe-associated molecular patterns and danger signals by pattern-recognition receptors." In: *Annu. Rev. Plant Biol.* 60, pp. 379–406.

Boller, T. and He, S. Y. (2009). "Innate immunity in plants: an arms race between pattern recognition receptors in plants and effectors in microbial pathogens." In: *Science.* 324.5928, pp. 742–744.

Bonardi, V. and Dangl, J. L. (2012). "How complex are intracellular immune receptor signaling complexes?" In: *Front. Plant Sci.* 3.October, p. 237.

Bonardi, V. et al. (2011). "Expanded functions for a family of plant intracellular immune receptors beyond specific recognition of pathogen effectors." In: *Proc. Natl. Acad. Sci. U. S. A.* 108.39, pp. 16463–16468.

Bossemeyer, D. et al. (1993). "Phosphotransferase and substrate binding mechanism of the cAMP-dependent protein kinase catalytic subunit from porcine heart as deduced from the 2.0 Å structure of the complex with Mn2+ adenylyl imidodiphosphate and inhibitor peptide PKI(5-24)." In: *EMBO J.* 12.3, pp. 849–859.

Bowman, S. M. and Free, S. J. (2006). "The structure and synthesis of the fungal cell wall." In: *BioEssays* 28.8, pp. 799–808.

Brodsky, I. and Medzhitov, R. (2007). "Two modes of ligand recognition by TLRs." In: *Cell* 130.6, pp. 979–981.

Brooks, D. M., Bender, C. L., and Kunkel, B. N. (2005). "The *Pseudomonas syringae* phytotoxin coronatine promotes virulence by overcoming salicylic acid-dependent defences in *Arabidopsis thaliana*". In: *Mol. Plant Pathol.* 6.6, pp. 629–639.

Brutus, A. et al. (2010). "A domain swap approach reveals a role of the plant wall-associated kinase 1 (WAK1) as a receptor of oligogalacturonides." In: *Proc. Natl. Acad. Sci. U. S. A.* 107.20, pp. 9452–9457.

Bücherl, C. A. et al. (2013). "Visualization of BRI1 and BAK1(SERK3) membrane receptor heterooligomers during brassinosteroid signaling." In: *Plant Physiol.* 162.4, pp. 1911–1925.

Buell, C. R. et al. (2003). "The complete genome sequence of the *Arabidopsis* and tomato pathogen *Pseudomonas syringae* pv. tomato DC3000." In: *Proc. Natl. Acad. Sci. U. S. A.* 100.18, pp. 10181–10186.

Buist, G. et al. (2008). "LysM, a widely distributed protein motif for binding to (peptido)glycans." In: *Mol. Microbiol.* 68.4, pp. 838–847.

Bulgarelli, D. et al. (2012). "Revealing structure and assembly cues for *Arabidopsis* root-inhabiting bacterial microbiota." In: *Nature* 488.7409, pp. 91–95.

Bulgarelli, D. et al. (2013). "Structure and functions of the bacterial microbiota of plants." In: *Annu. Rev. Plant Biol.* 64.1, pp. 807–838.

Cao, Y. et al. (2014). "The kinase LYK5 is a major chitin receptor in *Arabidopsis* and forms a chitin-induced complex with related kinase CERK1." In: *Elife* 3, e03766.

Catanzariti, A.-M. et al. (2010). "The AvrM effector from flax rust has a structured C-terminal domain and interacts directly with the M resistance protein." In: *Mol. Plant-Microbe Interact.* 23.1, pp. 49–57.

Cesari, S. et al. (2013). "The rice resistance protein pair RGA4/RGA5 recognizes the Magnaporthe oryzae effectors AVR-Pia and AVR1-CO39 by direct binding." In: *Plant Cell* 25.4, pp. 1463–1481.

Chang, J. H. et al. (2005). "A high-throughput, near-saturating screen for type III effector genes from *Pseudomonas syringae*." In: *Proc. Natl. Acad. Sci. U. S. A.* 102.7, pp. 2549–2554.

Chang, X. and Nick, P. (2012). "Defence signalling triggered by Flg22 and Harpin is integrated into a different stilbene output in Vitis cells." In: *PLoS One* 7.7, e40446.

Chao, Y.-P., Chiang, C.-J., and Hung, W.-B. (2002). "Stringent regulation and high-level expression of heterologous genes in *Escherichia coli* using T7 system controllable by the araBAD promoter." In: *Biotechnol. Prog.* 18.2, pp. 394–400.

Chen, J., Sawyer, N., and Regan, L. (2013). "Protein-protein interactions: General trends in the relationship between binding affinity and interfacial buried surface area." In: *Protein Sci.* 22.4, pp. 510–515.

Cheng, W. et al. (2011). "Structural analysis of *Pseudomonas syringae* AvrPtoB bound to host BAK1 reveals two similar kinase-interacting domains in a type III effector." In: *Cell Host Microbe* 10.6, pp. 616–626. arXiv: NIHMS150003.

Chinchilla, D. et al. (2007). "A flagellin-induced complex of the receptor FLS2 and BAK1 initiates plant defence." In: *Nature* 448.7152, pp. 497–500.

Chinchilla, D. et al. (2009). "One for all: the receptor-associated kinase BAK1." In: *Trends Plant Sci.* 14.10, pp. 535–541.

Chinchilla, D. et al. (2006). "The *Arabidopsis* receptor kinase FLS2 binds flg22 and determines the specificity of flagellin perception." In: *Plant Cell* 18.2, pp. 465–476.

Choi, J. et al. (2014). "Identification of a plant receptor for extracellular ATP." In: *Science* 343.6168, pp. 290–294.

Choi, M.-S. et al. (2013). "Harpins, multifunctional proteins secreted by gram-negative plant-pathogenic bacteria." In: *Mol. Plant-Microbe Interact.* 26.10, pp. 1115–1122.

Clark, R. M. et al. (2007). "Common sequence polymorphisms shaping genetic diversity in *Arabidopsis thaliana*." In: *Science.* 317.5836, pp. 338–342.

Clarke, C. R. et al. (2013). "Allelic variation in two distinct *Pseudomonas syringae* flagellin epitopes modulates the strength of plant immune responses but not bacterial motility." In: *New Phytol.* 200.3, pp. 847–860.

Clouse, S. et al. (2008). "Functional analysis and phosphorylation site mapping of leucine-rich repeat receptor-like kinases." In: *Plant Proteomics Technol. Strateg. Appl.* Ed. by G. Agrawal and R. Rakwal. Wiley Online Library. Chap. 32, pp. 469–484.

Collmer, A. et al. (2002). "Genomic mining type III secretion system effectors in *Pseudomonas syringae* yields new picks for all TTSS prospectors." In: *Trends Microbiol.* 10.10, pp. 462–469.

Cook, D. E., Mesarich, C. H., and Thomma, B. P. (2014). "Understanding plant immunity as a surveillance system to detect invasion." In: *Annu. Rev. Phytopathol.* 53, pp. 541–563.

Cooper, M. D. and Alder, M. N. (2006). "The evolution of adaptive immune systems". In: *Cell* 124.4, pp. 815–822.

Corda, A. (1847). "Pflanzenphysiologie und Pathologie. Beiträge zur Kunde der Kartoffel in Beziehung auf ihre Organisation und Krankheiten." In: *Oekonomische Neuigkeiten und Verhandlungen 73*, pp. 457–463.

Cui, H., Tsuda, K., and Parker, J. E. (2015). "Effector-Triggered Immunity: From pathogen perception to robust defense." In: *Annu. Rev. Plant Biol.* 66.1, pp. 487–511.

Cunnac, S., Lindeberg, M., and Collmer, A. (2009). "*Pseudomonas syringae* type III secretion system effectors: repertoires in search of functions." In: *Curr. Opin. Microbiol.* 12.1, pp. 53–60.

Dalton, G. D. and Dewey, W. L. (2006). "Protein kinase inhibitor peptide (PKI): A family of endogenous neuropeptides that modulate neuronal cAMP-dependent protein kinase function." In: *Neuropeptides* 40.1, pp. 23–34.

Dangl, J. L. and Jones, J. D. (2001). "Plant pathogens and integrated defence responses to infection." In: *Nature* 411.6839, pp. 826–833.

Danna, C. H. et al. (2011). "The *Arabidopsis* flagellin receptor FLS2 mediates the perception of Xanthomonas Ax21 secreted peptides." In: *Proc. Natl. Acad. Sci. U. S. A.* 108.22, pp. 9286–9291.

Danovaro, R. et al. (2008). "Major viral impact on the functioning of benthic deep-sea ecosystems." In: *Nature* 454.7208, pp. 1084–1087.

Dardick, C., Schwessinger, B., and Ronald, P. (2012). "Non-arginine-aspartate (non-RD) kinases are associated with innate immune receptors that recognize conserved microbial signatures." In: *Curr. Opin. Plant Biol.* 15.4, pp. 358–366.

Dawson, J. E. et al. (2009). "Elucidation of a pH-folding switch in the *Pseudomonas syringae* effector protein AvrPto." In: *Proc. Natl. Acad. Sci. U. S. A.* 106.21, pp. 8543–8548.

Day, B., Dahlbeck, D., and Staskawicz, B. J. (2006). "NDR1 interaction with RIN4 mediates the differential activation of multiple disease resistance pathways in *Arabidopsis*." In: *Plant Cell* 18.10, pp. 2782–2791.

De Coninck, B. et al. (2014). "What lies beneath: belowground defense strategies in plants." In: *Trends Plant Sci.* 20.2, pp. 91–101.

De Schutter, K. and Van Damme, E. (2015). "Protein-carbohydrate interactions as part of plant defense and animal immunity." In: *Molecules* 20.5, pp. 9029–9053.

Decreux, A. and Messiaen, J. (2005). "Wall-associated kinase WAK1 interacts with cell wall pectins in a calcium-induced conformation." In: *Plant Cell Physiol.* 46.2, pp. 268–278.

Deslandes, L. and Rivas, S. (2012). "Catch me if you can: Bacterial effectors and plant targets." In: *Trends Plant Sci.* 17.11, pp. 644–655.

Deslandes, L. et al. (2003). "Physical interaction between RRS1-R, a protein conferring resistance to bacterial wilt, and PopP2, a type III effector targeted to the plant nucleus." In: *Proc. Natl. Acad. Sci. U. S. A.* 100.13, pp. 8024–8029.

Diallo, M. D. et al. (2012). "*Pseudomonas syringae* naturally lacking the canonical type III secretion system are ubiquitous in nonagricultural habitats, are phylogenetically diverse and can be pathogenic." In: *ISME J.* 6.7, pp. 1–11.

Diévart, A. and Clark, S. E. (2004). "LRR-containing receptors regulating plant development and defense." In: *Development* 131.2, pp. 251–261.

Dodds, P. N. et al. (2006). "Direct protein interaction underlies gene-for-gene specificity and coevolution of the flax resistance genes and flax rust avirulence genes." In: *Proc. Natl. Acad. Sci. U. S. A.* 103.23, pp. 8888–8893.

Dominguez-Ferreras, A. et al. (2015). "An overdose of the *Arabidopsis* coreceptor BAK1 or its ectodomain causes autoimmunity in a SOBIR1-dependent manner." In: *Plant Physiol.* 168.July, pp. 1106–1121.

Dong, J. et al. (2009). "Crystal structure of the complex between *Pseudomonas* effector AvrPtoB and the tomato Pto kinase reveals both a shared and a unique interface compared with AvrPto-Pto." In: *Plant Cell* 21.6, pp. 1846–1859.

Donnelly, M. a. and Steiner, T. S. (2002). "Two nonadjacent regions in enteroaggregative *Escherichia coli* flagellin are required for activation of toll-like receptor 5." In: *J. Biol. Chem.* 277.43, pp. 40456–40461.

Eichmann, R. and Schäfer, P. (2015). "Growth versus immunity-a redirection of the cell cycle?" In: *Curr. Opin. Plant Biol.* 26, pp. 106–112.

Erbs, G. and Newman, M. A. (2012). "The role of lipopolysaccharide and peptidoglycan, two glycosylated bacterial microbe-associated molecular patterns (MAMPs), in plant innate immunity." In: *Mol. Plant Pathol.* 13.1, pp. 95–104.

Erickson, H. P. (2009). "Size and shape of protein molecules at the nanometer level determined by sedimentation, gel filtration, and electron microscopy." In: *Biol. Proced. Online* 11.1, pp. 32–51.

Esse, W. van et al. (2013). "A mathematical model for the coreceptors SOMATIC EMBRYOGENESIS RECEPTOR-LIKE KINASE1 and SOMATIC EMBRYOGENESIS RECEPTOR-LIKE KINASE3 in BRASSINOSTEROID INSENSITIVE1-mediated signaling." In: *Plant Physiol.* 163.3, pp. 1472–1481.

Fan, J. Y. et al. (2008). "Split mCherry as a new red bimolecular fluorescence complementation system for visualizing protein-protein interactions in living cells." In: *Biochem. Biophys. Res. Commun.* 367.1, pp. 47–53.

Fearon, D. T. and Locksley, R. M. (1996). "The instructive role of innate immunity in the acquired immune response." In: *Science.* 272.5258, pp. 50–53.

Feil, H. et al. (2005). "Comparison of the complete genome sequences of *Pseudomonas syringae* pv. syringae B728a and pv. tomato DC3000." In: *Proc. Natl. Acad. Sci. U. S. A.* 102.31, pp. 11064–11069.

Felix, G. et al. (1999). "Plants have a sensitive perception system for the most conserved domain of bacterial flagellin." In: *Plant J.* 18.3, pp. 265–276.

Fesel, P. H. and Zuccaro, A. (2015). "Beta-glucan: Crucial component of the fungal cell wall and elusive MAMP in plants." In: *Fungal Genet. Biol.*

Fett, W. F. and Dunn, M. F. (1989). "Exopolysaccharides produced by phytopathogenic *Pseudomonas syringae* pathovars in infected leaves of susceptible hosts." In: *Plant Physiol.* 89.1, pp. 5–9.

Feys, B. et al. (1994). "*Arabidopsis* mutants selected for resistance to the phytotoxin Coronatine are male sterile, insensitive to methyl jasmonate, and resistant to a bacterial pathogen." In: *Plant Cell* 6.5, pp. 751–759.

Fisher, M. et al. (2012). "Emerging fungal threats to animal, plant and ecosystem health." In: *Nature* 484.7393, pp. 186–194.

Flor, H. H. (1971). "Current status of the Gene-For-Gene concept." In: *Annu. Rev. Phytopathol.* 9.1, pp. 275–296.

Frankel, S., Sohn, R., and Leinwand, L. (1991). "The use of sarkosyl in generating soluble protein after bacterial expression." In: *Proc. Natl. Acad. Sci. U. S. A.* 88.4, pp. 1192–1196.

Freeman, B. C. and Beattie, G. A. (2009). "Bacterial growth restriction during host resistance to *Pseudomonas syringae* is associated with leaf water loss and localized cessation of vascular activity in *Arabidopsis thaliana*." In: *Mol. Plant-Microbe Interact.* 22.7, pp. 857–867.

Fritz-Laylin, L. K. et al. (2005). "Phylogenomic analysis of the Receptor-Like Proteins of rice and *Arabidopsis*." In: *Plant Physiol.* 138.June, pp. 611–623.

Furukawa, T. et al. (2014). "Two distinct EF-Tu epitopes induce immune responses in rice and *Arabidopsis*." In: *Mol. Plant-Microbe Interact.* 27.2, pp. 113–124.

Galán, J. E. and Wolf-Watz, H. (2006). "Protein delivery into eukaryotic cells by type III secretion machines." In: *Nature* 444.7119, pp. 567–573.

Gantner, B. N. et al. (2003). "Collaborative induction of inflammatory responses by dectin-1 and Toll-like receptor 2." In: *J. Exp. Med.* 197.9, pp. 1107–1117.

Gao, M. et al. (2009). "Regulation of cell death and innate immunity by two receptor-like kinases in *Arabidopsis*." In: *Cell Host Microbe* 6.1, pp. 34–44.

Garneau, J. E. et al. (2010). "The CRISPR/Cas bacterial immune system cleaves bacteriophage and plasmid DNA." In: *Nature* 468.7320, pp. 67–71.

Gassmann, W. and Bhattacharjee, S. (2012). "Effector-Triggered Immunity signaling: From gene-for-gene pathways to protein-protein interaction networks." In: *Mol. Plant-Microbe Interact.* 25.7, pp. 862–868.

Geldner, N. et al. (2007). "Endosomal signaling of plant steroid receptor kinase BRI1." In: *Genes Dev.* 21.13, pp. 1598–1602.

Geng, X. et al. (2014). "The phytotoxin coronatine is a multifunctional component of the virulence armament of *Pseudomonas syringae*." In: *Planta* 240, pp. 1149–1165.

Gill, SC; von Hippel, P. (1989). "Calculation of protein extinction coefficients from amino acid sequence data." In: *Anal. Biochem.* 182, pp. 319–326.

Göhre, V. et al. (2008). "Plant pattern-recognition receptor FLS2 is directed for degradation by the bacterial ubiquitin ligase AvrPtoB." In: *Curr. Biol.* 18.23, pp. 1824–1832.

Goldstein, B. et al. (1999). "The influence of transport on the kinetics of binding to surface receptors: application to cells and BIAcore." In: *J. Mol. Recognit.* 12.5, pp. 293–299.

Gómez-Gómez, L., Bauer, Z., and Boller, T. (2001). "Both the extracellular leucine-rich repeat domain and the kinase activity of FSL2 are required for flagellin binding and signaling in *Arabidopsis*." In: *Plant Cell* 13.5, pp. 1155–1163.

Gómez-Gómez, L. and Boller, T. (2000). "FLS2: an LRR receptor-like kinase involved in the perception of the bacterial elicitor flagellin in *Arabidopsis*." In: *Mol. Cell* 5.6, pp. 1003–1011.

Gou, X. et al. (2012). "Genetic evidence for an indispensable role of somatic embryogenesis receptor kinases in brassinosteroid signaling." In: *PLoS Genet.* 8.1, e1002452.

Gourion, B. et al. (2015). "Rhizobium-legume symbioses: The crucial role of plant immunity." In: *Trends Plant Sci.* 20.3, pp. 186–194.

Green, S. et al. (2010). "Comparative genome analysis provides insights into the evolution and adaptation of *Pseudomonas syringae* pv. aesculi on Aesculus hippocastanum." In: *PLoS One* 5.4, pp. 1–14.

Gregory, P. J. et al. (2009). "Integrating pests and pathogens into the climate change/food security debate." In: *J. Exp. Bot.* 60.10, pp. 2827–2838.

Griffiths, A. D. et al. (1994). "Isolation of high affinity human antibodies directly from large synthetic repertoires." In: *EMBO J.* 13.14, pp. 3245–3260.

Gross, D. and DeVay, J. (1977). "Production and purification of syringomycin, a phytotoxin produced by *Pseudomonas syringae*." In: *Physiol. Plant Pathol.* 11.1, pp. 13–28.

Grove, J. R. et al. (1987). "Recombinant fragment of protein kinase inhibitor blocks cyclic AMP-dependent gene transcription." In: *Science.* 238, pp. 530–533.

Guo, M. et al. (2009). "The majority of the type III effector inventory of *Pseudomonas syringae* pv. tomato DC3000 can suppress plant immunity." In: *Mol. Plant. Microbe. Interact.* 22.9, pp. 1069–1080.

Guo, Y.-L. et al. (2011). "Genome-wide comparison of Nucleotide-Binding Site-Leucine-Rich Repeat-encoding genes in *Arabidopsis*." In: *Plant Physiol.* 157.2, pp. 757–769.

Gust, A. A. (2015). "Peptidoglycan perception in plants." In: *PLoS Pathog.* 11.12, pp. 1–7.

Gust, A. a. and Felix, G. (2014). "Receptor like proteins associate with SOBIR1-type of adaptors to form bimolecular receptor kinases." In: *Curr. Opin. Plant Biol.* 21, pp. 104–111.

Gust, A. a. et al. (2012). "Plant LysM proteins: Modules mediating symbiosis and immunity." In: *Trends Plant Sci.* 17.8, pp. 495–502.

Gutierrez, J. R. et al. (2010). "Prf immune complexes of tomato are oligomeric and contain multiple Pto-like kinases that diversify effector recognition." In: *Plant J.* 61.3, pp. 507–518.

Guttman, D. S. et al. (2002). "A functional screen for the type III (Hrp) secretome of the plant pathogen *Pseudomonas syringae*." In: *Science.* 295.5560, pp. 1722–1726.

Guy, E. et al. (2013). "Natural genetic variation of Xanthomonas campestris pv. campestris pathogenicity on *Arabidopsis* revealed by association and reverse genetics." In: *MBio* 4.3, e00538–12.

Halter, T. et al. (2014a). "BIR2 affects complex formation of BAK1 with ligand binding receptors in plant defense." In: *Plant Signal. Behav.* 9.April 2015, pp. 1–4.

Halter, T. et al. (2014b). "The leucine-rich repeat receptor kinase BIR2 is a negative regulator of BAK1 in plant immunity." In: *Curr. Biol.* 24.2, pp. 134–143.

Hammond-Kosack, K. E. and Jones, J. D. (1996). "Resistance gene-dependent plant defense responses." In: *Plant Cell* 8.10, pp. 1773–1791.

Hann, D. R. et al. (2014). "The *Pseudomonas* type III effector HopQ1 activates cytokinin signaling and interferes with plant innate immunity." In: *New Phytol.* 201.2, pp. 585–598.

Hardoim, P. R., Overbeek, L. S. van, and Elsas, J. D. van (2008). "Properties of bacterial endophytes and their proposed role in plant growth." In: *Trends Microbiol.* 16.10, pp. 463–471.

Hauck, P., Thilmony, R., and He, S. Y. (2003). "A *Pseudomonas syringae* type III effector suppresses cell wall-based extracellular defense in susceptible *Arabidopsis* plants." In: *Proc. Natl. Acad. Sci. U. S. A.* 100.14, pp. 8577–8582.

Hawn, T. R. et al. (2003). "A common dominant TLR5 stop codon polymorphism abolishes flagellin signaling and is associated with susceptibility to Legionnaires' disease." In: *J. Exp. Med.* 198.10, pp. 1563–1572.

Hayafune, M. et al. (2014). "Chitin-induced activation of immune signaling by the rice receptor CEBiP relies on a unique sandwich-type dimerization." In: *Proc. Natl. Acad. Sci. U. S. A.* 111.3, E404–E413.

Hayashi, F. et al. (2001). "The innate immune response to bacterial flagellin is mediated by Toll-like receptor 5." In: *Nature* 410.6832, pp. 1099–1103.

He, K. et al. (2007). "BAK1 and BKK1 regulate Brassinosteroid-dependent growth and Brassinosteroid-independent cell-death pathways." In: *Curr. Biol.* 17.13, pp. 1109–1115.

He, P. et al. (2006). "Specific bacterial suppressors of MAMP signaling upstream of MAPKKK in *Arabidopsis* innate immunity." In: *Cell* 125.3, pp. 563–575.

He, S. Y., Huang, H. C., and Collmer, A. (1993). "*Pseudomonas syringae* pv. syringae harpinPss: A protein that is secreted via the hrp pathway and elicits the hypersensitive response in plants." In: *Cell* 73.7, pp. 1255–1266.

Heath, M. C. (2000). "Nonhost resistance and nonspecific plant defenses." In: *Curr. Opin. Plant Biol.* 3.4, pp. 315–319.

Heese, A. et al. (2007). "The receptor-like kinase SERK3/BAK1 is a central regulator of innate immunity in plants." In: *Proc. Natl. Acad. Sci. U. S. A.* 104.29, pp. 12217–12222.

Hirano, S. S. and Upper, C. D. (2000). "Bacteria in the leaf ecosystem with emphasis on *Pseudomonas syringae*–a pathogen, ice nucleus, and epiphyte." In: *Microbiol. Mol. Biol. Rev.* 64.3, pp. 624–653.

Hirano, S. S. and Upper, C. D. (1990). "Population biology and epidemiology of *Pseudomonas syringae*." In: *Annu. Rev. Phytopathol.* 28.1, pp. 155–177.

Hochuli, E., Bannwarth, W., and Döbeli, H. (1988). "Genetic approach to facilitate purification of recombinant proteins with a novel metal chelate adsorbent." In: *Nature* 6, pp. 1321–1325.

Hoorn, R. a. L. van der and Kamoun, S. (2008). "From Guard to Decoy: a new model for perception of plant pathogen effectors." In: *Plant Cell* 20.8, pp. 2009–2017.

Horn, M. A. and Walker, J. C. (1994). "Biochemical properties of the autophosphorylation of RLK5, a receptor-like protein kinase from *Arabidopsis thaliana*." In: *Biochim. Biophys. Acta (BBA)/Protein Struct. Mol.* 1208.1, pp. 65–74.

Horst, R. K. (2013). *Westcott's Plant Disease Handbook*. Ed. by R. K. Horst. 8th ed. Springer.

Horvath, P. and Barrangou, R. (2010). "CRISPR/Cas, the immune system of bacteria and archaea." In: *Science.* 327.5962, pp. 167–170.

Hothorn, M. et al. (2011). "Structural basis of steroid hormone perception by the receptor kinase BRI1." In: *Nature* 474.7352, pp. 467–471.

Houk, K. N. et al. (2003). "Binding affinities of host-guest, protein-ligand, and protein-transition-state complexes." In: *Angew. Chemie - Int. Ed.* 42.40, pp. 4872–4897.

Hu, C.-D., Grinberg, A. V., and Kerppola, T. K. (2005). "Visualization of protein interactions in living cells using bimolecular fluorescence complementation (BiFC) analysis." In: *Curr. Protoc. Cell Biol.* 21.3, pp. 1–21.

Huffaker, A., Pearce, G., and Ryan, C. A. (2006). "An endogenous peptide signal in *Arabidopsis* activates components of the innate immune response." In: *Proc. Natl. Acad. Sci. U. S. A.* 103.26, pp. 10098–10103.

Huffaker, A. et al. (2013). "Plant elicitor peptides are conserved signals regulating direct and indirect antiherbivore defense." In: *Proc. Natl. Acad. Sci. U. S. A.* 110.14, pp. 5707–5712.

Hutchison, M. L. and Gross, D. C. (1997). "Lipopeptide phytotoxins produced by *Pseudomonas syringae* pv. syringae: comparison of the biosurfactant and ion channel-forming activities of syringopeptin and syringomycin." In: *Mol. Plant. Microbe. Interact.* 10.3, pp. 347–354.

Hwang, M. S. H. et al. (2005). "Phylogenetic characterization of virulence and resistance phenotypes of *Pseudomonas syringae*." In: *Appl. Environ. Microbiol.* 71.9, pp. 5182–5191.

Imkampe, J. (2015). "Analysis on the BAK1 interacting RLKs BIR2 and BIR3, two proteins that differentially regulate BAK1 dependent pathways." PhD thesis. University of Tübingen.

Inada, N. and Ueda, T. (2014). "Membrane trafficking pathways and their roles in plant-microbe interactions." In: *Plant Cell Physiol.* 55.4, pp. 672–686.

Inoue, H., Nojima, H., and Okayama, H. (1990). "High efficiency transformation of *Escherichia coli* with plasmids." In: *Gene* 96.1, pp. 23–28.

Iwasaki, A. and Medzhitov, R. (2010). "Regulation of adaptive immunity by the innate immune system." In: *Science.* 327.5963, pp. 291–295.

Jaillais, Y. et al. (2011). "Extracellular leucine-rich repeats as a platform for receptor/-coreceptor complex formation." In: *Proc. Natl. Acad. Sci. U. S. A.* 108.20, pp. 8503–8507.

Jamir, Y. et al. (2004). "Identification of *Pseudomonas syringae* type III effectors that can suppress programmed cell death in plants and yeast." In: *Plant J.* 37.4, pp. 554–565.

Jelenska, J., Kang, Y., and Greenberg, J. T. (2014). "Plant pathogenic bacteria target the actin microfilament network involved in the trafficking of disease defense components." In: *Bioarchitecture* 4.4-5, pp. 149–153.

Jerabek-Willemsen, M. et al. (2011). "Molecular interaction studies using microscale thermophoresis." In: *Assay Drug Dev. Technol.* 9.4, pp. 342–353.

Jia, Y. et al. (2000). "Direct interaction of resistance gene and avirulence gene products confers rice blast resistance." In: *EMBO J.* 19.15, pp. 4004–4014.

Jin, R. et al. (2006). "Botulinum neurotoxin B recognizes its protein receptor with high affinity and specificity." In: *Nature* 444.7122, pp. 1092–1095.

Joardar, V. et al. (2005). "Whole-genome sequence analysis of *Pseudomonas syringae* pv. phaseolicola 1448A reveals divergence among pathovars in genes involved in virulence and transposition." In: *J. Bacteriol.* 187.18, pp. 6488–6498.

Johnson, L. N., Noble, M. E. M., and Owen, D. J. (1996). "Active and inactive protein kinases: Structural basis for regulation." In: *Cell* 85.2, pp. 149–158.

Johnsson, B., Löfås, S., and Lindquist, G. (1991). "Immobilization of Proteins to a Carboxymethyldextran-Modified Gold Surface for Biospecific Interaction Analysis in Surface Plasmon Resonance Sensors". In: *Anal. Biochem.* 198.2, pp. 268–277.

Jones, J. D. G. and Dangl, J. L. (2006). "The plant immune system." In: *Nature* 444.7117, pp. 323–329.

Jones, R. B. et al. (2006). "A quantitative protein interaction network for the ErbB receptors using protein microarrays." In: *Nature* 439.7073, pp. 168–174.

Josenhans, C. and Suerbaum, S. (2002). "The role of motility as a virulence factor in bacteria." In: *Int. J. Med. Microbiol.* 291.8, pp. 605–614.

Kadota, Y. et al. (2014). "Direct regulation of the NADPH oxidase RBOHD by the PRR-associated kinase BIK1 during plant immunity." In: *Mol. Cell* 54.1, pp. 43–55.

Kaiser, B. et al. (2015). "Parasitic plants of the genus Cuscuta and their interaction with susceptible and resistant host plants." In: *Front. Plant Sci.* 6.February, pp. 1–9.

Kang, J. Y. and Lee, J.-O. (2011). "Structural biology of the toll-like receptor family." In: *Annu. Rev. Biochem.* 80, pp. 917–941.

Kann, M. G. et al. (2005). "A structure-based method for protein sequence alignment." In: *Bioinformatics* 21.8, pp. 1451–1456.

Karaman, M. W. et al. (2008). "A quantitative analysis of kinase inhibitor selectivity." In: *Nat. Biotechnol.* 26.1, pp. 127–132.

Karlsson, R. and Fält, A. (1997). "Experimental design for kinetic analysis of protein-protein interactions with surface plasmon resonance biosensors." In: *J. Immunol. Methods* 200.1-2, pp. 121–133.

Kawai, T. and Akira, S. (2010). "The role of pattern-recognition receptors in innate immunity: update on Toll-like receptors." In: *Nat. Immunol.* 11.5, pp. 373–384.

Kawai, T. and Akira, S. (2011). "Toll-like receptors and their crosstalk with other innate receptors in infection and immunity." In: *Immunity* 34.5, pp. 637–650. arXiv: 120.

Kay, S. et al. (2007). "A bacterial effector acts as a plant transcription factor and induces a cell size regulator." In: *Science.* 318.5850, pp. 648–651.

Kearney, B. and Staskawicz, B. J. (1990). "Widespread distribution and fitness contribution of Xanthomonas campestris avirulence gene avrBs2." In: *Nature* 346.6282, pp. 385–386.

Keinath, N. F. et al. (2010). "PAMP (Pathogen-associated Molecular Pattern)-induced changes in plasma membrane compartmentalization reveal novel components of plant immunity." In: *J. Biol. Chem.* 285.50, pp. 39140–39149.

Kemmerling, B. et al. (2007). "The BRI1-associated kinase 1, BAK1, has a brassinolide-independent role in plant cell-death control." In: *Curr. Biol.* 17.13, pp. 1116–1122.

Kenakin, T. (2002). "Drug efficacy at G protein-coupled receptors." In: *Annu. Rev. Pharmacol. Toxicol.* 42, pp. 349–379.

Khan, M., Subramaniam, R., and Desveaux, D. (2016). "Of guards, decoys, baits and traps: Pathogen perception in plants by type III effector sensors." In: *Curr. Opin. Microbiol.* 29, pp. 49–55.

Kim, H.-S. et al. (2005a). "The *Pseudomonas syringae* effector AvrRpt2 cleaves its C-terminally acylated target, RIN4, from *Arabidopsis* membranes to block RPM1 activation." In: *Proc. Natl. Acad. Sci. U. S. A.* 102.18, pp. 6496–501.

Kim, J. F. et al. (1998). "Sequences related to transposable elements and bacteriophages flank avirulence genes of *Pseudomonas syringae*." In: *Mol. Plant-Microbe Interact.* 11.12, pp. 1247–1252.

Kim, M. G. et al. (2005b). "Two *Pseudomonas syringae* type III effectors inhibit RIN4-regulated basal defense in *Arabidopsis*." In: *Cell* 121.5, pp. 749–759.

Kim, T.-W. et al. (2011). "The CDG1 kinase mediates brassinosteroid signal transduction from BRI1 receptor kinase to BSU1 phosphatase and GSK3-like kinase BIN2." In: *Mol. Cell* 43.4, pp. 561–571.

Kim, Y. J., Lin, N. C., and Martin, G. B. (2002). "Two distinct *Pseudomonas* effector proteins interact with the Pto kinase and activate plant immunity." In: *Cell* 109.5, pp. 589–598.

Kjemtrup, S., Nimchuk, Z., and Dangl, J. L. (2000). "Effector proteins of phytopathogenic bacteria: Bifunctional signals in virulence and host recognition." In: *Curr. Opin. Microbiol.* 3.1, pp. 73–78.

Klemptner, R. L. et al. (2014). "Ergosterol, an orphan fungal microbe-associated molecular pattern (MAMP)." In: *Mol. Plant Pathol.* 15.7, pp. 747–761. arXiv: NIHMS150003.

Klinkowski, M. (1970). "Catastrophic plant diseases." In: *Annu. Rev. Phytopathol.* 8, pp. 37–60.

Kobayashi, I. (2001). "Behavior of restriction-modification systems as selfish mobile elements and their impact on genome evolution." In: *Nucleic Acids Res.* 29.18, pp. 3742–3756.

Kuiper, G. et al. (1997). "Comparison of the ligand binding specificity and transcript tissue distribution of estrogen receptors alpha and beta." In: *Endocrinology* 138.3, pp. 863–870.

Kunze, G., Zipfel, C., and Robatzek, S. (2004). "The N terminus of bacterial elongation factor Tu elicits innate immunity in *Arabidopsis* plants." In: *Plant Cell* 16.12, pp. 3496–3507.

Lacombe, S. et al. (2010). "Interfamily transfer of a plant pattern-recognition receptor confers broad-spectrum bacterial resistance." In: *Nat. Biotechnol.* 28.4, pp. 365–369.

Laemmli, U. (1970). "Cleavage of structural proteins during the assembly of the head of bacteriophage T4." In: *Nature* 227.5259, pp. 680–685.

Lalonde, S. et al. (2008). "Molecular and cellular approaches for the detection of protein-protein interactions: latest techniques and current limitations." In: *Plant J.* 53.4, pp. 610–635.

Lathe, W. C. and Bork, P. (2001). "Evolution of tuf genes: ancient duplication, differential loss and gene conversion." In: *FEBS Lett.* 502.3, pp. 113–116.

Lavermicocca, N. S. I. P., Grgurina, I., and Simmaco, M. (1992). "Phytotoxic properties of *Pseudomonas syringae* pv. syringae toxins." In: *Physiol. Mol. Plant Pathol.* 40, pp. 107–116.

Le Roux, C. et al. (2015). "An immune receptor pair with an integrated decoy converts pathogen disabling of defensive transcription factors into resistance." In: *Cell* 161.5, pp. 1074–1088.

Lee, H., Chah, O.-K., and Sheen, J. (2011). "Stem-cell-triggered immunity through CLV3p-FLS2 signalling." In: *Nature* 473.7347, pp. 376–379.

Lee, H. et al. (2012). "Complexity in differential peptide-receptor signaling: response to Segonzac et al. and Mueller et al. commentaries". In: *Plant Cell* 24.8, pp. 3177–3185.

Li, J. (2010). "Multi-tasking of somatic embryogenesis receptor-like protein kinases." In: *Curr. Opin. Plant Biol.* 13.5, pp. 509–514.

Li, J. et al. (2002). "BAK1, an *Arabidopsis* LRR receptor-like protein kinase, interacts with BRI1 and modulates brassinosteroid signaling." In: *Cell* 110.2, pp. 213–222.

Li, X. et al. (2005). "Flagellin induces innate immunity in nonhost interactions that is suppressed by *Pseudomonas syringae* effectors." In: *Proc. Natl. Acad. Sci. U. S. A.* 102.36, pp. 12990–12995.

Liang, Y. et al. (2013). "Nonlegumes respond to rhizobial Nod factors by suppressing the innate immune response." In: *Science.* 341.6152, pp. 1384–1387.

Liebrand, T. W. H. et al. (2013). "Receptor-like kinase SOBIR1/EVR interacts with receptor-like proteins in plant immunity against fungal infection." In: *Proc. Natl. Acad. Sci. U. S. A.* 110.24, pp. 10010–10015.

Lima, W. F. et al. (2009). "Human Dicer binds short single-strand and double-strand RNA with high affinity and interacts with different regions of the nucleic acids." In: *J. Biol. Chem.* 284.4, pp. 2535–2548.

Lindeberg, M., Cunnac, S., and Collmer, A. (2009). "The evolution of *Pseudomonas syringae* host specificity and type III effector repertoires". In: *Mol. Plant Pathol.* 10.6, pp. 767–775.

Lindgren, P. B., Peet, R. C., and Panopoulos, N. J. (1986). "Gene cluster of *Pseudomonas syringae* pv. 'phaseolicola' controls pathogenicity of bean plants and hypersensitivity on nonhost plants." In: *J. Bacteriol.* 168.2, pp. 512–522.

Liu, B. et al. (2012). "Lysin motif-containing proteins LYP4 and LYP6 play dual roles in peptidoglycan and chitin perception in rice innate immunity." In: *Plant Cell* 24.8, pp. 3406–3419.

Liu, J. et al. (2013a). "Heterotrimeric G proteins serve as a converging point in plant defense signaling activated by multiple receptor-like kinases." In: *Plant Physiol.* 161.4, pp. 2146–2158.

Liu, J. et al. (2009). "RIN4 functions with plasma membrane H+-ATPases to regulate stomatal apertures during pathogen attack." In: *PLoS Biol.* 7.6, e1000139.

Liu, Z. et al. (2013b). "BIK1 interacts with PEPRs to mediate ethylene-induced immunity." In: *Proc. Natl. Acad. Sci. U. S. A.* 110.15, pp. 6205–6210.

Lotze, M. T. et al. (2007). "The grateful dead: damage- associated molecular pattern molecules and reduction / oxidation regulate immunity." In: *Immunol. Rev.* 220.1, pp. 60–82.

Louws, F. J. et al. (2001). "Field control of bacterial spot and bacterial speck of tomato using a plant activator." In: *Plant Dis.* 85.5, pp. 481–488.

Lu, D., He, P., and Shan, L. (2010a). "Bacterial effectors target BAK1-associated receptor complexes: One stone two birds." In: *Commun. Integr. Biol.* 3.2, pp. 80–3.

Lu, D. et al. (2010b). "A receptor-like cytoplasmic kinase, BIK1, associates with a flagellin receptor complex to initiate plant innate immunity." In: *Proc. Natl. Acad. Sci. U. S. A.* 107.1, pp. 496–501.

Lu, D. et al. (2011). "Direct ubiquitination of pattern recognition receptor FLS2 attenuates plant innate immunity." In: *Science.* 332.6036, pp. 1439–1442.

Ludwig, C. F. W. (1856). "Diffusion zwischen ungleich erwärmten Orten gleich zusammengesetzter Lösungen". In: *Sitzungsberichte der Akad. der Wissenschaften der Math. Klasse* 20, p. 539.

Lundberg, D. S. et al. (2012). "Defining the core *Arabidopsis thaliana* root microbiome." In: *Nature* 488.7409, pp. 86–90.

Ma, L. et al. (2012a). "Molecular basis of effector recognition by plant NB-LRR proteins." In: *Mol. Plant Immun.* Pp. 23–40.

Ma, W. et al. (2006). "Type III effector diversification via both pathoadaptation and horizontal transfer in response to a coevolutionary arms race." In: *PLoS Genet.* 2.12, pp. 2131–2142.

Ma, Y. et al. (2012b). "Linking ligand perception by PEPR pattern recognition receptors to cytosolic Ca2+ elevation and downstream immune signaling in plants." In: *Proc. Natl. Acad. Sci. U. S. A.* 109.48, pp. 19852–19857.

Macho, A. P. and Zipfel, C. (2015). "Targeting of plant pattern recognition receptor-triggered immunity by bacterial type-III secretion system effectors." In: *Curr. Opin. Microbiol.* 23, pp. 14–22.

Macho, A. P. et al. (2014). "A bacterial tyrosine phosphatase inhibits plant pattern recognition receptor activation." In: *Science.* 343.6178, pp. 1509–1512.

Mackey, D. et al. (2003). "*Arabidopsis* RIN4 is a target of the type III virulence effector AvrRpt2 and modulates RPS2-mediated resistance." In: *Cell* 112.3, pp. 379–389.

Madej, T. et al. (2012). "MMDB: 3D structures and macromolecular interactions." In: *Nucleic Acids Res.* 40.D1, pp. 1–4.

Madej, T. et al. (2014). "MMDB and VAST+: tracking structural similarities between macromolecular complexes." In: *Nucleic Acids Res.* 42.1, pp. D297–D303.

Maekawa, T. et al. (2011). "Coiled-coil domain-dependent homodimerization of intracellular barley immune receptors defines a minimal functional module for triggering cell death." In: *Cell Host Microbe* 9.3, pp. 187–199.

Maekawa, T. et al. (2012). "Conservation of NLR-triggered immunity across plant lineages." In: *Proc. Natl. Acad. Sci. U. S. A.* 109.49, pp. 20119–20123.

Maki, L. R. et al. (1974). "Ice nucleation induced by *Pseudomonas syringae*." In: *Appl. Microbiol.* 28.3, pp. 456–459.

Mandell, D. J. and Kortemme, T. (2009). "Computer-aided design of functional protein interactions." In: *Nat. Chem. Biol.* 5.11, pp. 797–807.

Mansfield, J. et al. (2012). "Top 10 plant pathogenic bacteria in molecular plant pathology." In: *Mol. Plant Pathol.* 13.6, pp. 614–629.

Martin, G. B. et al. (1993). "Map-based cloning of a protein kinase gene conferring disease resistance in tomato." In: *Science.* 262.5138, pp. 1432–1436.

Mayo, C. S. and Hallock, R. B. (1989). "Immunoassay based on surface plasmon oscillations." In: *J. Immunol. Methods* 120.1, pp. 105–114.

McBlane, J. F. et al. (1995). "Cleavage at a V(D)J recombination signal requires only RAG1 and RAG2 proteins and occurs in two steps." In: *Cell* 83.3, pp. 387–395.

McCann, H. C. and Guttman, D. S. (2008). "Evolution of the type III secretion system and its effectors in plant-microbe interactions." In: *New Phytol.* 177.1, pp. 33–47.

McCann, H. C. et al. (2012). "Identification of innate immunity elicitors using molecular signatures of natural selection." In: *Proc. Natl. Acad. Sci. U. S. A.* 109.11, pp. 4215–4220.

Medzhitov, R. and Janeway, C. A. J. (1997). "Innate immunity: The virtues of a non-clonal system of recognition." In: *Cell* 91, pp. 295–298.

Melotto, M., Underwood, W., and He, S. Y. (2008). "Role of stomata in plant innate immunity and foliar bacterial diseases." In: *Annu. Rev. Phytopathol.* 46, pp. 101–122.

Melotto, M. et al. (2006). "Plant stomata function in innate immunity against bacterial invasion." In: *Cell* 126.5, pp. 969–980.

Meng, X. et al. (2015). "Differential function of *Arabidopsis* SERK family receptor-like kinases in stomatal patterning." In: *Curr. Biol.* 25.18, pp. 2361–2372.

Mersmann, S. et al. (2010). "Ethylene signaling regulates accumulation of the FLS2 receptor and is required for the oxidative burst contributing to plant immunity." In: *Plant Physiol.* 154.1, pp. 391–400.

Mesnage, S. et al. (2014). "Molecular basis for bacterial peptidoglycan recognition by LysM domains." In: *Nat. Commun.* 5.D4269, pp. 1–11.

Meyers, B. C. et al. (1999). "Plant disease resistance genes encode members of an ancient and diverse protein family within the nucleotide-binding superfamily." In: *Plant J.* 20.3, pp. 317–332.

Mills, E. et al. (2008). "Real-time analysis of effector translocation by the type III secretion system of enteropathogenic *Escherichia coli*." In: *Cell Host Microbe* 3.2, pp. 104–113.

Mithöfer, A. and Boland, W. (2008). "Recognition of herbivory-associated molecular patterns." In: *Plant Physiol.* 146.3, pp. 825–831.

Mohr, T. J. et al. (2008). "Naturally occurring nonpathogenic isolates of the plant pathogen *Pseudomonas syringae* lack a type III secretion system and effector gene orthologues." In: *J. Bacteriol.* 190.8, pp. 2858–2870.

Monteil, C. L. et al. (2013). "Nonagricultural reservoirs contribute to emergence and evolution of *Pseudomonas syringae* crop pathogens." In: *New Phytol.* 199.3, pp. 800–811.

Montillet, J. L. and Hirt, H. (2013). "New checkpoints in stomatal defense." In: *Trends Plant Sci.* 18.6, pp. 295–297.

Morin, M. J. (2000). "From oncogene to drug: development of small molecule tyrosine kinase inhibitors as anti-tumor and anti-angiogenic agents." In: *Oncogene* 19.56, pp. 6574–6583.

Morris, C. E., Monteil, C. L., and Berge, O. (2013). "The life history of *Pseudomonas syringae*: linking agriculture to earth system processes." In: *Annu. Rev. Phytopathol.* 51, pp. 85–104.

Morris, C. E. et al. (2007). "Surprising niche for the plant pathogen *Pseudomonas syringae*." In: *Infect. Genet. Evol.* 7.1, pp. 84–92.

Morris, C. E. et al. (2008). "The life history of the plant pathogen *Pseudomonas syringae* is linked to the water cycle." In: *ISME J.* 2.3, pp. 321–334.

Mucyn, T. S. et al. (2009). "Regulation of tomato Prf by Pto-like protein kinases." In: *Mol. Plant-Microbe Interact.* 22.4, pp. 391–401.

Mucyn, T. S. et al. (2006). "The tomato NBARC-LRR protein Prf interacts with Pto kinase in vivo to regulate specific plant immunity." In: *Plant Cell* 18.10, pp. 2792–2806.

Mueller, K. et al. (2012). "Contamination risks in work with synthetic peptides: flg22 as an example of a pirate in commercial peptide preparations." In: *Plant Cell* 24.8, pp. 3193–3197.

Mukhtar, M. S. et al. (2011). "Independently evolved virulence effectors converge onto hubs in a plant immune system network." In: *Science.* 333.6042, pp. 596–601.

Mur, L. a. J. et al. (2013). "Stomatal lock-up following pathogenic challenge: Source or symptom of costs of resistance in crops?" In: *Plant Pathol.* 62.S1, pp. 72–82.

Myszka, D. G. (1997). "Kinetic analysis of macromolecular interactions using surface plasmon resonance biosensors". In: *Curr. Opin. Biotechnol.* 8.1, pp. 50–57.

Myszka, D. G. et al. (1998). "Extending the range of rate constants available from BIACORE: interpreting mass transport-influenced binding data." In: *Biophys. J.* 75.2, pp. 583–94.

Nakano, S. I. et al. (1999). "Nucleic acid duplex stability: Influence of base composition on cation effects." In: *Nucleic Acids Res.* 27.14, pp. 2957–2965.

Navarro, L. et al. (2004). "The transcriptional innate immune response to flg22. Interplay and overlap with Avr gene-dependent defense responses and bacterial pathogenesis." In: *Plant Physiol.* 135.2, pp. 1113–1128.

Nicaise, V. et al. (2013). "*Pseudomonas* HopU1 modulates plant immune receptor levels by blocking the interaction of their mRNAs with GRP7." In: *EMBO J.* 32.5, pp. 701–712.

Nielsen, M. E. and Thordal-Christensen, H. (2013). "Transcytosis shuts the door for an unwanted guest." In: *Trends Plant Sci.* 18.11, pp. 611–616.

Nissen, K. S., Willats, W. G., and Malinovsky, F. G. (2016). "Understanding CrRLK1L function: Cell walls and growth control." In: *Trends Plant Sci.* NN.NN, pp. 1–12.

Nogueira, T. et al. (2009). "Horizontal gene transfer of the secretome drives the evolution of bacterial cooperation and virulence." In: *Curr. Biol.* 19.20, pp. 1683–1691.

Nolen, B., Taylor, S., and Ghosh, G. (2004). "Regulation of protein kinases: controlling activity through activation segment conformation." In: *Mol. Cell* 15.5, pp. 661–675.

Nomura, K. et al. (2006). "A bacterial virulence protein suppresses host innate immunity to cause plant disease." In: *Science.* 313.5784, pp. 220–223.

Nooren, I. M. A. and Thornton, J. M. (2003). "Structural characterisation and functional significance of transient protein-protein interactions." In: *J. Mol. Biol.* 325.5, pp. 991–1018.

Ntoukakis, V. et al. (2014). "The changing of the guard: the Pto/Prf receptor complex of tomato and pathogen recognition." In: *Curr. Opin. Plant Biol.* 20, pp. 69–74.

Ntoukakis, V. et al. (2013). "The tomato Prf complex is a molecular trap for bacterial effectors based on Pto transphosphorylation." In: *PLoS Pathog.* 9.1, e1003123.

Nürnberger, T. et al. (2004). "Innate immunity in plants and animals: Striking similarities and obvious differences". In: *Immunol. Rev.* 198, pp. 249–266.

O'Brien, H. E., Thakur, S., and Guttman, D. S. (2011). "Evolution of plant pathogenesis in *Pseudomonas syringae*: A genomics perspective." In: *Annu. Rev. Phytopathol.* 49, pp. 269–289.

Oerke, E. C. and Dehne, H. W. (2004). "Safeguarding production - Losses in major crops and the role of crop protection." In: *Crop Prot.* 23.4, pp. 275–285.

Oldroyd, G. E. D. et al. (2011). "The rules of engagement in the legume-rhizobial symbiosis." In: *Annu. Rev. Genet.* 45.1, pp. 119–144.

O'Neill, L. A. J. and Bowie, A. G. (2007). "The family of five: TIR-domain-containing adaptors in Toll-like receptor signalling." In: *Nat. Rev. Immunol.* 7.5, pp. 353–364.

Önell, A. and Andersson, K. (2005). "Kinetic determinations of molecular interactions using Biacore - Minimum data requirements for efficient experimental design." In: *J. Mol. Recognit.* 18.4, pp. 307–317.

Ottmann, C. et al. (2009). "A common toxin fold mediates microbial attack and plant defense." In: *Proc. Natl. Acad. Sci. U. S. A.* 106.25, pp. 10359–10364.

Parlevliet, J. E. and Zadoks, J. C. (1977). "The integrated concept of disease resistance: A new view including horizontal and vertical resistance in plants." In: *Euphytica* 26.1, pp. 5–21.

Peck, S. C. (2006). "Analysis of protein phosphorylation: methods and strategies for studying kinases and substrates." In: *Plant J.* 45.4, pp. 512–522.

Pedersen, S. et al. (1978). "Patterns of protein synthesis in E. coli: a catalog of the amount of 140 individual proteins at different growth rates." In: *Cell* 14.1, pp. 179–190.

Philippot, L. et al. (2013). "Going back to the roots: the microbial ecology of the rhizosphere." In: *Nat. Rev. Microbiol.* 11.11, pp. 789–799.

Piehler, J. (2005). "New methodologies for measuring protein interactions in vivo and in vitro." In: *Curr. Opin. Struct. Biol.* 15, pp. 4–14.

Plank, V. E. van der (1968). *Plant diseases: epidemics and control.* 1st ed. London: Academic Press Inc. (London) Limited.

Powell, N. (2012). "Interaction of plant parasitic nematodes with other disease-causing agents." In: *Plant Parasit. Nematodes*. Ed. by B. Zuckerman. Elsevier. Chap. 18, pp. 119–135.

Prats, E. et al. (2006). "Stomatal lock-open, a consequence of epidermal cell death, follows transient suppression of stomatal opening in barley attacked by Blumeria graminis." In: *J. Exp. Bot.* 57.10, pp. 2211–2226.

Preston, G. M. (2000). "*Pseudomonas syringae* pv. tomato: the right pathogen, of the right plant, at the right time." In: *Mol. Plant Pathol.* 1.5, pp. 263–275.

Pritchard, L. and Birch, P. R. J. (2014). "The zigzag model of plant-microbe interactions: is it time to move on?" In: *Mol. Plant Pathol.* 15.9, pp. 865–870.

Pruitt, R. N. et al. (2015). "The rice immune receptor XA21 recognizes a tyrosine-sulfated protein from a Gram-negative bacterium." In: *Sci. Adv.* 1.6, e1500245–e1500245.

Qi, D. and Innes, R. W. (2013). "Recent advances in plant NLR structure, function, localization, and signaling." In: *Front. Immunol.* 4.10, pp. 1–10.

Qi, Y. et al. (2011). "Physical association of pattern-triggered immunity (PTI) and effector-triggered immunity (ETI) immune receptors in *Arabidopsis*". In: *Mol. Plant Pathol.* 12.7, pp. 702–708.

Qutob, D. et al. (2006). "Phytotoxicity and innate immune responses induced by Nep1-Like Proteins." In: *Plant Cell* 18.12, pp. 3721–3744.

Ranf, S. et al. (2015). "A lectin S-domain receptor kinase mediates lipopolysaccharide sensing in *Arabidopsis thaliana*." In: *Nat. Immunol.* 16.4, pp. 426–433.

Rathjen, J. P. et al. (1999). "Constitutively active Pto induces a Prf-dependent hypersensitive response in the absence of avrPto." In: *EMBO J.* 18.12, pp. 3232–3240.

Rich, R. L. and Myszka, D. G. (2000). "Advances in surface plasmon resonance biosensor analysis." In: *Curr. Opin. Biotechnol.* 11.1, pp. 54–61.

Rixen, C., Stoeckli, V., and Ammann, W. (2003). "Does artificial snow production affect soil and vegetation of ski pistes? A review." In: *Perspect. Plant Ecol. Evol. Syst.* 5, pp. 219–230.

Robatzek, S., Chinchilla, D., and Boller, T. (2006). "Ligand-induced endocytosis of the pattern recognition receptor FLS2 in *Arabidopsis*." In: *Genes Dev.* 20.5, pp. 537–542.

Robatzek, S. and Kuhn, H. (2015). "Should I stay or should I go? Traffic control for plant pattern recognition receptors." In: *Curr. Opin. Plant Biol.* 28, pp. 23–29.

Robatzek, S. et al. (2007). "Molecular identification and characterization of the tomato flagellin receptor LeFLS2, an orthologue of *Arabidopsis* FLS2 exhibiting characteristically different perception specificities." In: *Plant Mol. Biol.* 64, pp. 539–547.

Rohmer, L., Guttman, D. S., and Dangl, J. L. (2004). "Diverse evolutionary mechanisms shape the type III effector virulence factor repertoire in the plant pathogen *Pseudomonas syringae*." In: *Genetics* 167.3, pp. 1341–1360.

Römer, P. et al. (2007). "Plant pathogen recognition mediated by promoter activation of the pepper Bs3 resistance gene." In: *Science.* 318.5850, pp. 645–648.

Rommens, C. M. et al. (1995). "Intergeneric transfer and functional expression of the tomato disease resistance gene Pto." In: *Plant Cell* 7.10, pp. 1537–1544.

Ronald, P. C. and Beutler, B. (2010). "Plant and animal sensors of conserved microbial signatures." In: *Science.* 330.6007, pp. 1061–1064.

Ronald, P. C. et al. (1992). "The cloned avirulence gene avrPto induces disease resistance in tomato cultivars containing the Pto resistance gene." In: *J. Bacteriol.* 174.5, pp. 1604–1611.

Roux, M. et al. (2011). "The *Arabidopsis* leucine-rich repeat receptor-like kinases BAK1/SERK3 and BKK1/SERK4 are required for innate immunity to Hemibiotrophic and Biotrophic pathogens." In: *Plant Cell* 23.6, pp. 2440–2455.

Russinova, E. et al. (2004). "Heterodimerization and endocytosis of *Arabidopsis* brassinosteroid Receptors BRI1 and AtSERK3 (BAK1)." In: *Plant Cell* 16.12, pp. 3216–3229.

Sakaguchi, S. et al. (2008). "Regulatory T cells and immune tolerance." In: *Cell* 133.5, pp. 775–787.

Sako, T. et al. (1988). "Contrasting actions of Staurosporine, a Protein Kinase C inhibitor , on human neutrophils and primary mouse epidermal cells." In: *Cancer Res.* 48, pp. 4646–4650.

Salmeron, J. M. et al. (1996). "Tomato Prf Is a member of the leucine-rich repeat class of plant disease resistance genes and lies embedded within the Pto kinase gene cluster." In: *Cell* 86.1, pp. 123–133.

Samatey, F. a. et al. (2001). "Structure of the bacterial flagellar protofilament and implications for a switch for supercoiling." In: *Nature* 410.6826, pp. 331–337.

Sarkar, S. F. and Guttman, D. S. (2003). "Evolution of the core genome of *Pseudomonas syringae*, a highly clonal, endemic plant pathogen." In: *Appl. Environ. Microbiol.* 70.4, pp. 1999–2012.

Sarkar, S. F. et al. (2006). "Comparative genomics of host-specific virulence in *Pseudomonas syringae*." In: *Genetics* 174.October, pp. 1041–1056.

Sarris, P. F. et al. (2015). "A plant immune receptor detects pathogen effectors that target WRKY transcription factors." In: *Cell* 161.5, pp. 1089–1100.

Saur, I. M.-L., Conlan, B. F., and Rathjen, J. P. (2015). "The N-terminal domain of the tomato immune protein Prf contains multiple homotypic and Pto kinase interaction sites." In: *J. Biol. Chem.* 290.18, pp. 11258–11267.

Sawada, H. et al. (1999). "Phylogenetic analysis of *Pseudomonas syringae* pathovars suggests the horizontal gene transfer of argK and the evolutionary stability of hrp gene cluster." In: *J. Mol. Evol.* 49.5, pp. 627–644.

Schechter, L. M. et al. (2004). "*Pseudomonas syringae* type III secretion system targeting signals and novel effectors studied with a Cya translocation reporter." In: *J. Bacteriol.* 186.2, pp. 543–555.

Schlumberger, M. C. et al. (2005). "Real-time imaging of type III secretion: Salmonella SipA injection into host cells." In: *Proc. Natl. Acad. Sci. U. S. A.* 102.35, pp. 12548–12553.

Schmid-Hempel, P. and Ebert, D. (2003). "On the evolutionary ecology of specific immune defence." In: *Trends Ecol. Evol.* 18.1, pp. 27–32.

Schmidt, E. D. et al. (1997). "A leucine-rich repeat containing receptor-like kinase marks somatic plant cells competent to form embryos." In: *Development* 124.10, pp. 2049–2062.

Schmidt, T. (2015). "In vivo-Interaktionsstudien des bakteriellen Effektorproteins AvrPto zu Virulenz-Zielproteinen". Master Thesis. Technische Universität Dresden.

Scholthof, K.-B. G. (2007). "The disease triangle: pathogens, the environment and society." In: *Nat. Rev. Microbiol.* 5.2, pp. 152–156.

Schulze, B. et al. (2010). "Rapid heteromerization and phosphorylation of ligand-activated plant transmembrane receptors and their associated kinase BAK1." In: *J. Biol. Chem.* 285.13, pp. 9444–9451.

Schulze-Lefert, P. and Panstruga, R. (2011). "A molecular evolutionary concept connecting nonhost resistance, pathogen host range, and pathogen speciation." In: *Trends Plant Sci.* 16.3, pp. 117–125.

Schwessinger, B. and Rathjen, J. P. (2015). "Changing SERKs and priorities during plant life." In: *Trends Plant Sci.* 20.9, pp. 531–533.

Schwessinger, B. et al. (2011). "Phosphorylation-dependent differential regulation of plant growth, cell death, and innate immunity by the regulatory receptor-like kinase BAK1." In: *PLoS Genet.* 7.4, pp. 1–17.

Scofield, S. et al. (1996). "Molecular basis of gene-for-gene specificity in bacterial speck disease of tomato." In: *Science.* 274.5295, pp. 2063–2065.

Segonzac, C. et al. (2012). "The shoot apical meristem regulatory peptide CLV3 does not activate innate immunity." In: *Plant Cell* 24.8, pp. 3186–3192.

Segonzac, C. et al. (2014). "Negative control of BAK1 by protein phosphatase 2A during plant innate immunity." In: *EMBO J.* 33.18, pp. 2069–2079.

Sessa, G., D'Ascenzo, M., and Martin, G. B. (2000). "Thr38 and Ser198 are Pto autophoshorylation sites required for the AvrPto-Pto-mediated hypersensitive respone". In: *EMBO J.* 19.10, pp. 2257–2269.

Shan, L. et al. (2000). "A cluster of mutations disrupt the avirulence but not the virulence function of AvrPto." In: *Mol. Plant-Microbe Interact.* 13.6, pp. 592–598.

Shan, L. et al. (2008). "Bacterial effectors target the common signaling partner BAK1 to disrupt multiple MAMP receptor-signaling complexes and impede plant immunity." In: *Cell Host Microbe* 4.1, pp. 17–27.

Shaner, N. C. et al. (2004). "Improved monomeric red, orange and yellow fluorescent proteins derived from Discosoma sp. red fluorescent protein." In: *Nat. Biotechnol.* 22.12, pp. 1567–1572.

Sheard, L. B. et al. (2010). "Jasmonate perception by inositol-phosphate-potentiated COI1-JAZ co-receptor." In: *Nature* 468.7322, pp. 400–405.

Shinya, T. et al. (2012). "Functional characterization of CEBiP and CERK1 homologs in *Arabidopsis* and rice reveals the presence of different chitin receptor systems in plants." In: *Plant Cell Physiol.* 53.10, pp. 1696–1706.

Shiu, S. H. and Bleecker, A. B. (2001). "Receptor-like kinases from *Arabidopsis* form a monophyletic gene family related to animal receptor kinases." In: *Proc. Natl. Acad. Sci. U. S. A.* 98.19, pp. 10763–10768.

Shiu, S.-h. and Bleecker, A. B. (2003). "Expansion of the receptor-like kinase / Pelle gene family and receptor-like proteins in *Arabidopsis*." In: *Plant Physiol.* 132.6, pp. 530–543.

Singh, P. and Zimmerli, L. (2013). "Lectin receptor kinases in plant innate immunity." In: *Front. Plant Sci.* 4.5, pp. 1–5.

Smith, K. D. et al. (2003). "Toll-like receptor 5 recognizes a conserved site on flagellin required for protofilament formation and bacterial motility." In: *Nat. Immunol.* 4.12, pp. 1247–1253.

Song, D. H. and Lee, J. O. (2012). "Sensing of microbial molecular patterns by Toll-like receptors." In: *Immunol. Rev.* 250.1, pp. 216–229.

Stavrinides, J., McCann, H. C., and Guttman, D. S. (2008). "Host-pathogen interplay and the evolution of bacterial effectors." In: *Cell. Microbiol.* 10.2, pp. 285–292.

Stenberg, E. et al. (1991). "Quantitative determination of surface concentration of protein with surface plasmon resonance using radiolabeled proteins." In: *J. Colloid Interface Sci.* 143.2, pp. 513–526.

Stotz, H. U. and Guimaraes, R. L. (2004). "Oxalate production by Sclerotinia sclerotiorum deregulates guard cells during infection." In: *Plant Physiol.* 136.11, pp. 3703–3711.

Stout, M. J., Thaler, J. S., and Thomma, B. P. H. J. (2006). "Plant-mediated interactions between pathogenic microorganisms and herbivorous arthropods." In: *Annu. Rev. Entomol.* 51, pp. 663–689.

Strange, R. N. and Scott, P. R. (2005). "Plant disease: A threat to global food security." In: *Annu. Rev. Phytopathol.* 43, pp. 83–116.

Stuart, L. M., Paquette, N., and Boyer, L. (2013). "Effector-triggered versus pattern-triggered immunity: how animals sense pathogens". In: *Nat. Rev. Immunol.* 13.3, pp. 199–206.

Sun, W. et al. (2006). "Within-species flagellin polymorphism in Xanthomonas campestris pv campestris and its impact on elicitation of *Arabidopsis* FLAGELLIN SENSING2-dependent defenses." In: *Plant Cell* 18.3, pp. 764–779.

Sun, X. et al. (2014). "The intrinsically disordered structural platform of the plant defence hub protein RPM1-interacting protein 4 provides insights into its mode of action in the host-pathogen interface and evolution of the nitrate-induced domain protein family." In: *FEBS J.* 281, pp. 3955–3979.

Sun, Y. et al. (2013a). "Structural basis for flg22-induced activation of the *Arabidopsis* FLS2-BAK1 immune complex." In: *Science.* 342.11, pp. 624–628.

Sun, Y. et al. (2013b). "Structure reveals that BAK1 as a co-receptor recognizes the BRI1-bound brassinolide." In: *Cell Res.* 23.11, pp. 1326–9.

Swords, K. M. et al. (1996). "Spontaneous and induced mutations in a single open reading frame alter both virulence and avirulence in Xanthomonas campestris pv. vesicatoria avrBs2." In: *J. Bacteriol.* 178.15, pp. 4661–4669.

T. J. Silhavy, D. Kahne and Walker, S. (2010). "The bacterial cell envelope." In: *Cold Spring Harb. Perspect. Biol.* 2.5, pp. 1–17.

Taguchi, F. et al. (2010). "Defects in flagellin glycosylation affect the virulence of *Pseudomonas syringae* pv. tabaci 6605." In: *Microbiology* 156, pp. 72–80.

Takai, R. et al. (2008). "Analysis of flagellin perception mediated by flg22 receptor OsFLS2 in rice." In: *Mol. Plant-Microbe Interact.* 21.12, pp. 1635–1642.

Takken, F. L. W. and Goverse, A. (2012). "How to build a pathogen detector: Structural basis of NB-LRR function." In: *Curr. Opin. Plant Biol.* 15.4, pp. 375–384.

Tampakaki, a. P. and Panopoulos, N. J. (2000). "Elicitation of hypersensitive cell death by extracellularly targeted HrpZPsph produced in planta." In: *Mol. Plant-Microbe Interact.* 13.12, pp. 1366–1374.

Tanaka, K. et al. (2010). "Extracellular ATP signaling in plants." In: *Trends Cell Biol.* 20.10, pp. 601–608.

Tang, W. et al. (2008). "BSKs mediate signal transduction from the receptor kinase BRI1 in *Arabidopsis*." In: *Science.* 321.5888, pp. 557–560.

Tang, X. et al. (1996). "Initiation of Plant Disease Resistance by Physical Interaction of AvrPto and Pto Kinase". In: *Science.* 274.21, pp. 3–6.

Tang, X. et al. (1999). "Overexpression of Pto activates defense responses and confers broad resistance." In: *Plant Cell* 11.1, pp. 15–29.

Tans-Kersten, J., Huang, H., and Allen, C. (2001). "Ralstonia solanacearum needs motility for invasive virulence on tomato." In: *J. Bacteriol.* 183.12, pp. 3597–3605.

Tao, Y. et al. (2003). "Quantitative nature of *Arabidopsis* responses during compatible and incompatible interactions with the bacterial pathogen *Pseudomonas syringae*." In: *Plant Cell* 15.2, pp. 317–330.

Tateda, C. et al. (2014). "Salicylic Acid regulates *Arabidopsis* microbial pattern receptor kinase levels and signaling." In: *Plant Cell* 26.10, pp. 4171–4187.

Tena, G., Boudsocq, M., and Sheen, J. (2011). "Protein kinase signaling networks in plant innate immunity." In: *Curr. Opin. Plant Biol.* 14.5, pp. 519–529. arXiv: NIHMS150003.

The UniProt Consortium (2015). "UniProt: a hub for protein information". In: *Nucleic Acids Res.* 43.D1, pp. D204–D212.

Thomma, B. P. H. J., Nürnberger, T., and Joosten, M. H. a. J. (2011). "Of PAMPs and effectors: the blurred PTI-ETI dichotomy." In: *Plant Cell* 23.1, pp. 4–15.

Tintor, N. and Saijo, Y. (2014). "ER-mediated control for abundance, quality, and signaling of transmembrane immune receptors in plants." In: *Front. Plant Sci.* 5.A65, pp. 1–6.

Tintor, N. et al. (2013). "Layered pattern receptor signaling via ethylene and endogenous elicitor peptides during *Arabidopsis* immunity to bacterial infection." In: *Proc. Natl. Acad. Sci.* 110.15, pp. 6211–6216.

Tonegawa, S. (1983). "Somatic generation of antibody diversity." In: *Nature* 302.5909, pp. 575–581.

Tsuda, K. and Katagiri, F. (2010). "Comparing signaling mechanisms engaged in pattern-triggered and effector-triggered immunity." In: *Curr. Opin. Plant Biol.* 13.4, pp. 459–465.

Tugizimana, F. et al. (2012). "Ergosterol-induced sesquiterpenoid synthesis in tobacco cells." In: *Molecules* 17.2, pp. 1698–1715.

Underwood, W., Melotto, M., and He, S. Y. (2007). "Role of plant stomata in bacterial invasion." In: *Cell. Microbiol.* 9.7, pp. 1621–1629.

Vaid, N., Pandey, P. K., and Tuteja, N. (2012). "Genome-wide analysis of lectin receptor-like kinase family from *Arabidopsis* and rice." In: *Plant Mol. Biol.* 80.4, pp. 365–388.

Van Der Biezen, E. A. and Jones, J. D. G. (1998). "Plant disease-resistance proteins and the gene-for-gene concept". In: *Trends Biochem. Sci.* 23.12, pp. 454–456.

Veronese, P. and Nakagami, H. (2006). "The membrane-anchored BOTRYTIS-INDUCED KINASE1 plays distinct roles in *Arabidopsis* resistance to necrotrophic and biotrophic pathogens." In: *Plant Cell* 18.1, pp. 257–273.

Vert, G. et al. (2005). "Molecular mechanisms of steroid hormone signaling in plants." In: *Annu. Rev. Cell Dev. Biol.* 21.1, pp. 177–201.

Vetter, M. M. et al. (2012). "Flagellin perception varies quantitatively in *Arabidopsis thaliana* and its relatives." In: *Mol. Biol. Evol.* 29.6, pp. 1655–1667.

Vivian, A. and Gibbon, M. J. (1997). "Avirulence genes in plant-pathogenic bacteria: Signals or weapons?" In: *Microbiology* 143, pp. 693–704.

Vorholt, J. A. (2012). "Microbial life in the phyllosphere." In: *Nat. Rev. Microbiol.* 10.12, pp. 828–840.

Wang, J. et al. (2014a). "Structural insights into the negative regulation of BRI1 signaling by BRI1-interacting protein BKI1." In: *Cell Res.* 24.11, pp. 1–14.

Wang, R. et al. (2004). "The PDBbind database: Collection of binding affinities for protein-ligand complexes with known three-dimensional structures". In: *J. Med. Chem.* 47.12, pp. 2977–2980.

Wang, X. et al. (2005). "Identification and functional analysis of in vivo phosphorylation sites of the *Arabidopsis* BRASSINOSTEROID-INSENSITIVE1 receptor kinase." In: *Plant Cell* 17.6, pp. 1685–1703.

Wang, X. et al. (2008). "Sequential transphosphorylation of the BRI1/BAK1 receptor kinase complex impacts early events in brassinosteroid signaling." In: *Dev. Cell* 15.2, pp. 220–235.

Wang, Y. et al. (2000). "Cn3D: sequence and structure views for Entrez." In: *Trends Biochem. Sci.* 25.6, pp. 300–302.

Wang, Y. et al. (2014b). "Assessment of BAK1 activity in different plant receptor-like kinase complexes by quantitative profiling of phosphorylation patterns." In: *J. Proteomics* 108, pp. 484–493.

Wang, Y. et al. (2010). "A *Pseudomonas syringae* ADP-ribosyltransferase inhibits *Arabidopsis* mitogen-activated protein kinase kinases." In: *Plant Cell* 22.6, pp. 2033–2044.

Weber, P. C. et al. (1989). "Structural origins of high-affinity biotin binding to streptavidin." In: *Science.* 243.4887, pp. 85–88.

Wei, C.-F. et al. (2007). "A *Pseudomonas syringae* pv. tomato DC3000 mutant lacking the type III effector HopQ1-1 is able to cause disease in the model plant Nicotiana benthamiana." In: *Plant J.* 51.1, pp. 32–46.

Weiler, E. W. et al. (1994). "The *Pseudomonas* phytotoxin coronatine mimics octadecanoid signalling molecules of higher plants." In: *FEBS Lett.* 345.1, pp. 9–13.

Werling, D. et al. (2009). "Variation matters: TLR structure and species-specific pathogen recognition." In: *Trends Immunol.* 30.3, pp. 124–130.

Westra, E. R., Buckling, A., and Fineran, P. C. (2014). "CRISPR–Cas systems: beyond adaptive immunity." In: *Nat. Rev. Microbiol.* 12.5, pp. 317–326.

Whitham, S. et al. (1994). "The product of the tobacco mosaic virus resistance gene N: Similarity to toll and the interleukin-1 receptor." In: *Cell* 78.6, pp. 1101–1115.

Willmann, R. (2011). "Charakterisierung von Proteinen mit Lysin-Motiven und ihre Rolle in der Peptidoglycanperzeption und der angeborenen Immunität in *Arabidopsis thaliana*". Dissertation. Universität Tübingen.

Willmann, R. and Lajunen, H. (2011). "*Arabidopsis* lysin-motif proteins LYM1 LYM3 CERK1 mediate bacterial peptidoglycan sensing and immunity to bacterial infection." In: *Proc. Natl. Acad. Sci. U. S. A.* 108.49, pp. 19824–19829.

Wilton, M. et al. (2010). "The type III effector HopF2Pto targets *Arabidopsis* RIN4 protein to promote *Pseudomonas syringae* virulence." In: *Proc. Natl. Acad. Sci. U. S. A.* 107.5, pp. 2349–2354.

Wofsy, C. and Goldstein, B. (2002). "Effective rate models for receptors distributed in a layer above a surface: application to cells and Biacore." In: *Biophys. J.* 82.4, pp. 1743–1755.

Wolber, P. K. et al. (1986). "Identification and purification of a bacterial ice-nucleation protein." In: *Proc. Natl. Acad. Sci. U. S. A.* 83.19, pp. 7256–7260.

Wu, W. et al. (2015). "Somatic embryogenesis receptor-like kinase 5 in the ecotype Landsberg erecta of *Arabidopsis* is a functional RD LRR-RLK in regulating brassinosteroid signaling and cell death control." In: *Front. Plant Sci.* 6.10, A852.

Wu, X. et al. (2012). "Transphosphorylation of E. coli proteins during production of recombinant protein kinases provides a robust system to characterize kinase specificity." In: *Front. Plant Sci.* 3.11, A262.

Wulf, J. et al. (2004). "The solution structure of type III effector protein AvrPto reveals conformational and dynamic features important for plant pathogenesis." In: *Structure* 12.7, pp. 1257–1268.

Xiang, T. et al. (2011). "BAK1 is not a target of the *Pseudomonas syringae* effector AvrPto." In: *Mol. Plant-Microbe Interact.* 24.1, pp. 100–107.

Xiang, T. et al. (2008). "*Pseudomonas syringae* effector AvrPto blocks innate immunity by targeting receptor kinases." In: *Curr. Biol.* 18.1, pp. 74–80.

Xiao, F. et al. (2003). "Pto mutants differentially activate Prf-dependent, avrPto-independent resistance and gene-for-gene resistance." In: *Plant Physiol.* 131.3, pp. 1239–1249.

Xie, D. X. et al. (1998). "COI1: an *Arabidopsis* gene required for jasmonate-regulated defense and fertility." In: *Science.* 280.5366, pp. 1091–1094.

Xin, X.-F. and He, S. Y. (2013). "*Pseudomonas syringae* pv. tomato DC3000: A model pathogen for probing disease susceptibility and hormone signaling in plants". In: *Annu. Rev. Phytopathol.* 51.1, pp. 473–498.

Xing, W. et al. (2007). "The structural basis for activation of plant immunity by bacterial effector protein AvrPto." In: *Nature* 449.7159, pp. 243–247.

Yamaguchi, K. et al. (2013). "Suppression of rice immunity by Xanthomonas oryzae type III effector Xoo2875." In: *Biosci. Biotechnol. Biochem.* 77.4, pp. 796–801.

Yamaguchi, Y., Pearce, G., and Ryan, C. A. (2006). "The cell surface leucine-rich repeat receptor for AtPep1, an endogenous peptide elicitor in *Arabidopsis*, is functional in transgenic tobacco cells." In: *Proc. Natl. Acad. Sci. U. S. A.* 103.26, pp. 10104–10109.

Yamaguchi, Y. et al. (2010). "PEPR2 is a second receptor for the Pep1 and Pep2 peptides and contributes to defense responses in *Arabidopsis*." In: *Plant Cell* 22.2, pp. 508–522.

Yan, L. et al. (2012). "Structural basis for the impact of phosphorylation on the activation of plant receptor-like kinase BAK1." In: *Cell Res.* 22.8, pp. 1304–1308.

Yoo, S.-D., Cho, Y.-H., and Sheen, J. (2007). "*Arabidopsis* mesophyll protoplasts: a versatile cell system for transient gene expression analysis". In: *Nat. Protoc.* 2.7, pp. 1565–1572.

Yoon, S.-i. et al. (2012). "Structural basis of TLR5-flagellin recognition and signaling." In: *Science.* 335.6070, pp. 859–864.

Yu, J. et al. (1999). "Involvement of the exopolysaccharide alginate in the virulence and epiphytic fitness of *Pseudomonas syringae* pv. syringae." In: *Mol. Microbiol.* 33.4, pp. 712–720.

Yue, J. X. et al. (2012). "Tracing the origin and evolutionary history of plant nucleotide-binding site-leucine-rich repeat (NBS-LRR) genes." In: *New Phytol.* 193.4, pp. 1049–1063.

Zamioudis, C. and Pieterse, C. M. J. (2012). "Modulation of host immunity by beneficial microbes." In: *Mol. Plant-Microbe Interact.* 25.2, pp. 139–150.

Zhang, J. et al. (2007). "A *Pseudomonas syringae* effector inactivates MAPKs to suppress PAMP-induced immunity in plants." In: *Cell Host Microbe* 1.3, pp. 175–185.

Zhang, J. et al. (2010). "Receptor-like cytoplasmic kinases integrate signaling from multiple plant immune receptors and are targeted by a *Pseudomonas syringae* effector." In: *Cell Host Microbe* 7.4, pp. 290–301.

Zhang, L. et al. (2014). "Fungal endopolygalacturonases are recognized as microbe-associated molecular patterns by the *Arabidopsis* receptor-like protein RESPONSIVENESS TO BOTRYTIS POLYGALACTURONASES1." In: *Plant Physiol.* 164.1, pp. 352–364.

Zheng, X. et al. (2014). "Functionally redundant RXLR effectors from Phytophthora infestans act at different steps to suppress early flg22-triggered immunity." In: *PLoS Pathog.* 10.4, e1004057.

Zhou, J. et al. (2013). "The *Pseudomonas syringae* effector HopF2 suppresses *Arabidopsis* immunity by targeting BAK1." In: *Plant J.* 2, pp. 1–11.

Zipfel, C. and Felix, G. (2005). "Plants and animals: a different taste for microbes?" In: *Curr. Opin. Plant Biol.* 8.4, pp. 353–360.

Zipfel, C., Robatzek, S., and Navarro, L. (2004). "Bacterial disease resistance in *Arabidopsis* through flagellin perception." In: *Nature* 428.4, pp. 15–18.

Zipfel, C. et al. (2006). "Perception of the bacterial PAMP EF-Tu by the receptor EFR restricts Agrobacterium-mediated transformation." In: *Cell* 125.4, pp. 749–760.

Zong, N. et al. (2008). "Blocking and triggering of plant immunity by *Pseudomonas syringae* effector AvrPto." In: *Plant Signal. Behav.* 3.8, pp. 583–585.

APPENDIX: SYNTHETIC OLIGONUCLEOTIDES

The following tables lists synthetic oligonucleotides generated in this work, which were used as primers for either cloning (table **A1**), sequencing (table **A2**), or SDM (table **A3**).

Table A1 Synthetic oligonucleotides: Cloning

Name	Sequence (5'-3')	Target
BAK1-Nde1-fw	ctgatccatatgtcggataattttagcaacaagaac	BAK1
BAK1-XhoI-rv	gtcgatctcgagttatcttggacccgaggggta	BAK1
BAK1-BamHI-fw	ctgatcggatcctcggataattttagcaacaagaac	BAK1
BRI1-NdeI-fw	ctgatccatatggaggcggagttggagatg	BRI1
BRI1-XhoI-rv	gtcgatctcgagttataattttccttcaggaacttc	BRI1
BRI1-BamHI-rv	gtcgatggatccttataattttccttcaggaacttc	BRI1
FLS2-NdeI-fw	ctgatccatatgacctgttgcaagaaaaaagaa	FLS2
FLS2-XhoI-rv	gtcgatctcgagttaaacttctcgatcctcgttac	FLS2
FLS2-BamHI-rv	gtcgatggatccttaaacttctcgatcctcgttac	FLS2
Pto-HindIII-fw	ctgatcaagcttatgggaagcaagtattctaag	Pto
Pto-BamHI-rv	gtcgatggatccttaaataacagactcttggag	Pto
mO-HindIII-fw	ctgatcaagcttgtgagcaagggcgaggagaat	mOrange
mO-link-BglII-rv	gtcgatagatcttccagatcctcctcccttgtacagctcgtccatgcc	mOrange
AP-link-BglII-fw	ctgatcagatctggctctggaggaaatatatgtgtcggcggatcc	AvrPto
AP-XhoI-rv	ctgatcctcgagtcattgccagttacggtacgg	AvrPto

Table A2 Synthetic oligonucleotides: Sequencing

Name	Sequence (5'-3')	Target
T7-fw	taatacgactcactataggg	T7 promoter
pJC40seq-rv	tgttagcagccggatcag	pJC40 MCS

Table A3 Synthetic oligonucleotides: Mutagenesis

Name	Sequence (5'-3')	Target
Y89D-fw	gacatgcagcatagggacatgacgggagcgt	mO-AvrPto
Y89D-rv	acgctcccgtcatgtccctatgctgcatgtc	mO-AvrPto
S286A-fw	gttttcattgcgtgaactacaagttgctgcggataattttagcaac	BAK1
S286A-rv	gttgctaaaattatccgcagcaacttgtagttcacgcaatgaaaac	BAK1
K317E-fw	ctgatggtactttagtggccgttgagaggctaaaagaggag	BAK1
K317E-rv	ctcctcttttagcctctcaacggccactaaagtaccatcag	BAK1
T324G-fw	gctaaaagaggagcgcggccaaggtggcgaactg	BAK1
T324G-rv	cagttcgccaccttggccgcgctcctcttttagc	BAK1
T324D-fw	gttttcattgcgtgaactacaagttgctgcggataattttagcaac	BAK1
T324D-rv	cagttcgccaccttggtcgcgctcctcttttagc	BAK1

ACKNOWLEDGEMENTS

Danksagung

Ich möchte mich bei Prof. Dr. Thorsten Nürnberger für die Bereitstellung eines spannenden und herausfordernden Promotionsthemas, die wissenschaftliche Betreuung und Unterstützung, das hervorragende Arbeitsklima sowie für das in mich gesetzte Vertrauen bedanken. Außerdem danke ich ihm für die Übernahme des Erstgutachtens dieser Arbeit.

Prof. Dr. Georg Felix danke ich für die Übernahme des Zweitgutachtens und für die vielen Denkanstöße und Anregungen, die mir dabei halfen, stets einen kritischen Blick sowohl auf die eigene als auch auf fremde wissenschaftliche Arbeit zu behalten.

Weiterhin möchte ich Dr. Libo Shan, Dr. Ping He, und Dr. Vardis Ntoukakis für die Bereitstellung einiger wissenschaftlicher Materialien danken. Gleiches gilt allen Mitgliedern der ZMBP-Pflanzenbiochemie für die ständige gegenseitige Hilfsbereitschaft, die einen reibungslosen Laboralltag erst möglich machte.

Ich danke Liane Schön für die große Geduld und Hilfsbereitschaft bei allen administrativen Aufgaben.

Besonderer Dank gilt Tanja Schmidt, die im Rahmen ihrer Masterarbeit wichtige Beiträge zu dieser Dissertation lieferte. Sie war außerdem die angenehmste Master-Studentin, die man sich als Betreuer überhaupt vorstellen kann - Danke für die stets gute Laune und Freundschaft!

Allen aktuellen und ehemaligen Mitgliedern der Pflanzenbiochemie danke ich für die gute Atmosphäre und Kooperation im Laboralltag und für die vielen Gelegenheiten, auch außerhalb des Labors schöne Zeiten miteinander zu verbringen. Ganz besonderer Dank gilt an dieser Stelle meinen ehemaligen Mitstreitern aus 'N3': Dr. Isabell Albert, Dr. Eric Melzer, Dr. Li Fan, Dr. Hannah Böhm, Katja Fröhlich, und Zana Kikic; ich werde unsere gemeinsame Zeit vermissen!

Meiner Familie danke ich für die moralische Unterstützung.

Zu guter Letzt möchte ich meiner Partnerin Julia für den Rückhalt, die Unterstützung und die Motivation während der letzten vier Jahre danken - ohne dich wäre diese Arbeit nicht möglich gewesen!